Queen Mary
University of London

School of Engineering and Materials Science

Culture of Mesenchymal Stem Cells on Nanosheets Assembled at the Surface of Liquid Microcarriers

Lihui Peng

Primary Supervisor: Prof. Julien Gautrot

Secondary Supervisor: Prof. Joost de Bruijn

This dissertation is submitted for the degree of

Doctor of Philosophy

October 2020

Declaration

I, Lihui Peng, confirm that the research included within this thesis is my own work or that where it has been carried out in collaboration with, or supported by others, that this is duly acknowledged below and my contribution indicated. Previously published material is also acknowledged below.

I attest that I have exercised reasonable care to ensure that the work is original, and does not to the best of my knowledge break any UK law, infringe any third party's copyright or other Intellectual Property Right, or contain any confidential material.

I accept that the College has the right to use plagiarism detection software to check the electronic version of the thesis.

I confirm that this thesis has not been previously submitted for the award of a degree by this or any other university.

Lihui Peng

October 2020

Details of collaboration and publications:

Dexu Kong performed X-ray photoelectron spectroscopy measurements, and Carlos Matellan performed magnetic tweezer measurements. All the sample preparation and data analysis were performed by me.

Parts of Chapter 2, 3 and 4 have been published (Faraday Discuss., 2017,204, 367-381 and ACS Nano., 2018,12, 9206-9213).

Acknowledgement

I would like to take this opportunity to express my gratitude to my supervisor Prof Julien Gautrot and Prof Joost de Bruijn for offering me such great opportunity to participate in such exciting project. Thanks for their continuous support for my research. I would like to thank Prof Julien Gautrot particularly, for the enlightening instruction and advice he has given which made the weekly meeting and discussion a really enjoyable moment for me.

I would also like to thank Chinese Scholarship Council, without whose funding support, completing this project would not have been possible.

My sincere appreciation also goes to my amazing colleagues in the group, without whom I would not have enjoyed last four years so much, their enthusiasm and passion were amazing. I would like to thank Dr Dexu Kong in particular for training on building liquid interfaces. Thanks Dr Yaqi You for qPCR training, Dr Danyang Li for the immunostaining training, Dr Minerva Bosch, Elijah Mojares and Christian Jones for those insightful discussions and proofreading my thesis. I really appreciate Dr William Megone and Dr Khai Duong Quang Nguyen's help on interfacial rheology.

Many thanks to all the technicians and researchers inside and outside the university. Thanks Chris Mole, Shafir Iqbal, Dr Dongsheng Wu and Dr Alice Williams for all their supports with maintaining the lab and providing trainings. I am extremely grateful to Dr Gary Warnes for his help on flow cytometry and Carlos Matellan on magnetic tweezer measurements.

Last but not the least, a special thanks to my parents and my girlfriend who always encourage me and support every decision I made. Without all the love and fully support from them I would not have the courage and determination to complete this challenge.

Abstract

Mesenchymal stem cells (MSC) are one of the prevalent cell types for potential clinical utility including cell therapies and tissue engineering. In order to meet massive demand for clinical usage, a large scale *in vitro* cell expansion is required. The culture of adherent cells like MSCs is typically thought to require cell spreading on a rigid substrate to sustain the formation of stable focal adhesions and the assembly of a contractile cytoskeleton. More recent studies suggest that cells may also actively respond to external stimuli despite the lack of bulk mechanics on underlying substrates, bringing liquid-liquid interface, which offers attractive features for the development of novel stem cell technologies as a potential culture platform. In particular, liquid emulsions can provide surface area comparable to current solid-microcarriers used in industry for cell culture, emulsion are also more advantageous in avoiding harsh enzymatic digestion for cell harvesting. The relative cheaper cost and potential recyclability also make emulsions a promising substrate for next generation platform for *in vitro* cell expansion. In this thesis, we aim at developing a protein nanosheet-assembled liquid-liquid interface with tuneable interfacial mechanical properties for the expansion of MSCs. In particular we focus on development of a protein-nanosheet stabilised oil in water (O/W) emulsion as a carrier for long-term cell culture.

Chapter one presents fundamental knowledge of this research, starting with a general description of integrin mediated cell adhesion and mechanotransduction, followed by an introduction to self-assembled polyelectrolyte multilayers (PEMs) for cell culture. The third part discusses the generation of emulsions by highlighting the important role of agitation and emulsifiers in its formation. Special attention is paid to the stability of the emulsion. In the final section of this chapter, we investigate the current cell expansion techniques with a major focus on microcarrier-based bioreactor systems.

In Chapter two, we focus on the design and characterisation of poly-L-lysine (PLL) nanosheets at the liquid-liquid interface between fluorinated oil and PBS. The impact of pro-surfactant, solution pH and

PLL molecular weight on PLL assembly at the interface are investigated. In particular, we focus on the impact on the interfacial mechanical properties, characterised by interfacial rheology. Upon the adjustment of these parameters, controllable PLL nanosheets with interfacial moduli of a wide range are obtained.

Chapter three demonstrates the culture of MSC on the interfaces prepared in chapter two. Cell adhesion is studied by imaging focal adhesion markers and actin, demonstrating that MSC adhesion at our liquid-liquid interface is mediated by classical integrin/acto-myosin machinery. Cellular proliferation is also found on such nanosheets, showing the effects of pro-surfactant and nanosheet mechanics on the ultimate cell output. Similar findings are also displayed by other non-fluorinated oil systems. Furthermore, we summarise interfacial mechanical properties of the nanosheets and the corresponding proliferation data, showing MSC proliferation at the liquid-liquid interface is seemingly regulated by the stress retention of the self-assembled PLL nanosheets.

In chapter four, O/W emulsion stabilised by the PLL assembled nanosheets is employed as a novel platform for the culture of MSCs. Based on the emulsion stability and cell proliferation, the optimum emulsion is selected to conduct long-term culture of MSCs and compared with commercially available microcarriers and tissue culture polystyrene (TPS, tissue culture treated). During this process cellular adhesion and morphology are monitored; the expression of MSC surface markers are characterised, whilst the stemness and multi-lineage differentiation potential are all characterised. These characterisations demonstrate minor difference in MSC phenotypes on three different platforms, suggesting the emulsion could be a potential candidate for the *in vitro* expansion of MSCs.

Chapter five summarises the main findings and conclusions of this thesis, addresses the challenges of the project and provides possible directions and improvements for future research.

List of Abbreviation

AFM	Atomic force microscopy
ALP	Alkaline Phosphatase
ARP2/3	Actin-related proteins-2/3
AuNPs	Gold nanoparticles
B2M	Beta-2-microglobulin
BMP2	Bone morphogenetic protein 2
BSA	Bovine serum albumin
CCK-8	Cell Counting Kit-8
CHI	Chitosan
CHS	Chondroitin sulfate
CIPAAm	2-carboxyisopropylacrylamide
COL	Collagen
COL1A1	Collagen type I alpha 1
COL2A1	Collagen type II alpha 1 chain
COL10A1	Collagen type X alpha 1 chain
Dapi	4,6-diamidino-2-phenylindole
DDR	Du Noüy Ring
DI	Deionised

DMEM	Dulbecco’s Modified Eagle’s Medium
DMSO	Dimethyl sulfoxide
DWR	Double Wall Ring
ECM	Extracellular matrix
EDC	N-(3-Dimethylaminopropyl)-N’-ethylcarbodiimide
ERK	Extracellular-signal-related kinase
ESCs	Embryonic stem cells
FABP4	Fatty acid binding protein 4
F-actin	Filamentous actin
FAD	Flavin adenine dinucleotide
FAK	Focal adhesion kinase
FAs	Focal adhesions
FBS	Fetal bovine serum
FH1	Formin homology-1
FMO	Fluorescence minus one
FN	Fibronectin
G-actin	Globular actin
GAGs	Glycosaminoglycans
GEFs	Guanine-nucleotide exchange factors
GEL	Gelatin

GO	Graphene oxide
GVHD	Graft-versus-host disease
HA	Hyaluronic acid
HDC	Heptadecanoyl chloride
HEP	Heparin
HLB	Hydrophilic-Lipophilic Balance
HSC	Hematopoietic stem cell
iPSCs	Induced pluripotent stem cells
ISCT	International Society for Cellular Therapy
LbL	Layer-by-Layer
LCST	Low critical solution temperature
LN	Laminin
LPL	Lipoprotein lipase
Lys	Lysozyme
MAPK	Mitogen-activated protein kinase
MSC	Mesenchymal stem cells
Mw	Molecular Weight
NADH	Nicotinamide adenine dinucleotide
NHS	N-hydroxysulfo-succinimide
OCN	Osteocalcin

O/W	Oil-in-water
OWLS	Optical waveguide lightmode spectroscopy
PA	p-diazonium diphenyl amine polymer
PAA	Poly(acrylic acid)
PAH	Poly(allylamine hydrochoride)
PAM	Polyacrylamide
PBS	Phosphate-buffered saline
PDAC	Poly(diallyldimethylammonium) chloride
PDMS	Poly(dimethyl siloxane)
PEI	Poly(ethylene imine)
PELs	Polyelectrolytes
PEMs	Polyelectrolyte multilayers
PFA	Paraformaldehyde
PFBC	Pentafluorobenzoyl chloride
PGs	Proteoglycans
PIPAAm	Poly(N-isopropylacrylamide)
PLL	Poly-L-lysine
PLL-g-PEG	Poly(l-lysine)-graft-polyethylene glycol
PSS	Polystyrene sulfonate
QCM-D	Quartz crystal microbalance

RGD	Arginine-glycine-aspartic
RPE	Retinal pigment epithelial
RT-PCR	Real-time polymerase chain reaction
RUNX2	Runt related transcription factor 2
SAMs	Self-assembled monolayers
SBC	Sebacoyl chloride
SEM	Scanning electron microscopy
SMCs	Smooth muscle cells
SOX9	SRY-box 9
TEA	Trimethylamine
Thy-1	Thymus cell antigen 1
TGF-β	Transforming growth factor β
TPS	Tissue culture polystyrene
VASP	Vasodilator-stimulated phosphoprotein
VB	Vinylbenzyl
VCAM1	Vascular cell adhesion molecule 1
VN	Vitronectin
WASP	Wiskott-Aldrich syndrome protein
W/O	Water-in-oil
XPS	X-ray photoelectron spectroscopy

Table of Contents

List of Figures

Chapter 1

Introduction

Mesenchymal stem cells (MSC) are famous for their *in vitro* self-renewal properties and multi-potency, are one of the prevalent cell types for potential clinical utility including cell therapies and tissue engineering. However, such cells are uncommon and relatively difficult to isolate in large numbers. In order to meet the massive demand for clinical usage, a large scale *in vitro* cell expansion is required. The culture of adherent cells like MSCs is typically thought to require cell spreading on a rigid substrate to sustain the formation of stable focal adhesions and the assembly of a contractile cytoskeleton. Such processes are crucial for the cell to build up proper and active intra- and extra-cellular connections, converting external signals into biochemical signals and generating appropriate cellular responses to extracellular cues. However, such solid rigid substrates present clear drawbacks, particularly in the case of cell harvesting, where an invasive enzymatic digestion is typically required, which can be harmful and induce cell phenotype changes. Moreover, since most of such substrates are made of plastic (normally polystyrene), massive plastic waste is also an issue. An alternative platform to address these challenges would be favoured. A number of recent studies suggest that cells may also actively respond to external stimuli despite the lack of bulk mechanics on underlying substrates, hence the surface of liquid could be a potential platform for cell culture. The culture of cells on more adaptive substrates such as liquid-liquid interface is particularly interesting especially in the case of designing oil-derived emulsion for cell culture purpose. The liquid emulsions provide surface area comparable to current solid-microcarriers used in industry for cell culture, and they are potentially more advantageous than the current industry choice by directly addressing the cell detachment and plastic waste issues mentioned above. This project is focusing on developing a protein nanosheet-assembled liquid-liquid interface with tuneable interfacial mechanical properties for the expansion of MSCs. In particular, we aim on the development of a protein-nanosheet stabilised O/W emulsion as a carrier for long-term cell culture.

This chapter presents fundamental knowledge of this research, starting with a general description of integrin mediated cell adhesion and mechanotransduction, followed by an introduction to self-assembled protein nanosheets for cell culture, including the mechanisms and methods of nanosheet

assembly and stiffening. The third part of this chapter discusses the generation of an emulsion and the mechanism is introduced by highlighting the important role of agitation and emulsifiers in its formation. Special attention is paid to the stability of the emulsion and common reasons for instability are discussed, including a theoretical mechanism and possible solutions. In the final section of this chapter, we investigate the current cell expansion techniques with a major focus on microcarrier-based bioreactor systems. The selection and operation parameters of this system are also reviewed.

1.1 Integrin Mediated Cell Adhesion and Mechanotransduction

The extracellular matrix (ECM), the microenvironment in which cells lives, is a three-dimensional network of proteins and polysaccharides secreted and remodelled by cells.[1] Cell adhesion to the ECM *in vivo* is essential for maintaining tissue structure and functionality, and its roles in regulating cell behaviour and phenotype such as spreading, motility, endocytosis, proliferation, differentiation and apoptosis have been widely recognised.[1–3] Cell-ECM adhesion has been at the centre of the study of cell-material interactions to aid the design of materials for biomedical applications.[1,4] The interaction between the ECM and cells is mainly mediated by a family of transmembrane heterodimeric surface receptors termed 'integrins', which interact with specific proteins of the ECM including fibronectin (FN), laminin (LN), vitronectin (VN) and collagen (COL). Such interaction directly activates signal transduction pathways converting extracellular environmental stimuli such as chemical, mechanical and topographical cues into intracellular molecular responses, guiding cells to adapt to various physiological changes. Understanding the detailed mechanisms of cell adhesion and the establishment of signalling pathways is of particular importance in designing biomaterials regulating cell phenotypes for tissue engineering and regenerative medicine applications.

ECM components such as elastic fibres, fibrillar collagens, glycosaminoglycans (GAGs) and proteoglycans (PGs) provide the basic mechanical properties of the ECM.[2,5] These mechanical properties are some of the major cues that cells sense from the ECM. The translation of such

mechanical cues into biochemical signals is a process termed mechanotransduction.[5,6] The process that cells use to sense the stiffness of their underlying substrates involve four steps: 1. cells begin by generating thin protrusions (filopodia), probing the new environment into which they spread; 2. these protrusions adhere to specific proteins of the ECM surrounding them; 3. cells exert forces to deform the surrounding substrate via adhesion; 4. finally, by measuring the forces applied via a transduction process, cells sense the stiffness of the area to which they adhere.[7] The entire process, which plays a critical role in various cellular activities (including motility, morphological changes, proliferation, differentiation and polarity formation, etc.) and pathogenesis of various diseases (including cardiovascular diseases, osteoporosis and cancer, etc.),[8] and requires the involvement of the actin cytoskeleton, focal adhesion and ECM (Figure 1.1).

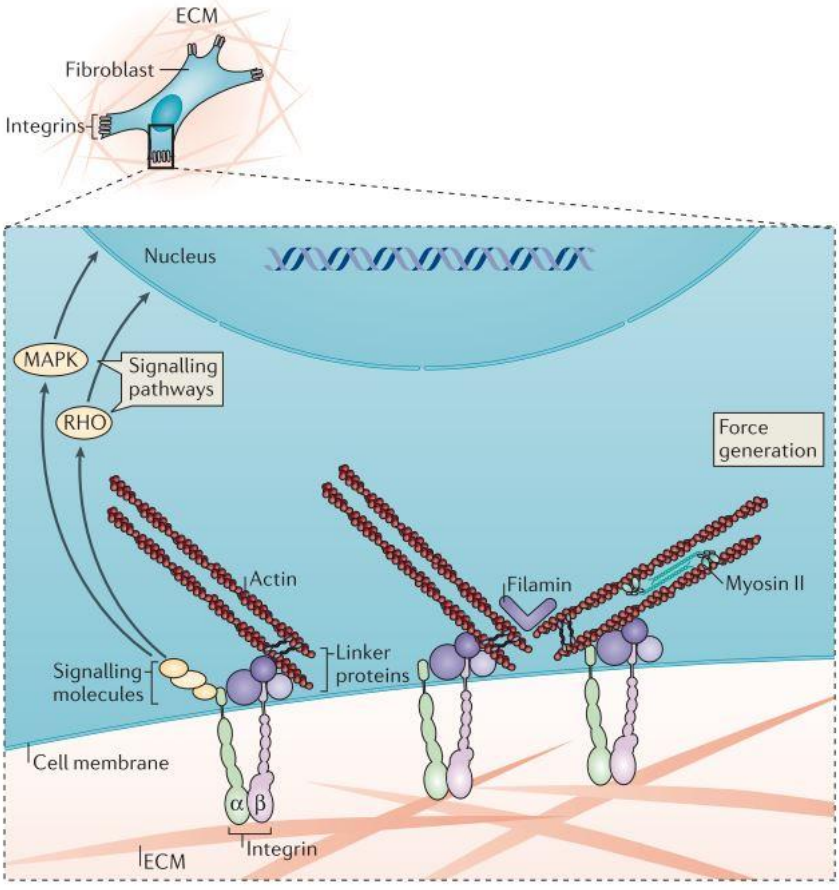

Figure 1.1. Schematic depicting the binding of the actin cytoskeleton to the ECM via integrin-mediated formation of a focal adhesion complex.[2] Reprinted with permission from [Springer Nature Customer Service Centre GmbH]: [Springer Nature] [Nature Reviews Molecular Cell Biology] [Humphrey, J. D., Dufresne, E. R. & Schwartz, M. A. Mechanotransduction and extracellular matrix homeostasis. [COPYRIGHT] (2014)

1.1.1 The Dynamic Process of Actin Filaments Assembly

Cell membrane protrusions forming at the leading edge of cells determine cellular morphology, and play an important role in initial cell contact with a given substrate.[9,10] Since protrusions require the

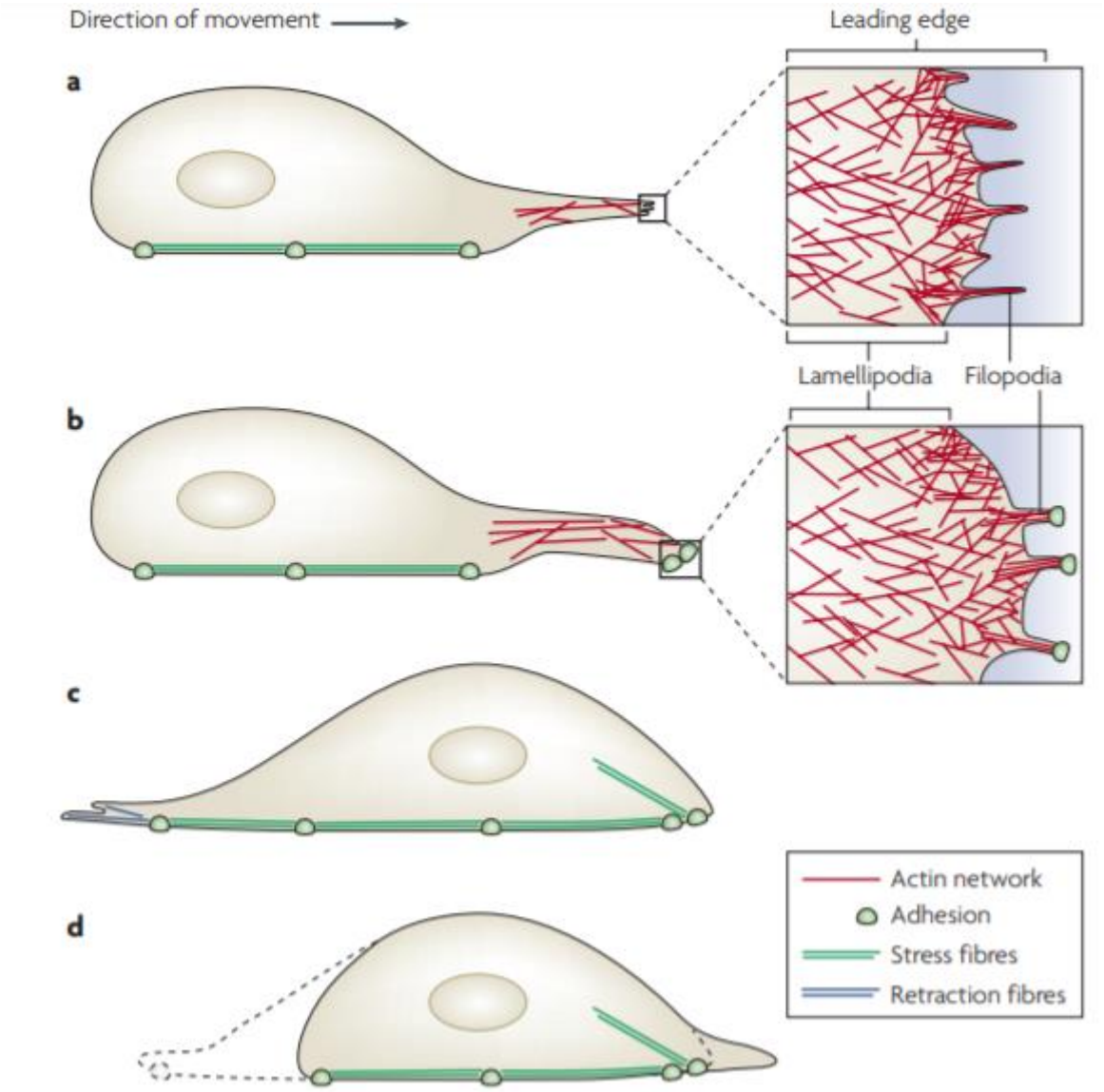

Figure 1.2 Schematic illustration of cellular migration and the role of different actin filament structures.[12] Reprinted with permission from [Springer Nature Customer Service Centre GmbH]: [Springer Nature] [Nature Reviews Molecular Cell Biology] [Mattila, P. K. & Lappalainen, P. Filopodia: Molecular architecture and cellular functions. [COPYRIGHT] (2008)

formation of actin microfilaments, it has been widely accepted that the formation of protrusions is driven by actin polymerisation.[10,11] Filamentous actin (F-actin) is known as the primary component cell spreading and motility and in combination with other associated proteins it forms the actin cytoskeleton which interacts with the ECM.[8] Globular actin (G-actin) molecules are the constitutive

subunits of F-actin, which assemble into F-actin at the front end and disassemble from the polymerised filaments at the rear end. This polymerisation and depolymerisation process is known as treadmilling, and allows the manifestation of cell-surface projections including dynamic structures such as sheet-like wide area protrusions called lamellipodia and thin rod-like protrusions termed filopodia (Figure 1.2) which form at the leading edge of cell.[12] Polymerisation of a single actin filament has been measured to generate a force of 1 pN[13] while filament bundles generate a force of as much as 300 nN.[14] With such significant protrusive forces generated by bundles of treadmilling F-actin, cells are able to deform their membranes, pushing their leading edges forward, protruding in some areas and retracting in others allowing them to explore new territories.[15]

1.1.1.1 Associated Proteins Regulating Filaments Assembly

This dynamic assembly and disassembly behaviour of actin filaments is regulated by hundreds of accessory proteins including formin, profilin, α-actinin, fascin and filamin in the cytoplasm (Figure 1.3).[1,10,12,16] These proteins normally bind to either F-actin or G-actin and permit cytoskeletal structures to react once signals are received from the extracellular or intracellular environment. The actin-related proteins-2/3 (ARP2/3), whose active configuration resembles the plus end of F-actin, can accelerate actin assembly by initiating G-actin polymerisation onto a filament, bypassing the rate-limiting step of filament nucleation upon the activation of Rho-type GTPases regulated by Wiskott-Aldrich syndrome protein (WASP) binding.[10,17] Similarly, formins can also promote actin nucleation under the influence of Rho-type GTPases. Formins associate with the plus end of the filament to sequester monomers once their autoinhibited conformation is relieved by Rho-type GTPases.[10,12,16] The proteins thymosin and profilin compete in binding free actin subunits instead of filaments. Monomers which bind to thymosin are in locked status and can neither associate with filaments nor be hydrolysed, and in this way F-actin assembly is inhibited. Those monomers bound to profilin can be readily bound to the formin homology-1 (FH1) domain at the plus end of the filament as the protein occupies the binding site, facilitating the elongation of F-actin.[10,12,16] Gelsolin and capping proteins function as plus-end cappers of F-actin, terminating the elongation process and limiting the filament

length.[18] Cofilin, which binds to both actin filaments and actin subunits, is known as an actin depolymerising factor which destabilises actin filaments by twisting the filaments tightly upon binding, producing a consequent force that weakens the connection between the subunits, gradually dissociating the monomers from the minus end.[19] These proteins work jointly to control the polymerisation and depolymerisation of actin filaments and consequently the treadmilling rate.

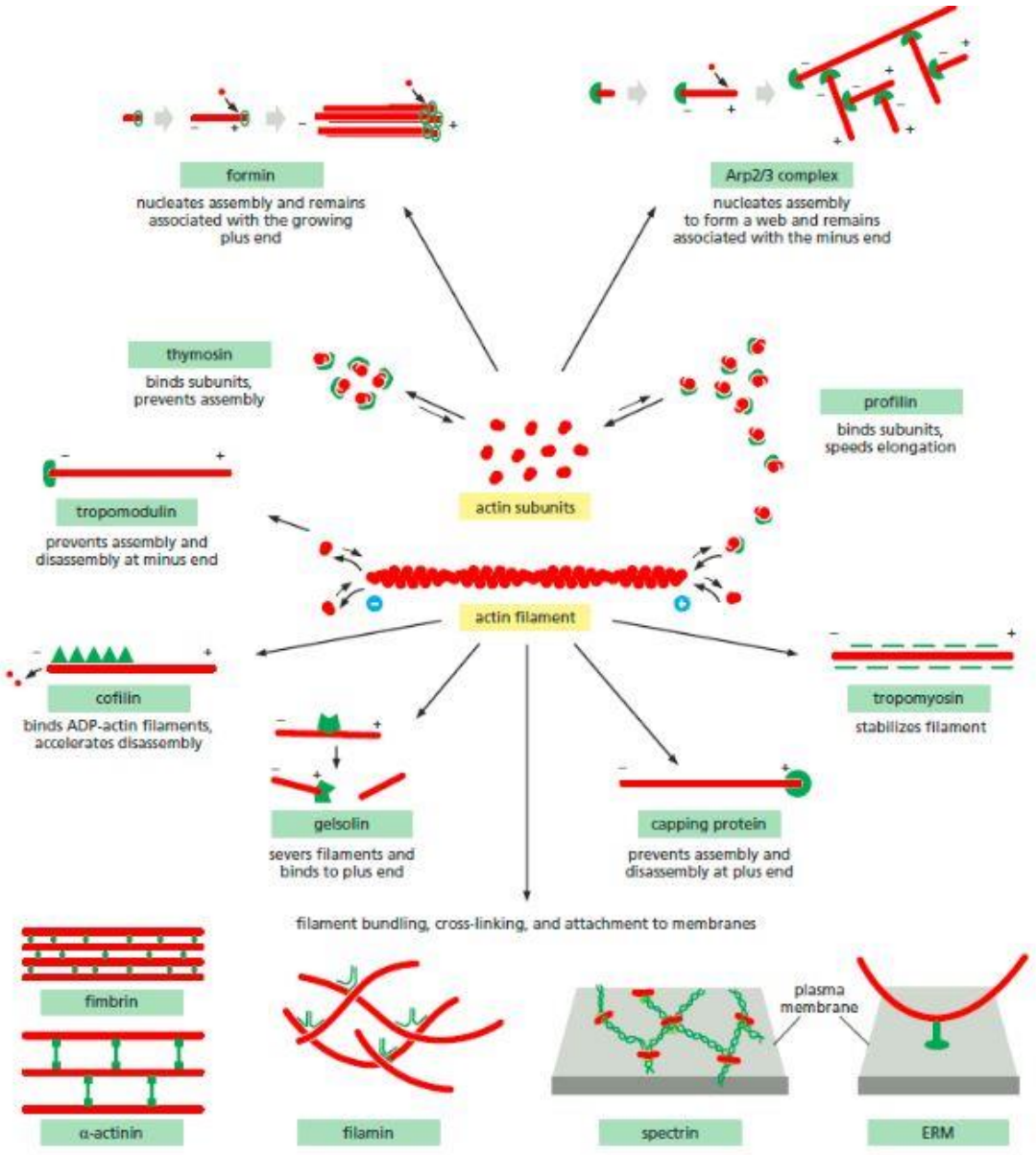

Figure 1.3. Schematic representation of accessory proteins regulating filament assembly and networking.[16]

1.1.1.2 Accessory Proteins Organised Actin Filament Networks

Actin filaments in cells exist in three forms: single filaments, meshworks (or isotropic gels) and bundles.[20] As mentioned above, bundle filaments generate forces orders of magnitude higher than those produced by a single filament.[13,14] In order to respond to mechanical stimuli, the actin cytoskeleton must form a network featuring mechanical integrity inside cells, which requires the organisation of each individual actin filament into a single interconnected structure. Filaments formed of different nucleating proteins differ in their higher-order structures: formins produce long and straight filaments and thus form bundled networks whereas the ARP2/3 complex-generated networks are weblike.[16] Accessory proteins are classified as either bundling proteins or gel-forming proteins and are known to assist in maintaining such structures. The gel-forming proteins, which typically feature comparably elevated molecular weights and elongated structures, produce more flexible filament webs.[20] A typical example is filamin, which roughly clamps filaments together forming an actin gel to extend cell-surface projection lamellipodia.[21] In contrast to gel-forming proteins, bundling proteins are often small and globular, providing stiff connections to align filaments in parallel,[20,22] with examples including fimbrin, α-actinin and fascin. Fimbrin, for instance, allows the formation of densely packed filaments featuring restricted contractility. By contrast, α-actinin forms a loosely packed network which allows the entry of myosin, a basic motor protein required for contractility, allowing the network to condense.[16] Fascin is another bundling protein that cross-links F-actin at the ends of stress fibres; it also prevents myosin entry as fimbrin does but it works alongside α-actinin to stiffen the cytoskeleton at cell protrusions against the rearward flow of actin.[1,22] Since fascin is strongly enriched in established filopodia, its role in bundling the tip of filopodia has been widely acknowledged.[12,23]

There are two common protrusions termed ‘lamellipodia’ and ‘filopodia’, the formation of which were proposed by the dendritic nucleation model and the convergent elongation model respectively.[18,23] Lamellipodia are seen as persistent protrusions over a substrate,[18] the formation of which starts with a WASP activated ARP2/3 mediated dendritic nucleation, followed by filament elongation and

importantly termination via capping proteins binding to keep filaments short and of a common length. However, filopodia which are recognised for sensory and exploratory functions are formed as a result of the reorganisation of abovementioned dendritic network with a subset of uncapped filaments.[12] During this process, Ena/vasodilator-stimulated phosphoprotein (VASP) is believed to be the key element which contributes to the anti-capping activity of the filaments, allowing continuous elongation.[12,18,23] Other models such as the de novo filament nucleation model and the working model have also been proposed for the formation of filopodia, though both suggested alternative nucleation routes other than the ARP2/3 mediated dendritic nucleation highlight the important role of Ena/VASP.[12]

1.1.2 Cell Adhesion via Integrin Mediated Focal Adhesions

Once lamellipodia and filopodia reach new areas, they must adhere to the substrate before a cell can apply any force to deform it. Integrin-mediated adhesions – termed 'focal adhesions' (FAs) frequently form at these sites. FAs are force-bearing protein complexes and serve as mechanical linkages connecting the ECM and the actin cytoskeleton via integrins. FAs not only provide resistance against the retrograde flow generated by myosin contraction but also convert such contractile forces into traction forces to deform the ECM.

1.1.2.1 Integrins

Since the cytoplasm is an enclosed region isolated from the external environment by the cell membrane, the interconnection and communication between the intracellular actin cytoskeleton and the ECM relies on a transmembrane heterodimer, the integrin. There are at least 24 types of integrins in human body all comprised of an α and a β subunit noncovalently bound to each other.[24] The intracellular portions of the subunits can adhere or detach from each other and the extracellular portions can be either folded or extended, through which process integrins can be inactivated or activated respectively. Such conformational change can be triggered via both inside-out and outside-

in pathways, allowing an integrin to transmit and convert signals bidirectionally[24] as shown in Figure 1.4. Each compatible combination of an α and a β subunit produces a different integrin, permitting it to bind specific adhesive ECM proteins include FN, COL, LN and VN, conferring each integrin a different adhesive role. For example, although both $\alpha_5\beta_1$ and $\alpha_v\beta_3$ integrins connect to FN, $\alpha_5\beta_1$ integrin determines the strength of the adhesion whereas $\alpha_v\beta_3$ integrin enables mechanotransduction.[25] A peptide sequence of three amino acids - arginine-glycine-aspartic (RGD) - has particular affinity to integrin heterodimers and has therefore been widely used for bioactive coating to promote cell adhesion to various culture substrates. The intracellular domain of an integrin does not directly bind to the actin cytoskeleton but requires a link in the form of intracellular proteins such as talin, vinculin and α-actinin, which are called integrin linker or adapter proteins. Talin, which contains 2 F-actin-binding sites and 11 vinculin-binding sites[5] is particularly important as a force bearing protein that directly binds to the β chain initiating an outside-in response and inside-out activation which triggers the assembly of FAs.[25]

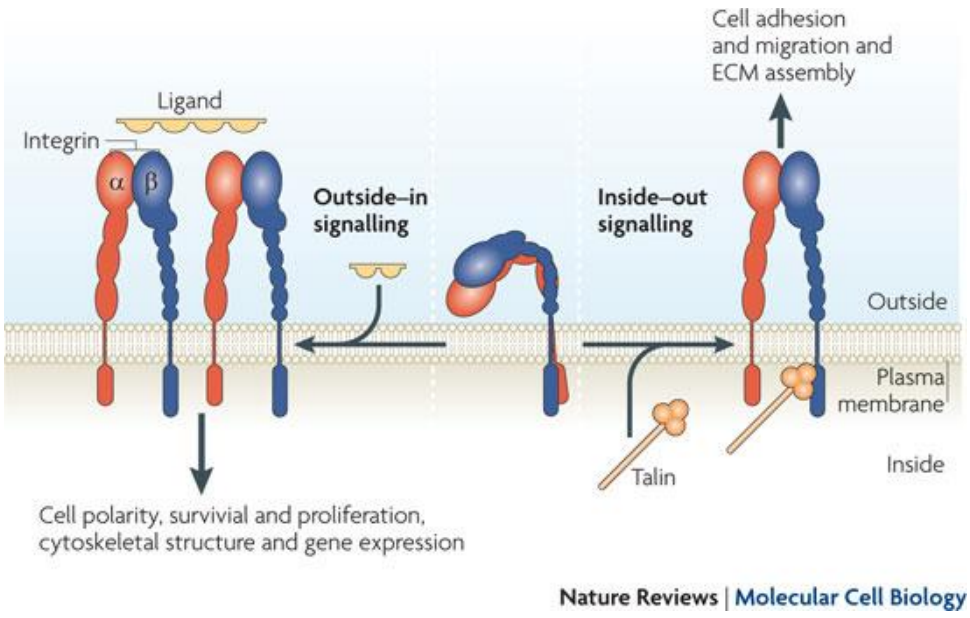

Figure 1.4. Schematic illustration of integrin activation via outside-in and inside-out pathways.[26] (Reprinted with permission from [Springer Nature Customer Service Centre GmbH]: [Springer Nature] [Nature Reviews Molecular Cell Biology] [Shattil, S. J., Kim, C. & Ginsberg, M. H. The final steps of integrin activation: the end game. [COPYRIGHT] (2010)

1.1.2.2 The formation of focal adhesions

The formation of FAs is initiated when an integrin binds to the ECM proteins at the protruding edge of the cell, forming integrin clusters or nascent adhesion. Such initial clusters serve as a platform for the tethering and polymerisation of F-actin.[27,28] By applying mechanical tensions to stretch FN, the cryptic sites on talin are exposed, initiating the sequential recruitment of adapter proteins, including vinculin, VASP, zyxin, and signalling proteins such as paxillin and focal adhesion kinase (FAK) to reinforce the adhesion.[1,29,30] During this process, the originally small and short-lived nascent adhesions forming at the leading edge of the lamellipodia gradually evolve into small (0.5-1 µm in diameter) transient 'dot-

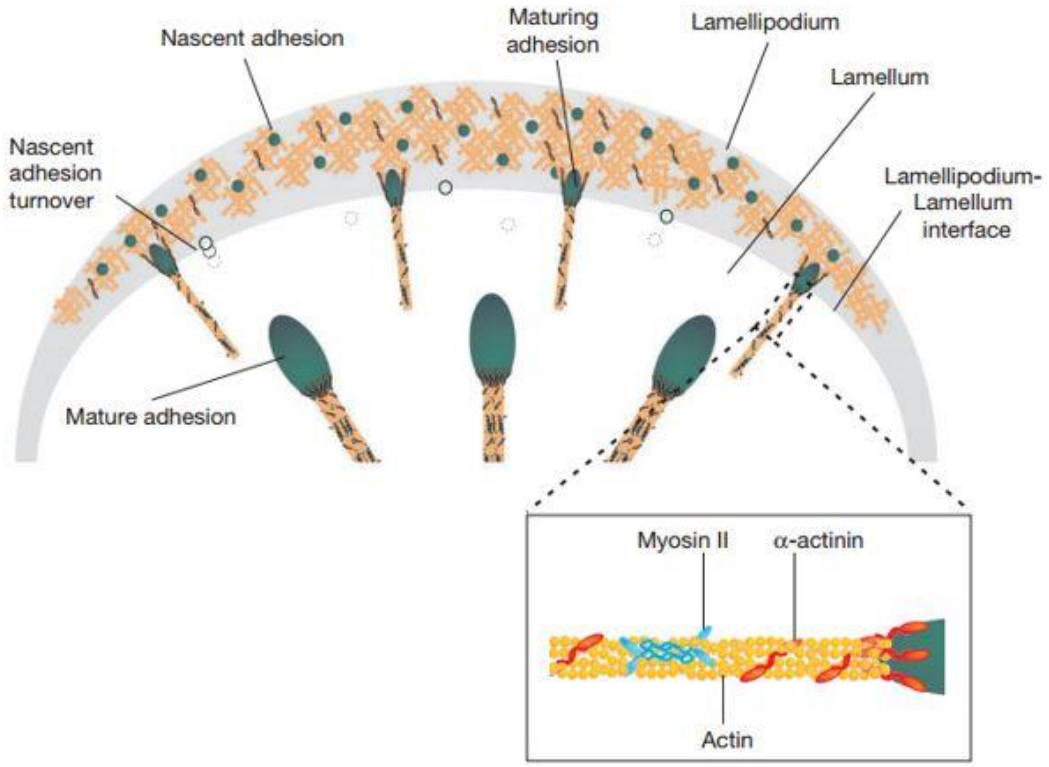

Figure 1.5. Schematic illustration of focal adhesion assembly, turnover and maturation.[330]Reprinted with permission from [Springer Nature Customer Service Centre GmbH]: [Springer Nature] [Nature Cell Biology] [Choi, C. K. et al. Actin and alpha-actinin orchestrate the assembly and maturation of nascent adhesions in a myosin II motor-independent manner. [COPYRIGHT] (2008)

like' contacts (focal complexes) and then mature into FAs (3-10 µm long and 2 µm wide) at the ends of stress fibres or actin bundles (Figure 1.5). FAs provide a more stable adhesion when associated with actin molecules such as myosin,[1,30,31] whilst the formation, maturation and disassembly of FAs are

continuous and dynamic processes regulated by the balancing of actin polymerisation and actomyosin contraction.[30]

Myosin is a motor protein that participates in various cellular activities, including organelle transport, mitosis, and cell locomotion.[32] Based on the differences of their C-terminal tails and N-terminal extensions, myosin has been classified into different classes, of which myosin II is particularly important for actin bundling and contractility.[33] Under a minor load, myosin shows a significant increase in its affinity to actin. By interacting with actin filaments and sliding them in opposite directions, myosin II generates the contractile forces to deform the substrate and allows the deformation of the cell membrane.[1] Myosin II can also work as a mechanosensor, as the exposure of talin's cryptic sites is regulated by forces generated by the contraction of myosin II[34] and cells no longer respond to external forces once it has been inhibited by blebbistatin.[35] It has also been reported that the maturation of a nascent adhesions and the speed of protrusion formation are dependent on the activity level of myosin II, suggesting that myosin II based contractility is related to adhesion formation, although this mechanism is not yet fully understood.[1,33]

1.1.3 Cell Measures and Responds to Mechanics via Signalling Processes

Cells can sense the underlying stiffness of a substrate if the counteracting forces they exert to deform the substrate are measured. Since many proteins can extend due to force resulting in altered conformations, functionalities or the kinetics of assembly and disassembly,[2] they can act as mechanical sensors that convert mechanical signals into biochemical signals. FAs act as signalling hubs that gather vast numbers of closely packed signalling proteins, and whose assembly and maturation are regulated by forces,[36,37] FAs are naturally regarded as mechanotransduction associated structures. Figure 1.6 illustrates the proposed structure of an FA, including a first 'integrin signalling layer' comprising FAK and paxillin; a 'force transduction layer' comprising talin and vinculin and a final 'actin-

regulatory layer' including zyxin, VASP and α-actinin. Such well-defined architecture reveals how forces are transmitted from the ECM, through the cell membrane, up to the actin cytoskeleton.[1]

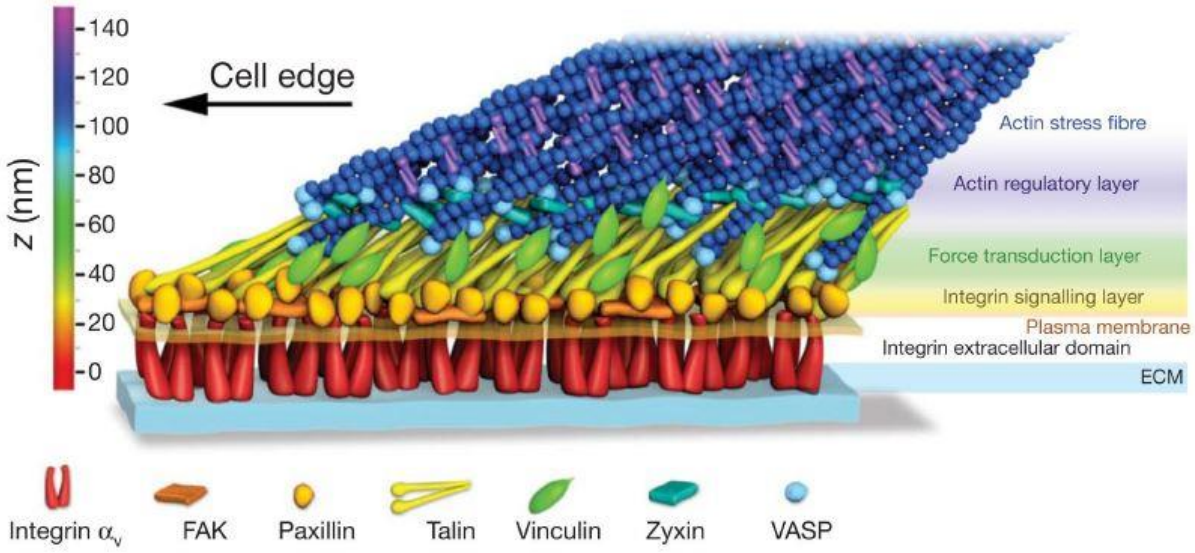

Figure 1.6. Schematic illustration of the focal adhesion nanoscale structure.[331] Reprinted with permission from [Springer Nature Customer Service Centre GmbH]: [Springer Nature] [Nature] [Kanchanawong, P. et al. Nanoscale architecture of integrin-based cell adhesions. [COPYRIGHT] (2010)

As mentioned in previous sections, some proteins such as talin and vinculin have binding sites hidden in the interior of bundles that are composed of several helices making them difficult to access. Such cryptic sites can be uncovered once tension is applied to unfold the protein, thus triggering the downstream binding processes which consequently translate the forces into biochemical information.[29,34] In addition to the exposure of cryptic sites, force-dependent phosphorylation is another common process in translating mechanical signals. A typical example is the adaptor protein p130Cas which connects actin and integrin. After being phosphorylated by Src family kinases, p130Cas binds to several guanine-nucleotide exchange factors (GEFs) activating a series of downstream signalling pathways. This phosphorylation process can be facilitated by mechanical stretching.[38] A concept called molecular clutch was proposed to describe these dynamic processes. This refers to the linkage between the integrin-bound ECM and the actin cytoskeleton and a more engaged clutch will more effectively transmit the described mechanical forces.[39] When myosin contractility is countered by a FA coupled to the ECM on a substrate with high elastic resistance, the retrograde flow of actin is

restricted, hence there is an increase in the force loading onto the FA, triggering subsequent downstream signalling including talin unfolding and vinculin recruiting or filament binding, which enables mechanosensation.[39–41] In the case of softer substrates where the actin retrograde flow is not restricted, talin does not unfold and the downstream signalling process ceases.

However research into this conformational change-based sensing system seems to be incomplete as the frequency of applied cyclic stretch or compression can have major impacts as well, which cannot be simply explained by this conformational change-based sensing system.[21] For example, whilst exposed to the same magnitude of stretch, gene expression in endothelial cells varies between steady stretch and cyclic stretch[42] and their alignment also changes when the frequency of the cyclic stretch is altered.[43] In fact, such mechanosensing processes are also dependent on the total duration rather than solely depending on the strength of the force. For example, a force of 50 pN induces in talin a conformational change within 25 ms, although 200 ms is required if only 20 pN of force is applied.[44] This might be explained by the slip and catch bonds that commonly bind to actin and α-actinin, and FN and integrin respectively. The existence of slip bonds whose lifetime can be shortened by forces terminates the force transmission after a short time, resulting the lack of sensing of high frequency forces. By contrast, more sensitive sensing can be achieved by catch bonds whose lifetime can be expanded under tension.[21] In fact, in order to properly differentiate different level of forces, at least two mechanosensory mechanisms with different properties are required. For example, in the case of FN-integrin-talin binding, FN-integrin binding is a catch bond while talin unfolding is a slip bond, so talin unfolding is only triggered when the applied force is above the threshold at which integrin binding (catch bond) sustains longer than talin unfolding (slip bond).[39]

Since the activation of an integrin is bidirectional, the signalling process between the actin cytoskeleton and the ECM is bidirectional as well, and thus a cell can not only sense the extracellular mechanical cues but also actively respond to them. Cells often generate mechanotransductory feedback loops by regulating cytoskeletal and adhesion structures.[21] For instance, mechanical stimuli

activate the myocardin-related transcription factor pathway, which then upregulates the genes encoding vinculin, filamin, actin etc., facilitating the generation of force-transmission pathways. Moreover, cells align either parallel or perpendicular to applied forces in a frequency-dependent manner under cyclic stretch. When the force application rate is faster than the remodelling rate of load-bearing subcellular structures, there is an induction of perpendicular alignment as cells are able to minimise stretching on these elements, whereas a higher remodelling rate enables cells to remodel themselves without risk, thus inducing alignment parallel to the stress direction.[21] Using similar feedback loops, cells are also able to actively remodel the substrate which they inhabit. For example, FN, an important ECM protein for cell attachment, also has cryptic sites in its structure. Once bound by integrins, the forces that are generated by actin-mediated contractility trigger its self-association process thus forming FN fibrils, stiffening the substrate.[45,46] Similarly, a given cell is also able to remodel COL fibres via integrin mediated actomyosin machinery to maintain and establish its mechanical state. However, an increase in stress may result in continuous ECM stiffening which ultimately leads to fibrosis.[2]

Through such complicated mechanosensory and menchanotransduction processes, cells are able to regulate their fate in response to mechanical stimuli. For example, osteogenic differentiation is upregulated when mesenchymal stem cells (MSCs) adhere to stiff substrates while adipogenic differentiation is preferential on soft substrates.[7] It has also been reported that cells on more compliant substrates with suppressed FAK signalling are more likely to undergo apoptosis.[2] However, beyond sensation of bulk mechanical properties, an increasing number of reports propose that other nanoscale physical cues may dominate in regulation of cellular phenotypes.[47] It was reported that the typical behavioural response of stem cells to the stiffness of silicone-based materials was not observed, in contrast to observations typically made with acrylamide hydrogels with a range of moduli from 0.1 kPa to 2 MPa. This was attributed to the differences in COL fibril anchoring densities modulating the activation of the extracellular-signal-related kinase (ERK)/mitogen-activated protein kinase (MAPK) signalling pathway.[48] Similarly, del Rio et al. studied the spread of human foreskin

derived primary fibroblasts cultured on surfaces coated with the RGD amino acid repeat sequence with varied tether length, proposing the possibility of modulating cellular behaviour by simply altering nanoscale tether length, as cell adhesion to RGD chains with longer tether length permits its integrin unhindered movement, leaving the force transducer inactivated, thus triggering fibroblast behaviour typically found on soft substrates (Figure 1.7).[49] In this study, they identified the critical tether length of fibroblasts falling between 40 and 200 nm, below which the substrate is analogous to a stiff material, while triggering a cellular response similar to that caused by a soft substrate if longer. Moreover, MSCs on soft nanofiborous mats and hydrogels also display a phenotype that is typically found on stiff substrates, for instance wider spreading and osteoblast differentiation were observed on the mats with high stress relaxation[50] and hydrogels with more viscoelastic substrates,[51] respectively. All these findings suggest to us the possibility of culturing cells on softer materials regardless of the bulk mechanical properties of the substrates.

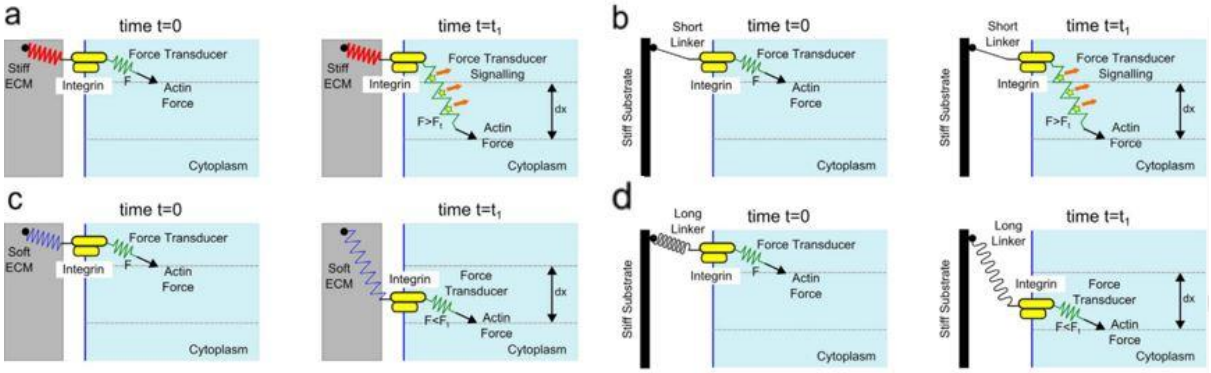

Figure 1.7. Proposed model to explain both rigidity and tether length sensing. (a) The integrin is fixed with limited motility on a stiff ECM, whilst the actin pulls the force transducer forward. Once greater than the trigger force (when time $t=t_1$), the cryptic binding sites are exposed, initiating the subsequent signalling pathway. (b) Cells on RGD with short tether experience a similar process, thus the short linker is analogous to a stiff substrate. (c) Integrins on soft ECM is not hindered and can move freely as actin moves forwards. The force transducer is subjected to a force lower than the trigger force, therefore the following signalling is not triggered. (d) Cells on a long tether undergo the same process, thus the long linker is analogous to a soft substrate.[49]

1.2 Modulating Interfacial Physicochemical Properties to Regulate Cell Culture

The culture of adherent cells is typically thought to require cell spreading on rigid substrates to allow the formation of stable focal adhesions and to enable actomyosin contractility.[52] In this way, cells establish mechanotransduction networks to convert extracellular mechanical signals into intracellular biochemical cues, generating appropriate cell adaptative responses. However, recent studies addressed the impact of nanoscale other than bulk mechanical properties in cell behaviour, making interfacial physicochemical properties modulation particular interested in regulating cell behaviours. Polyelectrolyte multilayers (PEMs) coating has emerged as a promising novel strategy to allow the modulation of the interfacial physicochemical properties of the substrate. Moreover, PEMs present additional advantages in terms of ease handling and cost-effectiveness, making them suitable for routine cell culture applications. PEMs are a new class of polymeric nanomaterials typically displaying thickness-dependent interfacial and mechanical properties such as noncovalent adhesiveness, tuneable flexibility and molecular permeability.[53] Although they have been used in various fields such as electrochemical devices, chemical and nano-mechanical sensors, their quasi-two-dimensional features are attractive for synthetically mimicking of the ECM which functions to promote cellular organisation *in vitro*.[54] In the field of biomedicine, PEMs have been widely used for wound dressing, tissue engineering and health-care monitoring.[55] Many technologies have been used for the fabrication of such multilayers, including spin-coating,[56] Langmuir-Blodgett method,[57] Layer-by-Layer (LbL) assembly[58,59] and sol-gel,[60] etc. Apart from solid substrates, recent studies have also successfully assembled protein PEMs at liquid-liquid interfaces, which have then been harvested via Langmuir-Blodgett method,[61–63] and subsequently used for cell culture. Understanding the mechanism through which polyelectrolytes (PELs) assemble and adsorb at interfaces is crucial to design proper PEMs for biomedical application.

1.2.1 Self-Assembled PEMs at Interfaces

1.2.1.1 Mechanism of PEL Self-Assembly at Interfaces

For cell culture purposes, ECM molecules including structural proteins and polysaccharides are commonly used for the build-up of PEMs. The adsorption of these molecules at the surface of substrates is a multistep process involving molecule diffusion, adsorption and conformational changes.[64–71] It starts with molecules transferring from the bulk phase to the surface, induced by diffusion or external forces such as gravitation. These molecules then adsorb to the surface or pre-adsorbed layer under the influence of electrostatic and van der Waals forces. Subsequently, these molecules, especially proteins, undergo a conformational change, immobilising at the surface as a result of interactions led by hydrogen bonding and surface roughness, etc.[71] Depending on the selection of the PELs, PEL concentration, solution temperature, pH and ion strength, the resulting PEMs can be very different. The modification of such parameters can be used to control the process to obtain a particular PEM with defined physicochemical properties.

Since the charge and conformation of weak PELs are easily affected by the pH values during the assembly, the pH adjustment has often been used to better control the nanosheet structure and formation. For example, poly-L-lysine (PLL) undergoes a conformation transition from random coil to α-helices and β-sheets at high pH.[68,72–74] It has been widely accepted that PELs exhibit greater adsorption at or near the isoelectric pH as a result of minimised electrostatic repulsion between molecules.[75] Since pH controls the linear charge density of the adsorbing and adsorbed PELs, the thickness of the nanosheets can be tailored by the pH as well, indeed the thickness tends to increase when the pH is close to its pKa value during adsorption.[76] In Shiratori and Rubner's study, the thickness of poly(acrylic acid) (PAA) and poly(allylamine hydrochoride) (PAH) paired PEMs' thickness can be adjusted to a range between less than 1 nm to more than 12 nm under different pH.[76] In light of the pH-dependant nature of PEMs, their thickness would inevitably affect the mechanical properties of the PEMs. With the same PEL pairs, Thompson and colleagues obtained PEMs adsorbed surfaces with stiffness ranging from 200 kPa to 142 MPa.[77] Similar to pH, the ion strength of the solution affects the

ionisation of the weak PELs and consequently the PEM thickness and mechanical properties.[78] Chitosan (CHI) is a weak polycation commonly used for the study of the impact of ionic strength on PEL assembly. The thickness of CHI-containing films is increased as a consequence of a higher ionic strength, while a loss of pH sensitivity and improper PEM formation were also observed at very high ionic strengths.[79,80] The authors of these studies attributed these effects to the decreased charge density of CHI under high ionic strength.

In addition to changing the properties of PEL solutions during assembly, modifying the surface of substrates that PELs adsorbed to can greatly impact the PEMs formation as well. As shown in Figure 1.8, the adsorption of PELs can be influenced by the chemistry, topography, roughness and wettability of the surface.[75] Self-assembled monolayers (SAMs) are commonly used to investigate the kinetics and amount of PEL adsorption on surfaces with different chemistries.[80] When PELs are deposited to $–CH_3$, $–NH_2$, –COOH or –OH terminated SAMs, it is not unexpected to find that the largest adsorbed mass was achieved on the surface with ionised groups of the opposite charge to the PEL. For example, $–NH_3^+$ and $–COO^-$ attract the highest amount of polyanions and polycations, respectively.[81,82] Apart from electrostatic surfaces, the PELs can also adsorb to non-electrostatic surfaces and even to electrostatically repulsed surfaces. Such process is driven by non-electrostatic short-range forces such as hydrogen bonding, van der Waals forces and hydrophobic forces, among which hydrophobic force is the most pronounced as mass PEL adsorption was found on $–CH_3$ terminated SAMs.[81,82] The hydrophobic force induced conformational change is an important step for the adsorption of those PELs with complex structures like proteins. During this process, PEL tends to unfold irreversibly at the hydrophobic interface, exposing its non-polar domain that is normally hiddenin its natural state. This can also lead to intermolecular interactions at high PEL density, resulting in different interfacial mechanical properties, especially at liquid-liquid interfaces. By using different oil subphases, Bergfreund and colleagues obtained liquid interfaces with different hydrophobicity and found that more hydrophobic interfaces led to faster and more oriented adsorption of β-lactoglobulin, resulting in a more viscoelastic protein network at the interface. Interestingly, they also found that polar

interfaces decelerated protein unfolding and consequently form softer nanosheets, which were resulted from the strong integration of the polar group in the oil and the hydrophilic surface of β-lactoglobulin.[83] Studies also revealed that protein conformation can also be altered by surface topography including surface curvature, nanopattern and roughness.[75,84,85] However, owing to the different characteristics of each individual protein, the impact of surface topography can be very different. Taking a globular protein bovine serum albumin (BSA) and a rod-shaped fibrinogen as an example, the increase of surface roughness (root-mean-square roughness from 2.0 to 32.9 nm) seems to induced a massive increase of fibrinogen adsorption but had little effect on BSA adsorption;[85] while the surface curvature with radii less than 30 nm resulted in a greater secondary structure loss of fibrinogen but maintained the native conformation of BSA.[84]

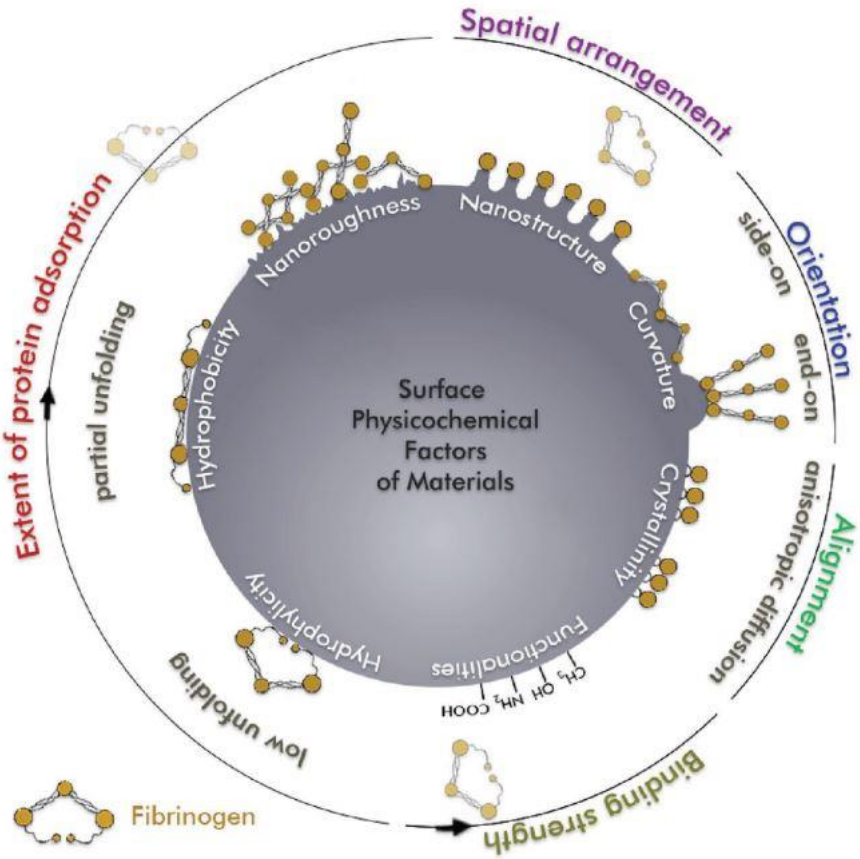

Figure 1.8. Schematic illustration of materials surface properties affecting fibrinogen adsorption.[75] Reproduced with permission. Copyright 2017 WILEY-VCH Verlag GmbH & Co. KGaA, Weinheim.

1.2.1.2 PELs Coupling at Liquid-Liquid Interface

Peptides and proteins containing less amphiphilic amino acids such as and arginine[67] are less likely to undergo conformational changes when adsorbed to substrates. In such cases, the interface between hydrophilic and hydrophobic liquids can be used to combine hydrophilic PELs with hydrophobic reaction partners, performing reactions that are impossible in homogenous solutions, thus supporting the formation of PEMs at liquid interfaces.[86] Interfacial reactions have been widely used in the field of polymer chemistry, for example, Nylon polymers, which also have repeating units linked by amide bonds like peptides and proteins, were firstly synthesised via interfacial polycondensation.[86] Since then, a large variety of diamines and diacid chlorides with different structures such as aliphatic, alicyclic, or aromatic, short- or long- chains were investigated for the synthesis of polyamides via interfacial polycondensation at interfaces between water and different oils.[87,88] These works inspired the introduction of oil soluble acid chlorides to form amines with peptides and proteins from aqueous solutions and effectively pin those less hydrophobic domains at the interfaces, inducing subsequent conformational changes. However, as the acid chloride is rather vulnerable to hydrolysis, the competition between the hydrolysis and the amidation is an important factor to take into account during the whole process.[86] We investigated the impact of such acid chloride on BSA nanosheet assembly at interface between fluorinated oil and PBS.[47,52] Additionally, we used the acid chloride for the generation stiff and stable nanosheets of less hydrophobic polypeptides, PLL.[89]

In addition to assisting PEL adsorption, these low molecular weight reagents can also induce PEL reorganisation at the interface. During such process, surfactant molecules compete with proteins for the interfacial area at high concentrations by penetrating into the defects between proteins at the interface, disrupting the protein network and weakening the interaction between proteins. In the case of non-ionic surfactants, the surfactant forms a surfactant-rich domain displaying greater surface pressure than the protein-rich domain, displacing proteins further from the interface. Whereas in the case of ionic surfactants, the surfactant compensates the protein charges until a net zero charge is reached, after which the surfactant continuously couple to the protein via hydrophobic forces,

forming a surfactant-protein complex at the interface, making the protein more hydrophilic and subsequently disassembling it from the interface.[90–93] However, protein nanosheets with higher interfacial shear viscosities resulted from higher levels of protein denaturation and interaction between proteins are more sustainable to such surfactant-led displacement.[92] On the other hand, surfactants can also function as a template inducing the crystallisation of PELs at liquid interfaces. Surfactant molecules organise or crystallise at the interface, coupling to PELs chain via either hydrogen bonding or ionic bonding, giving rise to its supramolecular assembly.[94,95]

1.2.2 Layer-by-Layer Assembled PEMs Modulate Cell Culture

The LbL method (Figure 1.9) involves the repetitive and alternative deposition of oppositely charged PELs driven mainly by electrostatically interactions.[54,58,59] The LbL method is particularly indicated for the assembly of biomedical PEMs as it allows a variety of biochemical PELs such as ECM proteins and polysaccharides to be integrated into the structure, and the properties such as thickness, roughness and surface chemistry can be precisely controlled.[96] Via this process, those biochemical molecules are assembled on either solid or liquid substrates, which are then for cell culture, tissue engineering and drug delivery among other biomedical applications.

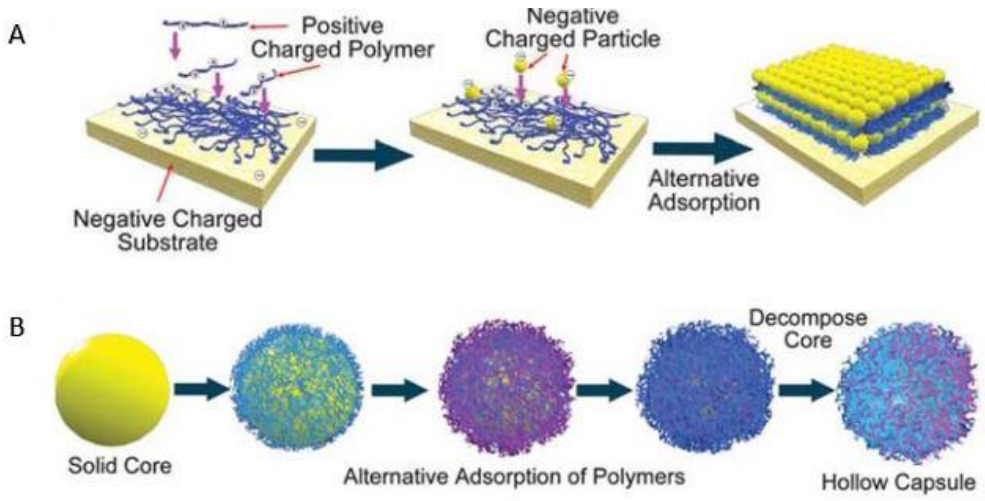

Figure 1.9. Schematic illustration of LbL assembly. (A) flat film mode and (B) colloidal mode.[97]

1.2.2.1 PEL Pairings for Cell Culture

LbL assembly is typically led by a reversal of interfacial charge to allow the adjacent oppositely charged PELs to adsorb.[98] Parameters that influence the assembly of nanosheets include the selection of PEL pairs, the ionic strength and pH of the polyelectrolyte solution. For example, pairs that prefer assembly by intrinsic compensation are more likely to form thinner, less permeable films;[99,100] high salt concentration is favoured to coil PELs and thus produce thicker layer; pH can affect the conformation and charge of the PELs assembled thus leading to the reorganization of the PEMs.[101,102] To assemble PEMs with controlled physicochemical properties and structure, these factors must be taken into consideration.

As mentioned in the previous section, ECM is a network of proteins and polysaccharides providing the necessary mechanical and chemical stimuli for cell adhesion, which eventually regulates cell behaviour. Therefore, ECM components such as FN, COL, hyaluronic acid (HA), chondroitin sulfate (CHS), gelatine and heparin (HEP) are necessary when preparing nanosheets for cell culture applications. Although these natural PELs are advantageous in mimicking cellular microenvironment and offering excellent bioactivity, the batch-to-batch variation and limited pH and ionic strength work range are issues for wider applications.[78] In addition to these natural PELs, some synthetic polymers with more choice of chemistries and structures are also used, those commonly applied in biomedical application include positively charged PLL, poly(ethylene imine) (PEI) and negatively charged polystyrene sulfonate (PSS) because of their biocompatibility and capacity of conjugating with bioactive molecules.[103,104] Due to the large varierty of biocompatible PELs available, different PEL pairings result in very different assembly mechanisms and material properties.

HA is the only non-sulfated glycosaminoglycan in ECM, it has shear dependent viscoelasticity, which makes it perfect for lubrication. It is known to bind CD44 receptor in chondrocytes,[103] acting both as a structural element as well as a signalling molecule in the ECM.[105] Paired with PLL, they form a PEM frequently used to promote cell adhesion. By conducting atomic force microscopy (AFM) tests, optical

waveguide lightmode spectroscopy (OWLS) and dissipation enhanced quartz crystal microbalance (QCM-D), C. Picart et. al.[103] monitored the absorption process and revealed that the assembly of HA/PLL nanosheets occurs in a two-step manner, where the polyelectrolytes form isolated but homogeneous islands at the initial stage, and once the continuous film is formed, an exponential increase of the film growth is observed. This was explained as a result of the PLL chains within the interior of films during the PLL treatment being able to diffuse out and further enable contact with the HA solution during the HA treatment. In a study showing PLL coupling with structurally similar but different in charge density PELs, namely, HEP, CHS and HA, the exponential growth was found on less charged PELs (CHS, HA), suggesting that such growth mode is charge density dependant.[78] Such exponential growth has also been reported for COL/HA paired nanosheets, and explained by the same mechanism.[59] In the case of PLL/FN pairing, FN experiences a conformation change during its assembly on PLL, with an increase of ß-strands and a decrease of random domains and ß-turn. Together with the observation of larger, globular island-like structure via scanning electron microscopy (SEM), these results suggested an enhanced FN-FN interaction and possibly FN fibrillogenesis in PLL/FN pairing.[98]

Apart from coupling with cell adhesion proteins such as FN, VN, COL and LN, synthetic PELs may also be presented as the final layer of the nanosheets for cell adhesion. The positively charged final layer seemly attracts negatively charged cell membranes. However, in many cases, the majority of cells prefer negatively charged PELs as it helps maintaining Na^+ that keeps cell hydrated and promotes the retention of negatively charged growth factors from serum and medium. For instance, hepatocytes and smooth muscle cells (SMCs) were found attached to nanosheets ending with negatively charged PSS but not to the positive poly(diallyldimethylammonium) chloride (PDAC) terminated in a PSS/PDAC pair.[106,107] Similarly, in the case of PSS/PAH pair, PSS-terminal layer promoted proliferation and differentiation of C2C12 skeletal muscle cells.[108] Moreover, with positively charged CHI as the outmost layer, different polyanion sublayers can also cause very different cell behaviours. Although MSCs displayed similar adhesion and spreading properties on GEL/CHI, HEP/CHI and HA/CHI PEMs, differences in MSC osteogenesis on these PEMs were observed when culturing in differentiation

medium as osteogenesis was promoted on HEP/CHI and HA/CHI PEMs but inhibited on GEL/CHI PEM.[109] This result was explained by the low adhesive of HEP and HA that allowed MSCs to migrate and aggregate into an osteogenesis-favoured 3D-environment.

1.2.2.2 Multilayers Stiffening

In the case of HA/PLL nanosheets, it has been reported that sometimes such PEMs do not necessarily support cell adhesion and proliferation,[96,110–113] even when using pre-adsorbed adhesive proteins such as FN.[112] The stiffness of the native HA/PLL nanosheets was pointed as the cause of such observation at it was found to be too low to support cell adhesion and proliferation.[96] Similar findings have also been reported for other polysaccharides assembled PEMs such as COL/HA.[59] Several approaches have been developed to increase the stiffness of multilayers, among which chemical cross-linking is the most frequently used. Cross-linked via the formation of amide induced by a water soluble carbodiimide (EDC) in combination with a N-hydroxysulfo-succinimide (NHS), the once viscoelastic HA-containing films become rigid and highly resistant to hyaluronidase.[111] By changing the concentration of EDC, up to two orders of magnitude (from 3 to 400 kPa) increase in the Young's modulus was observed.[113] Chondrosarcoma cells,[111,113] C2C12 myoblast[110] and MSCs[112] successfully adhere and proliferate on such stiffened surfaces. Photo cross-linking is another alternative to modify the PEM mechanical properties after assembly. Such strategies require photoreactive groups such as p-diazonium diphenyl amine polymer (PA)[114] and vinylbenzyl (VB)[115] to be inserted or grafted to one of the PEL building blocks. The increase of the photoreactive groups lead to more intense cross-linking and therefore more rigid multilayers. Even though, in the case of PLL/HA-VB, the maximum stiffness reached after being cross-linked by UV-irradiation remains significantly lower than chemically cross-linked due to limited linkages only provided within HA by photo-cross-linking other than between HA and PLL by chemical cross-linking.[78]

Although cross-linking has significantly increased the stiffness of the PEMs, it also reduces the motility of the polymer, prevents the film from incorporating bioactive agents and inhibits the biodegradation

of the film.[96] Another option to stiffen nanosheets is the combination with synthetic materials which are normally more charged and more flexible than their natural counterparts.[78] For example, PSS/PAH nanosheet has a Young's modulus of up to 100 MPa.[116] Upon depositing onto PLL/HA nanosheets, PSS can penetrate into the multilayers and greatly enhance the elasticity and viscoelasticity.[117,118] Progressively increasing PSS/PAH pairs in the system gradually stiffened the PLL/HA multilayers and enhanced the adhesion of kidney epithelial cells.[118] Similarly, the deposition of PAA on CHI/HA multilayers can destroy the soft diffuse matrix of HA by intercalating in the multilayer, making the exponential growth of the multilayers become linear, significantly increasing the mechanical strength.[119] Incorporating nanoparticles into the PEMs is another effective way for nanosheet stiffening, commonly used examples include gold nanoparticles (AuNPs), montmorillonite and carbon nanotubes, which can increase the Young's modulus as much as two orders of magnitude compared to substrates purely stiffened with PELs.[120] By depositing negatively charged AuNPs on the HA/PLL surface, Dmitry V. Volodkin's group[96] was also able to stiffen the nanosheet more than an order of magnitude (from 80 kPa to 1000 kPa, Figure 1.10). This is due to AuNPs clustering on the surface, exceeding the threshold of AuNPs percolation at the interfaces. In such situation the nanoparticles act as cross-linkers, stiffening and roughening the interface and promoting fibroblast adhesion but without affecting the motility of the polymers.

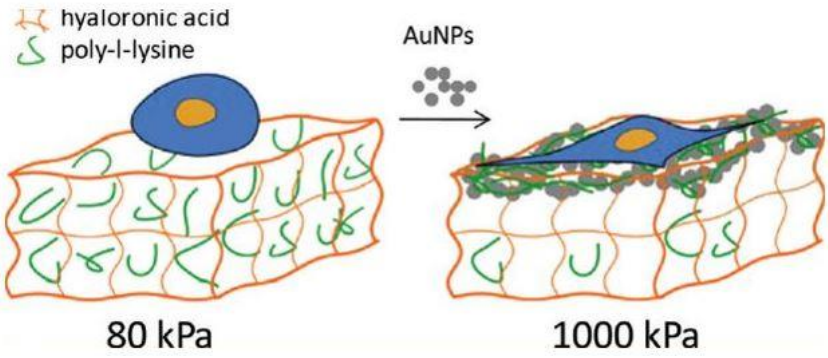

Figure 1.10 General scheme of adding AuNPs on HA/PLL film resulting in cellular adhesion.[96] Reprinted with permission. Copyright (2012) American Chemical Society.

In addition to nanoparticles, there has been an increasing number of works focused on graphene oxide (GO) because of the ability of this nanomaterial to influence cellular behaviour, such as adhesion and differentiation.[121] Graphene and its derivatives, which are two-dimensional monolayer of sp2-bonded carbon atoms with fascinating mechanical properties, have broadened their applications to the biomedical field. Compared with graphene, GO induces higher protein absorption and is less likely to denature native proteins,[121] thus it favours cell proliferation. With PLL/FN absorbed on the GO nanosheets, Yilei Zhang's group found that such films are an excellent cell culture substrate for MSCs as a result of the increased stiffness and high surface roughness provided by GO.[122] Similar findings were also reported by Wei Q et.al.[123] who found that the elastic modulus of nanomaterials could be increased by 1.81 fold if a layer of GO is deposited in 10 PSS and PAH paired bilayers, and such increase in elastic properties was found to promote the adhesion and proliferation of NIH-3T3 fibroblasts, which displayed increased spreading areas and better organised adhesions on the GO-based PEMs.

Instead of stiffening nanosheets via the introduction of covalent or non-covalent molecular assembly, fibrilisation of COL can stiffen the substrate as well. As the most abundant protein in tissues, COL has a triple helix structure which provides mechanical support in the ECM.[2,15] The diversity of polypeptide chains allows the triple helix structure to be built from different building blocks thus producing different types of COL. Among these, type I COL, classified as fibrillar collagen, can assemble into higher-order polymer networks known as COL fibrils and subsequently aggregate into COL fibers. Type I COL is the most abundant COL in human body and the key structural component for load-bearing tissues such as bone and tendons.[124] It has been reported that the concentration of COL is crucial for cell spreading. For example, fibroblast spreading is proportional to the COL density at the beginning, the relationship is however reversed beyond a certain concentration.[125] Paired with HA and incubated in PBS at 37 ℃ for 12 h, type I COL forms several large fibrillar structures.[59] During this process, 56% of the HA has been found dissociated from the multilayers just two hours after incubation, leaving COL molecules without polyanions to act as binders, an important parameter proposed to closely regulate the thermodynamic self-assembly of COL molecules into the long fibrils assembled.[59] In

comparison with non-fibril COL/HA multilayers, the elastic modulus of the fibril multilayer is three-fold greater. It is also associated with more elongated fibroblasts, observed on fibrous multilayers compared to the non-fibrous counterparts. Such cell adhesive properties can be easily tuned by changing the content of HA and COL fibrils.[59]

1.3 Generation and Stability of Emulsion

The physicochemical properties of interface clearly play an important role in regulating cell behaviour at interfaces. Although most of the studies reviewed above were made on solid-based interfaces, some encouraging progress has been made recently in the field to develop more adaptive interfaces for cell culture purposes, such as liquid-liquid interfaces.[47,52,61,62,89,126–129] However, due to the fluidity of liquids, the modulation and characterisation of the physicochemical properties of the PELs assembled multilayers at the liquid interfaces are not as straightforward as the characterisation of solid interfaces. Emulsions are often employed to characterise such liquid-liquid interfaces, and the stability of the emulsion is often regarded as a reflection of the interfacial properties. In this section, factors that affect the generation and stability of emulsions are reviewed.

1.3.1 Generation of Emulsions

An emulsion is a mixture of two immiscible liquids with one of them dispersed in the other, depending on which liquid is the continuous phase, emulsions are classified into either oil-in-water (O/W) or water-in-oil (W/O) emulsions. The process of generating emulsion is termed emulsification, involving the introduction of shearing energy into the system to overcome the interfacial tension that keep the liquids phase separated at the thermodynamically most stable state. The thermodynamic properties of emulsions are described by a Gibbs free energy equation derivation (Equation 1), where ΔG represents the free energy of emulsification, γ is the interfacial tension, A is the interfacial area, T is temperature and ΔS is entropy of mixing.

$$\Delta G = \gamma A - T\Delta S \quad \textbf{Equation 1}$$

Spontaneous formation only occurs when the value of *ΔG* is negative, given the fact that the value of the configurational entropy ($T\Delta S$) is much smaller than the value of the interfacial free energy (γA) in most of the emulsions, spontaneous formation is almost impossible. To aid in the formation of emulsions, surface reactive agents are introduced to lower the interfacial tension. Applying agitation, such as vigorous and high shear mixing, to introduce shearing energy as well as increase entropy are commonly applied processes for the formation of emulsions. The closer the value is from positive to zero, the easier the emulsification will be.[130]

1.3.1.1 Role of Agitation

As mentioned above, the two immiscible liquids stay phase separated as it minimises the contact area between two phases, minimising the free energy. The most thermodynamically stable status as such is maintained by the interfacial tension at the interface between two liquids. The generation of emulsion starts with an agitation process, breaking up one of the liquid phases into droplets. To do so, the disruptive forces introduced by agitation must be higher than the interfacial forces that hold the droplets together. In a perfect spherical droplet, the interfacial force is characterised by the Laplace pressure (Equation 2), where ΔP is the pressure difference between the outside and inside of the droplets, *r* is the radius of droplets and *γ* is the interfacial tension.[131] As it suggests, higher interfacial tension would result in larger droplets, and larger disruptive forces would be needed to generate smaller droplets. Apart from the disruptive forces, the duration of the forces being applied is also crucial for the formation of emulsion. It has to be longer than the droplets deformation duration to enable successful emulsion forming. The deformation duration (τ) is the defined as the ratio of oil viscosity (η) to the external stress (σ) acting on the drop as shown in Equation 3.[132,133]

$$\boldsymbol{\Delta P = \frac{2\gamma}{r}} \quad \textbf{Equation 2}$$

$$\boldsymbol{\tau = \frac{\eta}{\sigma}} \quad \textbf{Equation 3}$$

1.3.1.2 Role of Emulsifier

In addition to increasing entropy, the breakdown of droplets also significantly increases the surface area by creating smaller droplets. According to Gibbs free energy equation derivation (Equation 1), an increase in surface area would lead to an increase in ΔG, which is detrimental to the stability of the emulsion. Thus, the high frequency of collision during agitation may lead to coalescence, so the presence of emulsifiers would be necessary to avoid such coalescence. The emulsifiers adsorb at the interfaces between liquids, forming structured interfacial films and stabilising the emulsion via either long-ranged electrostatic repulsion or short-ranged steric repulsion. The concentration of the emulsifier must be sufficiently high to cover the whole surface of the emulsion, and the adsorption speed must be fast enough to modify the interface before collision.[134] As mentioned in the previous section, the amphiphilic characteristics of proteins allow them to strongly adsorb at the interface between water-oil and thus has been widely used in food industry[135–137] and drug delivery[136] as emulsifiers in stabilising O/W emulsion. In light of the role that polysaccharides play in increasing the viscosity of continues phase to slow down the destabilisation process,[138] there has been growing interests in developing polysaccharide–protein complexes as emulsifiers. Depending on how polysaccharides and proteins are complexed, three classes have been identified including naturally-occurring complexes, Maillard conjugates, and electrostatic complexes.[139] Among which, the naturally-occurring complexes offer very limited choices, gum Arabic is by far the most commonly used due to its ability to form thick interfacial multilayers.[135,138,140,141] Other natural complexes have been reported including pectin[142] and corn fibre gum,[139] meanwhile, attempts have also been made in developing gum Arabic alike polysaccharide–protein conjugates via Maillard reaction.[139] The Maillard reaction is a series of non-enzymatic browning reaction between reactive carbonyl groups of reducing sugars and nucleophilic amino groups of amino acids. Ever since it was first developed in 1912, it has been thoroughly investigated for its emulsifying potentials.[139,143–146] From which, Maillard reaction products (MRP) such as dextran-ovalbumin conjugates[147] and β-lactoglobulin-dextran conjugates,[148] successfully brought more enhanced emulsion stability than their purely native proteins

counterparts emulsified. However, the complicated reaction process and long reaction time are the issues for further application. In such concern, LbL assembly of polysaccharide–protein electrostatic complexes is a simpler and more controllable method, as previously described in 1.2.2. Given that most proteins and polysaccharides are PELs and would perform very differently under different pH, ionic strength, temperature, and etc. they would result in very different surface coverages and layer thickness – leading to emulsions with different stabilities.[137,149]

Since most emulsifiers are also amphiphilic, they also work as a surface active agent (surfactant), lowering the interfacial tension to compensate the increased surface area during emulsion formation and decelerate the increase of Gibbs free energy. In addition to proteins and polysaccharides, low molecular weight surfactant alone can function as emulsifiers as well. Compared to ionic surfactants, non-ionic surfactants are favoured for their stability, compatibility, and formulating flexibility as well as their inertness to ionic ingredients. Although these low molecular weight surfactants are more effective in reducing surface tension, they are unable to provide strong repulsion to prevent coalescence. Instead, they stabilise emulsion via Gibbs-Marangoni effect.[137] During the collision of two droplets, insufficient surfactant concentrations result in a concentration gradient and consequently an interfacial tension gradient at the surface of droplets. Less surfactant molecules are available at the region that droplets are close to each other, thus has higher interfacial tension in such area. The tension gradient results in the aqueous solution moving toward regions where interfacial tension are higher, driving the droplets away from each other. Although experiment is necessary to determine the optimum surfactant for a given system, the Hydrophilic-Lipophilic Balance (HLB) method is frequently used to select non-ionic surfactants. HLB value, calculated from the surfactant molecule structure or experimental data, is an important parameter to characterise the amphiphilicity of surfactants. High HLB values represent higher hydrophilicity while low HLB values represent higher hydrophobicity, and are favoured for the stabilisation of O/W and W/O emulsions, respectively, according to the Bancroft rule.[150,151] For instance, hydrophilic Tween and lipophilic Span are two commonly used non-ionic surfactants respectively for O/W and W/O systems.[152] By blending different surfactants together, a

wider range of surfactant options can be obtained, whose HLB values are determined by the corresponding weigh fraction (*x*) and HLB values of the components as shown in Equation 4.[133,152]

$$HLB = x_1 HLB_1 + x_2 HLB_2 \quad \textbf{Equation 4}$$

Apart from these abovementioned classical emulsifiers, another recently and commonly used choice is solid particles, by which the stabilised emulsion is referred as Pickering emulsion. Although the impact of solid particles on interfacial tension remain in doubt, the particles can stabilise emulsions by providing significant steric hindrance. Due to the larger size of the particle, it is more likely to form much thicker interfacial films than those classical emulsifiers and provide the most effective protection to coalescence.[135] However, others suggest otherwise as Tcholakova and colleagues' finding indicates no difference in stability was found among emulsions stabilised by globular protein, surfactant, or particles.[153] The adsorption of particles to the interface depends on its hydrophobicity. It stabilises O/W and W/O emulsion when the contact angles is more than 90° and lower than 90°, respectively.[154] Commonly used particles include silica, latex particles, polystyrene, metal oxides with sulphates, clays, and carbon, etc.[155] The presence of surfactants can modify the hydrophobicity of the particles. Some studies have been trying to combine surfactants with particles to make use of the advantages in emulsion stabilisation. Some progress has been made on such mixed-emulsifiers with enhanced emulsion stability.[156–158] For example, when Span®80 is added in silica particles stabilised water-in-paraffin oil emulsions, the resultant emulsions retain a longer stability and a narrower size distribution than emulsions prepared by the surfactant or the particle alone.[156]

1.3.2 Stability of Emulsions

An emulsion is a thermodynamically unstable state owing to its natural tendency for minimising its interfacial energy, thus property changes would sooner or later occur.[159] The emulsion stability is a kinetic stability, the longer the emulsion can maintain its properties, the more stable the emulsion is. Physical instability causes size distribution or structural reorganisation including creaming and

sedimentation, flocculation, coalescence, phase inversion, Ostwald ripening and ultimately complete phase separation (Figure 1.11).[133,159,160] To address the problem and provide long-term stability of emulsion, the mechanism of physical instability needs to be understood. However, chemical instability involving chemical changes such as oxidation and hydrolysis will not be discussed here.

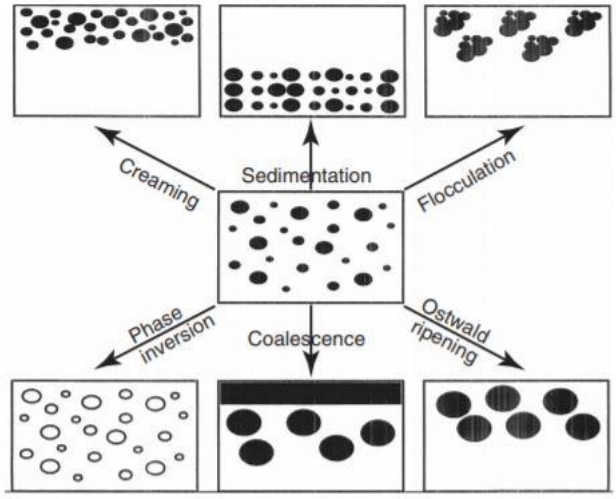

Figure 1.11. Schematic illustration of demulsification and instability of oil-water emulsion.[133] Reproduced with permission. Copyright 2013 WILEY-VCH Verlag GmbH & Co. KGaA, Weinheim.

1.3.2.1 Creaming and Sedimentation

Emulsions are made of two immiscible liquids that generally have different densities. Upon applying gravitational or centrifugal forces, the emulsion droplets tend to either cream at the top or sediment at the bottom of the emulsion, depending on the density differences. Creaming and sedimentation are not an actual breaking of the emulsion but a phase separation, the rate of which is determined by the density differences between two phases ($\Delta\rho$), radius of the dispersed phase droplet (R) and viscosity of the continuous phase (η_0) as calculated by Stokes' law (Equation 5, g is the acceleration due to gravity). Although the law is only applicable to diluted emulsions, it indicates potential pathways to slow down such emulsion instability. Possible solutions include minimising the density difference between two liquids by adding weighting agents in the lighter phase or using emulsifiers of different densities to vary the density of droplets; reducing the droplet sizes by introducing more

vigorous agitation or more concentrated emulsifiers, and increasing viscosity of the continuous phase with thickeners or gelling agents. [133,161]

$$v_0 = \frac{2\Delta\rho g R^2}{9\eta_0}$$ **Equation 5**

1.3.2.2 Flocculation

Flocculation is a type of aggregation where droplets stick to each other while each droplet keeps its own identity.[133,160] As mentioned above, in the formation of emulsions, droplets are surrounded by a thin layer of the continuous phase between droplets, which acts as a barrier preventing droplets from aggregation. To break up such barrier, a certain level of energy is required. Flocculation always occurs unless the energy barrier is significantly strong. Flocculation is normally driven by the van der Waals attraction when droplets are close to each other.[159] Although flocculation is reversible by mixing the emulsion again, severe flocculation can ultimately lead to phase separation of either creaming or sedimentation, as larger floc are subject to more gravitational effect.[159,161] Some mathematical models have been developed in predicting the influence of flocculation over emulsion stability in literature.[162–164] To manage the extent of flocculation, one of the choices is regulating steric, electrostatic and hydrophobic interactions between droplets. For sterically stabilised emulsion, it is necessary to ensure complete and thick coverage of the droplets by the emulsifiers and strong attachment of the emulsifiers to the droplets and it is also crucial to maintain the stabilising chain of the emulsifiers in good solvent conditions to avoid poor solvency. In the case of electrostatically stabilised emulsion that is easily sabotaged by electrolytes, keeping high surface potential while keeping the electrolyte concentration and ion valency low is important.[133]

1.3.2.3 Coalescence

Apart from flocculation, coalescence is another form of aggregation of droplets, but it is a non-reversible process. Coalescence is the merging of two or more droplets into a larger droplet that ultimately leads to the separation of two immiscible liquid layers. The mechanism of such emulsion failure mainly results in the thinning, disruption and eventual rupture of interfacial membrane – the

cause of which is complicated and depends on the properties of the liquids and emulsifiers. For example, coalescence increases when the viscosity of the interface or continuous phase is decreased, or the emulsion is agitated. In order to prevent coalescence, droplet contact and interfacial membrane rupture need to be minimised or avoided.[165] The introduction of mixed-emulsifiers such as the mixture of polysaccharide–protein complexes, low molecular weight surfactants, and nanoparticles that adsorb to the surface of droplets forming a mechanically strong, thick, and viscous layer as well as providing steric or electrostatic hindrance is a possible way to address this issue. Moreover, generating smaller emulsions also helps as smaller droplets are less susceptible to surface fluctuations.[133]

1.3.2.4 Ostwald Ripening

Ostwald ripening is another merging of emulsion droplets, appearing as the growth of larger droplets at the expense of smaller droplets. This process is driven by the difference in solubility among droplets of different sizes as smaller droplets are subjected to higher Laplace pressures (Equation 2) thus have higher solubility.[130,133] In light of that, the Ostwald ripening can be at least slowed down by narrowing the size distribution of emulsion to a slightly larger size. However, as mentioned above, larger emulsion would also increase the potential of flocculation and coalescence. A better alternative is to reduce the solubility of the dispersed phase by selecting less water-soluble oils. For example, use hexadecane instead of decane can effectively reduce the rate of Ostwald ripening. Moreover, many studies suggest that the rate of Ostwald ripening is determined by interfacial tension and diffusion coefficient of the dispersed phase.[130,132,166] Therefore by introducing protein or polysaccharides-based biopolymers will not only lower the interfacial tension, but also provide a mechanical resistance to droplet deformation, inhibiting the ripening.[130] The stability can be increased further by cross-linking the biopolymers or recruiting biopolymer multilayers via LbL methods.[167–169]

1.4 Microcarriers-based Bioreactors for *in vitro* Cell Expansion

Human stem cells such as embryonic, induced pluripotent and mesenchymal stem cells are favoured for cell therapy because of their intrinsic immunologic properties and multi-lineage differentiation potential.[170] For examples, embryonic stem cells (ESCs) have been investigated for retinal pigment epithelial (RPE) transplantation[171] and for treatment of spinal cord injury,[172] Induced pluripotent stem cells (iPSCs) have been utilised as models for disease tracing such as Parkinson's, Alzheimer's and Huntington diseases,[173] MSCs have been tested for acute graft-versus-host disease (GVHD), cardiovascular repair, bone and cartilage disease.[174] To fulfil these purposes, a large amount of cells would be needed, for instance, a dose ranged from 0.23 to 9 million MSCs per kilogram body weight were required per infusion for the treatment of GVHD.[175,176] Since most stem cells are sparse and rather difficult to be isolated from the body in a large amount, such massive demand cannot be easily met by traditional cell expansion on culture flasks (the current gold standard) because of their limited surface area and intensive labour work required on passages. Thus, a more efficient *in vitro* cell expansion at a larger scale would be required. Culturing cells on liquid provides an alternative cell culture platform. Due to the large surface-to-volume ratio, stable emulsions can provide significantly larger surface area with the same amount of medium than that of a traditional 2D culture flask does. However, since culturing on liquids is a novel cell culture platform, commercialised systems currently available on market are exclusively solid-based. Here, the existing cell culture platforms are reviewed.

1.4.1 Common Culture Systems for Cell Scale-Up

There is a variety of systems that have been developed for the scaling up of stem cells, such as multi-tray systems, roller bottles, and microcarriers (Figure 1.12). Since most stem cells are anchorage-dependent, all of these systems feature sufficiently large surface areas that provide significantly higher output of cells than the conventional tissue culture flask. Multi-tray systems, also known as cell factories, is a batch of trays stacked on top of each other (Figure 1.12A) that provides a surface area

up to 2.54×10^4 cm^2.[177] Although the employment of automated robotic arm dramatically reduced labour work and cell heterogeneity caused by manual culture, its inefficient gas exchange and unavailability of automatic monitoring and control system remains a challenge for large scale-up application. Roller bottle system provides surface area as much as more than 3.50×10^5 cm^2, far superior to the multi-tray systems. Additionally, it also allows the introduction of agitation to the system (Figure 1.12B), which not only enhances the gas exchange efficiency and lower the consumption of culture medium, but also minimise cell aggregation. However, similar to the multi-tray systems, it still lacks real-time monitoring and control, and still requires intensive labour work for cell passage.[177,178] Microcarrier-based systems overcome the abovementioned issues of the other two systems. A typical structure of microcarrier-based bioreactor is shown in Figure 1.12C, it contains an agitation paddle which guarantees the homogenous distribution of cells, mass transfer of oxygen and other nutrients, making the whole system cost-effective as it also prevents the formation of cell clusters.[179] The high surface-to-volume ratio of the microcarriers significantly increase the number of cells that could adhere and culture at the same time. It has been reported that a culture of 3 mg/mL Cytodex 1 microcarriers can provide a surface area of 1.32×10^4 cm^2 in 1 litre medium,[180] which is equivalent to 176 conventional T75 tissue culture flasks, and it can normally culture 4-fold higher cell density than planar platform with the same amount of medium used.[181] More importantly, microcarriers culture is also advantageous in allowing easy cell passage via bead-to-bead transfer,[182,183] this not only saves intensive labour work from cell passaging, but also minimises the risk of contamination. For the industrial application of cell scale-up, the cost-effectiveness is of particular importance, S-curve plots were proposed by Simaria et al. as shown in Figure 1.12D.[184] The optimal production range of different culture systems mentioned above is plotted against the R&D effort required, demonstrating that the microcarriers system would be of particular interest when a very large cell yield (4.7×10^{10} to 10^{12}) per lot is needed. Considering the industry would be continuing in high demand scenario, more R&D investment and effort will be required to move from tissue culture flask based culture system to microcarrier-based large-scale expansion system.[184]

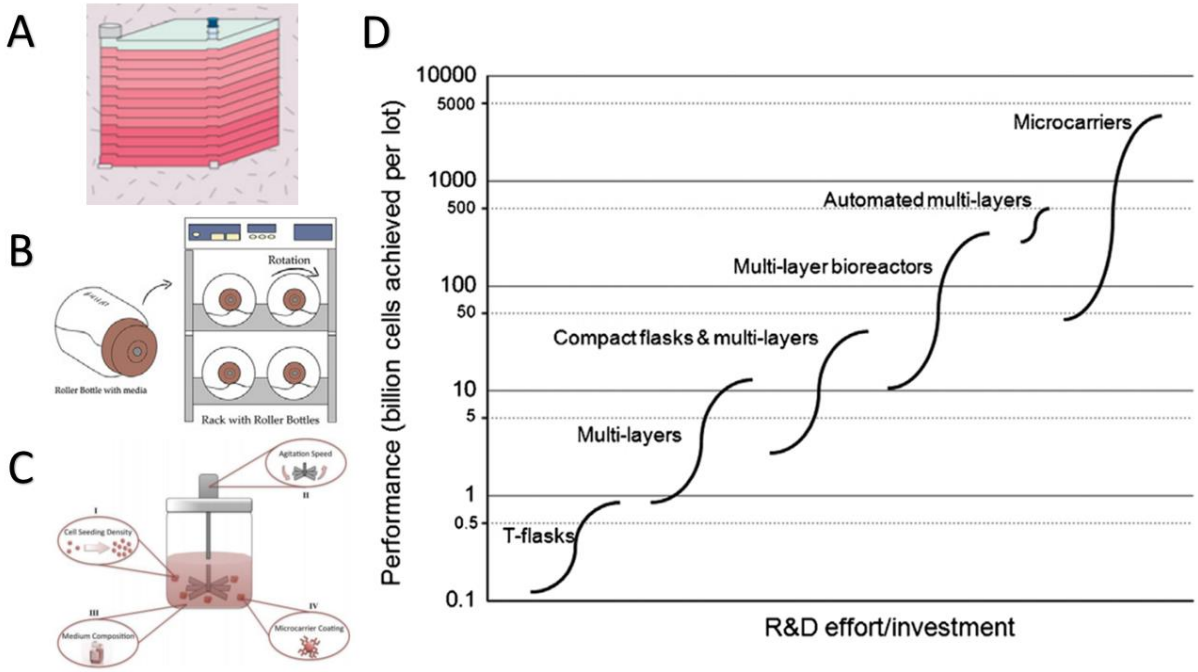

Figure 1.12. Different cell culture systems for *in vitro* expansion. (A) Multi-tray system,[185] (B) roller bottle system[178] (Reprinted with permission from Elsevier. Copyright (2018).), (C) microcarriers-based system[179] (Reprinted with permission from Elsevier, Copyright (2016).) and (D) Conceptual illustration of a technology S-curve illustrating the evolution of cell culture system for *in vitro* expansion. The R&D effort/investment values are calculated based on the direct costs (material, labor, QC testing) and indirect costs (equipment depreciation only) of the cell expansion process and assuming overheads are spread over 10 lots/year for all scenarios[184] (Reprinted with permission from John Wiley and Sons, Copyright (2013).).

1.4.2 Microcarriers

Microcarriers are small beads with diameters generally between 100-300 µm. These microcarriers provide anchoring points either via ECM proteins or electrostatic attraction for cell adhesion, proliferation, and potentially differentiation. Ideal microcarriers should enable the efficient harvest of expanded cells and should also have adequate physical mechanical properties to sustain the shear forces generated by the dynamic systems. Last but not the least, it must not be too expensive as the cost-effectiveness is the main concern for an industrial application.[179] The first introduction of microcarriers were dated back to 1967, when human cells were successfully cultured on a positively charged dextran particles.[186] Since then, the microcarrier technology have been developed further for

large scale cell expansion. Other materials such as cotton cellulose, polystyrene (PS), polyvinyl acetate (PVA) and ceramic have also been used for the fabrication of microcarriers.[180,183,187]

1.4.2.1 Microcarrier Classification and Selection

Microcarriers can be classified in different ways. When based on different materials used for fabrication, microcarriers can be classified into ceramic and polymer (natural and synthetic) microcarriers.[178] Microcarriers made from ceramic and synthetic polymer are advantageous due to in their excellent mechanical property, reproducibility, as well as cheap cost, but are poor in cell adhesion performance comparing to those made from natural polymers. Different materials with different resulting stiffnesses would ultimately lead to different cell phenotype. For example, MSCs are more likely to commit towards osteogenic lineage on rigid surfaces (stiffness higher than 34 kPa) but more likely to differentiate into chondrocytes and adipocytes on softer substrates.[7] Microcarriers can also be classified based on the surface topography: porous and non-porous. Porous microcarriers can be further subdivided into microporous (< 10 µm) and macroporous (10 to 70 µm) depending on different pore sizes.[180] Obviously, porous microcarriers provide significantly larger surface areas than non-porous microcarriers. Although microporous structures are too small for cells to grow in, it allows for the cells to create a microenvironment of its own inside the beads, which can potentially promote differentiation of cells such as osteogenesis.[188] In addition to extra spaces for cells to grow, macroporous structure also works as a shelter – shielding cells from the shear forces exerted by agitation.[189] However, the drawbacks of porous systems include limited transportation of nutrients and oxygen, and accumulation of metabolic waste in small pores. Poor diffusion of digestion enzyme such as trypsin into pores also leads to poor cell detachment and ultimately inefficient cell harvesting.[178,189,190] In such cases, pores over 20 µm in diameter should be suitable in accommodating most cells by allowing cell loading and sufficient penetration of the substances mentioned above.[191]

There is a range of microcarriers available in the market with various shape and properties and the commercial options have been extensively studied with different cells and thoroughly reviewed in

literature.[177,178,185,189,190,192] Owing to the complexity of cell culture process, many factors can affect the ultimate cell yield, therefore a universal rule for the selection of microcarriers is not yet established. Apart from the materials and porosity mentioned above, the size of microcarriers is another important factor affecting the cell proliferation and behaviour. For instance, it has been reported that MSCs prefer microcarriers larger than 150 µm in diameter while iPSCs are more likely to self-aggregate into cluster on microcarriers smaller than 100 µm.[178] Moreover, the curvature of microcarriers seems to be another factor to consider, as it could induce different shear forces on the cells in dynamic systems, which may lead to changes in MSCs proliferation rate and osteogenesis potential.[193] More recent studies also suggest that cell-scale curvature triggers a dynamic interplay between the nucleus and cytoskeleton, functions as an important regulatory cue in guiding cell migration, and potentially differentiation.[194,195] In addition to the cell type, cell proliferation, and differentiation potential, the intended use of the final cell product is also of great importance in selecting microcarriers. Non-biodegradable microcarriers such as ceramic or synthetic polymer-based can be used if the single cell suspension or cell pellet is wanted as the final product, otherwise only natural-polymer such as gelatin-based biodegradable microcarriers are allowed for direct infusion and transplantation purposes.[180]

1.4.2.2 Microcarrier Coatings

Cell attachment to microcarriers is an important factor in determining overall cell proliferation. Cells are attracted to microcarriers either via an electrostatic interaction or ECM protein adhesion, both of which can be effectively modulated by modifying the surface chemistry and coating of the microcarriers. For example, Cytodex microcarriers are made from cross-linked dextran-based matrix, of which Cytodex 1 is positively charged with N, N-diethylaminoethyl groups but Cytodex 3 is denatured COL coated, both of them are commonly used commercialised microcarriers for the expansion of ESCs[196] and MSCs.[197] Although ECM proteins coated microcarriers have reduced plating efficiency compared to simply positively charged microcarriers which electrostatically attract cells (which are negatively charged) at very high efficiency (about 90% within an hour), the ECM coated microcarriers usually support better growth of cells.[180] Commonly used ECM coating for microcarriers

include FN, VN, LN, COL and Matrigel. It was found that LN or Matrigel coating are essential in maintaining long-term proliferation and pluripotency of ESC on microcarriers.[198] However, these protein substances often originate from animal products, which suffer from batch-to-batch variability, and risk of contamination for clinic application. A possible solution is to use recombinant proteins produced by prokaryotic or eukaryotic cells, but these are typically more expensive. Another choice is to coat the surface with chemically synthesised adhesion motifs, such as RGD peptides.[185] A typical example is Synthemax microcarrier, which is coated with a short peptides sequence derived from VN. It performed similarly well for the prolonged culture of ESC,[199] iPSC[185] and MSC[200] compared to microcarriers coated with Matrigel, VN and FN, respectively. Modifying the surface chemistry of the microcarriers would also lead to different cell adhesion and fate, for instance, –COOH groups coated surfaces suppressed MSC spreading but enhanced chondrogenesis, while $–NH_2$ groups coating promoted MSC proliferation and osteogenesis.[201]

In addition to promoting cell adhesion, surface coating on microcarriers also affect cell harvesting. The cell harvesting after expansion on the microcarrier must provide an efficient cell-microcarrier separation and cell recovery without affecting the cell quality such as viability and differentiation potential.[179] A classical method used on planar platforms is enzymatic digestion which results in the damage of cell membrane receptors and other cell membrane proteins. However, this is not practical on large scale production as the concentration of the enzyme and the incubation time is difficult to control which would affect cell viability and recovery efficiency.[179] A cell sheet technology wherein cells are cultured on a thermo-responsive polymer has been developed. By switching the temperature and therefore altering the hydrophobicity of the polymer, cells can be harvested with ease as shown in Figure 1.13.[202] Poly(N-isopropylacrylamide) (PIPAAm), a thermo-responsive polymer has a low critical solution temperature (LCST) at 32 °C which promotes cell adhesion at temperature beyond its LCST when it is hydrophobic but repels cells when it hydrates and swells at the temperature below, is a common candidate for cell sheet technology.[202,203] Ever since this technology has been developed, it has been used for the culture of a wide range of cells including MSCs, iPSCs and ESCs for corneal,

cardiac and periodontal regeneration.[202,203] Such thermo-responsive properties can be transferred on the surface of microcarriers by radiation-induced grafting or living radical polymerisation.[204] However, complete detachment has yet to be achieved and initial cell adhesion is often relatively poor.[205] By introducing other substance such as polymer and protein into the system, cell performance can be further altered. For instance, when a positively charged quaternary amine monomer and a hydrophobic monomer was incorporated into PIPAAm, the terpolymer-grafted microcarriers facilitated cell proliferation and rapid cell detachment.[206] Apart from PIPAAm, other thermo-responsive copolymer such as 2-carboxyisopropylacrylamide (CIPAAm) and even other environmental-responsive materials such as pH-responsive and field-responsive materials were also used for the coating of microcarriers for the non-invasive cell harvesting.

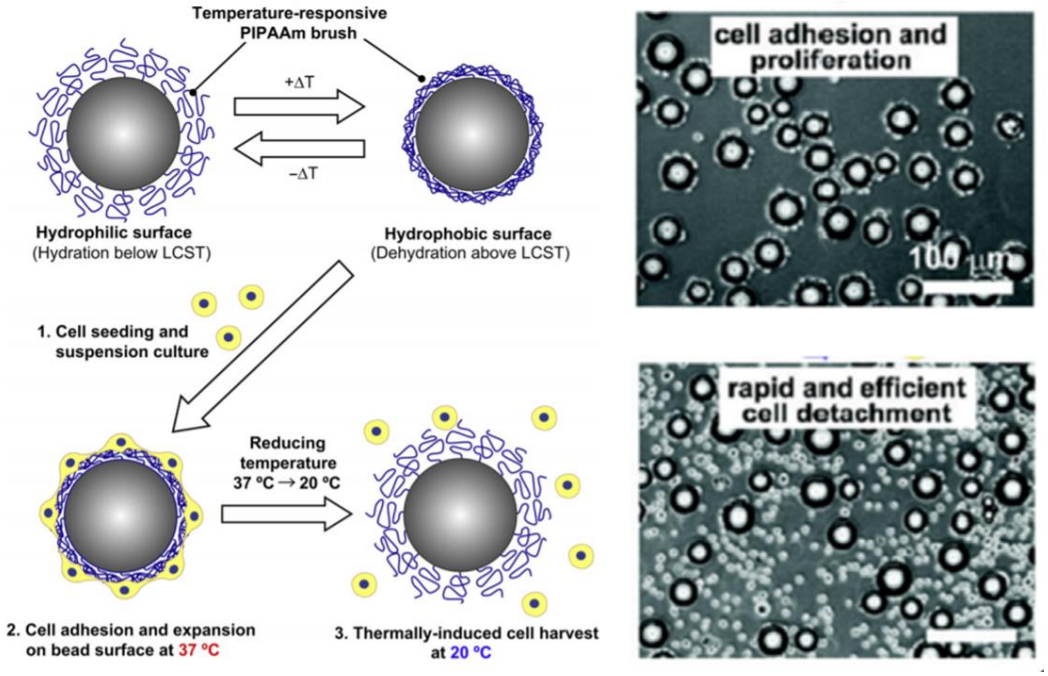

Figure 1.13. Schematic illustration of cell culture and harvest on thermo-responsive polymer coated microcarriers.[206,207] Reprinted with permission from Elsevier and American Chemical Society. Copyright (2012).

1.4.3 Operational Parameters of Microcarrier Systems

A typical cell proliferation profile can be divided into four phases as shown in Figure 1.14. The lag phase, also known as the inoculation phase, corresponds to the start of cell adhesion and spreading. It has been reported that the attachment efficiency at this point is crucial for the subsequent growth rate and cell yield.[208] In a dynamic culture system such as a microcarrier-based bioreactor system, applying agitation during this inoculation phase would affect the attachment efficiency. For example, MSC attachment efficiency can be increased to 55% under an intermittent agitation rate, 21% higher than using continuous agitation.[208] Reducing medium volume or increasing microcarrier density also helps as they increase cell-to-cell and cell-to-microcarrier collisions.[179] At the log phase, cells proliferate exponentially so it is also called exponential growth phase. The agitation rate is again the key parameter at this stage as it helps for effective and homogenous transportation of metabolic waste, nutrients, and oxygen, as well as prevents cell aggregation. It has also been found that introducing a certain amount of agitation could induce osteogenesis and chondrogenesis in MSCs.[196] Yuan et al. investigated three different agitation rates – 60, 90 and 115 rpm, and found that the increase of agitation leads to higher growth rate and lower doubling time of MSCs. However, a noticeable high level of cell debris was observed at the agitation rate of 115 rpm, the highest cell proliferation rate was therefore observed at 90 rpm.[208] Moreover, the selection of medium and frequency of medium exchange is another important parameter at this stage. It is difficult to perform a complete medium exchange in microcarrier culture, and so a partial medium replacement is often conducted instead. Sufficient and frequent medium exchange would therefore be required to avoid glucose depletion and ammonium accumulation which inhibits cell growth.[177] Although the supply of serum-protein in culture medium can protect cells from stress induced by agitation, it may also introduce contamination, chemically defined media is thus often preferred.[183] An increasing number of report shows that cells on confluent microcarriers are able to colonise newly added fresh microcarriers.[180,183,197,209] Many have found that cells bridge the gap between beads. This process would require sufficient cell migration and proliferation, and only occurs when cell proliferation

capacity is not impaired by over-confluency or metabolite inhibition.[183] It was also shown that continuously adding fresh microcarriers would extend the log phase, postponing the stationary phase to later time points,[197] which suggests that the stationary phase is determined by the maximum loading of the microcarriers which is the availability of surface area for adherent cell culture. Such feature is beneficial for industrial scale production as the intensive labour work associated with repeated passaging can be avoided. Since different cell sources on different microcarriers respond differently to these parameters, systematic study over all the conditions is lacking and unfeasible. It is of great importance to carry out high-throughput optimisation studies, to standardise parameters for cell expansion on microcarrier based on the type of cells and microcarriers.

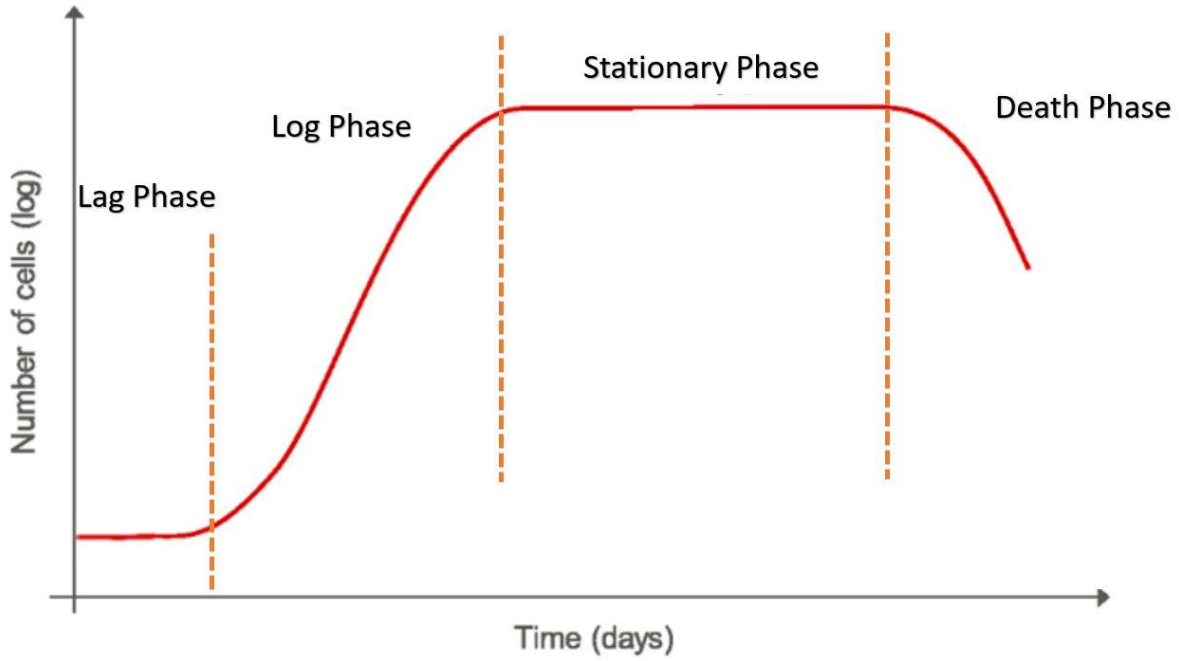

Figure 1.14. A typical growth curve of cells.

1.5 Aims and Objectives

Cell-material interactions are at the centre of the design of biomaterials for tissue engineering and regenerative medicine. A significant amount of research has focused on mimicking the natural microenvironments of cells via the assembly of nanosheets made from ECM proteins and

polysaccharides that are essential in maintaining tissue structure and functionality as well as providing mechanical support. The control of bulk mechanical properties of biomaterials is considered to be essential for the regulation of mechanotranduction process that control cell behaviour, such as proliferation and differentiation. However, many recent studies have suggested otherwise, as cell may response to changes in local ligand tethering[48,49] or viscoelasticity of substrates,[50,51] regardless of bulk mechanical properties. These reports suggest that the regulation of nanoscale mechanics may dominate over bulk mechanical properties and provide a new degree of flexibility for biomaterials design, whereby bulk mechanics can be tailored independently from interfacial mechanics to regulate structuring and scaffolding properties separately from the promotion of cell adhesion and spreading, as well as downstream cell phenotypes.

In this respect, the pioneering works of Keese and Giaever[126–129] have provided particularly striking examples of extreme scenarios, in which the culture of fibroblasts at liquid interfaces was shown to be possible. This opens the door to particularly novel technologies in which adherent cells can be cultured at surface of emulsions for the scale up of cell expansion, replacing solid substrates and enabling more affordable and simplified processing. However, the design of viable liquid-liquid systems for cell culture requires the understanding and control of interfacial mechanical properties and their impact on cell adhesion and proliferation. In this project, we aim to design protein nanosheet-assembled liquid interfaces whose interfacial mechanical properties are tuneable via the adjustment of pro-surfactant, pH and the molecular structure of protein or polymers. These interfaces are employed for the culture of MSCs to investigate the impact of interfacial mechanical properties such as the interfacial moduli and viscoelasticity on the adhesion and proliferation of MSCs. Overall, our aim is to formulate the improved interfaces that support the *in vitro* expansion of MSCs.

A major challenge in the field of regenerative medicine is the supply of cells at sufficient scales for therapeutic intervention, whilst controlling and retaining desired cell phenotypes. Hence this project also aimed to address these issues, by developing stable emulsions that can provide significantly larger

surface area for cell expansion as well as bypass enzymatic digestion in cell collection. Emulsions are stabilised by the assembly of protein-nanosheets at the liquid interface to provide steric repulsion to the coalescence of droplets and cell adhesive motifs. The stability of the emulsions was assessed under microscopy to help us understand the adsorption and assembly of the nanosheet under different conditions. Despite the fact that the assembly of proteins for the stabilisation of O/W emulsion has been extensively studied, its application and impact on cell culture remains mostly undocumented. In our study, the behaviour of MSCs, including their adhesion and proliferation, on emulsions are investigated. Formulations displaying improved emulsion stability and cell proliferation were then further explored for long-term culture. The prolonged culture of MSCs was carried out on selected emulsions as well as tissue culture polystyrene (TPS, tissue culture treated) and commercialised microcarriers for comparison. During this process, MSC phenotypes were continuously monitored and compared. We propose that such study demonstrates the potential of protein-nanosheet stabilised emulsions as an alternative to solid microcarriers for the *in vitro* scale-up of MSC production.

Chapter 2

Design of Poly-L-lysine Nanosheets at Liquid-Liquid Interfaces

2.1 Introduction

Adherent cell culture is typically thought to require cell spreading on rigid substrates to sustain the formation of stable focal adhesions and assembly of contractile cytoskeletal.[210] It has been extensively reported that the establishment of such cell adhesion is crucial for cell to convert external signals, such as mechanics and topography into biochemical signals, generating appropriate cellular response to extracellular cues, thus mechanical properties have become particularly important in the design of materials for biomedical applications.

Traditionally, bulk mechanical properties were regarded as key in regulating cell fate. However, more recent studies have suggested a more nuanced situation,[47,52] as the lack of cell response on Sylgard 184 poly(dimethyl siloxane) (PDMS) with wide range of moduli from 0.1 kPa to 2 MPa has been reported.[48] Moreover, it has been reported that cell culture at the surface of liquids is possible in the presence of mechanically strong nanosheets at corresponding interfaces to counterbalance forces that cells exert.[47,52,61–63,127,129]

To generate a strong interface to culture cells, proteins are obvious candidates due to their bioactivity and ability to form layers with strong interfacial rheology properties providing stability.[64] Protein adsorption to the interface is driven by the lowering of free energy via the reduction of surface area to restrict the exposure of hydrophobic groups to aqueous phase. This is a multistep process involving protein diffusion, adsorption and conformational change.[64–70] Parameters such as protein concentration, temperature, pH, ion strength, etc. can all contribute to this process.[67,68,70] By monitoring dynamic interfacial tension during protein adsorption, H.W. Blanch and co-workers[70] have divided protein adsorption at oil/water interfaces into three stages: induction, monolayer saturation and interface gelation. Induction, the regime when interface tension remained unchanged, was chiefly controlled by protein diffusion, where higher protein concentration and more hydrophobic protein result in shorter induction time, however, the difference in hydrophobicity can easily be levelled off if the oil phase strongly affects the proteins in solution. During monolayer saturation, interfacial tension

is sharply decreased as more proteins adsorb to the interface. At this point, while more proteins are still diffusing to saturate the interface, those adsorbed start to unfold and interact more with the oil phase. This stage was related to the hydrophobicity and the bulk stability of the protein. Finally, the tension slowly decreases as a result of the formation of a gel-like structure via entanglement and aggregation. At this stage, a multilayer structure is established. When the newly adsorbed layer become further distant from the interface, the environment becomes more bulk like, equilibrium is reached and adsorption ceased. The interfacial shear mechanical properties of the adsorbed multilayer are determined by the interaction among proteins as well as between proteins and interfaces,[64,67] which can be generally grouped as ionic or electrostatic interactions, hydrophobic interactions and hydrogen bonding. Likewise, by adjusting with buffer solution for example, ion strength, pH, temperature, or via changing the liquid-liquid interaction for instance, replacing the oil phase, or introducing surfactants, the protein layer can behave differently and display altered interfacial mechanical properties.

Based on their sequence of amino acids, proteins can be classified as globular or random coiled. In water, globular proteins such as BSA, lysozyme (Lys) and β-lactoglobulin can be conveniently described as colloidal particles (at least until they adsorb to the interface) whilst random coil proteins such β-casein, glycoproteins and lipoproteins, behave more as charged polymers or PELs.[67] Between these two classifications, exists another type of proteins which has reversible secondary or tertiary structures, such as gelatin (GEL) whose structure can be changed by temperature[13] and PLL whose structure is tunable upon the adjustment of pH.[68,72–74] In terms of mechanical performance, it has been widely reported that globular proteins are more likely to display higher interfacial shear viscosity and moduli because of their high packing density and unfolding level, whilst owing to their high flexibility, random coil proteins rearrange more easily in bulk or at the interface, thus are less likely to organise as ordered crystal structure and less likely to denature to build up intermolecular cohesion.[64,67,70,92,149]

Due to the amphiphilic character of some proteins, it is generally accepted that they can function as surfactants by adsorbing to any interface subjected to interface-adapted conformational change. However, owing to the mobility of liquid-liquid interfaces, the adapted conformational change is more transient and flexible, with random coil proteins being less affected than globular proteins, as mentioned above.[67] Low molecular weight surfactants might be needed in assisting protein adsorption and denaturation at interfaces,[91] especially for proteins composed of less hydrophobic amino acids such as lysine and arginine.[67] The protein-surfactant mixtures often cause a competitive adsorption phenomenon where low molecular surfactants penetrate into the defects between proteins at the interface, disrupting the protein network either by displacing proteins further (non-ionic surfactants) or forming an interface surfactant-protein complex (ionic surfactants).[90–93] When presented to an oil phase, non-ionic surfactants bound to proteins via hydrophobic binding and are less likely to cause dramatic conformational changes. In contrast, ionic surfactants, which electrostatically interact with proteins, tend to result in larger changes in conformation.[92] Therefore, the resultant interfacial mechanics may significantly differ between these two types. Another route to promote protein adsorption is to enhance amphiphilicity via chemical modification, as either the amino acid group or the carboxylic group of the amino acids can be substituted by hydrophobic tails to respectively form N-acylated anionic surfactants or C-substituted cationic surfactants.[211,212] These surfactants are favoured in food and pharmaceutical industries for their robust amphiphilicity and biocompatibility and have been thoroughly studied for their self-assembly behaviours and direct adsorption at liquid-liquid interfaces.[211,212]

A wide range of techniques have been employed to investigate protein adsorption at liquid interfaces. Interfacial rheology, which quantifies the relationship between applied forces and the corresponding shear deformation,[64,90,92,213] is amongst one of the most commonly used techniques to not only monitor the dynamic adsorption process but also characterise the interfacial shear properties. There are two types of deformations in interfacial rheology: dilatational deformation, which maintains the shape but change the area, and shear deformation which distorts the shape but keeps the interfacial

area unchanged.[64,90,213] These two methods are generally complementary with each other, with dilatation rheology more focused on short-term stability while shear rheology on long-term.[90,92] Ellipsometry is another powerful tool frequently used in measuring the thickness of an interfacial film by fitting the measured change in the polarisation of the polarised light reflected from the interface of interest to an existing optical model.[214–217] It has been widely used in the studies of the thickness of LbL assembled multilayer films.[111,216,218] In the field of protein adsorption at liquid interfaces, it was used to characterise the adsorption and destabilisation of the protein layers via monitoring the thickness[92,219,220] or ellipticity.[93] Other techniques that have also been employed in such study include neutron reflection,[67,69,221] dynamic light scattering,[72,73,136,221] second harmonic generation[68,222] and sum-frequency generation, etc.[219,223]

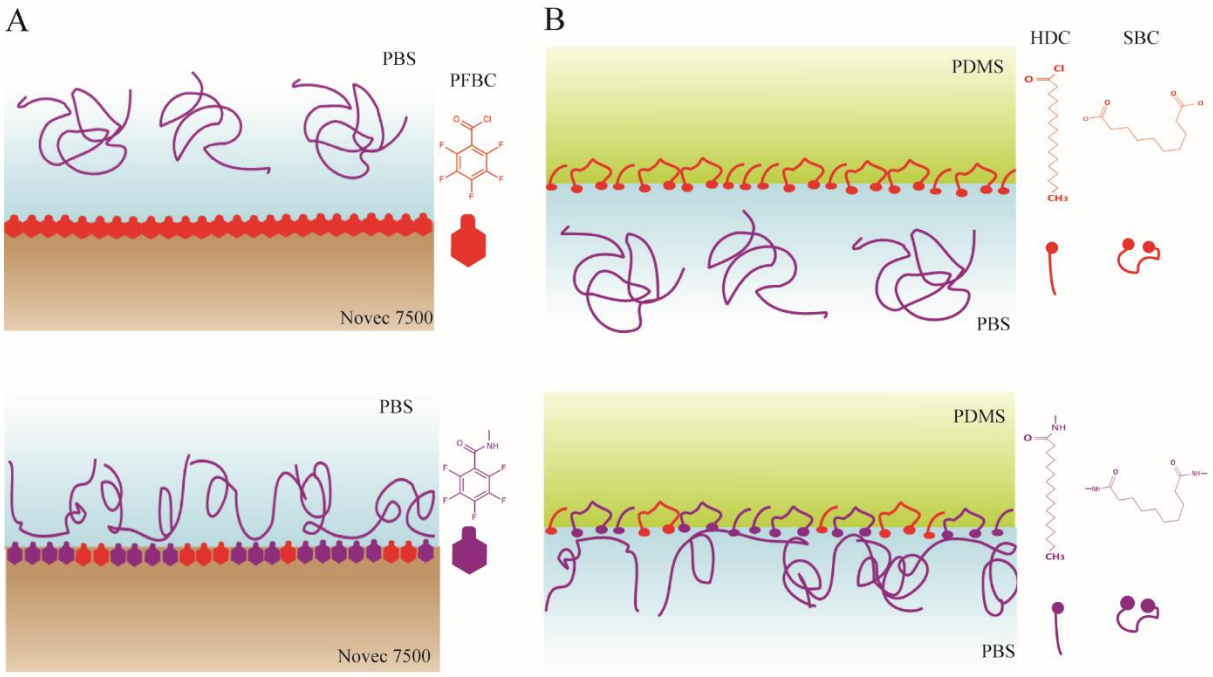

Figure 2.1. Schematic representation of PLL adsorption at oil interfaces, assisted by pro-surfactants. (A) PLL assembly at the interfaces between PBS and Novec 7500 containing PFBC. (B) PLL assembly at the interfaces between PDMS containing the mixture of HDC and SBC (mixed at 1:1 ration) and PBS.

In this chapter, PLL nanosheets were designed at liquid-liquid interfaces under different conditions to investigate the factors that affect interfacial mechanical properties. PLL, as a polypeptidic weak PEL,

displays pH-responsive conformation,[72] and has been widely used for biomedical applications such as cell adhesion,[224] cell encapsulation,[225–228] drug delivery[228,229] and bioactive coating[101,230] due to its biocompatibility and biodegradability. It can undergo conformational changes, switching between random coil, α-helix and β-sheet in response to pH,[68,72–74] temperature[231,232] and even shear force.[233] From this point of view, it is an excellent building block for protein nanosheets for cell culture at liquid interfaces. However, owing to the weak hydrophobicity of lysines, even at high pH, as mentioned above, low molecular weight reactive pro-surfactants such as pentafluorobenzoyl chloride (PFBC), sebacoyl chloride (SBC) and heptadecanoyl chloride (HDC) were introduced in the system we designed. We proposed that such molecules would function as pro-surfactants at oil-water interfcaces, reacting with amine side groups to form hydrophobic amide residues able to pin the corresponding protein or polypeptide at the liquid-liquid interfaces (Figure 2.1).[52,89] Interfacial shear rheology was conducted to explore the macroscopic mechanical properties of the nanosheet-reinforced interfaces. A platinum ring was placed at the interface between the two liquids, applying a sinusoidal shear deformation, and the resultant nanosheets response was then monitored. From the measured phase and amplitude shifts between the applied deformation and obtained response, the difference in viscoelasticity can be calculated (Figure 2.2A and B). Since cell-generated deformation are nano- to micro-scale, primary sensing of mechanics is local.[49,210,234] In light of the possible difference in macroscopic and microscopic mechanical performance, magnetic tweezers were also used to characterise the rheological properties of the nanosheets microscopically. Magnetic tweezers are a powerful technique allowing the application of controlled magnetic forces on magnetic beads bound to the entity of interest. The mechanical characteristic of the entity can therefore be extracted by tracking the beads displacement. This technique has been extensively used for single molecule mechanical characterisation, such as DNA stretching,[235] protein folding[236] or cellular mechanotransduction.[237] Hereby, magnetic beads were bound to the surface of nanosheets assembled at the interfaces to measure the microscopic mechanical performance as shown in Figure 2.2D. The Langmuir-Blodgett technique was also employed to harvest the nanosheets designed as

shown in Figure 2.2C, and subsequent characterisation was carried out by epifluorescence microscopy and ellipsometry.

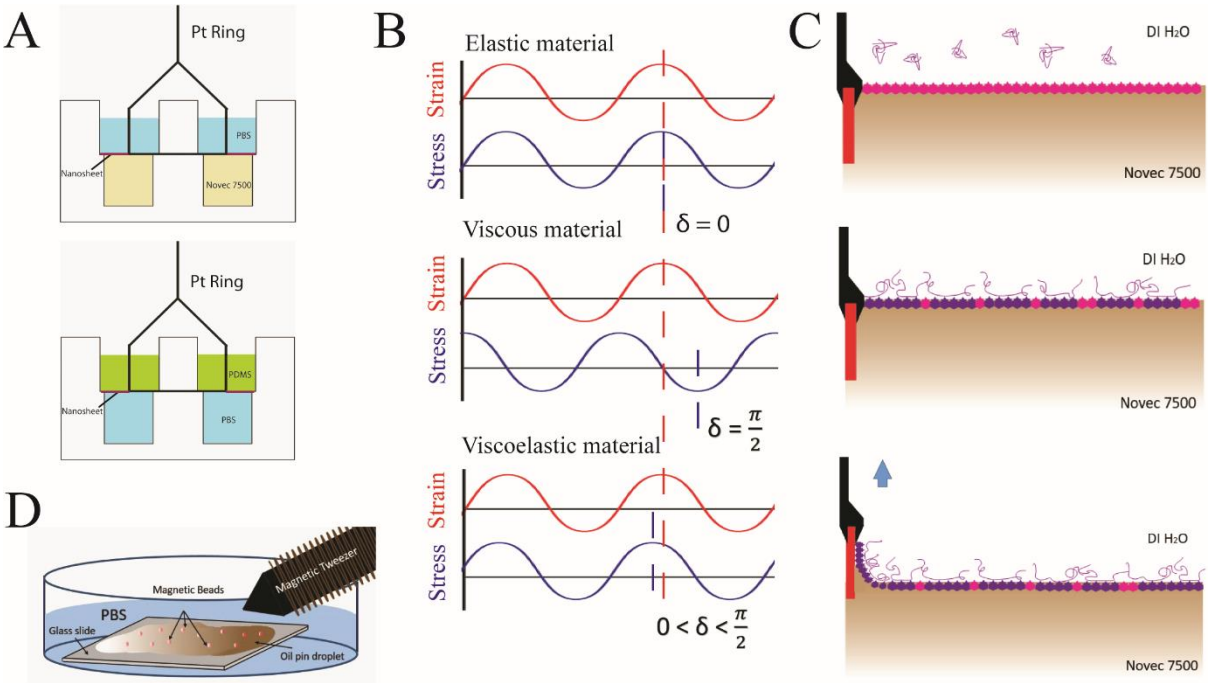

Figure 2.2. Schematic illustration of the characterisation of nanosheets assembled at the interfaces. (A) Cross-section illustration of interfacial shear rheology experiments set up for PBS/Novec 7500 interface (top) and PDMS/PBS interface (bottom). (B) Typical stress response to strain deformation for a pure elastic (top), a pure viscous (middle) and a viscoelastic material (bottom). (C) Schematic illustration of harvesting nanosheets via Langmuir-Blodgett Trough, substrate was placed at the interface between deionised water/Novec 7500 (top), the protein was then added and assembled at the interface with the presence of PFBC (middle), the nanosheets were harvested by slowly lifting the substrate out of the liquid. (D) Schematic representation of experiment set up for magnetic tweezer in this study to apply forces on beads bound to the nanosheets assembled at the PBS/Novec 7500 interface.

2.2 Materials and Methods

2.2.1 Materials and Chemicals

PFBC, PBS, sodium bicarbonate pellet ($NaHCO_3$), sodium hydroxide pellet (NaOH), PLL hydrobromide (mol wt 1-5 kDa, 4-15 kDa, 15-30 kDa, 30-70 kDa, 70-150 kDa, 150-300 kDa and >300 kDa), toluene (anhydrous, 99.8%), dimethyl sulfoxide (DMSO), trimethylamine (TEA), trichloro (1H, 1H, 2H, 2H-perfluorooctyl) silane, SBC, HDC, BSA and FN from human plasma were purchased from Sigma-Aldrich.

Fluorinated oil (Novec 7500) was from ACOTA. Foetal bovine serum (FBS) was from PAA. Cover glasses (25 × 60 mm) and pure ethanol were from VWR. PDMS (trimethylsiloxy terminated, viscosity 10 cSt) was from ABCR. Silicon wafers (100 mm diameter) were purchased from Pi-Kem Ltd. Dynabeads (M-450 epoxy), Alexa Fluor 488 NHS ester (succinimidyl ester), Alexa Fluor 488 goat anti-rabbit IgG (H+L) highly cross-adsorbed secondary antibody were purchased from Thermo Fisher Scientific. Mica Sheets (11mm x 11mm x 0.15mm thick) were from Agar Scientific Ltd. Polyclonal anti-fibronectin antibody from rabbit was from ABCAM.

2.2.2 Preparation of Fluorinated Oil-based Interfaces

24 well-plates were plasma oxidized via a plasma coater (Diener, 100% intensity) for 10 minutes. An amount of 500 µL pure ethanol pre-mixed with 10 µL TEA and 10 µL trichloro (1H, 1H, 2H, 2H-perfluorooctyl) silane was added into each well. The well-plates were then sealed with parafilm and left overnight. After 24 h, 500 µL Novec 7500 containing PFBC of desired concentrations was pipetted into the treated well after being washed twice with pure ethanol and three times with deionised (DI) water obtained from a Purelab® Chorus system. A 1 mL amount of pH 10.5 PBS was added dropwise on top of the oil in each well, 1 mL of PLL of interest solution (in pH 10.5 PBS unless otherwise specified) was then pipetted at 200 µg/mL, making the final PLL concentration at 100 µg/mL in each well. After an hour incubation allowing the PLL nanosheet to be formed, the excessive polymer solution was removed by diluting with PBS (pH 7.4) six times. When FN was required, 1 mL amount of 20 µg/mL FN solution (in pH 7.4 PBS) was pipetted on top of the PLL film and left for another hour incubation. The residual FN was then washed out by diluting with PBS (pH 7.4) six times.

For fluorescence imaging, conjugated PLL was used instead of normal PLL. The conjugated PLL stock solution was prepared by dissolving PLL powder in 0.1M $NaHCO_3$ buffer and reacting with Alexa Fluor 488 NHS ester (succinimidyl ester) dissolved in DMSO, as suggested by the user manual. The conjugated PLL was mixed with normal PLL at 1:9 ratio and added into each well at 100 µg/mL as the

final concentration. The incubation and washing process was the same as described above. To image FN film, primary antibody (rabbit-anti-fibronectin, at 1:400 dilution in 3% BSA solution) was incubated with the film for an hour first before secondary antibody was incubated for another hour. Extensive washing was performed after each incubation. Samples were imaged by Leica DMI4000 fluorescence microscopy.

2.2.3 Interfacial Rheology

Rheological measurements were carried out on a hybrid rheometer (DHR-3) from TA Instruments fitted with a double wall ring (DWR) geometry and a Delrin trough with a circular channel. The double wall ring used for this geometry has a radius of 34.5 mm and the thickness of the platinum–iridium wire is 1 mm. The diamond-shaped cross-section of the geometry's ring provides the capability to pin directly onto the interface between two liquids and measure the interface properties without complicated sub-phase correction. 19 mL of the fluorinated oil pre-mixed with PFBC at desired concentrations was placed in the Delrin trough and the ring was lowered, ensuring contact with the surface, via an axial force procedure. The measuring position was set 500 µm lower than the contact point of the ring with the oil-phase surface. Thereafter, 15 mL of the PBS buffer (pH 10.5 for PLL, pH 7.4 for FBS) was carefully syringed on top of the oil phase. For PDMS-based system, 19 mL of pH 10.5 PBS buffer was placed as bottom phase while 15 mL of the PDMS pre-mixed with the pro-surfactants (mixture of SBC and HDC at 1:1 ratio) at 0.1 or 0.01 mg/mL was added as top phase when the measuring position was set as mentioned above. Time sweeps were performed at a constant frequency of 0.1 Hz and a temperature of 25°C, with a displacement of 1.0×10^{-3} rad to follow the formation of the protein layers at the interface. The concentration of PLL and FBS used for all rheology experiments were 100 µg/mL and 1 g/mL (with respect to aqueous phase volume), respectively. After the time sweep, a frequency sweep (with a constant displacement of 1.0×10^{-3} rad) was conducted to examine the frequency-dependant characteristics of the interface. Before an amplitude sweep (with

constant frequencies of 0.1 Hz) was carried out to ensure that the selected displacement was within the linear viscoelastic region (the limit of which was defined as the point where 5% deviation from the value of the previous point in storage modulus was observed), stress relaxation was performed at 1% strain for 120 s. The strain in the interfacial shear rheology test is defined as angular displacement relative to a reference length, calculated by the Equation 6. The γ represents the shear strain; θ is the angular displacement in radians, displaying the circular path an object moves; and K_γ is the strain constant determined by measurement geometry and/or initial sample dimensions.

$$\gamma = \theta \times K_\gamma \qquad \textbf{Equation 6}$$

For creep-recovery measurements, a double wall Du Noüy Ring (DDR, 20 mm in diameter and 400 µm in thickness) geometry and a smaller trough was used. An amount of 3 mL of the fluorinated oil pre-mixed with 0.01 mg/mL PFBC was placed in the Delrin trough and the ring was lowered, ensuring contact with the surface, via an axial force procedure. The measuring position was set 200 µm lower than the contact point of the ring with the oil-phase surface. Thereafter, 4 mL of the pH 10.5 PBS buffer was carefully syringed on top of the oil phase. Time sweep was performed at a constant frequency of 0.1 Hz and a temperature of 25°C, with a displacement of 1.0×10^{-3} rad to follow the formation of the protein layers at the interface. A 40 µL amount of 10 mg/mL (in DI water) PLL with molecular weight of interest was pipetted to the aqueous phase, making the final concentrations at 100 µg/mL. When the time sweep measurement was finished, the excessive polymer solution was washed by diluting with PBS (pH 7.4) six times. The creep-revocery experiment was then conducted by applying a 1×10^{-3}, 5×10^{-3} or 10×10^{-3} Pa stress for a duration of 30 s, followed by a 30 s recovery without applying any stress.

Since the creep ringing issues are inevitably resulted by the coupling of instrument inertia and sample elasticity in a stress-controlled rheometry.[238–241] The initial creep ringing parts were discarded via a smoothing tool in Origin and the creep results were fitted with a 6-element modified Burger's model (a Burger's model[242] with an extra Kelvin-Voigt element in series, Figure 2.3) via MATLAB. The

constitutive equation of the form is showing below (Equation 7). The *J* represents creep compliance (the ratio of the measured strain to the applied stress), *G* is the elastic modulus, *η* is the viscosity and *t* is the time. τ is the retardation time given by *η/G*, defined as the time required for the strain to reach approximately 63% of its final asymptotic value.

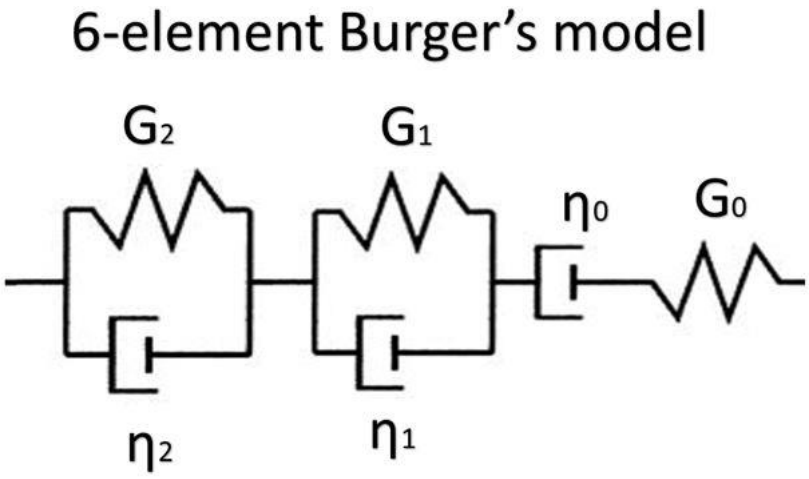

Figure 2.3. Schematic illustration of a 6-element Burger's model. It consists of two Kelvin–Voigt elements (a spring and a dashpot in parallel) in series with a Maxwell element (a dashpot and a spring in series).

$$J = \frac{1}{G_0} + \frac{1}{G_1}\left(1 - e^{-t/\tau_1}\right) + \frac{1}{G_2}\left(1 - e^{-t/\tau_2}\right) + \frac{t}{\eta} \qquad \textbf{Equation 7}$$

Instantaneous Deformation	Viscoelastic Effect (2 characteristic times)	Long-term viscous flow

A modified Jeffreys model (a dashpot in series with a Kelvin–Voigt element and the instrument inertia, Figure 2.4) was also used in the creep results fitting to extract viscoelasticity properties from the creep ringing.[238–241] The raw data was fitted via MATLAB with the equation showing below (Equation 8, with parameters defined by Equation 9,10,11), where *I* is the instrument inertia and *b* is determined by the

specific instrument and geometry used, can be calculated by the angular velocity (*Ω)*, torque(*T*), shear rate (*Ÿ*) and shear stress (*σ*) as *Ÿ T/ Ω σ.*

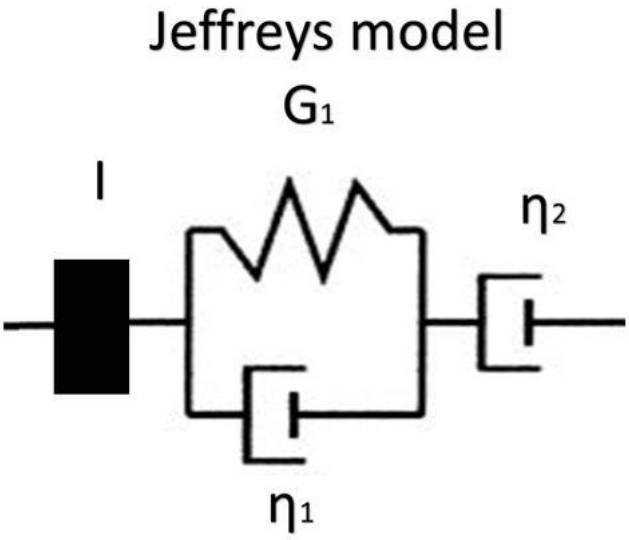

Figure 2.4. Schematic illustration of a linear viscoelasticity Jeffreys model. It consists of a Kelvin–Voigt element (a spring and a dashpot in parallel) in series with a dashpot and an instrument inertia element.

$$J = \frac{t}{\eta_2} - B + e^{-At}\{B\cos(\omega t) + \frac{A}{\omega}[B - \frac{1}{\eta_1 A}]\sin(\omega t)\} \quad \textbf{Equation 8}$$

$$A = \frac{G_1 + \eta_1\eta_2 b/I}{2(\eta_1+\eta_2)} \quad \textbf{Equation 9}$$

$$B = \frac{\eta_1+\eta_2}{G_1\eta_1}(\frac{2AI}{\eta_2 b} - 1) \quad \textbf{Equation 10}$$

$$\omega = \sqrt{\frac{G_1 b}{I}\frac{\eta_2}{(\eta_1+\eta_2)} - A^2} \quad \textbf{Equation 11}$$

2.2.4 Magnetic Tweezer Measurements

To prepare fluorophilic glass slides, thin glass slides (25 mm × 60 mm) were plasma oxidized for 10 minutes and placed into a staining jar. An amount of 1 mL toluene pre-mixed with 30 µL trichloro (1H, 1H, 2H, 2H-perfluorooctyl) silane was added in a glass vial. The staining jar containing the glass slides and the glass vial with the silane solution were placed into a desiccator under vacuum for 5 min and then left under reduced atmosphere but sealed overnight. The fluorinated glass slides were washed with ethanol and dried in air before being cut into chips and placed into a petri-dish, where 5 mL of PBS (normally at pH 10.5 otherwise specified) was filled. Droplets of 100 µL fluorinated oil with PFBC at desired concentrations were deposited on top of the glass slide and formed a fluorinated oil droplet spreading over the entire substrate. An amount of 50 µL 10 mg/mL PLL solution (in DI water) was pipetted into the dish, making a final concentration of 100 µg/mL. After 1 hour incubation, the polymer solution was then diluted with PBS (pH 7.4) six times. Meanwhile, epoxylated dynabeads were diluted by 100 times in PBS, and 50 µL of which was homogeneously pipetted into the dish and left to incubate for 15 mins. The excess beads in the dish were removed by diluting with PBS (pH 7.4) six times before measurement.

The creep-recovery measurement was performed by magnetic tweezer, where the beads attached to the nanosheets were subjected to a force pulse with a magnitude of 6 nN (40 µm distance between the bead and the tip) and a duration of 30 seconds, and their trajectories recorded for a total of 1 minute per bead with a frame every 20 ms. Around 30 traces were obtained per dish. Bead tracking was achieved by MATLAB and fitted with a 6-element modified Burguer's model (Equation 7) described above.

2.2.5 X-ray photoelectron spectroscopy (XPS)

A 1 mL amount of fluorinated oil containing the pro-surfactant PFBC at 0.01 mg/mL was added in a 50 mL centrifuge tube with 2 mL of PLL solution of desired molecular weight (200 µg/mL, in pH 10.5 PBS).

The tube was vigorously vortexed to generate emulsion and subsequently left to incubate at room temperature for 1 h. The top liquid phase that above the settled emulsion was aspirated and replaced with DI water 4 times. Droplets of emulsion were then transferred to silicon substrates and left to dry in air. The samples were further washed by ethanol and dried in air before conducting the measurement.

XPS was performed via a Kratos Axis Ultra DLD electron spectrometer with a monochromated Al Kα source (1486.6 eV) operated at 150 W. A pass energy of 160 eV and a step size of 1 eV were used for survey spectra. For high energy resolution spectra of regions, a pass energy of 20 eV and a step size of 0.1 eV were used. The spectrometer charge neutralising system was used to compensate sample charging and the binding scale was referenced to the aliphatic component of C 1s spectra at 285.0 eV. The concentrations obtained (error less than ±10%) are reported as the percentage of that particular atom species (atomic %) at the surface of the sample (< 10 nm analysis depth) without any correction. The analysis area (0.3 × 0.7 mm^2), the angle of incidence and the beam intensity were kept constant for all measurements. To determine the functionalisation level of PLL, the molar mass of lysine repeat units before and after functionalisation with PFBC were used to predict a reference curve to which experimental data was compared.

2.2.6 Nanosheet Harvesting via Langmuir-Blodgett Deposition

To prepare fluorophilic substrates, mica sheets or silicon wafers (11 mm × 11 mm) were plasma oxidized for 10 minutes and placed in a petri dish. An amount of 1 mL toluene pre-mixed with 30 µL trichloro (1H, 1H, 2H, 2H-perfluorooctyl) silane was added in a glass vial. The petri dish containing the mica sheets or silicon wafers and the glass vial with the silane solution were placed into a desiccator under vacuum for 5 min and then left under reduced atmosphere but sealed overnight. The fluorinated sheets or wafers were washed with ethanol and dried in air.

20 mL of fluorinated oil containing PFBC at the relevant concentration were pipetted into the tray of a Langmuir-Blodgett trough (Kibron). The functionalised substrates was clamped by the dip coater combined with the instrument, then was lowered to be perpendicularly fully immersed into the oil phase, and 60 mL of DI H_2O was added dropwise on the top of the oil phase. To form a nanosheet at the interface, 600 µL PLL solution (10 mg/mL in DI H_2O) of desired molecular weight was pipetted into the aqueous phase, making a final concentration of 100 µg/mL. After an overnight incubation, the PLL nanosheet was harvested by lifting the substrate completely out of the top phase via the clamp at a speed of 0.5 mm/min.

For imaging, the mica sheet was used as the substrate, and the conjugated PLL that prepared as described in 2.2.2 was mixed with normal PLL at 1:9 ratio and pipetted into the aqueous phase at the final concentration of 100 µg/mL. After harvesting the nanosheet as described above, the mica was placed in a well of 24-well plate and imaged by Leica DMI4000 fluorescence microscopy.

2.2.7 Ellipsometry

The thickness of nanosheets harvested via Langmuir-Blodgett deposition on silicon wafers (as in 2.2.6) was monitored by spectroscopic ellipsometry (JA Woollam, SE). The measurement was individually conducted in dry condition on the silicon wafer after plasma and after the fluorination treatment. When the nanosheet was harvested, the measurement was also conducted in DI H_2O and PBS. For wet ellipsometry measurements, the wafer was placed in a chamber where 6 mL of the corresponding solution was gently injected. In each measurement, three different positions were measured.

2.2.8 Statistical Analysis

Statistical analysis was carried out using Origin 2019 through one-way ANOVA with Tukey test for posthoc analysis. Significance was determined by * $P < 0.05$, ** $P < 0.01$, *** $P < 0.001$ and n.s., non-significant.

2.3 Results and Discussions

2.3.1 Impact of Pro-surfactant on Protein Assembly at Liquid Interface

2.3.1.1 Impact of PFBC on FBS Assembly

As a common composition in cell culture medium, FBS adsorption to the surface of liquid-liquid interfaces generated between fluorinated oil and PBS was studied via interfacial rheology. As shown in time sweep experiments (Figure 2.5A), upon the injection of 10% FBS after 900 s, the storage shear modulus was rapidly increased roughly by two orders of magnitude, and reached a plateau within 30 min. The presence of 0.01 mg/mL PFBC promoted an increase in the modulus significantly higher than without (31.5 ± 2.8 mN/m and 16.2 ± 1.9 mN/m, respectively). PFBC dependent variations were also found in stress relaxation (Figure 2.5C) measurements where significantly higher stress retention was found in FBS-assembled interfaces in the presence of PFBC. Based on amplitude sweeps measurements, an oscillation stress-strain curve (Figure 2.5D) was plotted up to the point where fracture occurs (the limit within linear viscoelastic region) and toughness was calculated as the total area below the curve. The resilience represents the maximum energy the nanosheet can adsorb during elastic deformation, calculated as the area below curve up to elastic point (the point where the slope is significantly decreased). Similarly, the toughness and resilience were also significantly improved when PFBC was introduced. These findings suggest that PFBC assisted FBS assembly at the interface, and that its coupling with FBS generated a stiffer, yet more elastic, tougher and more resilient interfaces.

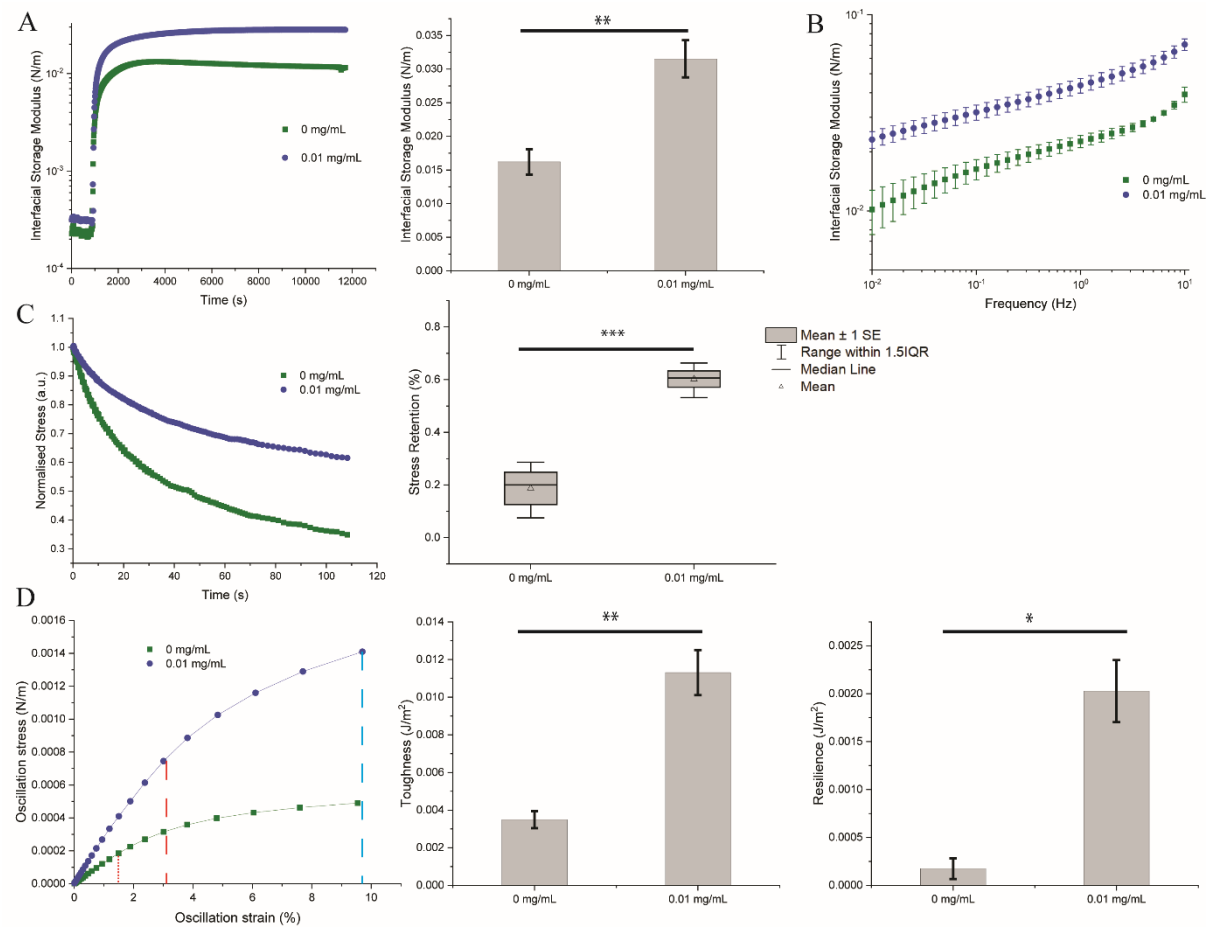

Figure 2.5. Interfacial mechanical properties of interface between Novec 7500 containing PFBC (0 and 0.01 mg/mL) and PBS containing 10% FBS. (A) Representative time sweep measurement profiles (left) and the corresponding interfacial shear moduli (right), (error bars are s.e.m.; n=4). (B) Frequency sweep measurement profile. (C) Representative stress relaxation curves for different PFBC concentrations (left) and summarised stress retentions obtained from the corresponding curves (right), (error bars are s.e.m.; n=4). (D) Representative oscillation stress-strain curves (left) and summarised toughness (middle; calculated as the area within the curves and the blue dash line in the oscillation stress-strain curves) and resilience (right; calculated as the area within the curves and the red dash lines in the oscillation stress-strain curves), (error bars are s.e.m.; n=4).

2.3.1.2 Impact of PFBC on PLL Assembly

Apart from globular proteins such as albumin present in FBS, PFBC was found to assist the adsorption of PLL at the Novec 7500 and PBS interface as well. All of the five concentrations (0, 1.25, 2.5, 5 and 10 µg/mL) that have been explored showed very similar time sweep profiles (Figure 2.6A). However, it is noticeable that the presence of PFBC accelerated PLL assembly, higher concentrations resulting in stiffer interfaces. The adsorption of PLL took a much longer time to equilibrate, owing to the modest

hydrophobicity and the less compact structure of PLL which would need a longer time to adsorb and unfold than more hydrophobic and more compact globular proteins, such as albumin. However, significantly higher plateau values were observed in PLL than in FBS (without PFBC, 45.7 ± 6.6 mN/m v.s. 16.2 ± 1.89mN/m; with PFBC, 1522 ± 115 mN/m v.s. 31.5 ± 2.8 mN/m). This implies PLL adsorption to the interface is significantly different to that of proteins contained in FBS, perhaps involving higher degree of cross-linking or network formation and more closely packed assemblies (amide formation). Interestingly, stress retention was reduced compared to those observed for FBS (Figure 2.5C), with trends showing weaker retentions at higher PFBC concentrations resulting in less elastic interfaces (Figure 2.6C). A possible explanation for that is that at lower PFBC concentrations, the slower adsorption of PLL may result in lower densities at the available interface areas, resulting in more stretched but less densely packed PLL at the interface, inducing more cross-linking but less adsorption at the surface of oil therefore more elastic but softer in mechanics. Whereas for FBS, the adsorption occurred in a very fast manner at almost the same rate in with and without the presence of PFBC. This is in agreement with the proposal that PFBC is not driving the interfacial adsorption of proteins from FBS, in contrast to PLL. Moreover, as the unfolding of globular proteins (such as albumin, the main component) from FBS is limited, the protein density may dominate the elasticity rather than the unfolding, leaving stiffer and more elastic mechanics in the presence of PFBC. Frequency sweeps suggest that at 10 μg/mL of PFBC, the profile was the least frequency dependant (Figure 2.6B), suggesting less viscous nanosheets, more compact PLL assemblies. Although the oscillation stress-strain curves may indicate that higher PFBC concentrations lead to tougher and less resilient nanosheet, no significant difference was yet found (Figure 2.6D). Overall, the contrasting trends observed from the frequency sweeps and stress-strain profiles, compared to the stress relaxation profiles, suggested that multiscale mechanical and relaxation behaviours regulated the overall macroscale mechanics of nanosheet-reinforced liquid-liquid interfaces.

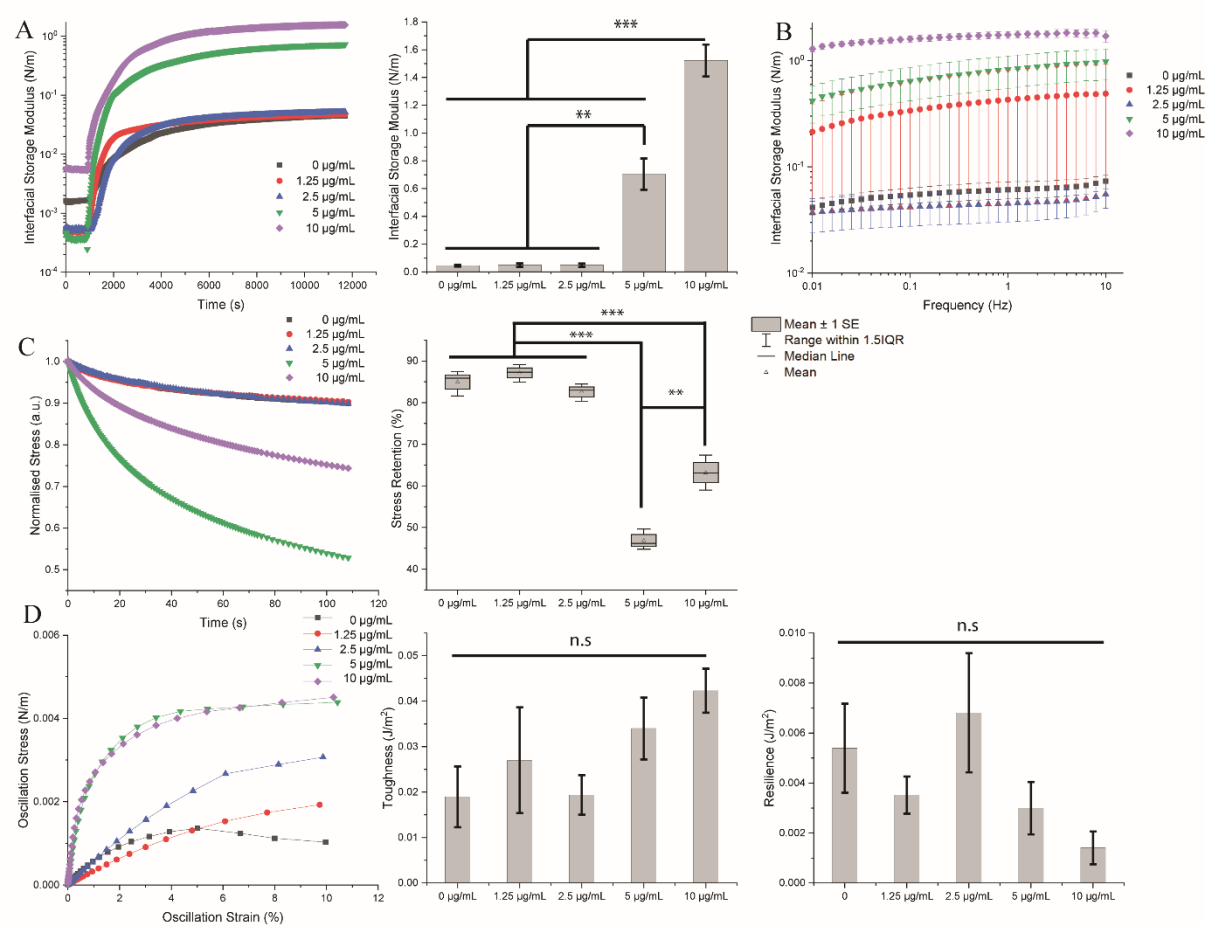

Figure 2.6. Interfacial mechanical properties of interface between Novec 7500 containing PFBC (0, 1.25, 2.5, 5 and 10 µg/mL) and pH 10.5 PBS containing 100 µg/mL PLL. (A) Representative time sweep measurement profiles (left) and the corresponding interfacial shear moduli (right), (error bars are s.e.m.; n=3). (B) Frequency sweep measurement profile. (C) Representative stress relaxation curves for different PFBC concentrations (left) and summarised stress retentions obtained from the corresponding curves (right), (error bars are s.e.m.; n=3). (D) Representative oscillation stress-strain curves (left) and summarised toughness (middle) and resilience (right) calculated from the corresponding curves, (error bars are s.e.m.; n=3).

To investigate the local mechanics of nanosheets assembled at liquid-liquid interfaces, their microscale mechanical behaviour was characterised with a magnetic tweezer assay, performing creep-recovery tests. The results of this assay are displayed as displacement against time (Figure 2.7C). Nanosheets generated at higher PFBC concentrations were found to be stiffer, as indicated by the lower initial creep displacement subjected to the same stress (Figure 2.7C) and confirmed by the quantification (Figure 2.7D), consistent with the interfacial rheology findings at the macroscale (Figure 2.6A). However, in contrast to the macroscale behaviour observed, it was also found that higher

concentrations gave significantly higher elasticity (Figure 2.7C, F). One possible explanation for that is the formation of domains during PLL nanosheet formation at higher PFBC concentrations, perhaps resulting from the stiffer and more brittle assemblies. Such finding is predictable as the protein layers consist of denatured, partly denatured and native proteins can be expected.[67] When the experiment performed at the microscale, beads on rigid domains display a more elastic behaviour while those on inter-domain spaces are more fluid-like, giving a bimodal distribution of viscosity (Figure 2.7E) and

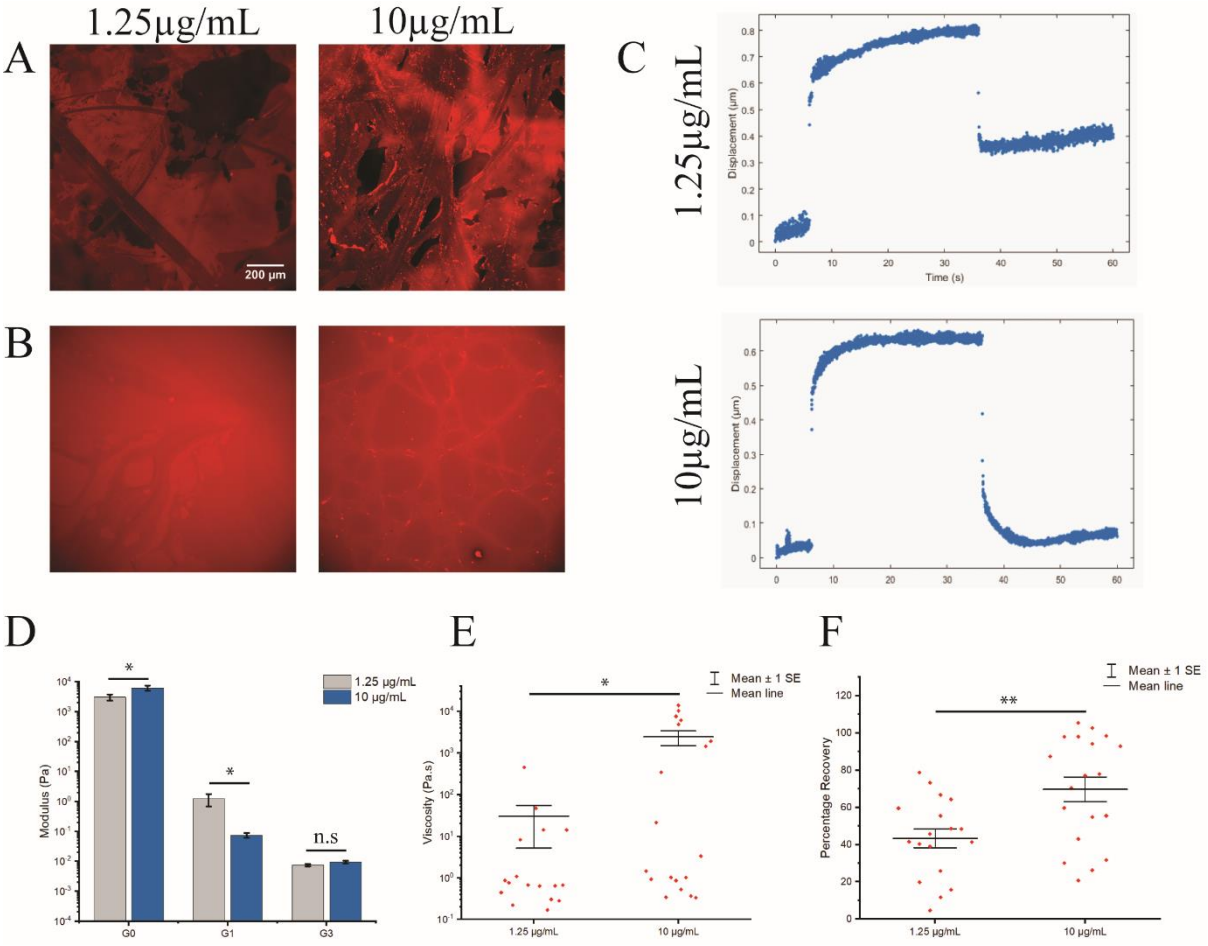

Figure 2.7. Characterisation of PLL assembled nanosheets assisted by PFBC at different concentrations (1.25 µg/mL and 10 µg/mL). (A) Epifluorescence images of PLL nanosheet harvested on mica via Langmuir-Blodgett Trough. (B) Epifluorescence images of PLL nanosheet assembled at the interfaces between Novec 7500 containing PFBC and PBS. (C) Creep-recovery curves obtained by magnetic tweezer at the interfaces between Novec 7500 containing PFBC (1.25 µg/mL, top, and 10 µg/mL, bottom) and pH 10.5 PBS containing 100 µg/mL PLL. A 6-element Burger's model was fitted to the raw data with viscoelasticity parameters quantified shown as (D) elastic modulus, (E) viscosity and (F) percentage recovery. Error bars are s.e.m.; n≥17.

elasticity (Figure 2.7F). At macroscale, the ring embedded at the interface, the fracture or brittleness of the inter-domain prevents the translation of such elasticity to the macroscale. Epifluorescence

images of PLL nanosheets also show less PLL fracture at higher PFBC concentrations than the lower (Figure 2.7A) and some domains like structure can be observed (Figure 2.7B). The low elasticity at lower PFBC concentration observed at the microscale, could possibly result from slippage or flow of PLL within the monolayer, as the nanosheet is more fluidic.

2.3.1.3 Impact of SBC/HDC on PLL Assembly

At the interfaces between PDMS and PBS, another pro-surfactant mixture (SBC and HDS mixed at 1:1 ratio) was used due to the hydrophobic nature of PDMS. The pro-surfactant also accelerated the adsorption of PLL and led to an increase in modulus to a higher level (Figure 2.8A). The resulting moduli

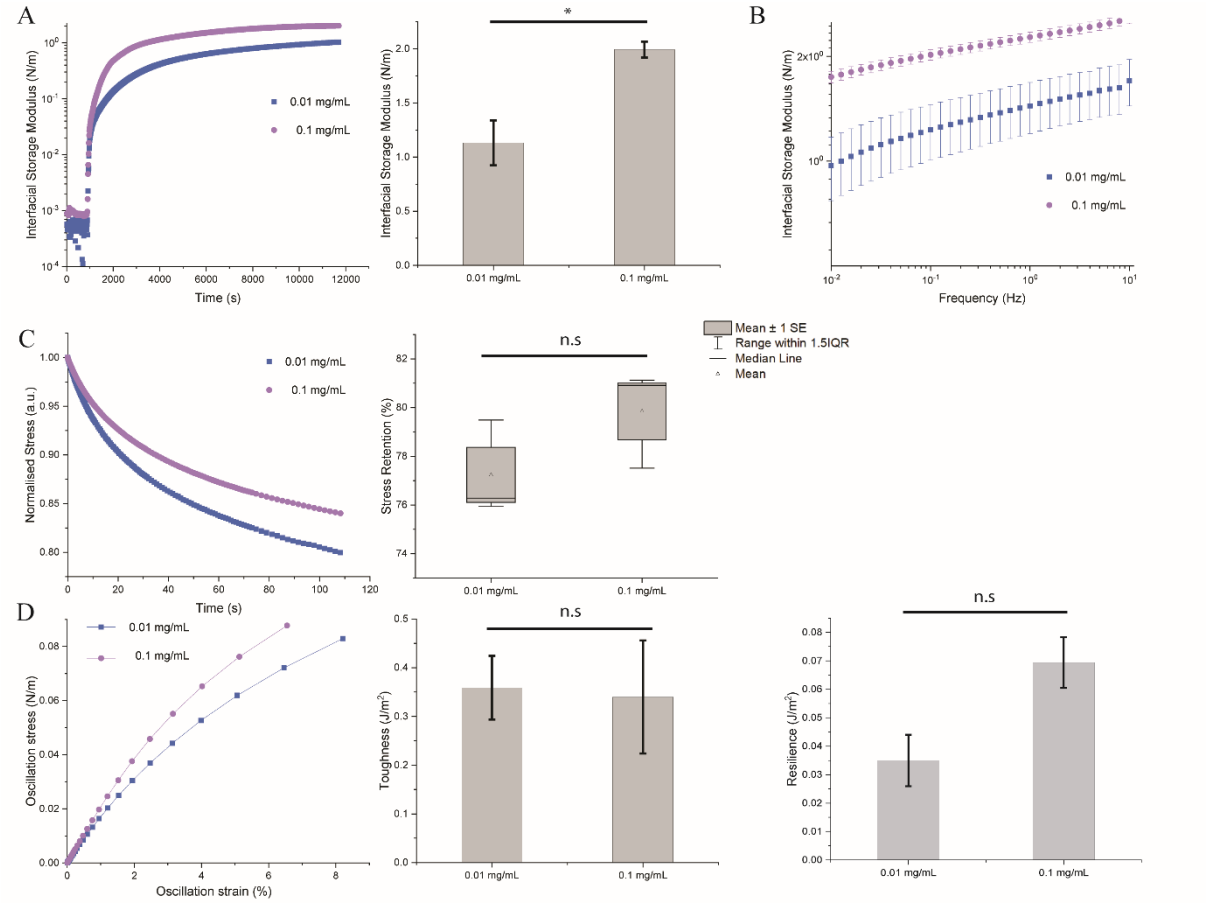

Figure 2.8. Interfacial mechanical properties of interface between PDMS containing SBC and HDC mixed at 1:1 ratio (0.01 and 0.1 mg/mL) and pH 10.5 PBS containing 100 µg/mL PLL. (A) Representative time sweep measurement profiles (left) and the corresponding interfacial shear moduli (right), (error bars are s.e.m.; n=3). (B) Frequency sweep measurement profiles. (C) Representative stress relaxation curves for different PFBC concentrations (left) and summarised stress retentions obtained from the corresponding curves (right), (error bars are s.e.m.; n=3). (D) Representative oscillation stress-strain curves (left) and summarised toughness (middle) and resilience (right) calculated from the corresponding curves, (error bars are s.e.m.; n=3).

were similar to those of PLL nanosheets assembled at Novec 7500-based interfaces with PFBC at similar concentrations. No significant difference was observed in terms of stress retention, toughness and resilience (Figure 2.8C and D). Interestingly, values of toughness and resilience from PDMS-based PLL nanosheets were orders of magnitude higher than that of Novec 7500-based system, this could be attributed to the higher flexibility and polar imbalance of HDC and SBC compared to PFBC, potentially impacting on the morphology of the nanosheets assembled as well as their mechanical behaviour.

2.3.1.4 Summary

As frequently found in the studies of protein adsorption at oil-water interfaces, non-reactive surfactants were often reported to compete with proteins for the interfacial areas, reducing the adsorption of proteins as well as the interfacial modulus.[92,93] Some others reported that the polarity of the oils also affects the unfolding of proteins at the interface, as higher oil polarity often promotes stronger interaction with outer hydrophilic residues of proteins such as albumins and β-lactoglobulin, restricting protein unfolding and subsequently reduces the shear moduli of the protein layers.[83] However, in all the systems we tested, though polar as those acyl chloride-based pro-surfactants are, they all helped to stiffen the nanosheets formed at the interface. This is due to the reaction between acyl chlorides of the pro-surfactants and amine residues in the proteins assembling, forming pro-surfactant and protein couplings at the interface. Higher pro-surfactant concentration obviously assists and accelerates the formation of such couplings therefore resulting higher moduli. Instead of relying on protein bulk concentrations in controlling the adsorption rate,[243] the pro-surfactant concentration can also be adjusted to control the rate of adsorption and subsequently control protein unfolding. Different mobility and flexibility resulted by different pro-surfactant structures may also contribute to different interfacial mechanical properties. The interaction between the couplings also provides physical crosslinking that is expected to alter the viscoelastic behaviour of nanosheets but its impact on toughness and resilience is not pronounced.

2.3.2 Impact of pH on Protein Assembly at Liquid Interfaces

Since PLL displays a conformational change in response to different pHs, the role of pH in PLL assembly was investigated. At higher pH, the assembly of PLL nanosheets resulted in increased interfacial storage moduli (Figure 2.9A). As PLL has an isoelectric point in the range from 9 to 11,[68,74] PLL should be more deprotonated and neutralised at a higher pH (around pH 10.5), which leads to more compact shape with reduced steric hindrance and electrostatic repulsion between polymers,[68] accelerating the assembly of PLL. This is in consistent with other studies, where the random coil structure PLL formed at lower pH has significantly lower coverage density than those with α-helix and/or β-sheet structures

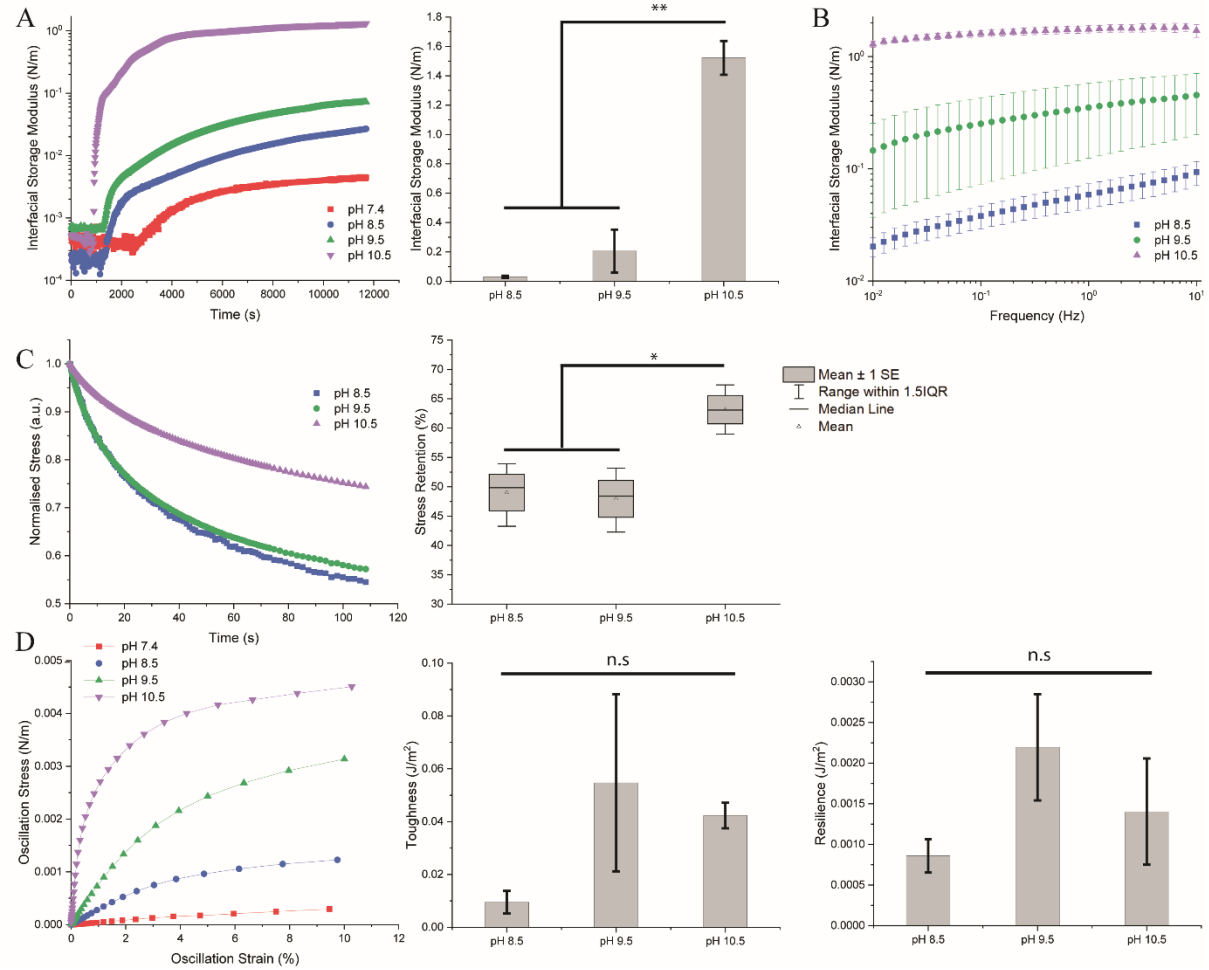

Figure 2.9. Interfacial mechanical properties of interface between Novec 7500 containing 0.01 mg/mL PFBC and PBS at different pH (pH 8.5, 9.5 and 10.5) containing 100 µg/mL PLL. (A) Representative time sweep measurement profiles (left) and the corresponding interfacial shear moduli (right), (error bars are s.e.m.; n=3). (B) Frequency sweep measurement profiles. (C) Representative stress relaxation curves for different pHs (left) and summarised stress retentions obtained from the corresponding curves (right), (error bars are s.e.m.; n=3). (D) Representative oscillation stress-strain curves (left) and summarised toughness (middle) and resilience (right) calculated from the corresponding curves, (error bars are s.e.m.; n=3).

at higher pH.[244] More importantly, in this neutral state, lysine residues are able to form covalent bonds with acyl chloride, resulting in amide formation. It was also reported that the discharge of amide groups in high pH solution induces an α-helix structure with hydrogen bonds, leads to a rigid rod structure,[68,72] which was also suggested by significantly higher dynamic viscosity observed at higher pH (Figure 2.10), as globular conformation usually significantly more viscous than random coil conformation.[67] By contrast, the protonated lysine residues at lower pH can hardly react with the pro-surfactant due to the electrostatic repulsion or even dissociate from the interface, leaving more viscoelastic (Figure 2.9B) and less elastic (Figure 2.9C) nanosheets. However, it remains unclear why such difference did not translate into significant differences in toughness and resilience (Figure 2.9D).

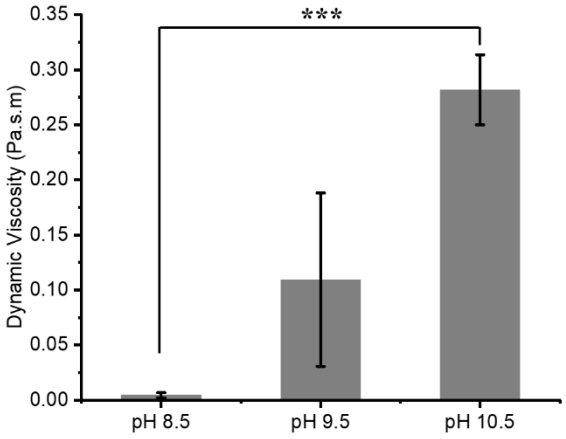

Figure 2.10. PLL nanosheets assembled at higher pH display higher dynamic viscosity. (Error bars are s.e.m.; n=3).

In light of the impact of pH on PLL adsorption at the interface, we further looked into whether the mechanical properties of adsorbed PLL nanosheets at the interface would still be affected by switching pH from 10.5 to 7.4. PLL nanosheets were adsorbed at pH 10.5 (the pH PLL was fully adsorbed compare to others as shown above), then was washed with pH 7.4 PBS to neutralise the pH as well as remove excess PLL in solution, a stress relaxation test was conducted before and after the washing step. As shown in Figure 2.11A, the washing step (neutralising pH) made little change on the stress relaxation profile, except for slightly reduced residual stress, which may be resulted from the removal of excess

PLL or loosely bound PLL in the solution. No significant difference was found on stress retention (Figure 2.11B), confirming that neutralising pH has little impact on the mechanics of adsorbed PLL nanosheets once they are covalently bind to the pro-surfactant at pH 10.5.

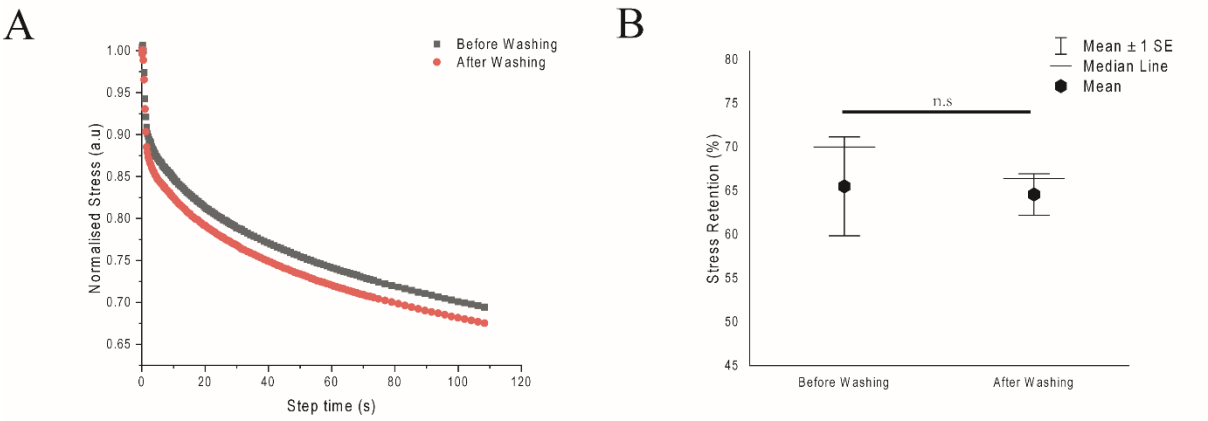

Figure 2.11. Neutralising pH has little impact on the mechanics of PLL nanosheets adsorbed at pH 10.5. (A) Representative stress relaxation curves for adsorbed PLL nanosheets at pH 10.5 (before washing, black) and after being neutralised by pH 7.4 PBS (after washing, red). (B) Summarised stress retentions obtained from the corresponding curves (right), (error bars are s.e.m.; n=3).

2.3.3 Impact of Molecular Weights on Protein Assembly at Liquid Interface

With PFBC concentration fixed at 0.01 mg/mL and PBS pH fixed at 10.5, the adsorption of PLL chains with different Mw was also investigated. Most of these polymers presented very similar time sweep profiles and interfacial storage moduli except for the lowest Mw (1-5 kDa), whose modulus was significantly lower than the rest (Figure 2.12A). A possible explanation for this could be the lack of sufficient interlocking or cross-linked PLL domains associated with low Mw chains. It has also been reported that mass density of PLL adsorbed at the interface was lower with shorter PLL chain length,[68] which may also result in reduced moduli. The stability of emulsions was consistent with this explanation, as 1-5 kDa PLL failed to form stable emulsions (Figure 2.13A), suggesting insufficient steric hindrance to coalescence. However, it was surprising that 1-5 kDa PLL maintained a high stress retention (Figure 2.12C), indicating high elasticity. Although such softer but more elastic PLL nanosheets were also found in those formed by lower PFBC concentrations (Figure 2.6) and the cause of such may be explained by the unfolding of PLL. As less sterically hindered, 1-5 kDa PLL chains could

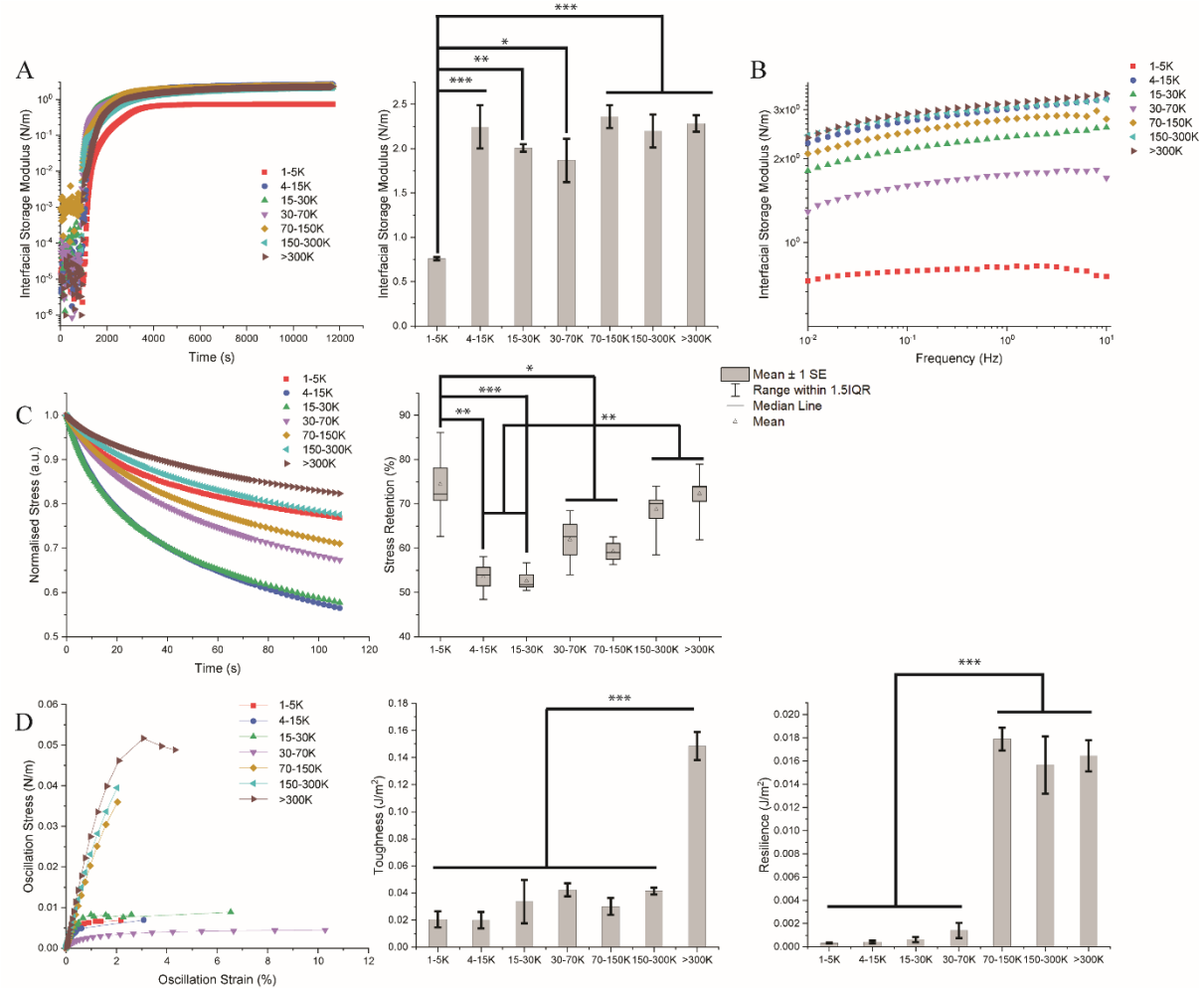

Figure 2.12. Interfacial mechanical properties of interface between Novec 7500 containing 0.01 mg/mL PFBC and pH 10.5 PBS containing 100 µg/mL PLL at different Mws (1-5, 4-15, 15-30, 30-70, 70-150, 150-300 and >300 kDa). (A) Representative time sweep measurement profiles (left) and the corresponding interfacial shear moduli (right), (error bars are s.e.m.; n≥3). (B) Frequency sweep measurement profiles. (C) Representative stress relaxation curves for different PLL molecular weights (left) and summarised stress retentions obtained from the corresponding curves (right), (error bars are s.e.m.; n≥3). (D) Representative oscillation stress-strain curves (left) and summarised toughness (middle) and resilience (right) calculated from the corresponding curves, (error bars are s.e.m.; n≥3).

more fully unfold than longer chains, inducing higher degree of networking and higher elasticity. This explanation is supported by the frequency sweep measurements (Figure 2.12B) as a less frequency dependant modulus suggests more extended crosslinked networks. However, it should also be noted that the reduced modulus observed for short chain PLL nanosheets may also resulted in too fast relaxation to be quantified via our assay.

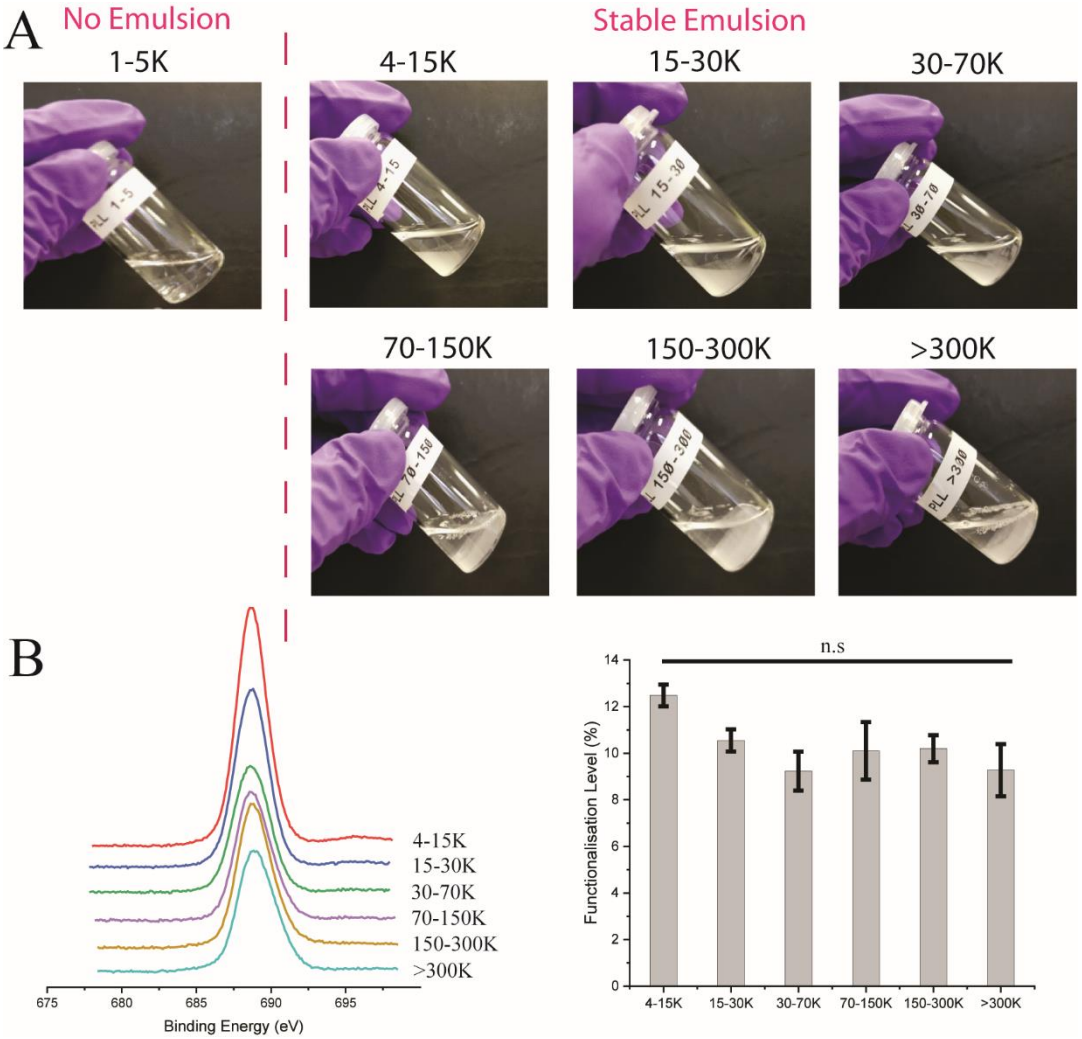

Figure 2.13. Characterisation of different Mw PLL ((1-5, 4-15, 15-30, 30-70, 70-150, 150-300 and >300 kDa)) assembly at the interfaces. (A) Images of emulsions formed by Novec 7500 containing PFBC and 10.5 PBS containing PLL. (B) XPS spectra (F 1S) obtained for dried emulsions (right) and summarised functionalisation level of the corresponding PLL (left), (error bars are s.e.m.; n=3).

In addition, amongst all the stable emulsions, it is worth mentioning that emulsions became more sticky, with restricted flow, and more likely to aggregate at the bottom of a vial, at higher molecular weights (Figure 2.13A). This might be related to entanglement caused by longer polymer chains or the formation of intermolecular (and inter-droplets) physical crosslinks and/or β-sheets.[72] Such entanglement or intermolecular β-sheets could also contribute to higher elasticity as the incremental Mw leads to incremental stress retention (Figure 2.12C). XPS analysis of the resulting PLL nanosheets collected from emulsions revealed comparable levels of PFBC functionalisation for all Mw tested (near

10%, Figure 2.13B), suggesting comparable levels of covalent coupling of the pro-surfactant to PLL. This is compatible with the similar storage moduli observed for all molecular weight PLLs. Although significantly tougher nanosheets were only assembled by PLL over 300 kDa, significantly more resilient nanosheets were found in nanosheets assembled by PLL over 70 kDa.

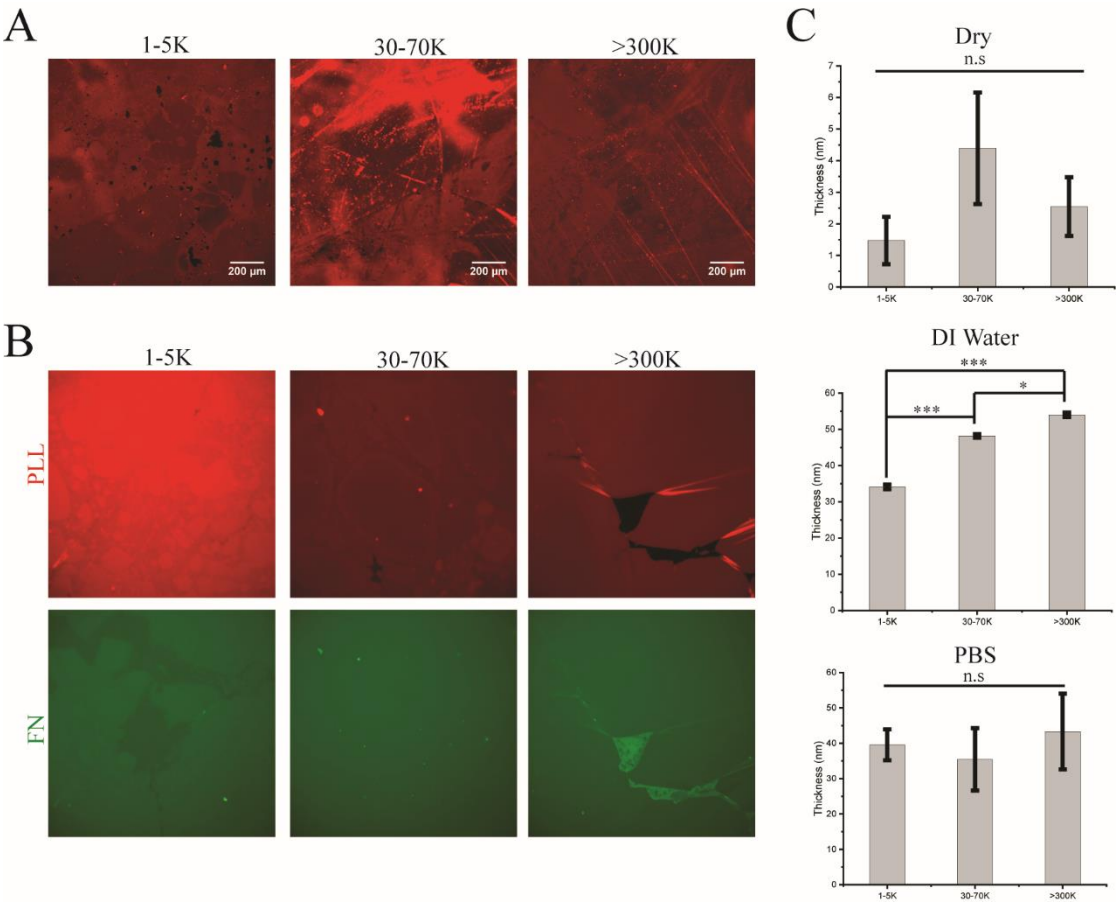

Figure 2.14. Characterisation of different Mw (1-5, 30-70 and >300 kDa) PLL assembled nanosheets. (A) Epifluorescence images of PLL nanosheet harvested on mica via Langmuir Blodgett Trough. (B) Epifluorescence images of PLL/FN nanosheet assembled at the interfaces between Novec 7500 containing 0.01 mg/mL PFBC and PBS. (C) Summarised thickness of different Mw PLL nanosheet harvested on silicon wafer via Langmuir Blodgett Trough, measured by ellipsometry in dry (top), DI water (middle) and PBS (bottom), (error bars are s.e.m.; n=3).

Interestingly, even though 1-5 kDa PLL formed relatively softer nanosheet, epifluorescence images (Figure 2.14A and B) showed that the adsorption densities were comparable to the others molecular weight PLLs. This implies that the weaker modulus of low Mw PLL nanosheets may be due to the lack of interlocking of polymer chains. Some domain-like structures can be observed at the interfaces with

1-5 and 30-70 kDa PLL, but not with >300 kDa PLL, and were also seen with FN (Figure 2.14B), indicating weaker PLL assembly at inter-domain areas.

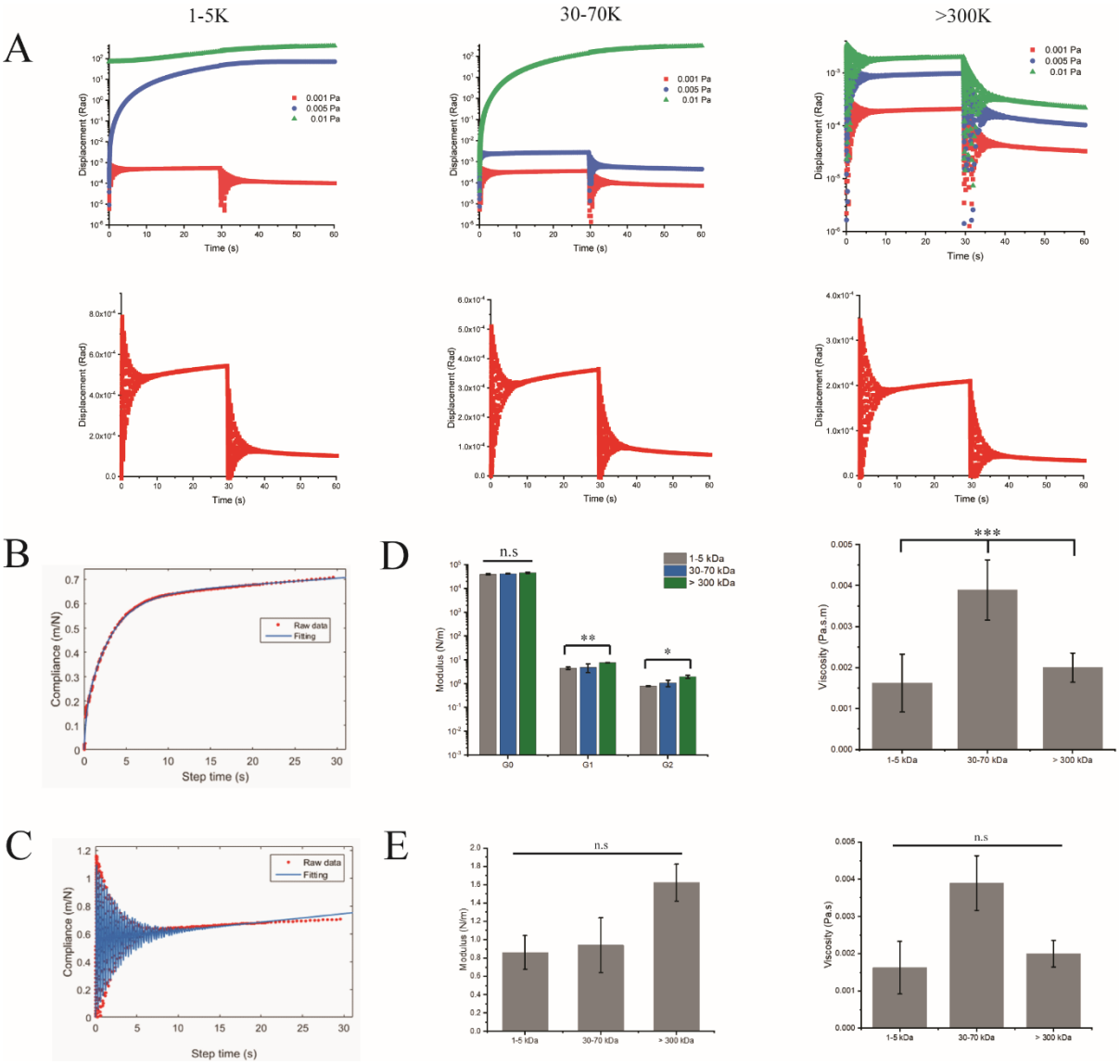

Figure 2.15. Creep experiments via interfacial rheology at the interfaces between Novec 7500 containing 0.01 mg/mL PFBC and pH 10.5 PBS containing 100 µg/mL PLL at different Mws (1-5, 30-70 and >300 kDa). (A) Representative creep and recovery curves at different oscillation stresses (top) and at stress of 0.001 Pa alone (bottom). (B) Representative creep curves fitted with a 6-element Burger's model and (D) the corresponding viscoelasticity parameters (elastic modulus, G_0, G_1 and G_2, left; and viscosity η, right). (C) Representative creep curves fitted with a modified Jeffreys model and (E) the corresponding viscoelasticity parameters (elastic modulus G_1, left; and viscosity η_1, right.). Error bars are s.e.m.; n=3.

Ellipsometry measurements were carried out to characterise the thickness of PLL nanosheets harvested on silicon substrates. The dry thickness of nanosheets were around 3 nm (Figure 2.14C),

comparable to other PLL monolayers studied via ellipsometry,[101,214,216,218] but much shorter than our previous study on nanosheets harvested from dried emulsions via AFM, which was around 14 nm.[234] Measurements carried out in DI water suggested significantly thicker layers for higher Mw PLLs, as longer polymer chains swell more. Maldonado et al. also suggested that α-helix could be truncated by lysine yielding with higher Mw, giving more elongated structures.[72] However, such differences in thickness were not observed in PBS, presumably due to electrostatic screening and partial collapse of chains. Therefore, more compact structures were perhaps the reason for higher stiffness at higher Mws.

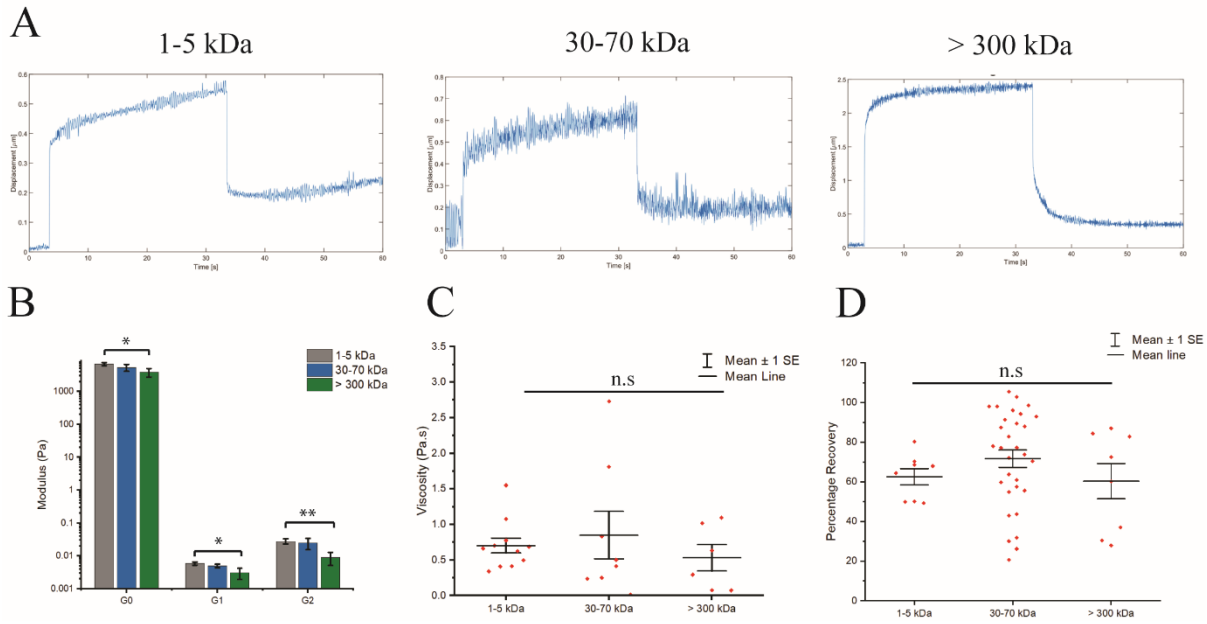

Figure 2.16. Creep experiments via magnetic tweezer at the interfaces between Novec 7500 containing 0.01 mg/mL PFBC and pH 10.5 PBS containing 100 µg/mL PLL at different Mws (1-5, 30-70 and >300 kDa). (A) Representative creep and recovery curves and the corresponding viscoelasticity parameters extract from a 6-element Burger's model fitting (B) elastic modulus (G_0, G_1 and G_2); (C) viscosity (η); and (D) percentage recovery. Error bars are s.e.m.; n≥7.

Creep-recovery experiments were performed at both macroscale via interfacial rheology and microscale via magnetic tweezer. The stress was sequentially increased in the test performed by interfacial rheology. 1-5 kDa nanosheets broke at a stress of 0.005 Pa and 30-70 kDa nanosheets broke at a stress of 0.01 Pa. PLL with Mw > 300 kDa maintained intact nanosheets at all stress investigated,

further confirming the difference in yield strength observed (Figure 2.15A). At the macroscale, initial displacements were inversely proportional to the PLL Mw, when subjected to 0.001 Pa stress, in agreement with the incremental moduli as a function of Mw. To overcome the creep ringing issue, which is a ramped oscillatory strain response at the beginning of the creep experiments via a stress-controlled rheometry,[241,242] a Jeffreys model with an instrument inertia was also introduced in addition to the 6-element Burger's model that commonly used to described a gel-like structure to fit the results (a Burger's model was used for the fitting first but did not fit well, thus we introduced an extra Kelvin–Voigt element to improve the fitting). Similar to other reports used Jeffreys model to fit creep ringing, the model fits well at short time but progressively deviates from the raw data as the total strain accumulates.[240] In general, both Burger's model (Figure 2.15B) and Jeffreys model (Figure 2.15C) fittings displayed a very similar trend that higher Mw PLL nanosheet had higher elastic modulus compared to low Mw PLL (Figure 2.15D and E), but the difference was not significant when the instrument inertia was taken into account (Figure 2.15E). However, the trend was exactly the opposite at the microscale (Figure 2.16A, B). This was possibly an indication of the stretching of polymer chains by beads independent of the nanosheet modulus. It was also worth noting that the viscosity and percentage recovery displayed a bimodal distribution (Figure 2.16C, D), which was again an indication to the formation of different domains. After the initial deformation, the profile obtained for > 300 kDa PLL nanosheets almost flattened while that of lower Mw PLL nanoshets experienced a rather pronounced increase (Figure 2.16A), which suggests that nanosheet formed by > 300 kDa PLL was more solid like than fluid like. Overall, although the creep curves presented similar profiles at different scales that suggests nanosheets behave similarly macroscopically and microscopically, there were some microscale variations that were not probed at macroscale.

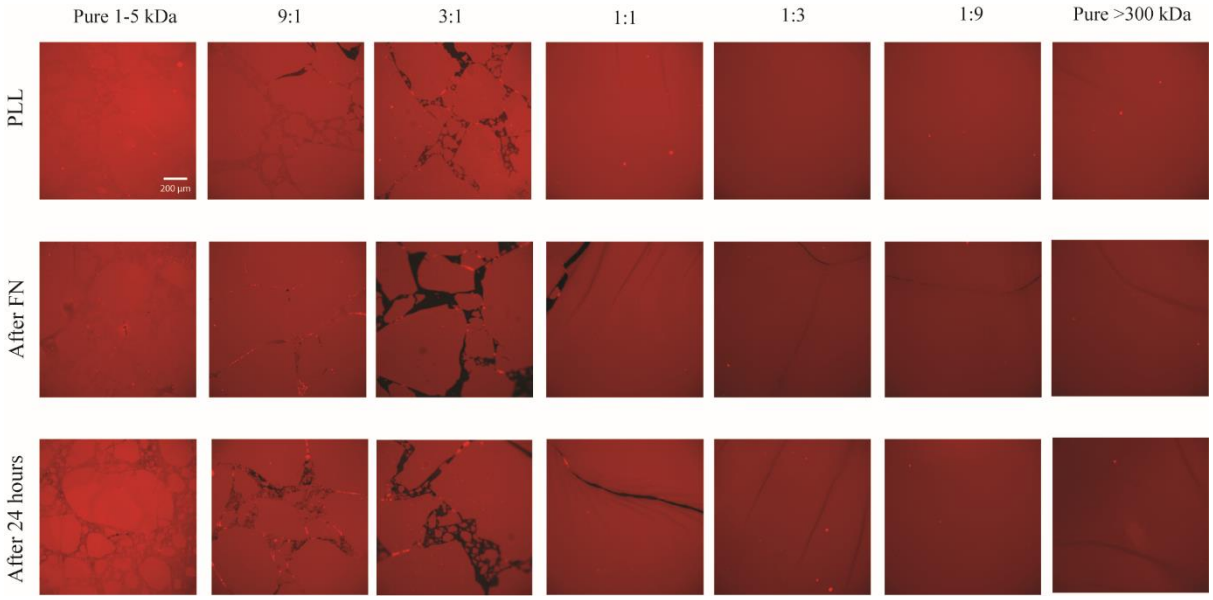

Figure 2.17. Epifluorescence images of 1-5 kDa and > 300 kDa PLLs mixed at different ratios assembled at the interfaces between PBS and Novec 7500 containing 0.01 mg/mL PFBC. Images were taken after PLL incubation (top), then FN incubation (middle) and after 24 hours (bottom).

We also mixed 1-5 kDa PLL with > 300 kDa PLL at different ratios, and imaged interfacial nanosheets under epifluorescence microscopy. As shown in Figure 2.17, fractures were spotted when a small amount of the high Mw PLL was introduced, however, when the percentage of high Mw was increased, more intact and continuous nanosheets were formed. Small domains were also observed at the interfaces with higher 1-5 kDa contents, and became much clearer after FN incubation and after 24 h. Apart from such PLL/FN pairs, similar finding was also reported in PLL/HA pairs on a solid surface when HA was added on PLL monolayer.[103] It was attributed to the complex coacervates formed by the interaction between HA and PLL. Upon the increase of > 300 kDa PLL content, the domains became larger. From 50% onwards, the domains disappeared and nanosheets appeared continuous. In some protein-surfactant mixtures, it has been reported that the interfacial nanosheet networks formed by globular proteins can be penetrated by low molecular weight surfactants through a process called 'orogenic displacement', through which the surfactants self-assemble into small domains among the network and gradually expand in size and eventually disrupt the protein network.[240,245] This theory may also be used to describe the domain formation among nanosheets formed by different Mw PLL

mixtures. Since only limited PLL residues (roughly 10%) are able to react with the PFBC thus pinned at the interface according to the XPS measurements (Figure 2.13B), those residues that do not bound to the PFBC may penetrate into the network and assemble into domains. This could possibly explain the reason that the higher >300 kDa PLL contents had larger domains, as it is more difficult for higher Mw PLL to penetrate into the network.

2.4 Conclusions

The aim of the work in this chapter is to design mechanically strong protein nanosheets to support cell culture at liquid-liquid interfaces. We started with nanosheets formed from FBS which is often used in cell culture media. We found that nanosheets with relatively weak storage moduli at the interfaces between PBS and Novec 7500 even with the presence of the pro-surfactants PFBC. Therefore, a further modification of the interfaces would be needed before being presented for cell culture. In light of the mechanical requirements as well as its biocompatibility and bioactivity (In particular for extracellular matrix protein adsorption and cell adhesion), PLL was selected as the candidate for such purpose. The interfacial storage moduli of PLL varied from 5×10^{-3} N/m to 2.5 N/m, as confirmed by interfacial shear rheology, under different conditions including pro-surfactant concentrations, oil phase, pH and PLL Mw. As PLL adsorption on liquids was a rather complicated process, those factors can easily affect the mechanical performance by changing the interfacial interactions sustained by nanosheets. This must be taking into careful consideration in designing the naonsheets. It is worth noting that even the softest PLL nanosheets still had higher moduli than that of FBS nanosheets. Despite the relative homogeneous adsorption of PLL at the interface, the microscale creep experiments reveal there is a heterogeneous in viscosity and elasticity. This is also found in other proteins in similar adsorption experiments in literature,[67] and it was mostly attributed to the mixture of proteins of different denaturation levels in the adsorbed layers. Knowing the high functionalisation level of PLL (around 10%) and the small domain-like structures observed in the PLL nanosheets, we propose that the

formation of PLL-surfactant rafts at liquid-liquid interfaces resulted in nanosheets with high rigidity.[89] In addition to interfacial storage moduli, PLL nanosheets also exhibited very different stress retention or elasticity behaviour at the interface where higher elasticity nanosheets had lower moduli. It was also found that although pro-surfactants and pH had impact on PLL assembly, as well as stiffness and viscoelasticity, they had very little influence on toughness and resilience, for which Mw seems to contribute more.

Overall, we demonstrated the formation of PLL nanosheets with tunable interfacial storage moduli and viscoelasticity at liquid-liquid interface. These nanosheets provide a possible substrate to support cell culture on liquids. The detailed study of cell adhesion and proliferation at such interfaces is presented in the next chapter.

Chapter 3

Culture of Mesenchymal Stem Cells on Liquid interfaces Mediated by Protein Nanosheets

3.1 Introduction

The importance of cell adhesion to ECM in regulating cell behaviour and phenotype has been addressed extensively, particularly in the study of cell-material interactions.[1,4] Cell adhesion is mainly mediated by integrins, which are transmembrane heterodimeric surface receptors that connect intracellular and extracellular environments. Common ECM proteins binding to integrins include FN, LN, VN and COL. These proteins selectively bind to different integrin families. For example FN mainly binds to α5β1, αIIbβ3 and the αvβ integrins;[246] LN to α3β1, α6β1, α6β4 and α7β1;[247] VN to αvβ1, αvβ3, αvβ5 and αIIbβ3;[248] and COL to α1β1, α2β1, α10β1 and α11β1.[247,249] Thus, these proteins have been widely used for coating the surface of materials for biomedical applications. The organisation and presentation of these proteins to integrins have a great impact on cell adhesion, behaviour and, subsequently, cell phenotype. For example, mechanical,[7,250] topographical[251,252] and chemical modifications are among those properties that have been shown to play a key role in regulating cell adhesion, motility, proliferation and differentiation.[7,253] In the case of mechanics, the impact of substrate elasticity has been thoroughly investigated. A molecular clutch model has been widely used to explain the effects of matrix stiffness.[5,10,39,254] This model proposes that the actin retrograde flow exerts forces on integrins bound to the ECM, via adaptor proteins such as talin, resulting in their unfolding and further recruitment of vinculin, among other effectors. This behaviour is modulated by integrin binding strength, the density of ligands and the mechanics of the ECM. This results in the remodelling of the actin network, that is sufficiently stable to resist myosin-based contractility, and in the subsequent downstream signalling events, mediating further mechanosensing and mechanotransduction.[39–41] In the case of softer substrates where integrin mobility is not restricted, talin unfolding is not activated and downstream signalling ceased resulting in ECM detachment. Under such model, cell displays distinct adhesion behaviour in response to different elasticity[255] and subsequently leading to different differentiation lineages even in the absence of soluble induction factors.[7,253] However, whether substrate bulk mechanics controls cell fate regulation was challenged as the lack of cell response to PDMS with different stiffnesses was reported.[48] ECM molecule tethering

was proposed as an explanation for such finding as a loosely bound ECM on stiffer substrates was suggested to impair ECM mechanical feedback. Study of cell adhesion on substrates tethered with adhesive ligands with different lengths also revealed that cell adhesion was restricted on stiff substrate with RGD ligands linked by longer tethers, similarly to the lack of adhesion on soft subtrates.[49] Since most of the studies were conducted on elastic (solid or highly cross-linked hydrogel) substrates, the impact of viscoelasticity was not clear. In light of the importance of ECM presenting viscoelasticity in physical environments,[51,254,256] further study and a deeper understanding of the impact of viscoelasticity on cell adhesion is particularly important. Weak cross-linked hydrogel systems were therefore used to address the role of viscoelasticity in cell behaviour. By adjusting the initial combination of monomer acrylamide and cross-linker bis-acrylamide concentrations, Cameron et al. prepared a range of polyacrylamide (PAM) gels with similar storage moduli but different loss moduli and, hence, different creep characteristics.[257] They found that MSC motility, spreading area, proliferation and differentiation were promoted on surfaces displaying higher viscosity. Such difference was proposed to be the result of the reduction in contractile forces resulting from the inherent energy dissipation in substrates displaying high creep. Similar findings were also reported by Mooney's group,[254] as they used covalent and ionic cross-linking to regulate the elastic and viscoelastic properties of alginate gels, whilst retaining the comparable elastic moduli (at least in part of the range of frequency and strain probed). They observed enhanced U2OS cell spreading and focal adhesion formation on substrates displaying stress-relaxation. They also attributed this to the energy dissipation of viscoelastic interfaces and the requirement of cells to generate greater work than on purely elastic substrates of the same elastic modulus in order to spread. A later work reported by the same group used alginate-polyethylene glycol coupling to prepare hydrogels with extended relaxation time.[51] MSC spreading and proliferation were suppressed on slow relaxing gels but enhanced on the faster relaxing systems. In turn, adipogenesis and osteogenesis were also found to be promoted on gels with faster relaxation. These cell behaviours on rapid relaxing hydrogels were explained by the greater malleability of the hydrogels that enable substrate remodelling and ligand clustering by cells.

In these studies, it was hypothesised that one effect of stress-relaxation was to mediate integrin clustering and associated cell adhesion, via adaptor molecules involved in the clutch model.[5,41] This was further confirmed by a mathematical model.[41,51,254] Developed from such hypothesis, Ze Gong and colleagues[258] addressed the importance of the stress relaxation time of the substrates. They proposed that the maximum cell spreading would be achieved on highly viscous and low rigidity substrates with a relaxation time comparable to the life time of focal adhesions (10^{-1} to 10^{3} s) and clutch engagement time (around 1 s), so that clutch mediated spreading at the high initial stiffness could be maintained as actin retrograde flow was minimised via stress relaxation.

In light of the importance of ECM viscoelasticity, the culture of cells on liquid interface is particular interesting as the fluid and reconfigurable properties of liquids provide a more adaptive system than rigid substrates. It is also surprising as fast and complete relaxation should prevent energy storage and the activation of the molecular clutch. Keese and Giaever were the pioneers who reported the proliferation of fibroblasts at the surface of fluorinated and silicone oils.[127–129] Their work highlighted the importance of surfactant molecules to enable cell expansion, without developing on the nature of the structures assembled and the mechanisms enabling such cell proliferation, even with normal adherent fibroblasts, although they noted a change in interfacial mechanics.[128] Such system was later studied on other anchorage-dependent cell types in addition to fibroblasts, such as epithelial cells,[259] myoblast,[61,259] investigating their proliferation and differentiation on liquid substrates. Upon culture on fluorinated oil-based liquids, the myogenic differentiation of myoblast was suppressed,[61] and the osteogenesis, adipogenesis and chondrogenesis of MSCs were unchanged compared to TPS[260] while the neurogenesis was promoted,[62] although these results could not be repeated (presumably due to the lack of pro-surfactants in the work reported). These reports mainly focused on the chemistry of different fluorinated oils while the analysis and characterisation of interfacial mechanics were missing or insufficient. Previous works in our group studied the culture of HaCaT cells (I contributed to the interfacial rheology characterisation of FBS at liquid interface)[47,52] and keratinocytes[89] and MSCs (I contributed to the MSCs culture)[89] on pro-surfactant assisted protein nanosheets assembled at

fluorinated oil interfaces. This work highlighted the importance of interfacial, rather than bulk, mechanical properties in regulating cell adhesion and fate decision.

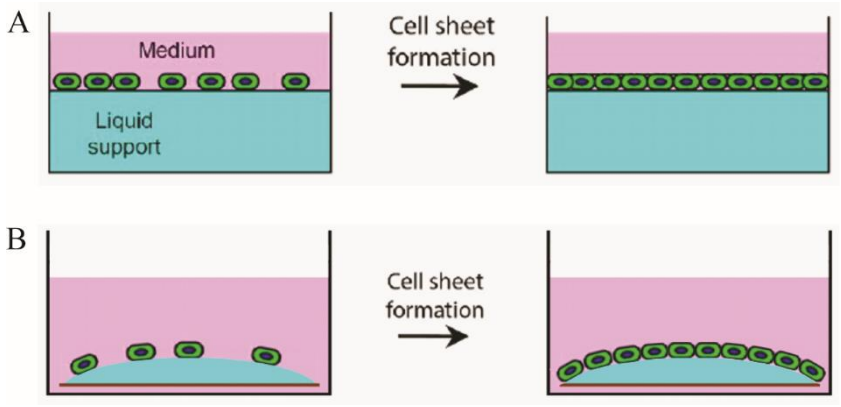

Figure 3.1. Schematic Illustration of Cell Culture on Oil Interface. (A) Cell culture on flat Novec 7500 interface. (B) Cell culture on oil droplet pinned on glass slides.

This chapter aims at culturing MSCs on nanosheets assembled at oil interfaces and describing the processes that regulated by the substrate mechanical properties. The interfacial mechanics of nanosheets has been characterised by interfacial rheology, showing clear dependency on protein type, pro-surfactant concentration and pH, as discussed in Chapter 2. The impact of these nanosheets on cell adhesion and proliferation are examined in this chapter. MSCs were cultured at the interfaces between the oil and the medium. Additionally, owing to the lighter mass density of non-fluorinated oils such as PDMS, the oil was pinned on glass slides via hydrophobic treatment (Figure 3.1), to allow simple imaging. Although previous reports from our group suggested successful culture of HaCaT cells on serum adsorbed oil interfaces (I contributed to the interfacial rheology characterisation of FBS at liquid interface),[47,52] it was not the case for adherent stem cells such as primary keratinocytes and MSCs, which typically required more adhesive environments. Hence, we hypothesise that poor proliferation was the result of insufficient cell adhesion to the oil surface. ECM proteins such as FN were therefore introduced in our system to promote cell adhesion. However, FN could not be introduced directly as it did not stabilise on liquid-liquid interfaces sufficiently. To tackle this issue, a PLL nanosheet was self-assembled at the interface in the presence of the pro-surfactant, allowing FN

electrostatically binding to the interface. Cell adhesion was studied via immunostaining of actin and FA markers such as vinculin, talin, paxillin and phosphotyrosine. MSCs were found to adhere on oil interfaces at levels comparable to those observed for solid substrates and hydrogel culture systems. We also demonstrated the expansion of cells on oil substrates, at similar rates to those observed on TPS, though the potential toxicity and the fracture of the nanosheets were found to be issues impairing the expansion of cells in some systems. Finally, based on the viscoelasticity of the nanosheets assembled interface and the corresponding cell proliferation, a correlation between the stress retention and the MSC proliferation was drawn, which we propose is an essential feature for the design of liquid-liquid interfaces for cell culture.

3.2 Materials and Methods

3.2.1 Materials and Chemicals

MSC (human bone marrow derived), MSC growth medium, freezing medium Cryo-SFM and accutase solution were purchased from PromoCell. PFBC, PBS, $NaHCO_3$ pellet, NaOH pellet, PLL hydrobromide (molecular weights: 1-5 kDa, 4-15 kDa, 15-30 kDa, 30-70 kDa, 70-150 kDa, 150-300 kDa and >300 kDa), Lys (from chicken egg white), toluene (anhydrous, 99.8%), DMSO, TEA, trichloro (1H, 1H, 2H, 2H-perfluorooctyl) silane, triethoxy(octyl) silane, SBC, HDC, BSA, GEL (from cold water fish skin), FN (from human plasma), paraformaldehyde (PFA), Triton X-100, tetramethyl rhodamine isothiocyanate phalloidin, 4,6-diamidino-2-phenylindole (Dapi), monoclonal anti-vinculin antibody from mouse, monoclonal anti-talin antibody from mouse and anti-phosphotyrosine antibody were purchased from Sigma-Aldrich. Live/Dead kit, VN were from Life Technologies. Fluorinated oil (Novec 7500) was from ACOTA. FBS was from PAA. COL (rat tail, type 1) was from First Link (UK) Ltd. HA was provided by GlaxoSmithKline. Cover glasses (25 × 60 mm) and pure ethanol were from VWR. PDMS (trimethylsiloxy terminated, viscosity 10 cSt) was from ABCR. Mr. Frosty™ freezing container, Alexa Fluor 488 NHS ester (succinimidyl ester), Alexa Fluor 488 goat anti-rabbit IgG (H+L) highly cross-adsorbed secondary

antibody, Alexa Fluor 488 goat anti-mouse IgG (H+L) highly cross-adsorbed secondary antibody, Hoechst 33342 (1 mg/mL) were purchased from ThermoFisher Scientific. Monoclonal anti-paxillin antibody from rabbit was from ABCAM. Sticky-slide 8 Well was from Thistle Scientific. Rapeseed oil was from Sainsbury. Blandol® White Mineral Oil was purchased from Sonneborn.

3.2.2 MSCs Culture

MSCs were directly cultured in MSC growth medium on a T75 flask. The flask was placed in an incubator with a humidified atmosphere (37 ℃ and 5% CO_2). Growth medium was completely replaced every two days. When a 70-80% confluence was reached, medium was aspirated and cells were washed with PBS to remove serum and protein traces and cells were detached through incubating 5 min with 4 mL accutase-solution at 37 ℃. Cells were then transferred to a centrifuge tube and centrifuged at 1,200 rpm for 5 min, the supernatant was aspirated and the cells were re-suspended in 10 mL growth medium and counted using a haemocytometer. For proliferation experiments, 5,000 cells were seeded per well, and half of the old medium was replaced by fresh medium every two days. For cell passage, 300,000 cells were seeded in a T75 flask. Cells were disposed after being passaged for more than six times. For cryopreservation, the harvested cells were re-suspended in Cryo-SFM freezing medium at a density of 5,000 cells/mL. 1 mL of cell suspension was transferred to each cryovial and stored in a Mr. Frosty™ freezing container. The container was kept at -80 ℃ for 24 hours before transferring the vials a cell bank filled with liquid nitrogen. The same batch of cells was not cryopreserved more than once.

3.2.3 Preparation of Fluorinated Oil-based Interfaces for Cell Culture

To generate flat interfaces, 24 well-plates were plasma oxidized via a plasma coater (Diener, 100% intensity) for 10 minutes. A solution containing 500 µL pure ethanol pre-mixed with 10 µL TEA and 10

µL trichloro (1H, 1H, 2H, 2H-perfluorooctyl) silane was added into each well. The well-plates were then sealed with parafilm and left overnight at room temperature. After 24 h, 500 µL of fluorinated oil containing PFBC at the desired concentrations was pipetted into the treated well after being sterilised twice with 70% ethanol and washed three times with DI water obtained from a Purelab® Chorus system. 1 mL of pH 10.5 PBS was added dropwise on top of the oil in each well, 1 mL of 200 µg/mL PLL (30-70 kDa unless otherwise specified) solution (in pH 10.5 PBS unless otherwise specified) was then added to the wells, making the final PLL concentration at 100 µg/mL in each well. After an hour incubation allowing the PLL nanosheet to form, the excess PLL solution was removed by diluting with PBS (pH 7.4) six times. For Lys, the final concentration was 1 mg/mL in pH 10.5 PBS. To promote cell adhesion, 1 mL of 20 µg/mL FN solution (in pH 7.4 PBS, making the final concentration 10 µg/mL) was pipetted on top of the PLL film and left for another hour incubation. For VN, FN/BSA mixture or BSA, the final concentrations were also at 10 µg/mL. The residual FN and other proteins were then washed out by diluting with PBS (pH 7.4) four times, after another two more dilutions with MSC growth medium, the interface was ready for cell culture.

In the case of the PLL-HA-COL nanosheet, 1 mL of 200 µg/mL HA solution (in pH 7.4 PBS, making 100 µg/mL the final concentration) was pipetted on top of the PLL film and left for another hour incubation. The residual FN was then washed out by diluting with PBS (pH 7.4) six times before 1 mL of 20 µg/mL COL solution (in pH 7.4 PBS, making the final concentration 10 µg/mL) was added. After 30 min incubation, the well was washed by diluting with PBS (pH 7.4) four times, after another two more dilutions with MSC growth medium, the interface was ready for cell culture.

For fluorescence imaging of PLL, Alexa Fluor 488-conjugated PLL was used instead of normal PLL. The conjugated PLL stock solution was prepared by dissolving PLL powder in 0.1M $NaHCO_3$ buffer and reacting with Alexa Fluor 488 NHS ester (succinimidyl ester) dissolved in DMSO, as suggested by the user manual. The conjugated PLL was mixed with normal PLL at 1:9 ratio and added into each well at

a final concentration of 100 µg/mL. The incubation and washing process was the same as the one described above.

3.2.4 Preparation of Non-fluorinated oil-based Interfaces for Cell Culture

Since the non-fluorianted oils used were lighter in mass density than the aqueous solution, the oils were pinned at the surface of hydrophobic slides. The hydrophobic glass slides were plasma oxidized for 10 minutes and placed into a staining jar filled with toluene containing 100 µL triethoxy(octyl) silane and 100 µL TEA. After 24 hours incubation, the glass slides were washed with ethanol and air-dried. The resulting hydrophobic glass slides were cut into 1 × 1 cm chips and placed into a 24-well plate. After being sterilized with 70 % ethanol, the wells were washed with PBS and filled with 2 mL pH 10.5 PBS. A 70 µL volume of non-fluorinated oil such as PDMS, mineral oil or rapeseed oil was pre-mixed with the corresponding pro-surfactants (mixture of SBC and HDC at different ratio) at the corresponding concentrations (100 µg/mL or 10 µg/mL) was added on the surface of the glass slides to generate droplets. 1 mL of 200 µg/mL PLL solution (in pH 10.5 PBS) was pipetted into each well to final concentration of 100 µg/mL, and incubated for 1 hour. The solution was then diluted with PBS (pH 7.4) six times. For FN adsorption, 20 µL of FN solutions (1 mg/mL) was pipetted into each well (after PLL coating), to make a final concentration of 10 µg/mL, and incubated for 1 h. The protein solution was diluted with PBS (pH 7.4) four times and then with growth medium twice.

3.2.5 Immunostaining and Analysis

To obtain higher resolution images of cells growing on liquid-liquid interfaces, imaging was carried out on droplets pinned on thin glass slides mounted at the bottom of a sticky-slide 8 well.

Thin fluorinated glass slides were plasma oxidized for 10 minutes and placed into a staining jar. 1 mL toluene and 30 µL trichloro (1H, 1H, 2H, 2H-perfluorooctyl) silane were added in a glass vial. The staining jar containing the glass slides and the glass vial with the silane solution were placed into a desiccator under vacuum for 5 min and then left under a reducing atmosphere but sealed overnight.

The fluorinated glass slides were washed with ethanol and dried in air before being mounted at the bottom of a sticky-slide 8 well. After sterilisation with 70% ethanol, the wells were washed twice with PBS and then filled with 300 µL pH 10.5 PBS. 10 µL droplets of fluorinated oil with pro-surfactant PFBC at desired concentrations were deposited on top of the glass slide and formed a fluorinated oil droplet spreading over the entire substrate. 200 µL of the desired PLL solution (in pH 10.5 PBS) was pipetted into each well, making a final concentration of 100 µg/mL, and incubated for 1 hour. The PLL solution was then diluted with PBS (pH 7.4) six times. For the coating of the following proteins (FN, VN, FN/BSA mixture or BSA), 200 µL protein solution at the desired concentration was pipetted into each well, to make a final concentration of 10 µg/mL, and incubated for 1 h. The protein solution was diluted with PBS (pH 7.4) four times and then with growth medium twice. An amount of 3,000 cells was seeded on each well.

For PDMS, the hydrophobic glass slide was prepared as described in 3.2.4 and then mounted to the sticky-slide 8 well. The preparation of PDMS samples for immunostaining was the same as for the preparation for the fluorinated oil sample except for the use of PDMS and hydrophobic pro-surfactants (HDC and SDC).

Cells were cultured for either 24 or 48 hours before fixation. Each well was diluted with PBS six times and the samples were fixed with 8% PFA for 10 minutes, then washed by diluting with PBS six times. Samples were then permeabilized with 0.4% Triton X-100 for 5 min at room temperature. Followed an hour blocking tetramethyl rhodamine isothiocyanate phalloidin (1:500, in blocking buffer). Samples were subsequently incubated with the corresponding primary antibody (anti-vinculin, 1:200; anti-talin, 1:200; or anti-paxillin, 1:250, in blocking buffer) for 1 hour at room temperature. The staining solution was washed out by diluting with PBS six times. Samples were then incubated with the corresponding Alexa Fluor 488-conjugated secondary antibody (1:500 in blocking buffer) and Dapi (1:500) for 1 hour at room temperature. For anti-phosphotyrosine antibody staining, since it was conjugated, it was directly stained at 1:500 dilution together with Dapi staining for an hour. The

samples were finally washed by diluting six times with DI water. Confocal microscopy images were acquired with a Zeiss Laser scanning confocal mycoscope (LSM710). To determine cell adhesion areas, images were analyzed by thresholding and watershedding fluorescence images of the cytoskeleton (F-actin staining) using ImageJ. Cell-cluster areas were removed when analysing results.

3.2.6 Live/Dead, Hoechst Staining and Cell Counting

Cell proliferation and viability at the interfaces were assessed via Live/Dead and Hoechst staining, for which, half of the medium was replaced with pre-warmed PBS containing 1 µL/mL calcein, 4 µL/mL ethidium from Live/Dead kit and 2 µL/mL Hoechst. After 40 min incubation, the cells were imaged using a Leica DMI4000B epifluorescence microscope. Cell counting was carried out by thresholding and watershedding nuclear images via ImageJ.

3.2.7 Statistical Analysis

Statistical analysis was carried out using Origin 2019 through one-way ANOVA with Tukey test for posthoc analysis. Statistical significance was indicated a follows: *, $P < 0.05$; **, $P < 0.01$; ***, $P < 0.001$; and n.s., non-significant.

3.3 Results and Discussions

3.3.1 MSCs Adhesion on Liquid Mediated by Protein Nanosheets

Although our previous works showed successful results for the growth of HaCaT cells on albumin-assembled oil interfaces,[47,52] such interfaces were inadequate to support the adhesion of MSCs. We hypothesised that such poor adhesion was the result of the lack of adsorption of ECM protein to albumin nanosheets, an important issue owing to the crucial role of ECM proteins in regulating cellular behaviour.[1] Therefore, FN was used to coat the surface of PLL nanosheets to promote MSC adhesion.

To investigate cell adhesion at oil interfaces, MSCs were seeded on PLL/FN functionalised oil interfaces for 24 and 48 hours, enabling the assembly of FAs. In light of the impact of PFBC concentration on the interfacial mechanics of PLL nanosheets mechanics as described in the Chapter 2, the effect of PFBC concentrations on MSCs adhesion was studied by confocal microscopy. As shown in Figure 3.2, the

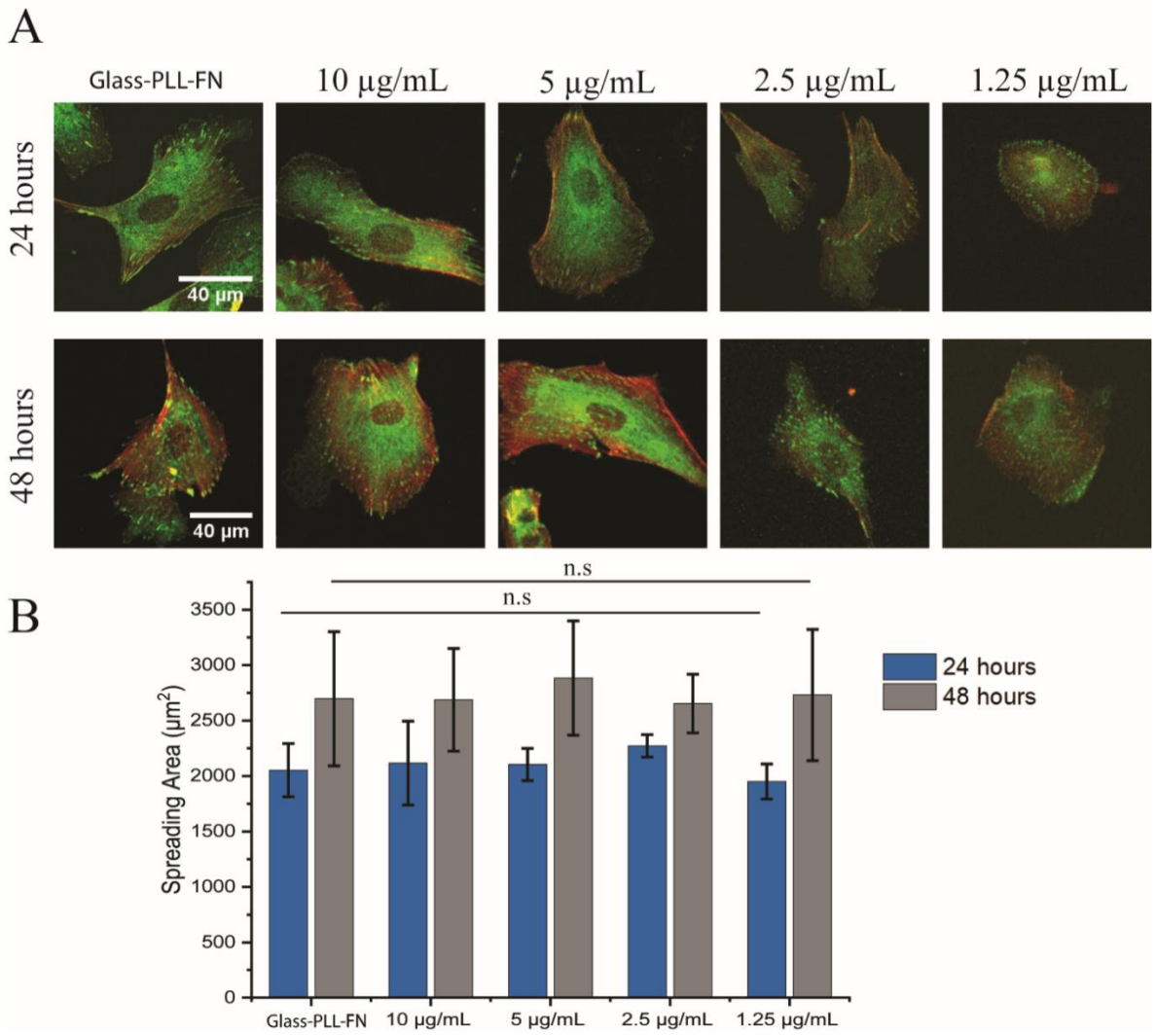

Figure 3.2. Impact of PFBC concentrations on MSC spreading on PLL/FN functionalised Novec 7500 interfaces. (A) Confocal microscope images of MSCs cultured at the interfaces for 24 hours (top) and 48 hours (bottom), green, vinculin; red, actin. (B) Summarised spreading area on the corresponding interfaces calculated from actin images. Error bars are s.e.m; n represents number of experiments, n ≥ 3, more than 20 cells for each condition were measured in each experiment.

formation of FA was already observed at all interfaces in cells growing for 24 hours, and less diffuse and more frequent FAs were seen after 48 hours of culture, indicating that the mechanics of the PLL/FN nanosheets at the interfaces was sufficiently strong to sustain the formation of FA. We next analysed the organisation of the actin cytoskeleton and observed actin cytoskeleton in all samples,

but stress fibres were only found in cells spreading on stiffer interfaces (higher PFBC concentrations), whereas on softer interfaces (lower PFBC concentrations), more actin-rich protrusions were observed. This is in agreement with previous findings on hydrogels, where a higher stiffness often results in more prominent and oriented stress fibres[35] as it allows cells to better generate traction forces.[261] Although MSCs on softer interfaces seem to be less elongated than on the stiffer interfaces, no statistically significant difference was found in their spreading area, similarly to the observations made by Chaudhuri et al. for hydrogels displaying controlled viscoelasticity, compensating the effect of decreased stiffness and enabling spreading associated with local substrate remodelling.[254]

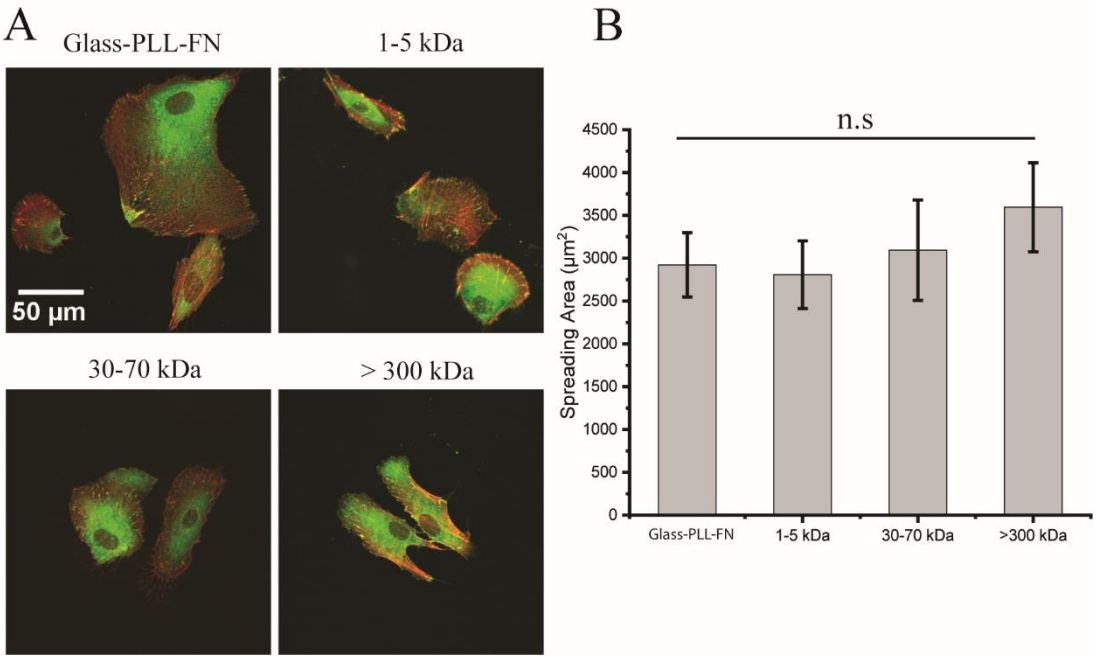

Figure 3.3. Impact of PLL Mw on MSC spreading on PLL/FN functionalised Novec 7500 interfaces. (A) Confocal microscope images of MSCs cultured at the interfaces for 24 hours, green, vinculin; red, actin. (B) Summarised spreading area on the corresponding interfaces calculated from actin images. Error bars are s.e.m; n represents number of experiments, n ≥ 3, more than 20 cells for each condition were analysed in each experiment.

The impact of PLL molecular weight on cell behaviour was then studied with the PFBC concentration fixed at 10 µg/mL. Again, 24 hours after cell seeding, focal adhesion and stress fibres were comparable to PLL/FN functionalised glass and clearly seen at the corresponding oil interfaces (Figure 3.3A and Figure 3.4). Although MSCs on nanosheets of higher molecular weight PLL (stiffer nanosheets) seem

to spread more, no statistically significant difference was found (Figure 3.3B). As shown in Figure 3.4, MSCs on all nanosheets, formed with PLL with different molecular weights, presented mature FAs and stress fibres, implying success in building-up adhesion complexes and associated mechanosensing processes.

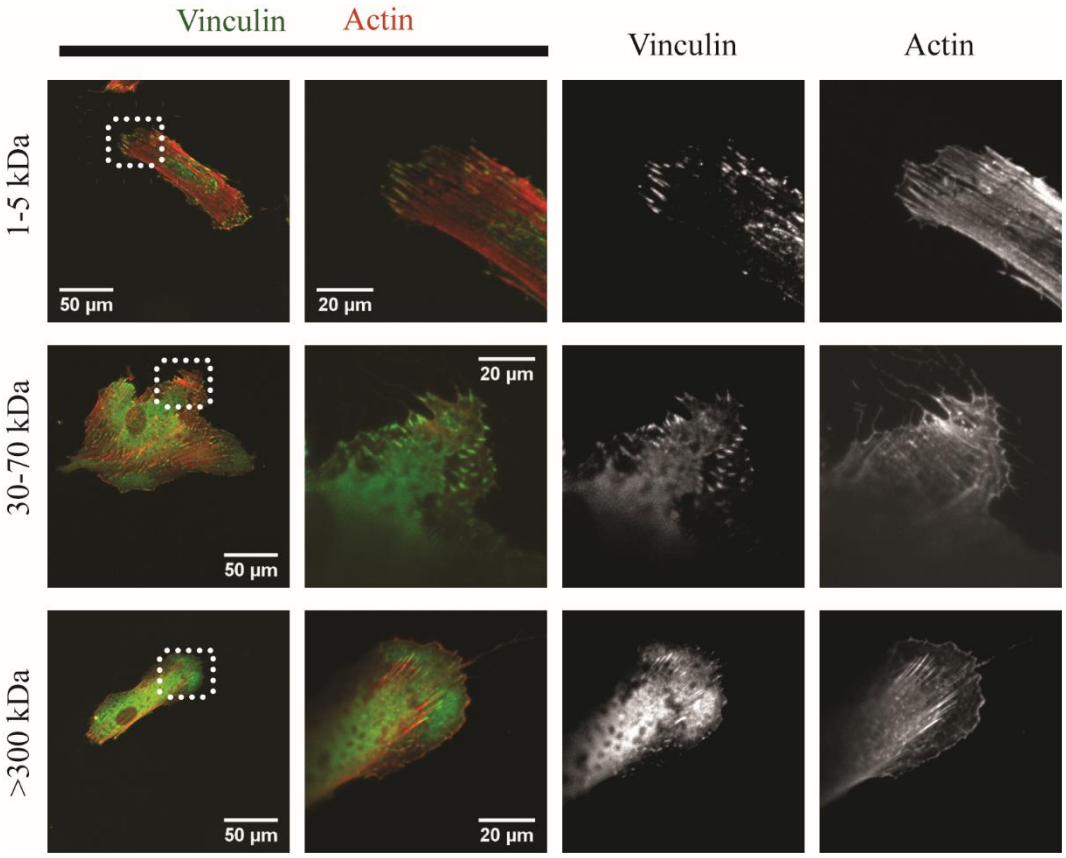

Figure 3.4. Confocal microscopy images of MSCs spreading (after 24 h) on PLL/FN functionalised Novec 7500 interfaces. Zoom-ins correspond to the dotted boxes.

Our findings on keratinocytes growing on liquid-liquid interfaces suggested that cell adhesion to the interface was largely promoted by the β1 integrin-FN interactions.[89] In the case of MSCs, cells were cultured at the interface of PLL coated with different FN dilutions in BSA (100%, 50%, 20% and 0, dilutions from an initial concentration of 10 µg/mL). As shown in Figure 3.5, it was clear that MSC adhesion decreased with FN concentration, as the spreading area was significantly lower in FN concentration of 20% and 0. This highlighted the importance of FN density in regulating MSC spreading

at oil interfaces. Interestingly, cells on oil seem to be less affected by such FN reduction than cells on glass, which was in agreement with many other studies conducted on cell spreading on viscoelastic surfaces,[254] suggesting it would be easier for cells to remodel the matrix on more viscoelastic surfaces while maintaining cell spreading. However, MSC spreading was unaffected when FN was completely replaced by VN on the top of PLL nanosheets, since VN is an ECM protein that mainly binds to β3

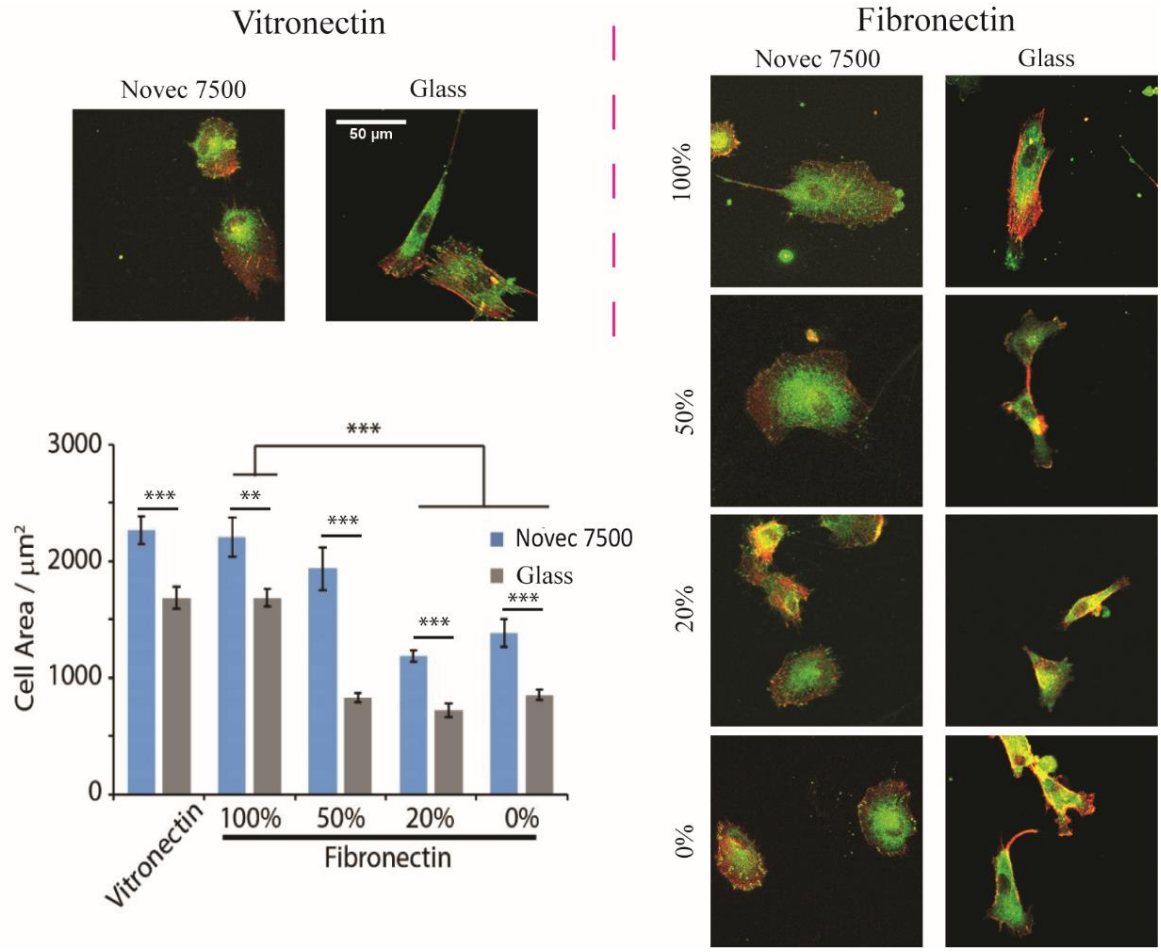

Figure 3.5. Impact of ECM adsorbed to PLL nanosheets on cell spreading (after 48 hours). Confocal microscope images of MSCs on PLL/VN (left) and PLL/FN, PLL/FN-BSA (FN was diluted by BSA to 50% and 20%) and PLL/BSA (right) functionalised Novec 7500 interfaces (1.25 µg/mL PFBC). Green, vinculin, red; actin. The spreading area was quantified.

integrin, this finding indicates that β3 integrin may also promote MSCs adhesion on PLL nanosheets assembled oil interfaces (as on solid substrates).

Apart from vinculin, the recruitment of other focal adhesion markers (namely, talin paxillin and tyrosine phosphorylation) was also studied on PLL/FN functionalised oil (Figure 3.6). Tyrosine phosphorylation is known as a major type of protein phosphorylation, commonly found in signalling

process, especially in integrin-mediated cell adhesion. Indeed, tyrosine phosphorylation of focal adhesion kinase (FAK), paxillin and p130cas has been widely linked to the regulation of both focal adhesion assembly as well as the dynamics of the actin network.[250,262–264] For example, increased tyrosine phosphorylation in response to the stiffer substrates would typically lead to the formation of mature and stable FAs.[250] The comparable levels of phosphotyrosine staining observed on cell growing on oil and glass substrates suggest a similar signalling environment, further confirming that oil interfaces display sufficiently strong mechanical properties to sustain the maturation of focal complexes. Talin activates integrins in an inside-out manner and directly binds to integrins in a slip bond, acting as a force-bearing protein. The unfolding of talin is a crucial process in focal adhesion formation as talin contains cryptic binding sites for other focal adhesion proteins.[44] Upon the

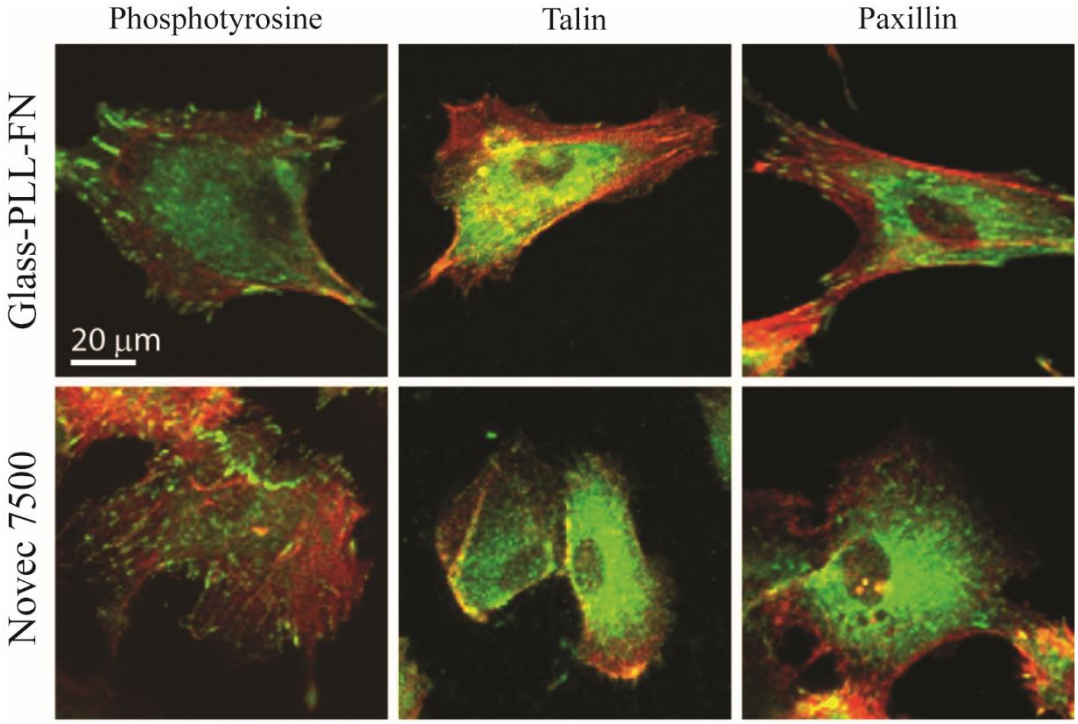

Figure 3.6. Confocal microscope images of focal adhesion protein recruitment on PLL/FN assembled Novec 7500 interfaces (1.25 µg/mL PFBC). Cultured for 48 hours, stained with different focal adhesion markers (phosphotyrosine, talin and paxillin, green) and phalloidin for actin, red.

application of mechanical forces via coupling to the actin retrograde flow, the cryptic binding sites of talin are exposed, recruiting proteins promoting focal adhesion strengthening and cytoskeleton reorganisation, such as vinculin and paxillin.[44,265] Paxillin works as a scaffold at the integrin signalling

layer of focal adhesion, contributing to the recruitment of signalling proteins such as FAK and Src.[266,267] Its role in recruiting vinculin at adhesions has also been reported.[264] The successful recruitment of these molecules in MSCs growing on the nanosheets, further confirmed the establishment of mature focal adhesions by cells adhering to oil interfaces, indicating that even at the lowest PFBC concentrations (1.25 µg/mL), the PLL nanosheets were sufficiently strong to sustain contractile forces generated by cells.

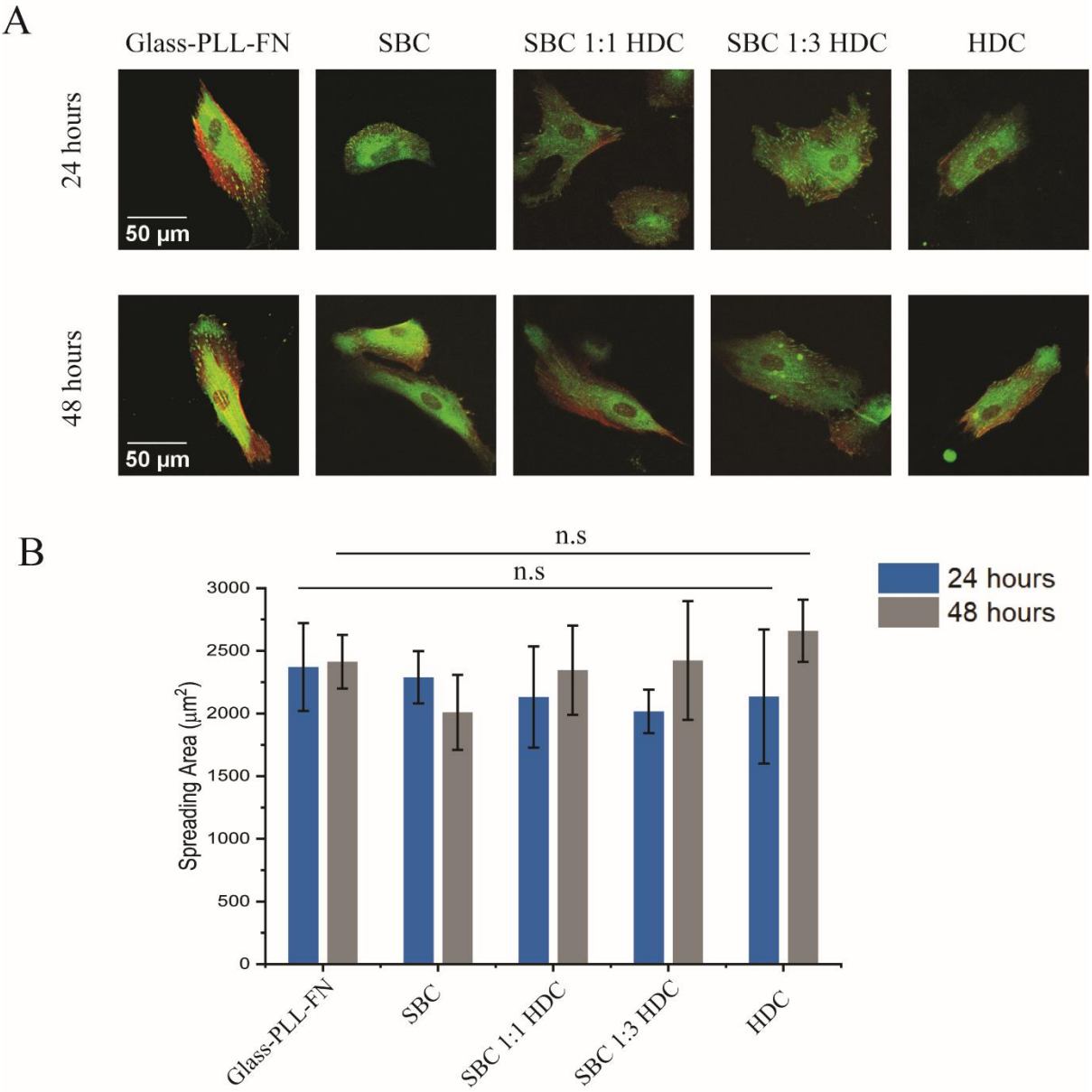

Figure 3.7. Impact of pro-surfactant combinations (0.1 mg/mL) on MSC spreading on PLL/FN functionalised PDMS interfaces. (A) Confocal microscope images of MSCs cultured at the interfaces for 24 hours (top) and 48 hours (bottom), green, vinculin; red, actin. (B) Summarised spreading area on the corresponding interfaces calculated from actin images. Error bars are s.e.m,; n ≥ 3, more than 20 cells for each condition were measured in each experiment.

On PDMS-based systems, focal adhesions and stress fibres were abundantly found after 24 h spreading (Figure 3.7A), consistent with the high interfacial storage moduli measured for these interfaces (Table 1). Despite different pro-surfactant combinations, all the combinations had very similar interfacial mechanical performance and their impacts on cell spreading were also very similar. Although the spreading area of MSCs on oil containing SBC was slightly reduced after 48 hours compared to 24 hours, no statistically significant difference was found.

3.3.2 MSCs Proliferation on Liquid Mediated by Protein Nanosheets

3.3.2.1 MSCs Proliferation on Fluorinated Oil

In the previous section, the establishment of cell adhesion to the PLL/FN nanosheet assembled oil interfaces was confirmed. MSCs were then cultured on such interfaces for longer times to study cell proliferation.

Since PFBC is an acyl chloride, its acidity leads to a decrease in the pH of the culture medium at high concentrations, causing toxicity to cells. This effect was not observed at the concentrations used in our system,[52] but may have a moderate impact on cell expansion. A Live/Dead staining was performed at early culture stages (days 1 and 3) to examine the cytotoxicity induced by the interfaces. Although our previous findings showed the pH of the medium was unchanged in these conditions (at this concentration of pro-surfactants) and HaCaT cells grew well in the presence of 10 µg/mL PFBC,[52] MSCs seemed more sensitive to the PFBC concentration at the interface. As shown in Figure 3.8A, an increasing amount of cell death was observed on oils with increased PFBC concentrations. Cell viability was significantly lower on interfaces in the presence of higher PFBC concentrations (10 and 5 µg/mL) than on TPS (Figure 3.8B). Such high death rate could either be directly linked to the toxicity of high PFBC amounts or unfavourable microenvironment, as we showed in Chapter 2 that PLL interfaces displayed significantly less elastic behaviours at higher PFBC concentrations. However, the healthy morphology observed for cells growing on interfaces with high PFBC concentrations (with mature FAs

and stress fibres) may suggest little direct cytotoxicity under these conditions, and points towards a role of the mechanical environment. However, the dead and unhealthy cells could have also been removed or washed off during staining procedures which involved several extensive washing steps. In such case, the PFBC cytotoxicity cannot be completely ruled out. A further cytotoxicity test, culturing MSCs with PFBC, could be conducted to confirm the possible effects of PFBC. In any case, such difference in viability severely affected MSC proliferation, as the cell densities on oil containing higher PFBC concentrations (10, 5 and 2.5 µg/mL) were significantly lower than that of TPS after a culture of 7 days (Figure 3.8C). The number of cells on interfaces containing 10 µg/mL was almost unchanged, indicating no proliferation on these interfaces over the period of 7 days.

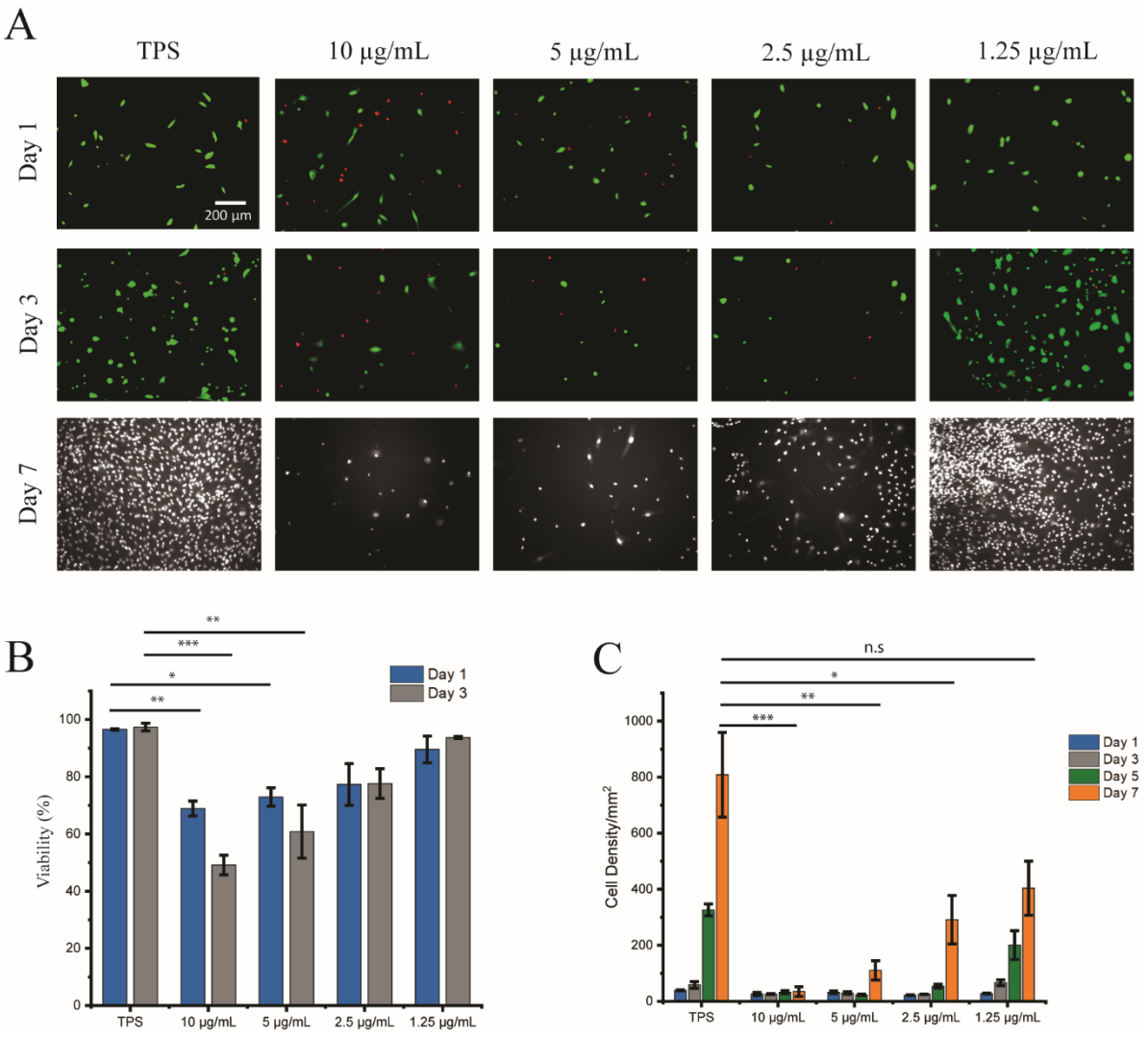

Figure 3.8. Impact of PFBC concentrations on MSC proliferation on PLL/FN functionalised Novec 7500.

(A) Epifluorescence microscopy images of MSCs cultured on TPS and oil for 1, 3 and 7 days. Day 1 and 3 were stained with Live/Dead staining, green, live cells; red, dead cells; the corresponding viability was summarised in (B), Day 7 was stained with Hoechst. (C) Summarised cell densities at different culture times. Error bars are s.e.m,; n ≥ 3.

Interfacial shear rheology indicated that the pH had an important impact on PLL adsorption and resulted in different interfacial mechanics. However, when MSCs were cultured on PLL/FN nanosheets prepared at different pH, it was surprisingly found that MSCs did not show any statistically significant difference in proliferation (Figure 3.9). In the presence of 10 µg/mL PFBC, MSC densities at the oil interfaces at day 6 were sparse compared to those on TPS, in agreement with the results presented above. In contrast, at 1.25 µg/mL PFBC, cells proliferated on all the interfaces regardless of the pH, although on the softest interfaces MSCs seem to proliferate less, this result was not statistically significant.

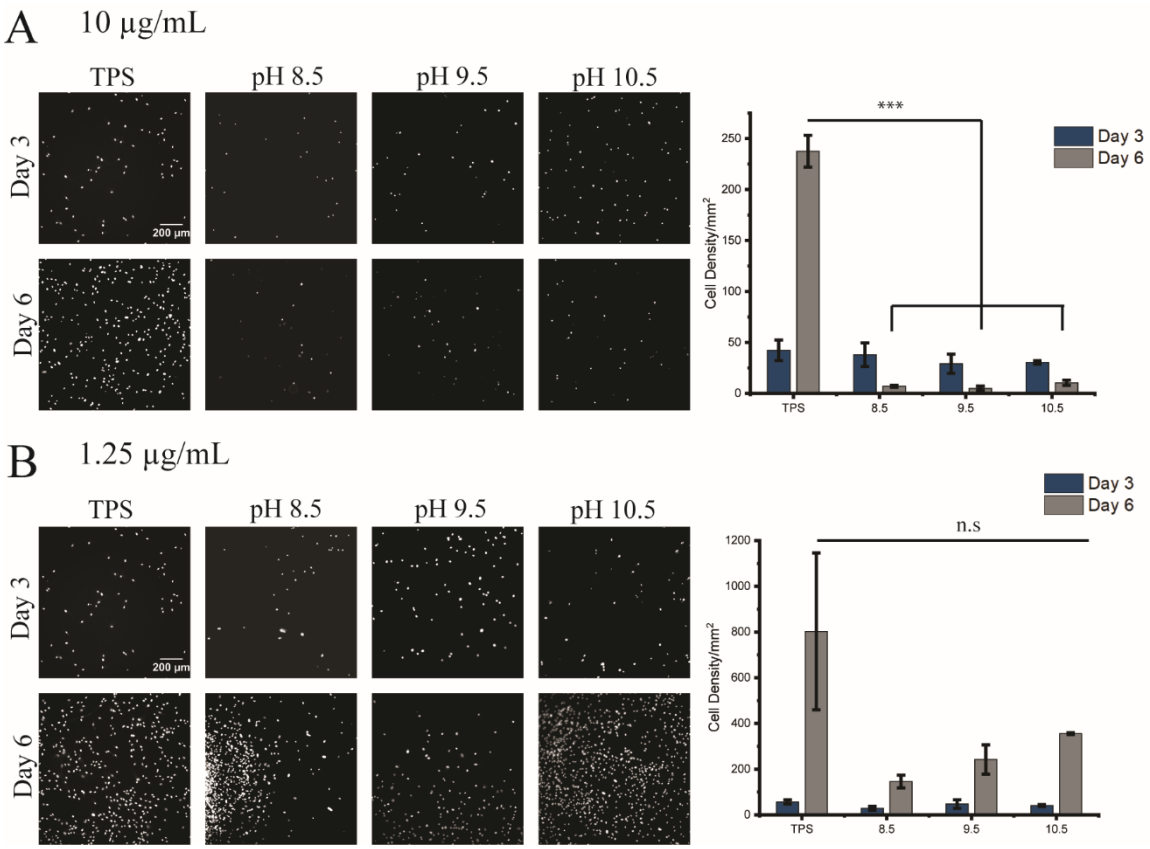

Figure 3.9. Impact of pH on MSC proliferation on PLL/FN functionalised Novec 7500. Epifluorescence microscopy images (left) of MSC nuclei on PLL adsorbed at pH 8.5, 9.5 and 10.5 on Novec 7500

containing (A) 10 µg/mL and (B) 1.25 µg/mL. Cell density was quantified and summarised (right). Error bars are s.e.m,; n ≥ 3.

With PFBC concentration fixed at 1.25 µg/mL, the impact of different PLL Mws was then characterised (Figure 3.10). Likewise, Live/Dead staining was performed first. Under such low PFBC concentrations, all of the Mws analysed allowed a high cell viability, comparable to that on TPS (Figure 3.10B). Even though no significant difference was found regarding cell viability, the proliferation was significantly different, with cell proliferating significantly higher on TPS than on all of the PLL/FN functionalised oil interfaces (Figure 3.10C). When being cultured on oils, there was a clear impact of the Mw of PLL on proliferation, as MSC proliferation gradually increased with longer PLL molecules, with the exception of PLL with a Mw > 300 kDa. Interfaces assembled with 150-300 kDa PLL had the highest proliferation rate and MSCs proliferated significantly more on these interfaces than on interfaces generated with 1-5 kDa and 4-15 kDa PLL.

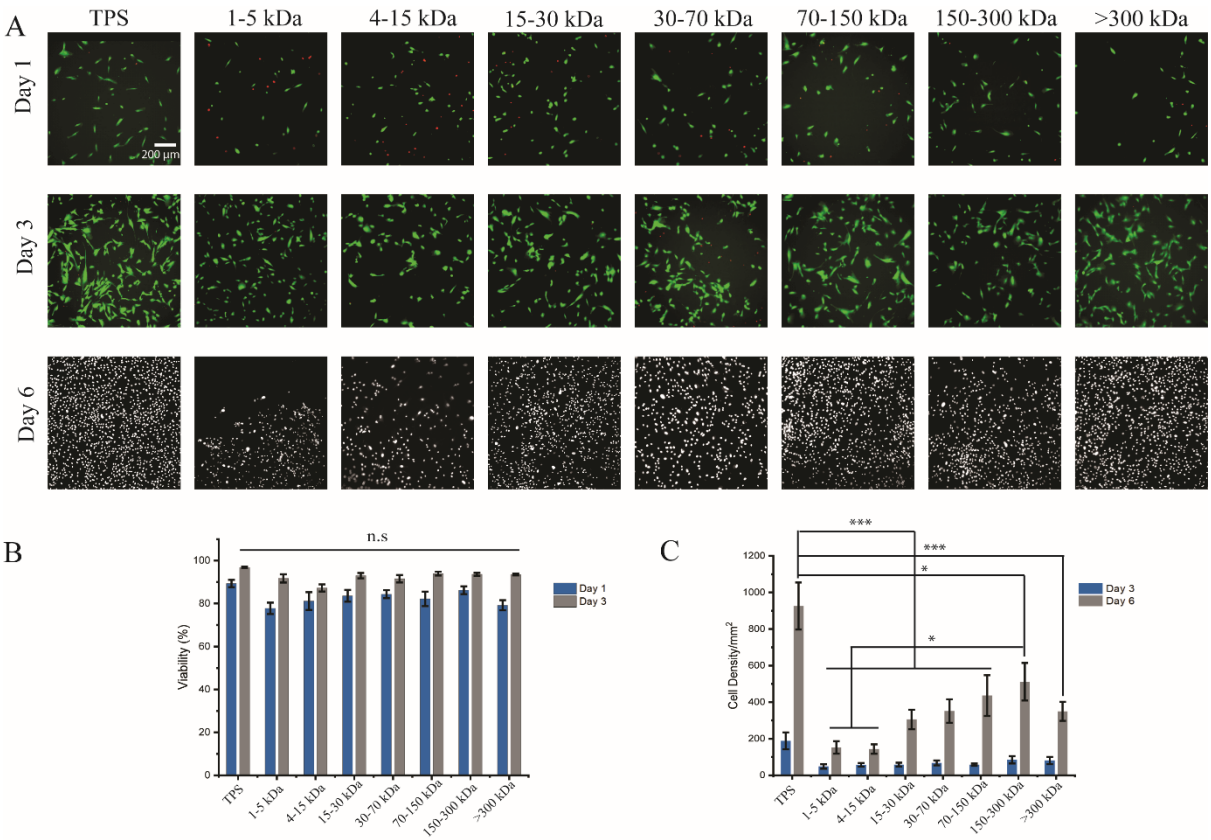

Figure 3.10. Impact of PLL Mw on MSC proliferation on PLL/FN functionalised Novec 7500. (A) Epifluorescence microscopy images of MSCs cultured on TPS and oil for 1, 3 and 6 days. Day 1 and 3 were stained with Live/Dead staining, green, live cells; red, dead cells; the corresponding viability was

summarised in (B), Day 6 was stained with Hoechst. (C) Summarised cell densities at different culture time. Error bars are s.e.m,; n ≥ 3.

When culturing of MSCs on nanosheet assembled oil interfaces, some areas devoid of cells surrounded by dense cell areas were systematically observed (Figure 3.11). In some cases, folded cell sheets were also found nearby. We proposed that such cell-free areas were caused either by the detachment of cell sheets with poor adhesion strength or the fracture of PLL nanosheets. To investigate this phenomenon, PLL molecules were conjugated with fluorescent tags. After FN incubation, the nanosheets displayed the formation of domains with increasing size as the higher PLL Mw increased, similarly to the trend previously reported in Chapter 2. However, some fractures were already observed at this stage especially at low PFBC concentration (1.25 μg/mL), suggesting weaker nanosheets. Such fracture is proposed to be the result of the dissociation of PLL nanosheets, upon FN binding and the associated forces exerted. Then, MSCs at a high density (200,000), similar to the density of cells reached on later culture stage, were directly seeded onto the oil interfaces (Figure 3.12). After 24 hours incubation, extensive damage on the nanosheet could be observed on interfaces generated with 1.25 μg/mL PFBC. Cells stayed only on the nanosheet, with folded cell sheets also visible, confirming that the cell-devoid areas were a consequence of nanosheet fracture led by contraction at high cell density and not by cell detachment due to low adhesion forces. With PFBC concentration at 10 μg/mL, although fracture was also observed, it was not as pronounced. Higher Mw also resulted in fewer fractured nanosheets. This could explain the relatively higher MSC proliferation on high Mw PLL interfaces. However, even at the highest Mw, the nanosheets could not fully sustain the cell contractions generated at high densities and nanosheet rupture could still be observed.

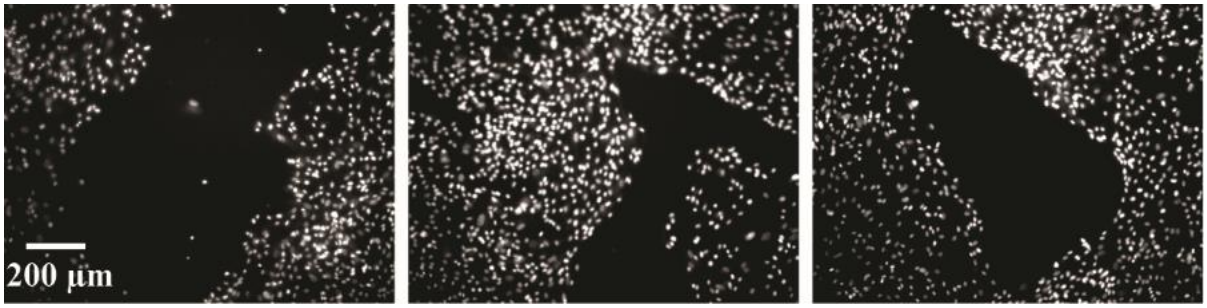

Figure 3.11. MSC devoid area on PLL/FN nanosheets. Representative images of MSC culture on nanosheets for 6 days.

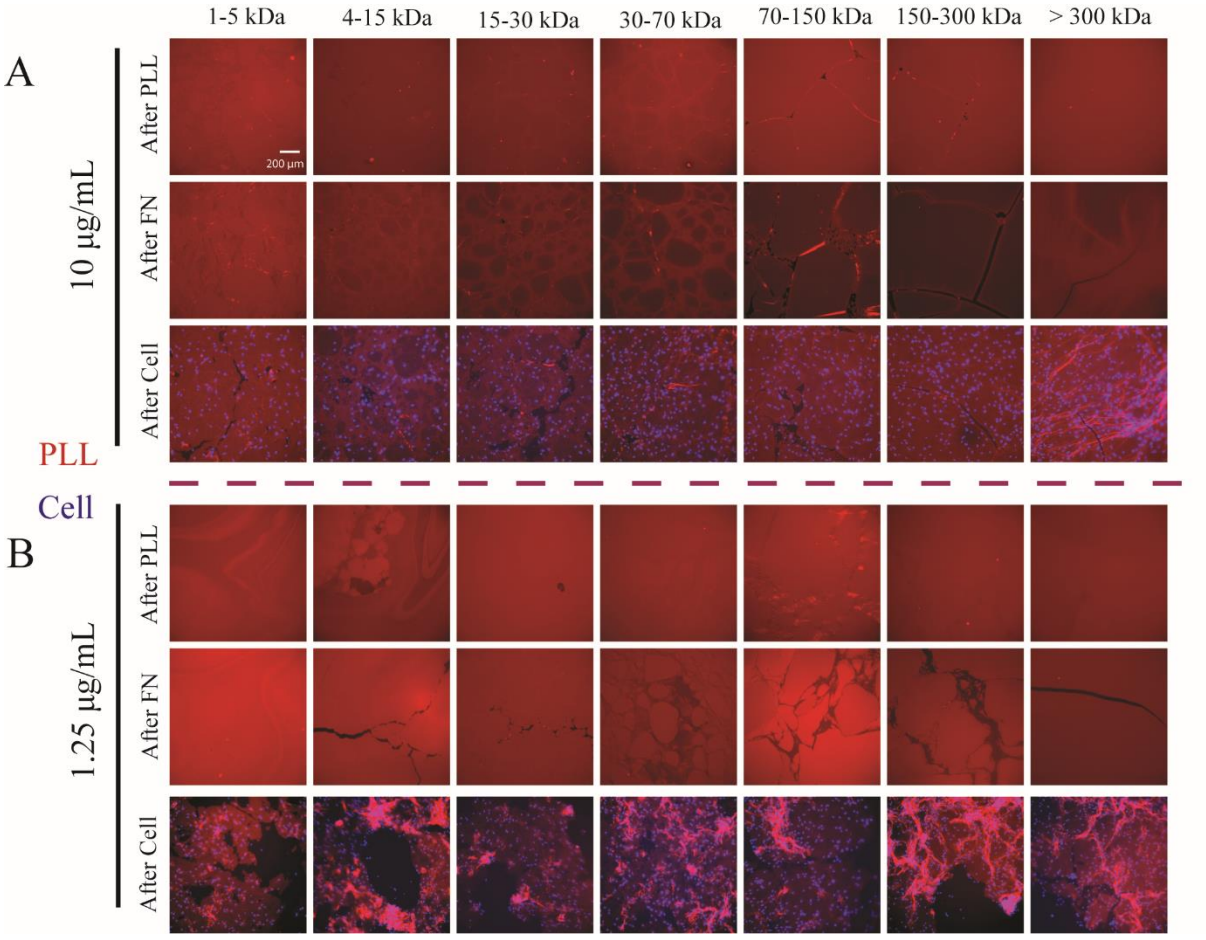

Figure 3.12. Highly confluent MSC fractures PLL/FN nanosheets assembled at the surface of Novec 7500. Epifluorescence microscopy images of PLL nanosheets (top) and after FN adsorption (middle) and 24 hours after seeding 200K cells (bottom), red, PLL; blue, nuclei. Both (A) 10 µg/mL and (B) 1.25 µg/mL PFBC were used for PLL adsorption.

Apart from PLL/FN nanosheets, other combinations of proteins and PELs were also tested to sustain MSC proliferation. HA and COL are common components of ECM and both contribute to the regulation of cell phenotype and have been widely used for mimicking the cell microenvironment *in vitro*. Since HA is negatively charged at neutral pH, whilst COL is positively charged (high isoelectric point), we proposed to form LbL assemblies on top of positively charged PLL nanosheets, resulting in PLL-HA-COL

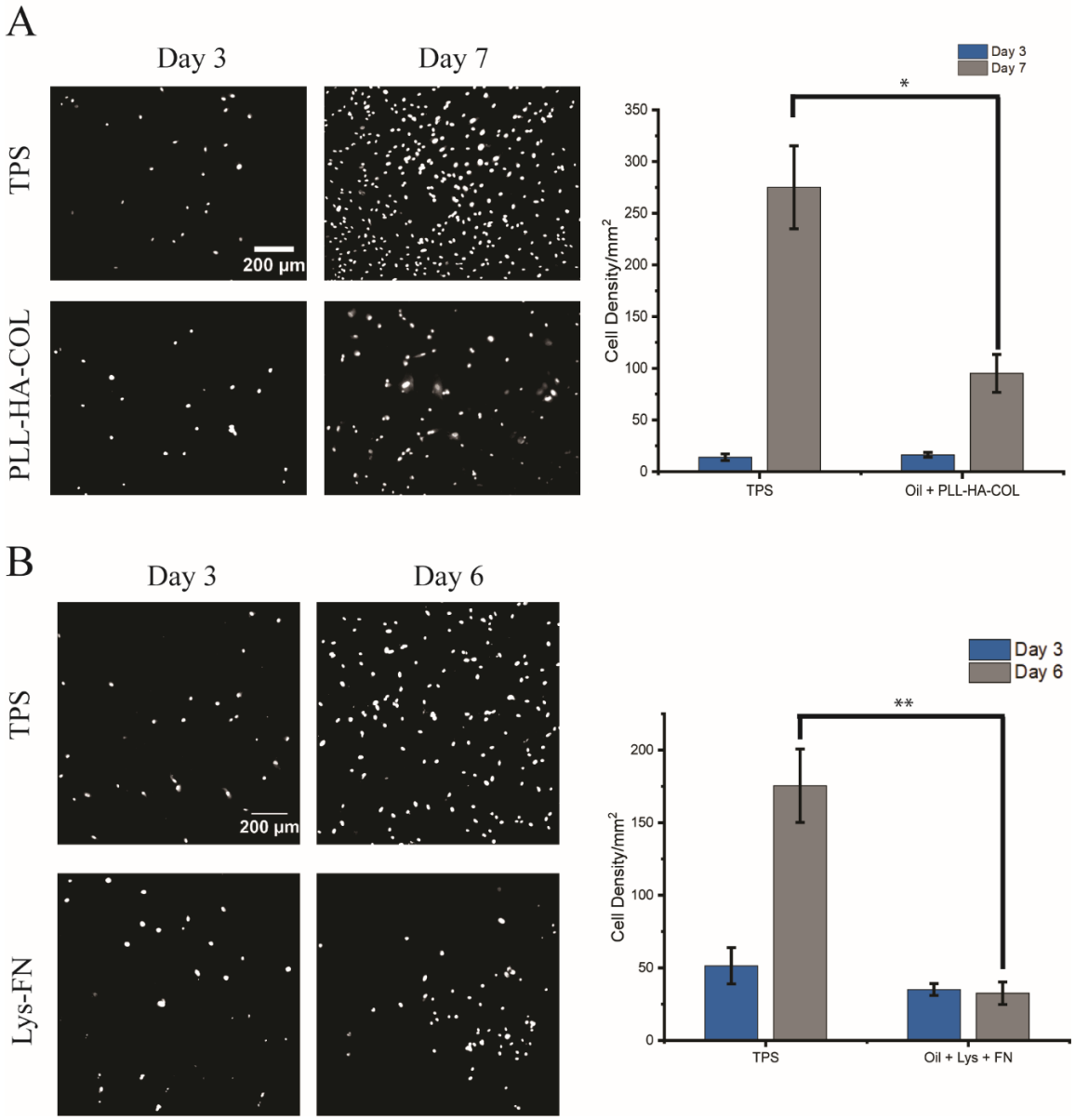

Figure 3.13. MSC proliferated on other protein assembled Novec 7500 interfaces. Epifluorescence microscopy images (left) of MSC nuclei on (A) PLL-HA-COL and (B) Lys-PLL functionalised Novec 7500 interfaces (1.25 µg/mL). Cell density was quantified and summarised (right). Error bars are s.e.m,; n ≥ 3.

nanosheets, in the presence of 1.25 µg/mL PFBC. Some extent of proliferation was observed on such

functionalised oil interfaces, but still significantly less than on TPS (Figure 3.13A). Since COL is a specific ligand for β1 integrin heterodimers, it could be useful for the culture of other stem cells poorly adhering to FN. As mentioned above, MSCs did not grow on albumin-coated interfaces, owing to the poor cell adhesion to albumin. Another natural globular protein Lys, which was incorporated with FN because of its positive charge at neutral pH, was also tested for MSC proliferation. As shown by interfacial shear rheology, it forms soft and less elastic nanosheets (Table 1). Lys-FN nanosheets on oil containing 1.25 μg/mL enabled MSC proliferation on day 3 as the density was similar to that on TPS but did not proliferate further at later time points (Figure 3.13B). This may suggest that such Lys-FN nanosheets degraded at later time points, although this process was not investigated.

3.3.2.2 MSCs Proliferation on Non-fluorinated Oil

Live/Dead assays were also carried out on PDMS-based systems to examine the likelihood of cytotoxicity brought by pro-surfactants. No cytotoxicity was observed on both low (0.01 mg/mL) and high (0.1 mg/mL) pro-surfactant concentrations for the different pro-surfactant combinations studied, except for the 0.1 mg/mL SBC (Figure 3.14A), whose cell viability was significantly reduced at day 3. As SBC contains two chloride groups that can react with PLL, it would possibly lead to higher acidity and thus be more toxic than others pro-surfactant combinations at the same concentrations. However, it is worth noting that even though the cell viability on PDMS containing 0.1 mg/mL SBC was significantly reduced after 3 days, it still maintained at a high level (around 80%) and showed no significant difference compared to TPS. Interestingly, MSC proliferated similarly in all of the conditions tested, at levels comparable to those of TPS (Figure 3.14). This is consistent with the fact that all of the pro-surfactant combinations presented displayed comparable interfacial mechanics, even for different concentrations which only differ slightly in their interfacial storage moduli (Table 1).

Similar to Novec 7500 oil-based interfaces, nanosheet fracture was also observed at the surface of PDMS. At day 5, the fracture was quite prominent already (Figure 3.15) with the oil containing SBC alone displaying the most significant fractures. As indicated in the Figure 3.14B, MSC grew at PDMS-

based interfaces containing 0.1 mg/mL pro-surfactant and reached high densities even on day 3. However, their proliferation rate slowed down on day 5. Such slowing down could possibly be attributed to such fractures. The nanosheet fracture was clearly a major issue affecting the ultimate cell density at oil interface, a nanosheet toughening is therefore needed to prevent such surface fracture.

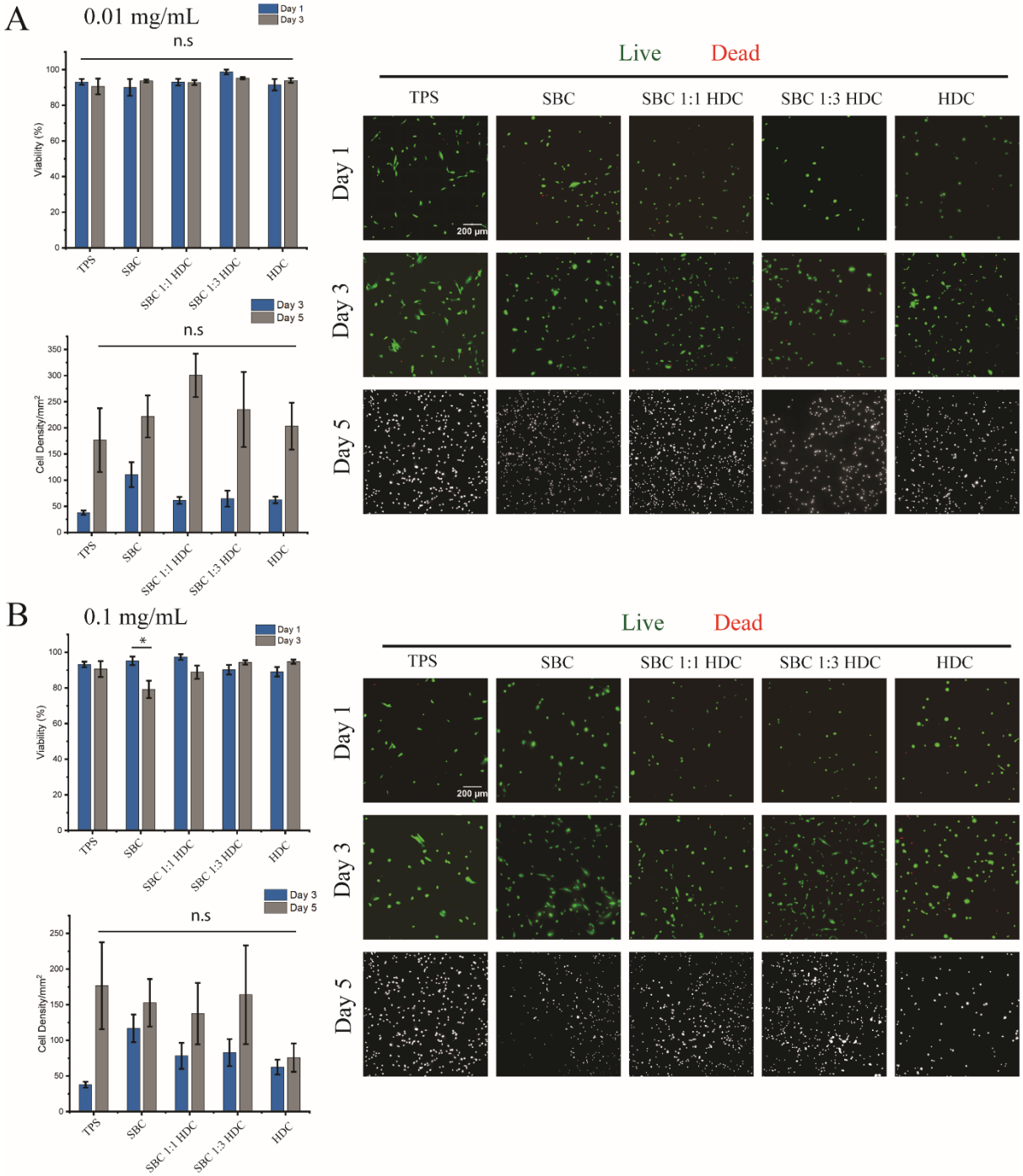

Figure 3.15. Impact of pro-surfactant on MSC proliferation on PLL/FN functionalised PDMS. Epifluorescence microscopy images of MSCs cultured on TPS and oil for 1, 3 and 5 days (right). Day 1 and 3 were stained with Live/Dead staining, green, live cells; red, dead cells; day 5 was stained with

Hoechst on nuclei. The corresponding viability and cell density were quantified and summarised (left). Both low pro-surfactant concentration (0.01 mg/mL, A) and high pro-surfactant concentration (0.1 mg/mL, B) were studied. Error bars are s.e.m,; n ≥ 3.

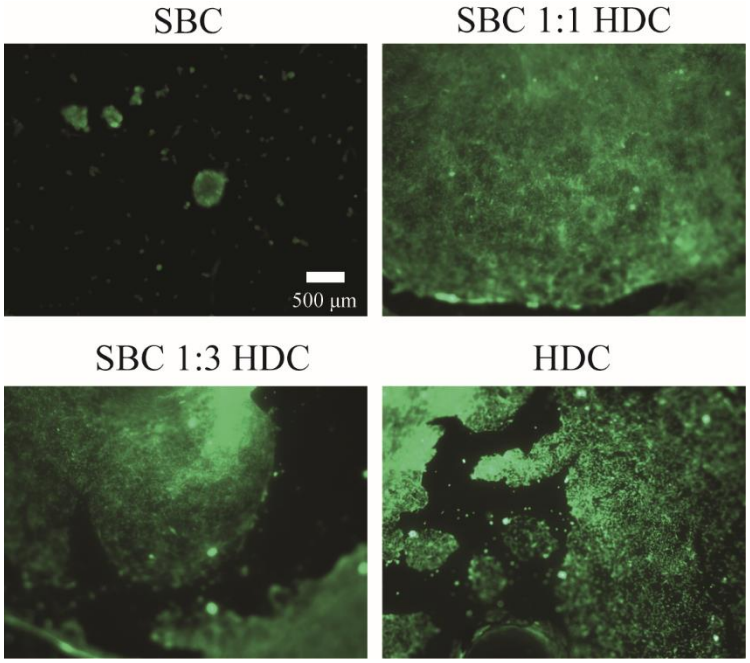

Figure 3.16. MSC fractures PLL/FN nanosheets assembled at the surface of PDMS. Epifluorescence microscopy images MSCs cultured on PLL/FN functionalised PDMS containing 0.1 mg/mL pro-surfactant for 5 days. MSCs were stained with calcein, green, live cells.

In addition to PDMS, other non-fluorinated oil systems were also examined for the culture of MSCs. Mineral oil is commonly used in a wide range of healthcare products and rapeseed oil is a common cooking oil used in food industry, containing short peptides and other nutrients, in addition to lipids, that may promote cell proliferation. Both of them are inexpensive and accessible, and would be favoured for industrial applications. Upon the deposition of PLL/FN nanosheets, MSCs proliferated on these oils at levels comparable to those of TPS (no statistically significant difference; Figure 3.16). This highlighted the universality of such protein nanosheets assembled oil-based cell culture systems.

Since these non-fluorinated oils we have looked into were generally lighter than water, the culture of cell was made on oil droplets that had been pinned on hydrophobic slides, which inevitably would introduce curvature. As many reports have highlighted the importance of substrate curvature in regulating cell behaviour,[194,268,269] the impact of curvature was difficult to be isolated or neglected in our non-fluorinated oil-based systems. The existence of convex geometries, which was reported to

induce more contractile actin cytoskeleton,[194] could be another possible reason for early nanosheets rupture on PDMS in addition to fast proliferation rates. However, owing to the hydrophobicity of the underlying slides used and the small amount of oil pipetted, the convex structures introduced was believed to be negligible,[268] with the influence of substrate curvature typically requiring higher curvature.

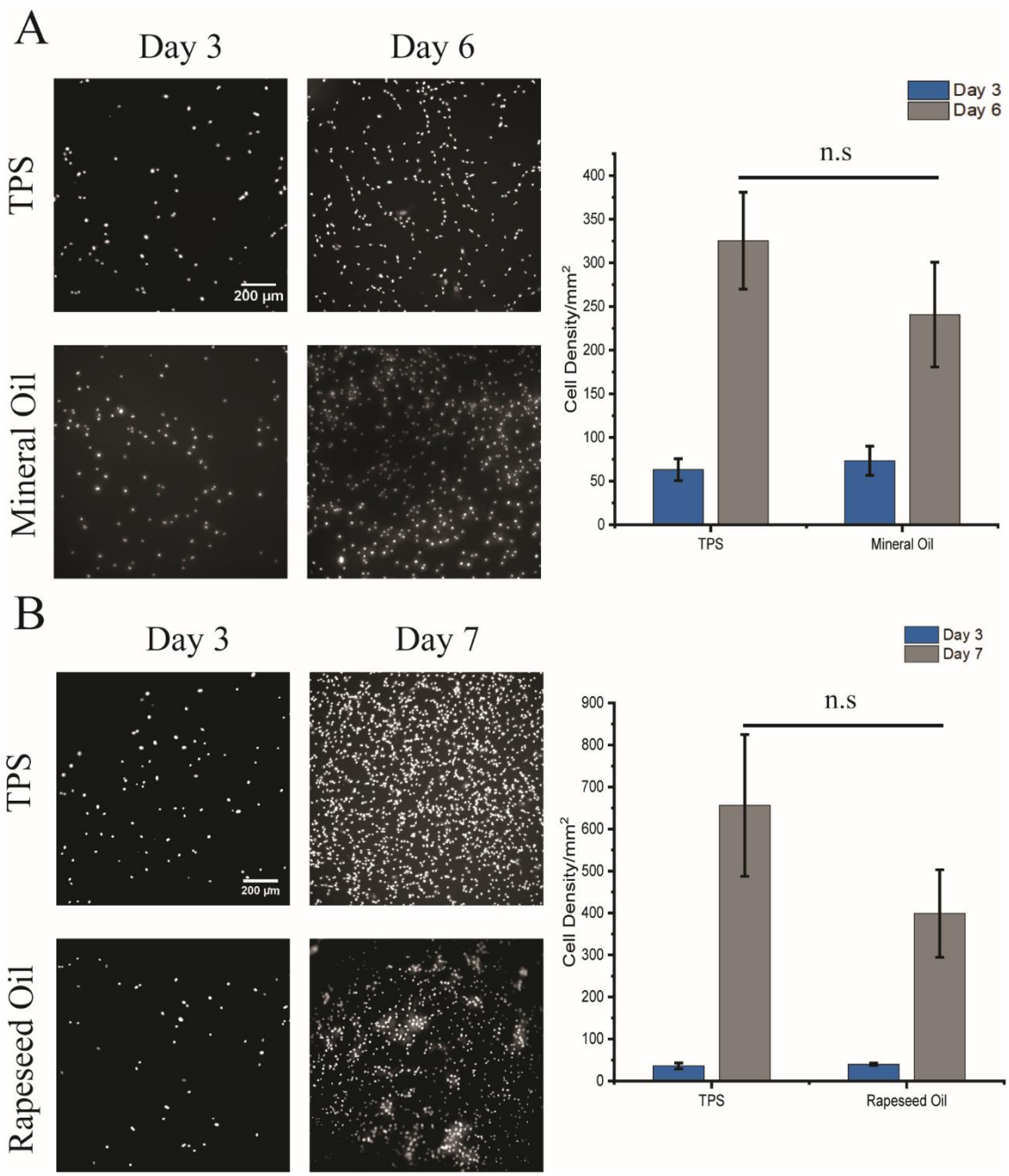

Figure 3.17. MSC proliferated on other PLL/FN assembled interfaces. Epifluorescence microscopy images (left) of MSC nuclei staining on (A) mineral oil interface and (B) rapeseed oil interface containing

0.01 mg/mL HDC, functionalised with PLL/FN. Cell density was quantified and summarised (right). Error bars are s.e.m,; n ≥ 3

3.3.3 Correlation of Interfacial Mechanics to MSC Proliferation

With all the conditions that had been studied for proliferation, a summary of MSC proliferation on the nanosheets assembled relative to that observed on TPS was gathered in Table 1, in addition to key mechanical properties of associated interfaces. When the relative proliferation was plotted against the stress retention, a correlation suggested that MSCs tends to proliferate more on nanosheets that have stress retention higher than 60% (Figure 3.17A). It was also suggested in Table 1 and Figure 3.17C that the storage modulus does not seem to have a great impact on MSC proliferation as cells were able to proliferate on nanosheets with moduli ranging from around 3.67 ± 1.4 mN/m (PLL nanosheet formed at pH 8.5 on Novec 7500 with 1.25 μg/mL PFBC) to 2.30 ± 0.61 N/m (PLL nanosheet formed at pH 10.5 on PDMS containing 0.1 mg/mL HDC). Similarly to the impact of hydrogel viscoelasticity on fibroblast spreading,[270] cell culture at liquid-liquid interfaces seems to be more sensitive to viscoelastic properties, rather than simply shear moduli of the corresponding materials. To avoid a possible misleading result stemming from the potential toxicity of PFBC, the PFBC concentrations (10 and 5 μg/mL) that have impaired cell viability characterised by Live/Dead staining were labelled as high concentrations and marked differently in the plot. This correlation was not unexpected, as many literatures had reported the influence of viscoelasticity on cell proliferation.[51,254,257] Generally, higher stress relaxation results in higher proliferation and it was proposed that the local remodelling of the matrix generated by cells and the force dissipation resulting from substrate creep might be the reason behind this behaviour, though the exact mechanism remains unclear. However, in our findings, the trend was exactly the opposite of what was reported, as we found that interfaces with more stress retention (reduced stress relaxation) promoted the proliferation of MSCs. Although in this study MSC proliferation seems to be insensitive to the interfacial storage modulus, the stiffness was not controlled in this experiment as was possible in hydrogels reported in the literature.[270] Thus, the

impact of the stiffness cannot be completely ruled out. The differences observed could also be attributed to the synergistic influence of both the stress retention and the interfacial moduli. More detailed studies are needed to confirm the exact mechanism via which cells sense interfacial mechanics. However, our studies indicate that interfaces displaying high stress retention and able to store energy upon cell-mediated contractility promote cell proliferation. This may be related to the better long range mechanical stability of corresponding interfaces and the stabilisation of cell adhesions, although mature FAs were also observed on stiff yet fast relaxing interfaces.

Table 1. List of Oil Systems Cultured with MSC

Oil	Protein	pH	Pro-surfactant	Concentration (µg/mL)	Stress retention (%)	Storage modulus (N/m)	Relaxation time (s)	Relative proliferation
Novec 7500	30-70 kDa PLL	8.5	PFBC	10**	49.02	0.03019	60.66	0.02974
Novec 7500	30-70 kDa PLL	9.5	PFBC	10**	47.95	0.2062	57.68	0.02022
Novec 7500	30-70 kDa PLL	10.5	PFBC	10**	59.37	1.522	78.32	0.04401
Novec 7500	30-70 kDa PLL	8.5	PFBC	1.25	N.A*	0.003667	N.A*	0.1819
Novec 7500	30-70 kDa PLL	9.5	PFBC	1.25	64.09	0.004336	61.15	0.3017
Novec 7500	30-70 kDa PLL	10.5	PFBC	1.25	87.12	0.04945	78.31	0.7763
Novec 7500	30-70 kDa PLL	10.5	PFBC	2.5	82.58	0.04812	73.33	0.5019
Novec 7500	30-70 kDa PLL	10.5	PFBC	5**	35.02	0.7043	63.40	0.1365
Novec 7500	1-5 kDa PLL	10.5	PFBC	1.25	48.45	0.8191	48.45	0.1646

Novec 7500	> 300 kDa PLL	10.5	PFBC	1.25	51.20	1.505	56.17	0.3776
Novec 7500	lysozyme	10.5	PFBC	1.25	42.88	0.09160	60.36	0.1852
PDMS	30-70 kDa PLL	10.5	SBC	100	78.18	2.138	81.54	0.8646
PDMS	30-70 kDa PLL	10.5	SBC 1:1 HDC	100	79.85	1.993	73.20	0.7785
PDMS	30-70 kDa PLL	10.5	SBC 1:3 HDC	100	78.62	1.914	75.71	0.9283
PDMS	30-70 kDa PLL	10.5	HDC	100	72.52	2.297	88.66	0.4292
PDMS	30-70 kDa PLL	10.5	SBC	10	79.43	1.411	70.97	1.256
PDMS	30-70 kDa PLL	10.5	SBC 1:3 HDC	10	77.39	1.120	69.80	1.332
PDMS	30-70 kDa PLL	10.5	HDC	10	76.97	0.7951	97.20	1.151
PDMS	30-70 kDa PLL	10.5	SBC 1:1 HDC	10	77.23	1.993	72.05	1.702

***The nanosheets formed at pH 8.5 was too fragile to performed stress relaxation, thus the result was not available.**

**** PFBC concentrations at 10 and 5 µg/mL were defined as high concentrations, as they were showing significantly impaired viability in Live/Dead staining in Figure 3.8.**

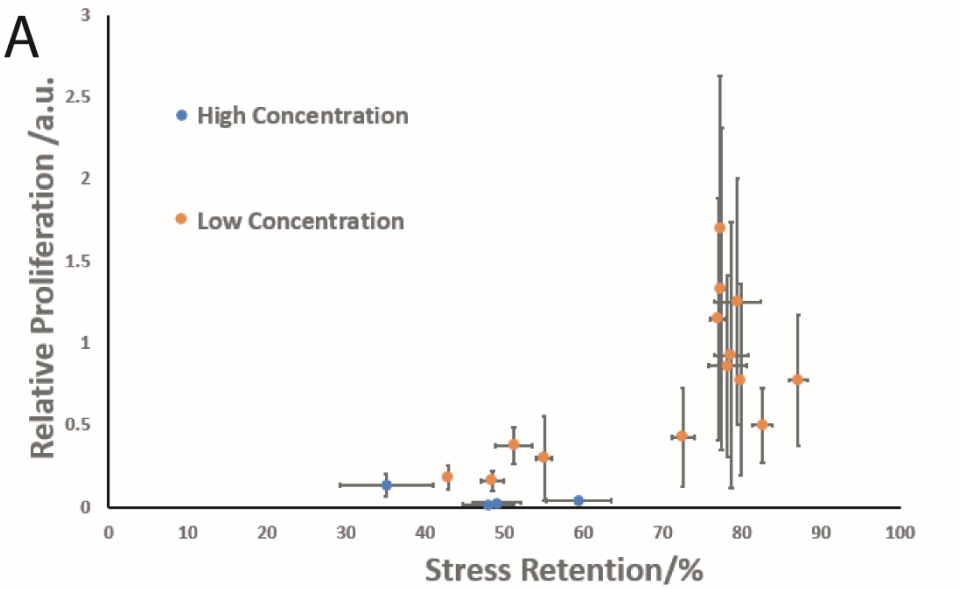
A
Relative Proliferation /a.u.
High Concentration
Low Concentration
Stress Retention/%
0
0.5
1
1.5
2
2.5
3
0
10
20
30
40
50
60
70
80
90
100

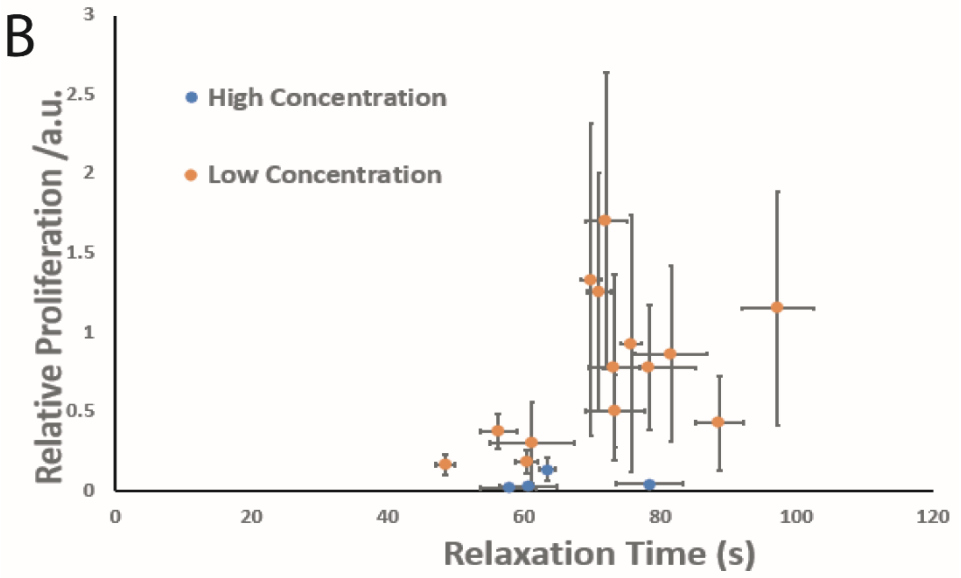
B
Relative Proliferation /a.u.
High Concentration
Low Concentration
Relaxation Time (s)
0
0.5
1
1.5
2
2.5
3
0
20
40
60
80
100
120

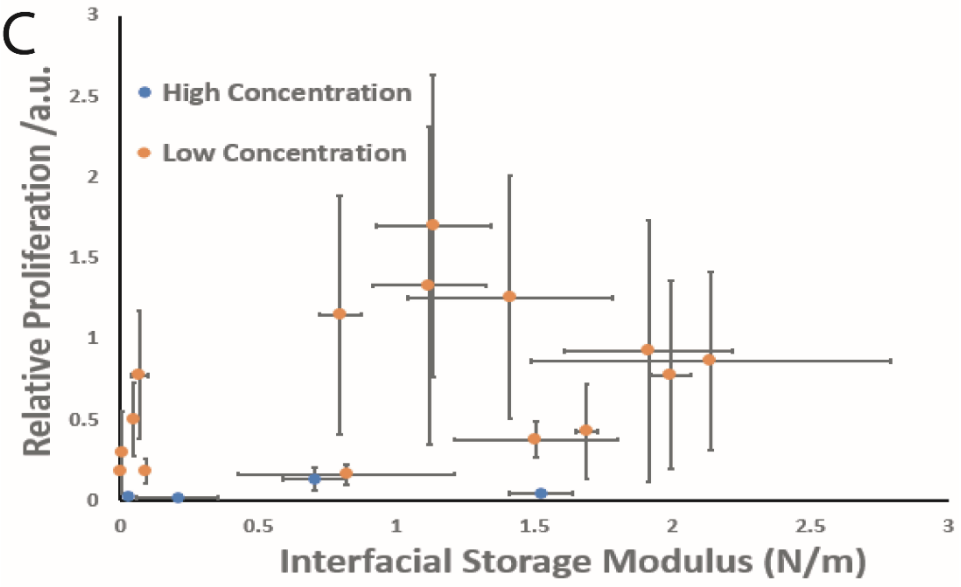
C
Relative Proliferation /a.u.
High Concentration
Low Concentration
Interfacial Storage Modulus (N/m)
0
0.5
1
1.5
2
2.5
3
0
0.5
1
1.5
2
2.5
3

Figure 3.18. MSC proliferation on protein nanosheets assembled oil interface was mediated by the stress retention. MSC were cultured at different protein functionalised oil interface for a given time, MSC density on oil was relative to that on TPS. (A) Stress retention; (B) relaxation time and (C) interfacial storage modulus were obtained from the interfacial rheology measurements and individually plotted against relative MSC density. High concentration pro-surfactants were PFBC at 10 or 5 μg/mL (those had significantly lower cell viability in Live/Dead test) and low concentrations were the rest (those did not significantly affect cell viability in Live/Dead test). Error bars are s.e.m,; n ≥ 3

3.4 Conclusions

In this chapter, MSC adhesion and proliferation on PLL/FN nanosheets assembled at oil interfaces were studied. The successful establishment of FAs was observed after 24 h of culture on corresponding oil interfaces, though more evident stress fibre assembly was only found on more rigid interfaces, similar to observations reported for solid substrates and hydrogels. Such difference did not have a significant impact on MSC spreading, which could be associated to the viscoelasticity of corresponding interfaces. We identify that the adsorption of ECM proteins such as FN and VN would be sufficient to promote MSC adhesion, a process mediated by integrin adhesion to which both β1 and β3 integrins can contribute. In MSC proliferation experiments, we demonstrated that the possible toxicity of the pro-surfactants and nanosheet fracture caused by high cell density were the major hurdles to cell proliferation. Although our nanosheets may be able to counterbalance the forces exerted by cells at early stages of the formation of FAs, they might not be able to sustain the contractile forces generated at high cell densities, leading to nanosheet rupture and disruption of cell sheets. Interfacial toughening is therefore required. However, since lowering pro-surfactant concentration would normally weaken the nanosheets, as we found by interfacial rheology, the gain in elasticity is counter-balanced by a loss in modulus, and the toughness of the corresponding interfaces may not increase significantly. The concept of culturing cells on a wider range of nanosheets and on oils was also explored. We broadened it to other ECM protein combinations, such as HA/COL pair and other oils such as inexpensive mineral oil and rapeseed oil. These observations imply the universality of the system developed and demonstrate the potential of these platforms for industrial applications (e.g. for the scale up of cell culture in 3D bioreactors). Finally, we reported a correlation between stress retention of nanosheets

and MSC proliferation, suggesting the importance of viscoelasticity of the nanosheets to support the growth of MSCs. Although the exact mechanism via which cells sense such properties remains unclear, this correlation provides a key insight for the design of protein nanosheets assembled at oil interfaces for cell expansion. Moreover, as many have described the damage resulting from harsh enzymatic digestion during cell harvesting,[271–273] these oil-based culture systems provide alternative methods for cell recovery, such as direct pipetting,[129,260] Langmuir-Blodgett transfer[61] or emulsion disruption (e.g. via filtration or centrifugation)[89] to help retaining cell phenotype over long term expansion. This aspect will be the focus of the following chapter.

Chapter 4

Culture of Mesenchymal Stem Cells on Nanosheets Assembled Emulsions

4.1 Introduction

Since the discovery of MSCs in bone marrow in the late 1960s,[174,274] MSCs have been isolated from almost every tissue in the human body.[275,276] MSCs were defined by the International Society for Cellular Therapy (ISCT) as a plastic-adherent cell that maintain self-renewal properties and differentiating potential towards adipogenic, osteogenic and chondrogenic lineages. MSCs should also express CD73, CD90 and CD105 while be negative for CD45, CD34, CD14 or CD11b, CD79a or CD19 and HLA-DR.[277] Because of its self-renewal ability and multi-potency, it is one of the favourite cell type for clinical applications such as cell therapy and tissue engineering.[183,208,277,278] An increase in the number of clinical trials registered using MSCs has developed in recent years [174,276] since the first clinical trial with MSCs in 1995.[279] On-going clinical applications of MSCs include treatment for acute graft-versus-host disease (GVHD), bone and cartilage disease, as well as cardiovascular repair strategies.[174] More recent studies also revealed the potential of using MSC to treat Covid-19 induced pneumonia.[280,281] However, in the case of the Covid-19 treatment, a dose of one million clinical grade MSCs per kilogram body weight was used for intravenous infusion,[280] while for GVHD, doses ranged from 0.23 to 9 million cells per kilogram body weight were used per infusion for the treatment.[175,176] Since MSCs are sparse and rather difficult to be isolated in a large amount, scaled-up *in vitro* expansion is required. However, like most of other somatic cells, MSCs progressively lose their ability to replicate and differentiate after a certain amount of divisions as a result of differentiation and senescence, which leads to increased heterogeneity of the cell population and uncertainty of treatment outcomes. This constitutes a major hurdle that restricts the clinical application of MSCs.[282–284] Cell senescence is a complicated process resulting from several factors including oxidative stress, DNA damage and telomere shortening.[282–284] Genetic engineering has allowed to induce the ectopic expression of telomerase thus preventing *in vitro* senescence[285,286] but was inadvisable concerning its effects on cell differentiation.[283] Other methods developed to tackle senescence include incubating MSCs with hydrogen gas[287] or isothiocyanate[288] to reduce oxidative stress and hence extend MSCs lifespan. Considering the huge impact of cell senescence on MSC proliferation and differentiation, it is

important to monitor and control the entire culture process to enable the homogeneity of MSCs. A cost-effective way for *in vitro* scale-up to meet such demands would be culturing MSCs on solid microcarriers which offer large surface areas in bioreactors, allowing excellent control of culture parameters as well as high cell output.[289–291]

Microcarriers are small beads with diameters generally ranging from 100 to 300 μm fabricated from various materials such as dextran, cellulose, polystyrene and polyvinyl acetate.[180,183,187] Owing to the large surface-to-volume ratio, microcarriers can provide significantly larger surface area than traditional 2D culture plates. This is particularly suitable for the culture of anchorage-dependent cells like MSCs which require a large surface area to support their expansion. Apart from higher outputs, microcarrier cultures are also advantageous in allowing cell passaging via bead-to-bead transfer without enzymatic treatment.[182,183] This not only saves intensive labour required for cell passage but also minimises the risk of contamination. The selection of the adequate microcarriers is key to the success of cell culture as it can impact the growth kinetics and phenotype of expanded cells.[292] As mentioned in Chapter 1, suitable microcarriers should provide sufficient anchorage for cell growth, allow the expanded cells to be easily and efficiently harvested, and should also display adequate physical mechanical properties to be applied into dynamic systems. In addition, microcarriers should not be too expensive as the cost-effectiveness is a key concern for industrial applications.[179,180] Many studies have been conducted on currently commercially available microcarriers to select the optimum one for MSC culture.[180,183,187,197,293] Although the results cannot be directly compared to determine which one is the best for MSC culture owing to the variation of culture conditions and batch-to-batch differences of cells and their sources, it is unanimously highlighted the importance of the surface coating of microcarriers to promote cell adhesion and proliferation and even differentiation potential. Common ECM protein-coated microcarriers used for MSC culture include cross-linked dextran-based and denatured COL-coated microporous Cytodex 3 and a cross-linked GEL-based macroporous CultiSpher-S.[177,180,197,200,205,291,294] More recently, the adhesion peptide grafted synthetic polymer-coated polystyrene Synthemax II microcarriers have become the most frequently used microcarrier

for MSC culture.[183,187,200] On Synthemax II microcarriers, a continuous culture of MSCs for more than 50 days was achieved and the MSCs were found retained their phenotypic marker expression (CD73 and CD105) and trilineage differentiating potential (adipogenesis, osteogenesis and chondrogenesis) at passage 9.[200,295] Despite of all the above mentioned advantages, a clear drawback of such solid bead-based culture system is that enzymatic digestion is still needed for cell detachment, which might be invasive and affect cell phenotype, resulting in potential damage to cell membrane receptors and other cell membrane proteins.[179] Moreover, enzymatic digestion might not be practical on large scale production as the concentration of enzyme and the incubation times are difficult to control, which would severely impair cell viability and recovery efficiency.[179] Alternative methods avoiding cell-damaging enzymatic treatments include culturing cells on microcarriers coated with thermoresponsive polymers such as PNIPAAm on which cell sheets can spontaneously detach from the substrate by simply decreasing the temperature below the switching temperature (LCST, representing a transition from hydrophobic coating to hydrophilic cell repellent coating). The problem of this method is that complete detachment has not been achieved yet and the initial cell adhesion is often relatively poor.[205] Other approaches include the culture of cells on dissolvable microcarriers which can be easily removed by non-invasive treatments such as pectinase digestion.[179] Previous work in the Gautrot's lab proposed another potential alternative. It was demonstrated that human primary keratinocytes and MSCs can be cultured at the surface of liquids,[47,52,89] while the culture of fibroblast,[126–129] myoblast[61,259] on similar systems have also been reported by others. Based on such liquid-liquid cell culture platforms, Keese et al.[126,127,129] proposed that using proteins as stabilisers, emulsion of fluorocarbons can be generated in an aqueous phase for cell culture.

Emulsions are mixtures of two immiscible liquids with one of them dispersed in the other. Emulsions are classified into either O/W or O/W emulsions depending on which liquid is the continuous phase. To form emulsions, agitations are commonly applied to bring shear energy into the system, breaking the thermodynamic stable state and forming droplets. During this process, droplets initially formed are constantly moving, colliding or even coalescing, forming droplets of different sizes determined by

the flow regime,[149] disruptive forces, interfacial tensions and the presence of emulsifier.[92] Emulsifiers are used to avoid droplet coalescence by forming a layer at the droplet surface inducing either electrostatic or steric repulsion between droplets.[135,139,149] In such cases, the concentration of the emulsifier is of great importance. It must be sufficiently high to cover the droplet surfaces, otherwise coalescence would occur between adjacent droplets.[139] Moreover, the adsorption speed of emulsifiers is also important. Faster adsorption leads to reduced coalescence as it modifies the interface before disruption can occur. Because of their greater biocompatibility, proteins are one of preferred emulsifiers, providing long-term stability against coalescence. Depending on the protein surface coverage, the layer thickness, surface potential, pH and the ionic strength of the aqueous solution; proteins act differently when adsorbing at the surface of droplets, resulting in emulsions of different stability.[137,149] By bringing the pH away or close to the isoelectric point of the proteins adsorbed, the emulsions can be either neutral or charged, blocking or providing electrostatic binding sites for further modification of the surfaces. Since most emulsifiers are also amphiphilic, they also work as a surface active agent (surfactant), as reported in many studies,[150,151,296] promoting interactivity between two liquids hence reducing interfacial tensions. In the generation of emulsions, interfacial tension needs to be overtaken by the disruptive forces generated by agitation to break up initially formed large droplets into smaller droplets. The introduction of surfactant facilitates such process. The size of emulsions can be estimated by the Laplace equation (Equation 2), which indicates that higher concentrations of surfactant result in reduced interfacial tension and consequently smaller droplets. Theoretically, an emulsion is typically a thermodynamically unstable state (especially in the absence of surfactants) owing to the increased interfacial area. Thus, morphology changes would sooner or later occur.[159] Common instability of emulsions include phase separation, flocculation and coalescence.[159,297,298] Among these, creaming and sedimentation are led by the density difference between two liquids under the influence of gravity[297] and can be avoided by adding weighting agents in the lighter phase to minimise the density difference between two liquids. Common strategies include using emulsifiers of different densities to vary the density of droplets, reducing the droplet

sizes by introducing more vigorous agitation or more concentrated emulsifiers[161] or increasing viscosity of the continuous phase by gelling. Flocculation is a type of aggregation in which droplets stick to each other,[299] resulting from low interaction energy barriers between two particles.[159,298,299] Similar to flocculation, coalescence is another type of droplet aggregation occurring on emulsions, however, unlike flocculation, droplets retain their structure and integrity.[298] During coalescence, droplets merge together forming larger droplets and ultimately lead to the separation of two immiscible liquid layers.[297] In order to prevent flocculation and coalescence, droplet contact and interfacial membrane rupture need to be minimised or avoided,[165] the introduction of emulsifiers or stabilisers which can adsorb to the surface of droplets forming a mechanically strong layer as well as providing steric or electrostatic hindrance is a possible way to address the issue, maintaining long-term stability.

In this chapter, we focus on the development of nanosheet assembled emulsion systems for the culture of MSCs. In the previous two chapters, we have demonstrated that the pro-surfactant assisted protein absorption at the liquid-liquid interface would generate a mechanically strong nanosheet that can sustain the forces exerted by cells, allowing cell adhesion and proliferation. The protein nanosheets absorbed at the oil-water interfaces can also function as stabilisers providing steric and electrostatic repulsion to prevent oil in water droplets from coalescence, thus allowing the formation of stable O/W emulsions. Such emulsions provide high surface-to-area ratio, hence posing a potential platform for high-throughput *in vitro* cell expansion. We investigated the stability and characterised the structure of such emulsions, highlighting the importance of protein selection and the role of pro-surfactants. We also provide a proof-of-concept for culturing MSCs on emulsions and demonstrate the feasibility of simple cell passaging and harvesting methods on such platforms. Solid microcarrier-based cell culture systems have long been used for *in vitro* cell expansion because of their high yields and ease of handling, as mentioned above. Our emulsions not only present properties that resemble those of microcarriers, but also offer advantages over them by providing an alternative less-invasive cell harvesting method, which we proposed may help cells to preserve their phenotype. Oils are also

significantly cheaper (>50 fold). On that account, a long-term culture study and associated characterisation of MSC phenotype, including proliferation, adhesion, stemness retention and multi-potency was conducted on emulsions in comparison to 2D TPS and commercialised solid microcarriers.

4.2 Materials and Methods

4.2.1 Materials and Chemicals

MSCs, MSC growth medium, osteogenic differentiation medium, adipogenic differentiation medium, chondrogenic differentiation medium, freezing medium, Cryo-SFM and accutase solution were purchased from PromoCell. PFBC, PBS, $NaHCO_3$ pellet, NaOH pellet, PLL hydrobromide (mol wt 15-30 kDa, 30-70 kDa, 70-150 kDa and >300 kDa), DMSO, TEA, trichloro (1H, 1H, 2H, 2H-perfluorooctyl) silane, triethoxy(octyl) silane, SBC, HDC, isopropanol (99%), BSA, FN from human plasma, Dulbecco's Modified Eagle's Medium (DMEM, low glucose), L-glutamine, PFA, Triton X-100, tetramethyl rhodamine isothiocyanate phalloidin, Dapi, monoclonal anti-vinculin antibody from mouse, microcarriers (low concentration Synthemax II), Mowiol, BCIP/NBT tablet (SigmaFast™ BCIP-NBT), Alizarin Red S powder, Oil Red O powder, Alcian Blue powder (8GX) and acetic acid (glacial ≥99.7%) were purchased from Sigma-Aldrich. FBS was from PAA. Live/Dead kit was from Life Technologies. Fluorinated oil (Novec 7500) was from ACOTA. HA was provided by GlaxoSmithKline. Poly(l-lysine)-graft-polyethylene glycol (PLL-g-PEG) was from SuSoS AG. Cell Counting Kits-8 (CCK-8) was purchased from Dojindo. Cover glasses (25 × 60 mm) and pure et, cell strainer (70 µm), CyQUANT® Cell Proliferation Assay Kit, Taqman® Gene Expression Assay and TaqMan™ Fast Advanced Master Mix were purchased from Thermo Fisher Scientific. Blandol® White Mineral Oil was purchased from Sonneborn. QuantiTect®Reverse Transcription Kit and RNeasy® Plus Mini Kit were from Qiagen. 8 Well µ-Slide was from Ibid. Mouse anti-human monoclonal antibodies of CD105-FITC, CD105-RPE, CD90-APC, CD73-RPE, CD73-FITC, CD34-FITC, CD45-RPE, CD19-Pacific Blue were purchased from Bio-Rad.

4.2.2 Generation of Emulsions

For fluorinated oil emulsion, Novec 7500 containing PFBC at final concentration of 0.01 mg/mL and PLL solution (200 μg/mL in pH 10.5 PBS) were added into a 50 mL centrifuge tube at the ratio of 1:2. The tube was vigorously shaken via a vortex for the generation of emulsions, then left to incubate at room temperature for 1 hour. The top liquid phase which above the emulsion level was aspirated and replaced with normal PBS for washing for four times. Such washing step was repeated four times to ensure that excess PLL was removed and PBS pH was neutralised. For non-fluorinated oil-based emulsion, the oil was pre-mixed with 0.1 mg/mL of the corresponding surfactants (HDC or HDC and SBC mixture) and added into a glass vial that had been plasma oxidized for 10 minutes. PLL solution (200 μg/mL in pH 10.5 PBS) of the volume doubled to the oil was then pipetted into the vial before the vial was vigorously shaken by vortexing. After an hour incubation, the bottom phase below the emulsion level was gently aspirated by a springe with needle, normal PBS was slowly and gently pipetted to the vial, such washing step was repeated four times to ensure that excessive PLL was removed and PBS pH was neutralised.

For cell culture experiment, FN (20 μg/mL) or HA (200 μg/mL) solution of the same volume as the above mentioned PLL solution was added into the PLL-coated emulsion. After an hour incubation, the emulsion was washed with PBS three times as described above and washed with medium once.

To image emulsion droplets in bright field microscope, emulsion was gently pipetted into a well of a 24-well plate with a certain amount of PBS (500 μL for Novec 7500-based emulsion or 200 μL for non-fluorinated oil-based). To characterise emulsion surface area, the visible emulsions were all outlined by imageJ via a Trainable Weka Segmentation plugin and had the corresponding area calculated. The total cell culture area provided by emulsions in the field was calculated by quadrupling the sum of the emulsion surface area in the field calculated as mentioned above. For fluorescence imaging, conjugated PLL was used instead of normal PLL. The conjugated PLL stock solution was prepared by dissolving PLL powder in 0.1M $NaHCO_3$ buffer and reacting with Alexa Fluor 488 NHS ester

(succinimidyl ester) dissolved in DMSO, as suggested by the user's manual. The conjugated PLL was mixed with normal PLL at 1:9 ratio and added into each well to a 100 µg/mL final concentration. The incubation and washing process was the same as the one described above. For polarised optical microscopy, droplets were then transferred to a glass coverslip placed on a polarized optical microscope (Olympus BX51) and photographed between crossed polarisers.

4.2.3 MSC Culture, Passaging and Harvesting

To avoid cell adhesion on TPS and therefore maximise the amount of cell adhesion on emulsion or solid microcarriers, 300 µL of 25 µg/mL PLL-g-PEG coating of the well was used as cell repellent. After an hour incubation, PLL-g-PEG solution was aspirated and the well was washed with PBS twice before a certain amount of growth medium (500 µL for Novec 7500-based emulsion and microcarriers or 200 µL for non-fluorianted oil-based) was added into each well, around 100 µL of emulsion or 20 mg of microcarriers pre-incubated with 500 µL MSC growth medium was then transferred to the well to fully cover of the whole surface. MSC was then gently seeded in each well at a density of 20,000 cells/well.

When 70-80% cell confluence was reached, cell passage on emulsions and mirocarriers was carried out via a drop-to-drop (bead-to-bead) transfer method without trypsin usage. In such case, around 1/3 of the emulsion/microcarriers cultured with confluent cells were transferred to a new well containing fresh emulsion/microcarriers with medium. The well-plate was placed on an orbital shaker (VWR) at a speed of 40 rpm located in an incubator (37 °C and 5% CO_2), after 24 hours, the speed was increased to 70 rpm. To perform live imaging of cells migrate from emulsion, emulsion with confluent cell on was transferred to a new well without PLL-g-PEG coating but containing growth medium. A Lumascope 720 microscope was used to image the well every 15 min over a period of 24 hours.

To harvest cells on emulsions, the emulsion was transferred by pipetting to a centrifuge tube, the residual excess medium was removed before the emulsion was washed with PBS three times. The tube was then centrifuged for 5 min at a speed of 1,500 rpm to break the emulsion. The cell pellets

were collected at the interface between the PBS and the oil after centrifugation. For microcarriers, the microcarriers were collected in a centrifuge tube by pipetting as well. When the microcarriers were settled at the bottom of the tube, the medium was removed before the PBS was added into the tube to wash off excess medium, the microcarriers were then incubated with accutase solution for 5 minutes in the incubator for cell detachment. The solution was transferred to another centrifuge tube capped with a cell strainer to separate detached cells from the microcarriers. The flow through was saved and the cell pellet was collected after 5 minutes centrifugation at a speed of 1,200 rpm.

4.2.4 Cell Counting Assay

Since the curvature of the emulsion and microcarriers, cell density cannot be directly measured by ImageJ via nuclei staining, thus indirect measurements including metabolic activity via Cell Counting Kit-8 (CCK-8) and DNA measurements via Cyquant Kit were conducted.

4.2.4.1 Metabolic Assay

CCK-8 contains a water-soluble tetrazolium salt (WST-8 [2-(2-methoxy-4-nitrophenyl)-3-(4-nitrophenyl)-5-(2,4-disulfophenyl)-2H-tetrazolium, monosodium salt]), which would be reduced by electron mediators producing a water-soluble formazan dye. Samples at desired time points were incubated in medium containing 10% CCK-8 for four hours. After which, an amount of 100 µL medium was transferred to a 96-well plate and placed in a plate reader to measure the absorbance at 450 nm wavelength. The absorbance can roughly reflect the number of cells alive.

4.2.4.2 Cyquant Assay

For DNA measurement via Cyquant, emulsion/microcarriers cultured with cells were collected at desired time points, transferred into a 2 mL microcentrifuge tube and washed with PBS three times before being stored at -70 ℃ for cell lysis. The cells were thawed at room temperature and reacted with Cyquant Kit by following the user manual. The reacted solution was then transferred into a 96-well plate and measured with a fluorescence microplate reader set up with excitation at 480 nm and

emission at 520 nm. To convert absorbance into cell density, standard curves of cells on TPS and emulsion/microcarriers were prepared by plotting absorbance against cell numbers, which were determined by haemocytometer counting, and the relations were linearly fitted by Excel.

4.2.5 Staining and Imaging

Cell viability were assessed via Live/Dead and Hoechst staining, for which, half of the medium was replaced by pre-warmed PBS containing 2 µL Hoechst and 1 µL/mL calcein, 4 µL/mL ethidium from Live/Dead kit. After 40 min incubation, the cells were imaged via a Leica DMI4000B epifluorescence microscope.

Cell adhesion was studied via immunostaining of vinculin and phalloidin. To stain cells on emulsion, the emulsion was transferred into a well of a µ-Slide 8 Well containing 300 µL PBS. The sample was then fixed with 300 µL 8% PFA for 10 minutes and diluted with PBS six times before being permeabilized with 300 µL 0.4% Triton X-100 for 5 min at room temperature. Followed by an hour blocking and actin staining in blocking buffer (PBS containing 3 wt% BSA) combining with tetramethyl rhodamine isothiocyanate phalloidin (1:500). Samples were subsequently incubated with the corresponding primary antibody (anti-vinculin, 1:200 in blocking buffer) for 1 hour at room temperature, diluted with PBS for six time then incubated with Alexa Fluor 488-conjugated secondary antibody (1:500 in blocking buffer) and Dapi (1:500 in blocking buffer) for 1 hour at room temperature. The sample was imaged after another six times dilution with DI water. Confocal microscopy images were acquired with a Zeiss LSM710 Confocal.

To study cell adhesion from long-term culture, cells were harvested from different substrates as described in 4.2.3 and reseeded on glass slides pre-coated with FN. After 24 hours, the samples were stained as described above but with halved reagent concentrations. The stained samples were mounted by Mowiol on a coverslip and imaged by a Leica DMI4000B epifluorescence microscope. To determine cell spreading and adhesion areas and cell morphologies, images were analysed by

thresholding and watershedding fluorescence images of the cytoskeleton (phalloidin stained) via ImageJ. The area of cell clusters was removed when analysing the results. Focal adhesions were analysed by ImageJ via a previously reported widely adopted method,[59] only focal adhesion sized between 0.5 and 10 μm^2 were considered for the analysis.

4.2.6 MSC Differentiation Characterisation

MSCs were cultured at a density of 50,000 cells per well in 48-well plates. After 24 to 72 hours incubation when 100% confluency was reached, the differentiations were induced by replacing the growth medium with either osteogenic differentiation medium for osteogenesis or adipogenic differentiation medium for adipogenesis, while control group was continuously cultured with the growth medium. The media were replaced every three-day over a period of two weeks. For chondrogenesis, cell were seeded in U-bottom 96-well plates (Greiner Bio-One) for 72 hours to allow the formation of spheroids. The chondrogenesis was induced by culturing with chondrogenic differentiation medium while the undifferentiated control group was cultured with DMEM with 2 mM L-glutamine and 10% FBS. The media were replaced three times a week for a period of three weeks.

4.2.6.1 Oil Red Staining

Oil Red solution reacts with lipid droplets produced during adipogenesis and marks them in a red-orange colour. Oil Red staining stock solution was prepared by dissolving 150 mg of Oil Red O powder with 50 mL of 99% isopropanol. The solution was filtered and stored in dark after the powder was fully dissolved. The working solution was prepared by mixing the Oil Red stock solution with DI water at 3:2 ratio for 10 minutes, the mixture was then filtered via a 0.2 mm 0.2 µm filter. Samples were washed twice with PBS before being fixed with 4% PFA for 10 minutes. After which the samples were washed three times with PBS to remove excess PFA and then stained with Oil Red working solution. After an hour incubation, samples were washed six times with PBS and imaged by microscope.

4.2.6.2 Alkaline Phosphatase (ALP) Staining

ALP activity has been found peaked at early stage of osteogenesis,[60,61] therefore is used as an indicator of MSC commitment to osteogenic lineage. Substrate solution was prepared by dissolving one BCIP/NBT tablet in 10 mL DI water. The sample was washed with 0.1M PBS for three times and then fixed by 90% ice cold ethanol for 4 minutes. After being washed three times with DI water, the substrate solution was added to each sample and incubated for 1 hour at room temperature. After incubation, samples were washed three times with DI water and imaged by microscope.

4.2.6.3 Alizarin Red Staining

Alizarin Red is an anthraquinone derivative that can react with calcium to form a bright red complex, thus was used to identify the calcium deposition or the mineralisation of osteogenesis. Alizarin Red solution was prepared by dissolving 1 g Alizarin Red S powder in 50 mL DI water, once the pH of the solution was adjusted below 4.2 by hydrochloric acid, the solution was filtered via a 0.2 µm filter and stored in the dark. Samples were washed twice with PBS before being fixed with 4% PFA for 10 minutes. Before being stained with Alizarin Red solution, the samples were washed three times with DI water. After an hour incubation, samples were washed six times with DI water and imaged by microscope.

4.2.6.4 Alcian Blue Staining

Typical cartilage matrix such as aggrecan, which can react with copper-containing dye become dark blue, is produced during chondrogenesis, thus Alcian Blue was selected as an indicative staining for chondrogenesis.

Alcian Blue staining solution was prepared by dissolving 10 mg Alcian Blue 8 GX in solution prepared by 6 mL ethanol and 4 mL acetic acid. A destaining solution for washing was prepared by mixing 12 mL ethanol with 8 mL acetic acid. After washing twice with PBS to remove excess medium, the spheroid was fixed with 4% PFA for 45 minutes at room temperature. After rinsing with PBS three times, the sample was left with the Alcian Blue staining solution overnight. The staining solution was carefully

removed and the spheroid was washed three times with the destaining solution for 10 minutes, the sample was then ready for photograph.

4.2.7 Flow Cytometry

The antibody panels were designed as as CD105-FITC, CD73-RPE and CD-90 or CD105-RPE, CD73-FITC and CD90-APC for positive panel, CD34-FITC, CD45-RPE and CD19-Pacific Blue for negative panel. Unstained control, single colour controls and fluorescence minus one controls (FMO, samples are stained for all the flurochromes in the panel, except for the one that is being measured) were also performed respectively for voltage adjustment, compensation and positive gating. All the antibodies were prepared in PBS containing 1% BSA at dilutions suggested by the user's manual. After cultured from passage 3 cells on TPS, emulsion and microcarriers at passage 4, 6, 8 and 10, MSCs were harvested by accutase-solution as single cells from the corresponding substrates and transferred to 2 mL microcentrifuge tubes at a density of 1×10^6 cells/tube. Cells from each substrate were individually stained with one of the panels at a volume of 100 µL for 30 min on ice. After washing with 1.5 mL PBS, each microcentrifuge tube was filled with 300 µL ice cold PBS. Flow cytometry was performed on a FACS Canto II instrument (BD Biosciences), excited by 405 Coherent VioFlame, 488 Coherent Sapphire and 635 JDS Uniphase HeNe lasers. The results were analysed by Flowjo.

4.2.8 Real-Time Polymerase Chain Reaction (RT-PCR)

After being cultured for the desired time points, the RNA of MSCs was extracted via a Qiagen RNeasy Kit by following the user's manual. The concentration of extracted RNA was measured by a Nanodrop (Thermo Fisher) and the RNA was then reverse-transcribed by using QuantiTect® Reverse Transcription Kit by following the user manual. The cDNA obtained was preserved at -20 °C. The RT-PCR experiments were set up and performed by following the Taqman® Gene Expression Assay protocol using the kit in a QuantStudio™ Real-Time PCR System (Applied Biosystems™), Beta-2-

microglobulin (B2M, Hs00187842_m1) was chosen as the housekeeping gene, and the results were shown as the relative value obtained when comparing all the samples to newly thawed P3 cells control. Since some of the differentiation markers did not express under growth medium condition, the P4 cell cultured on TPS in differentiation medium was used as the control for differentiation. Analysis of the results was performed according to $2^{-\Delta\Delta Ct}$ method. The rest of the target genes are presented in the Table 2.

Table 2. List of Primers for PCR

Gene Name	Assay ID
Beta-2-microglobulin (B2M)	Hs00187842_m1
Nestin	Hs04187831_g1
Thy-1 cell surface antigen (THY)	Hs00174816_m1
Vascular cell adhesion molecule 1 (VCAM1)	Hs01003372_m1
Fatty acid binding protein 4 (FABP4)	Hs01086177_m1
Lipoprotein lipase (LPL)	Hs00173425_m1
Runt related transcription factor 2 (RUNX2)	Hs01047973_m1
Collagen type I alpha 1 (COL1A1)	Hs00164004_m1
Bone morphogenetic protein 2 (BMP2)	Hs00154192_m1
Osteocalcin (OCN)	Hs01587814_g1
SRY-box 9 (SOX9)	Hs00165814_m1
Collagen type II alpha 1 chain (COL2A1)	Hs00264051_m1
Collagen type X alpha 1 chain (COL10A1)	Hs00166657_m1

4.2.9 Statistical Analysis

Statistical analysis was carried out using Origin 2019 through one-way ANOVA with Tukey test for posthoc analysis. Significance was determined by * $P < 0.05$, ** $P < 0.01$, *** $P < 0.001$ and n.s., non-significant.

4.3 Results and Discussions

4.3.1 Characterisation of Emulsion Stability and Nanosheet Structure

In Chapter 2, where the impact of Mw on PLL assembly was studied, XPS characterisation showed that all PLLs were able to form stable emulsions with the assistance of 10 µg/mL PFBC except for the lowest Mw (1-5 kDa), which was believed to be unable to provide sufficient steric repulsion for emulsion stabilisation. However, it was also found that for molecular weights above 30 kDa, emulsion droplets were found to be significantly smaller, were flowing less freely and were more likely to stick to the wall of glass vials (Figure 4.1). Bright field microscopy images of emulsions transferred to well-plates (Figure 4.1) showed that droplets were generally smaller at higher Mw, and tended to gel. This may be explained by the steric hindrance associated with longer chains, favouring lower radii of curvature, and suggested that long chains may bridge across two droplets resulting in their gelation. Some literature suggested that cells are sensitive to the size of beads on which they are cultured, as smaller sizes and higher curvatures were found to impact cell adhesion and proliferation.[178,198] Moreover, in microcarrier-based culture systems, the carriers are expected to be flowable and to allow sufficient bead-to-bead transfer for cell passaging. Obviously, for cell culture applications, emulsions generated at high Mw may not be optimal and our choice was limited to 4-15 kDa and 15-30 kDa PLL. In Chapter 3, we studied the impact of PLL Mw on MSC adhesion and proliferation at PLL/FN nanosheet assembled oil interfaces and found that higher Mws PLL nanosheets may be better to sustain the

fracture resulting from cell contractility at high cell density and therefore afforded higher cell yields. In conclusion, 15-30 kDa PLL was selected to prepare emulsions for the following MSC culture.

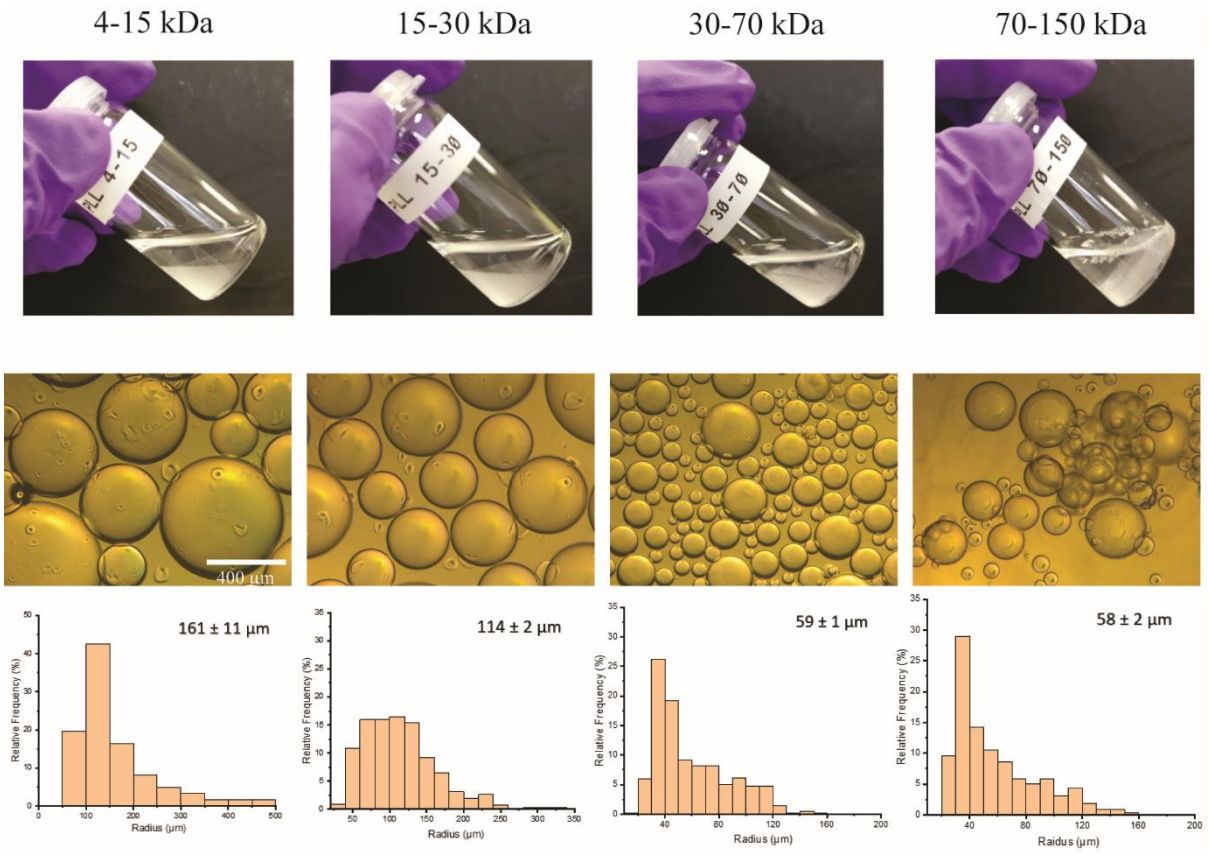

Figure 4.1. PFBC assisted PLL assembly stabilising Novec 7500 emulsion. Photos of Novec 7500 emulsion formed and stabilised by different Mw PLLs (top) and the corresponding bright field microscope images (middle) and histogramme of the emulsion size distribution (bottom, numbers are the corresponding average radius ± s.e.m).

The long-term stability of emulsions was further studied and the impact of cell proliferation on emulsion stability was investigated. As shown in Figure 4.2A, over a period of a week of culture, emulsions maintained a spherical shape without any significant distortion. Although at later time points MSCs were bridging across droplets, no significant droplet merging was observed during the first week. The corresponding histograms show no obvious size distribution shift, further confirming the stability of emulsions (Figure 4.2B). However, it is noticeable that the size of emulsion with cells are generally larger than without, which maybe resulted by cell bridging between droplets.

Considering that the average radius of emulsions without cells was around 123 ± 3 µm, a monolayer of droplets expanded the culture area of a well to roughly 2.5-fold. Further increase can be achieved by introducing more emulsion in each well.

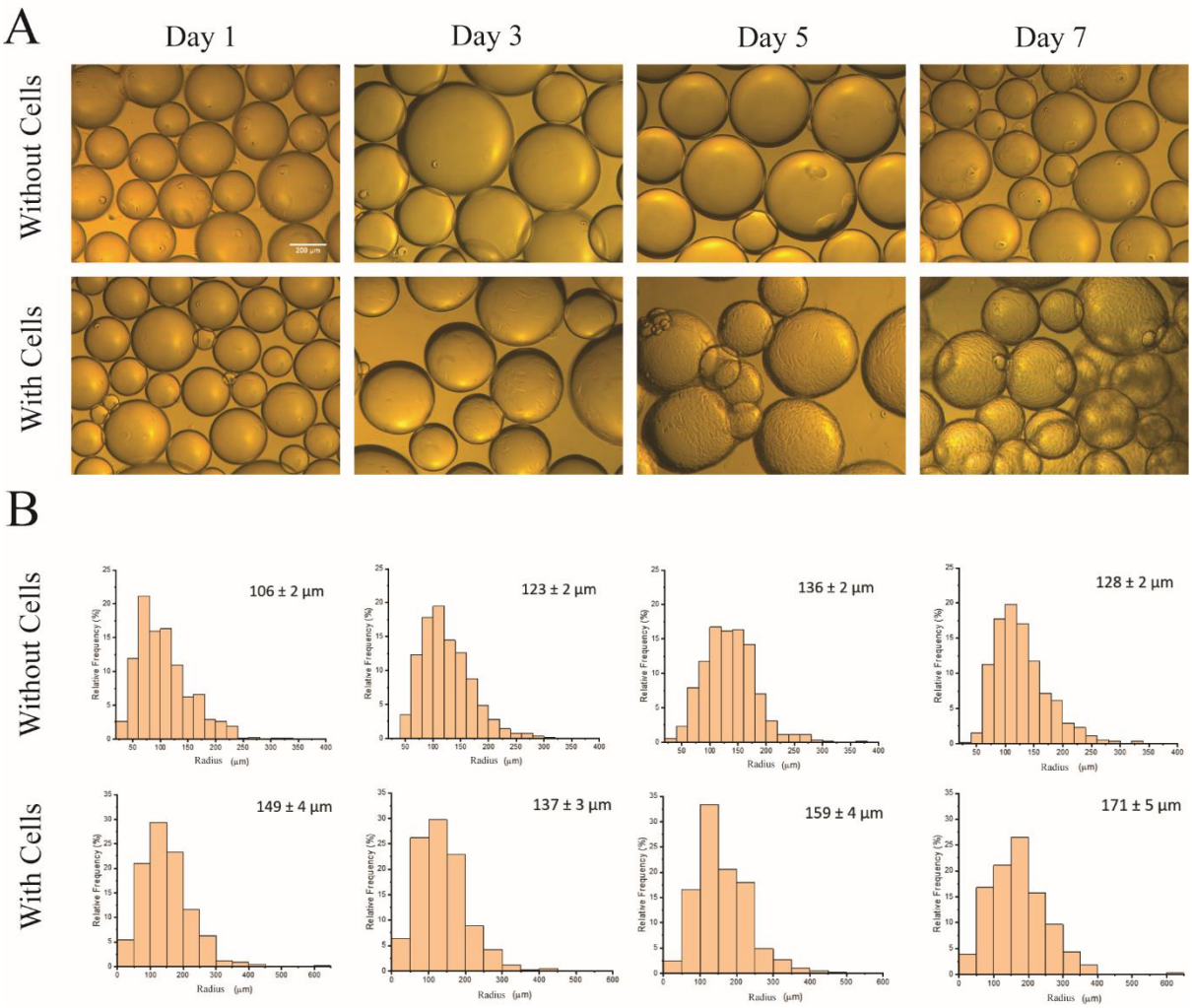

Figure 4.2. PLL/FN assembled emulsion maintains stability in the presence of cells over a period of 7 days. (A) Bright field microscope images of emulsion with and without cells cultured for week and (B) the corresponding histogramme of the emulsion size distribution and average radius ± s.e.m.

The structure of nanosheets at the interface of emulsions was studies via a polarised optical microscopy, which illuminates samples with a polarised light to reveal existing birefringent structures. As a globular protein, BSA can quickly adsorb to the surface of oils, providing sufficient steric repulsion to stabilise emulsions. However, as shown in Figure 4.3, the birefringent structure was not clearly seen

under cross-polarised illumination, in the absence of pro-surfactant. With the assistance of PFBC (for Novec 7500) or HDC (for hexadecane), clear birefringence was observed at the periphery of droplets, indicating the role that the pro-surfactants play in helping BSA form a more ordered structure at the interface. A similar ordered structure was also found on PLL formed emulsion, though it was less clear than the BSA one formed under the same condition. This makes sense as PLL is more flexible than BSA, thus it would be harder for PLL to form an ordered structure like BSA does. It was also found that a higher PFBC concentration (10 µg/mL) brought clearer birefringence than the lower concentration (1.25 µg/mL), highlighting the importance of pro-surfactants.

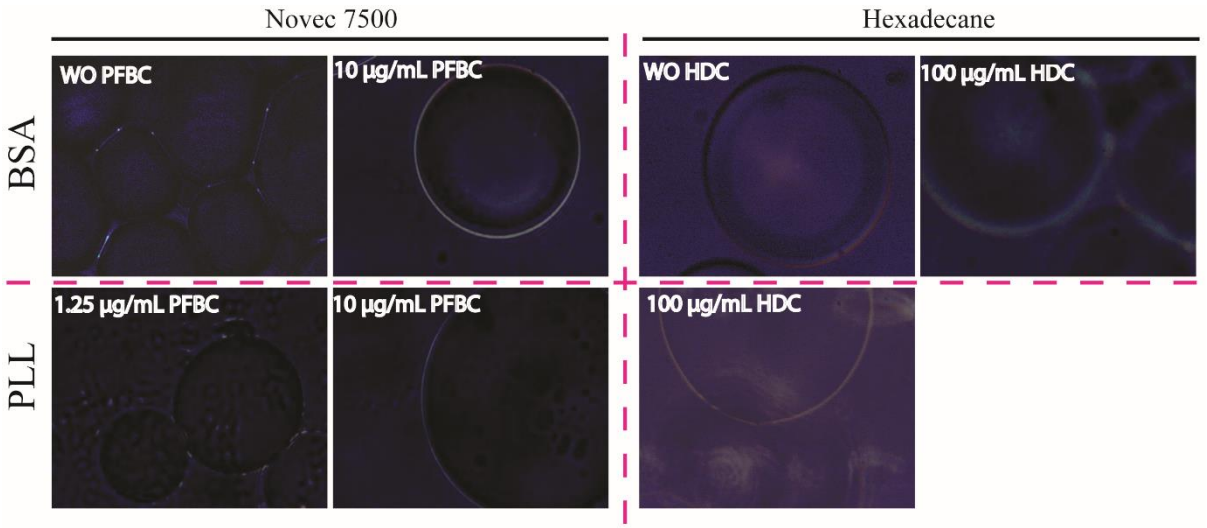

Figure 4.3. Protein formed a birefringent structure on the surface of the emulsion. Polarised optical microscope images of emulsion formed by Novec 7500 (left) or hexadecane (right) with BSA (top) or PLL (bottom) with or without the corresponding pro-surfactants.

In Chapter 3, we also showed the successful culture of MSCs on LbL assembled PLL-HA-COL nanosheets. However, in the case of emulsions, the addition of HA disrupted the PLL stabilised emulsions. As shown in the Figure 4.4, upon the injection of HA, the droplets in the previously stable emulsion gradually coalesced in just 30 min. After 24 hours, the formation of irregular clump was maintained, which was a sign of partial coalescence.[300] HA is known for its large chain persistence length (> 10 nm) and strong hydrophilicity, therefore may be poorly diffusing upon adsorption.[301] In the study of PLL/HA nanosheets layer-by-layer assembly on solid substrates, it was found that PLL/HA

islets were formed first upon the deposition of HA and subsequently coalesced and restructured into homogeneous islands.[103] This mechanism could be used to explain the instability of PLL/HA assembled emulsion. Owing to the high viscosity and limited diffusion of HA, it slowly adsorbed to the surface of PLL-coated emulsions and destabilised PLL nanosheets by electrostatic interactions. This led to the coalescence of adjacent droplets before complete coverage of the droplet surface with HA to provide electrostatic repulsion. The elasticity of PLL nanosheets initially resisted such merging process, but once the Laplace pressure was equilibrated, it could not prevent coalescence.[302] Since both PLL and HA are classified as weak polyelectrolytes which are partially charged only, the assembly of which would be largely affected by pH and ionic strength,[303] we have been working on adjusting ionic strength to compensate such interactions, and some progress has been made, but the following MSC culture on emulsion would remain focused on the PLL-FN nanosheet system only.

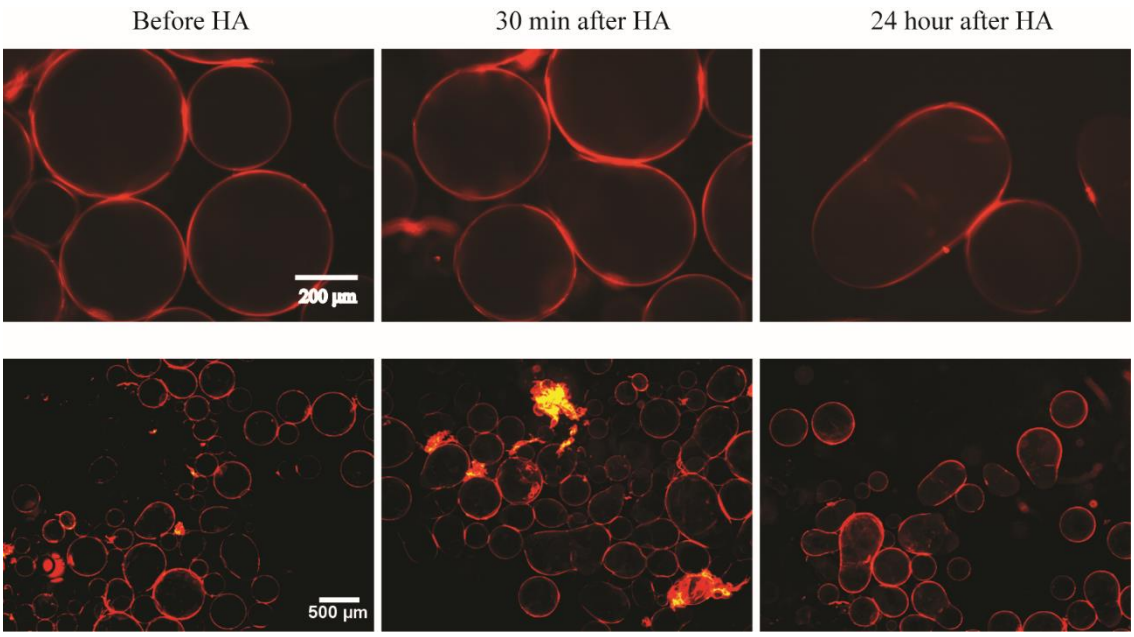

Figure 4.4. The addition of HA destabilises PLL assembled emulsion. Epifluorescence microscopy images of PLL assembled emulsion prior to the addition of HA (left), 30 min (left) and 24 hours (right) after the addition of HA. Red, PLL.

4.3.2 MSCs Culture on Emulsions

Results from section 4.3.1. suggested that our PLL/FN assembled Novec 7500-based emulsions were able to maintain its stability for at least a week. MSCs were cultured on these emulsions (Figure 4.5). The metabolic activity of MSCs on emulsions was at the same level as on TPS on day 6, which can be roughly interpreted as an indication that MSCs proliferated similarly on emulsions and on TPS at this time point. It was also noticeable that the metabolic activity of cells on TPS on day 3 showed little difference compared to that of day 6 whereas the metabolic activity of cells on emulsions was much lower on day 3 than on day 6. MSCs on TPS already reached a high level of confluency on day 3 as evidenced by the Live/Dead and Hoechst staining (Figure 4.5C). The limited culture area provided by the well-plate was the major hurdle preventing MSCs from proliferating further, the images also showed little difference in cell density on TPS between different time points. In the case of emulsions, a much larger surface area was available which could extend the lag phase of MSC proliferation, thus the initial proliferation was delayed resulting in lower activity on day 3. However, we also found that the metabolic activity measurements were insensitive to higher cell densities and the values were likely to underestimate the actual MSC density on emulsions when we prepared the standard curve to convert metabolic activity into cell numbers (Appendix Figure 2). In any case, the metabolic assay suggests that MSC proliferation on emulsions is at least comparable to that on TPS. MSC adhesion to the surface of emulsions was also studied by immunostaining for vinculin and actin after culturing for 6 days. MSCs clearly spread on emulsions adopting an elongated shape. Stress fibres and FAs were also clearly visible (Figure 4.5D), confirming that the PLL/FN nanosheets on curved emulsions were mechanically strong enough to sustain forces exerted by MSCs for the formation of FAs and assembly of a contractile cytoskeleton favouring the establishment mechanotransduction at the oil interface.

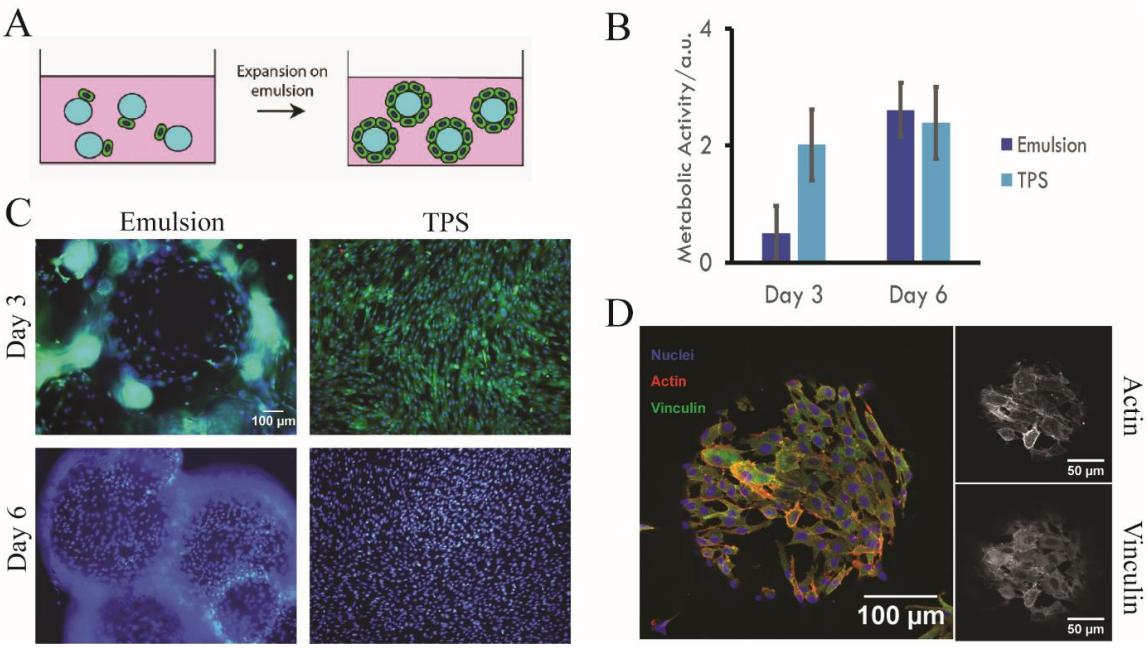

Figure 4.5. MSCs adhere and proliferate on PLL/FN assembled emulsion. (A) Schematic illustration of MSCs proliferate on emulsions. (B) Metabolic activity of MSCs cultured on emulsion compare to that of TPS on day 3 and on day 6. n represents number of experiments, n ≥ 3. (C) Epifluorescence microscopy images (Live/Dead and Hoechst stainings) of MSCs cultured on emulsion and TPS for 3 days and 6 days. Green, live cells, red, dead cells; blue, nuclei. (D) Confocal microscopy images of MSCs spread on the surface of emulsion. Green, vinculin; red, actin; blue, nuclei.

One of the advantages of culturing cells on microcarrier-based systems is that cells can be easily passaged via bead-to-bead transfer or bead-to-TPS transfer by simply adding fresh emulsions (Figure 4.6A) or transferring emulsions to a new well. As shown in Figure 4.6B, MSCs had been cultured on emulsion for 7 days and reached a very high confluency. After addition of red-labelled fresh emulsions, cells were found bridging the gap between old and new emulsions and transferring to these last ones. Cells were already growing on new droplets 3 days after the addition of fresh emulsions. Moreover, emulsions can also allow cell transfer to solid substrates as shown in Figure 4.6C and was also confirmed by live imaging over a period of 5 hours (Figure 4.6D), during which cells bridged the gap between droplets and gradually moved from droplets to new droplets and to TPS.

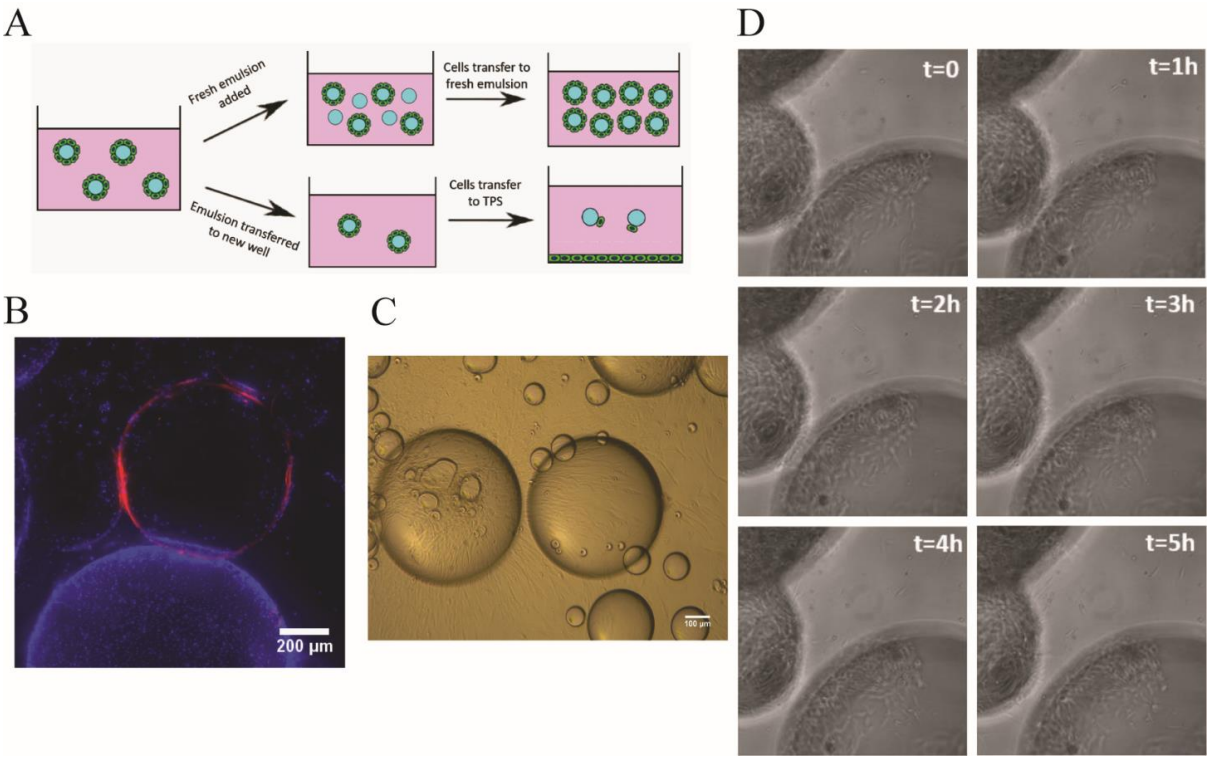

Figure 4.6. MSCs on emulsion migrate from emulsion to other substrates. (A) Schematic illustration of passaging cells via emulsion-to-emulsion transfer or emulsion-to-TPS transfer. (B) An epifluorescence microscopy image of MSCs cultured on an old emulsion for 7 days migrating to a fresh emulsion, day 3. Blue, nuclei; Red, fresh emulsion made from fluorophore-tagged PLL. (C) A bright field image of MSCs transferring from emulsions to TPS, day 2. (D) Lumascope images of MSCs transferred from emulsion to emulsion and TPS over a period of 5 hours.

Another advantage of our emulsion-based system in addition to other commercial solid microcarriers is that cells on emulsion could be harvested by centrifugation without the need of trypsin or other enzymatic treatments (Figure 4.7A). When a high cell density was reached on emulsions, nanosheet fracture is likely to occur as described in Chapter 3. Those defects on the surface provide weak points where coalescence could be induced as droplets collide. The broken emulsions merged into an oil phase that settle down at the bottom of the tube after the centrifugation, whilst cells accumulate at the interface between the oil phase and the aqueous phase (Figure 4.7B). Since no enzymatic digestion was used, cells maintained the organisation as a cell sheet with intact cell-cell junctions (Figure 4.7C). Such harvested cell sheets can quickly

adhere to TPS and mostly maintained in a complete cell sheet form (Figure 4.7D), displaying a high level of viability (Figure 4.7E).

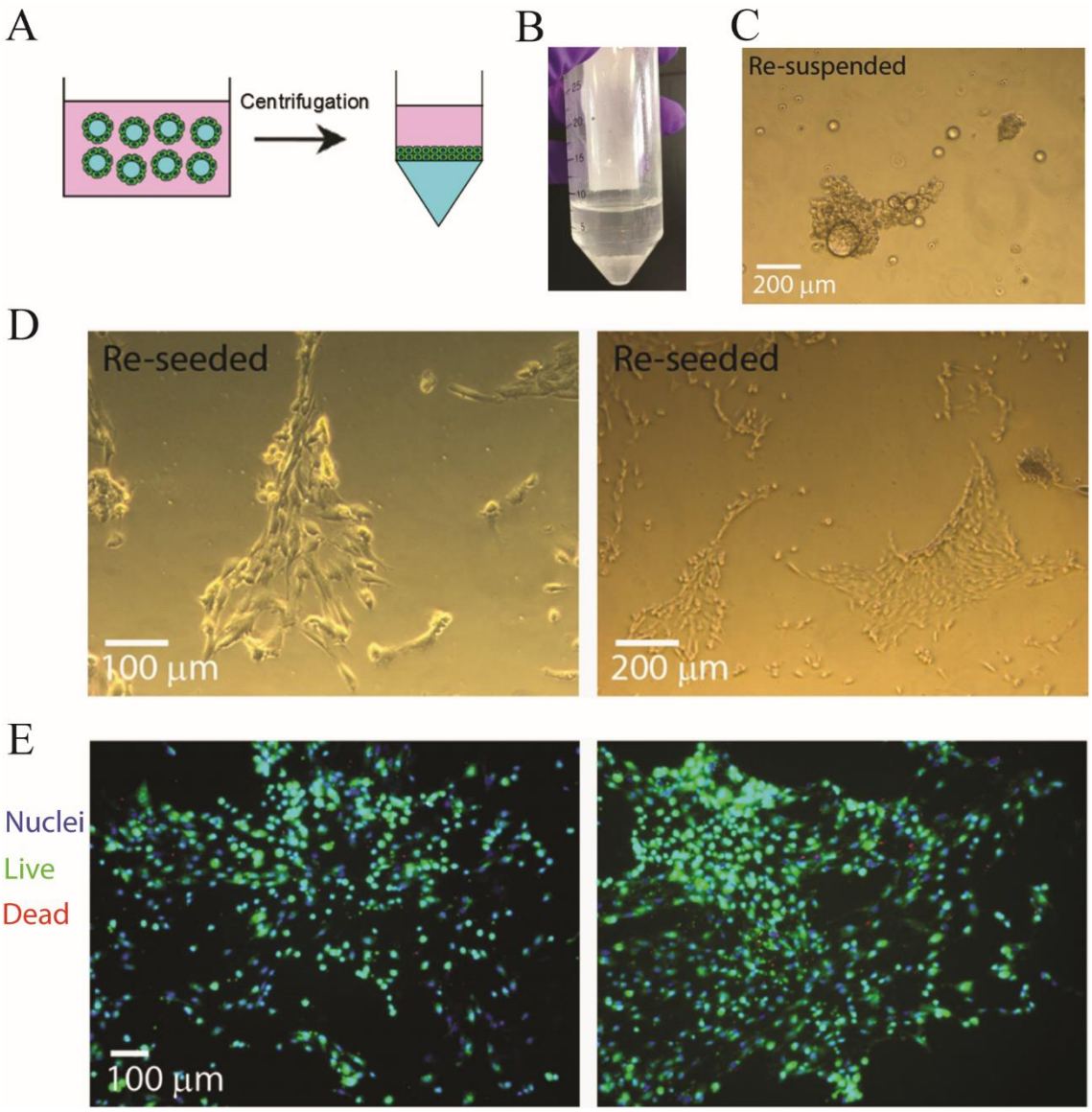

Figure 4.7. MSCs cultured on emulsions is non-invasively harvested via centrifugation. (A) Schematic illustration of harvesting cells from emulsion via centrifugation. (B) A photo of broken emulsion after centrifugation, cells were collected at the interface between the aqueous solution and the oil. (C) A bright field image of MSCs re-suspended immediately after centrifugation. (D) Bright field images of harvested MSCs re-seeded on TPS for 24 hours. (D) Epifluorescence microscopy images (live/dead and nuclear stainings) of MSCs harvested via centrifugation and re-seeded on TPS for 24 hours. Green, live cells, red, dead cells; blue, nuclei.

Apart from fluorinated oils, non-fluorinated oils such as PDMS and mineral oils were also used to generate emulsions for cell culture purposes. In Chapter 3, MSC culture was achieved on these non-fluorinated oil pinned droplets, showing the generality of such nanosheets assembled at liquid interfaces for MSC culture. Such generality also applies to emulsions as shown in Figure 4.8, where high cell density was observed on both mineral oil and PDMS emulsions on day 7. However, a few challenges remained concerning the use of non-fluorinated oil systems. Due to the viscosity of these non-fluorinated oils, the emulsions formed were very likely to stick together. The hydrophobicity and density of the oils also drove the emulsion to the wall of the well plate and the stability of the non-fluorinated oil emulsion was poorer than that of the fluorinated oil emulsions. Unlike fluorinated oils, whose density is higher than water hence stays at the bottom, the non-fluorinated oils are lighter and tend to float, which causes difficulties for cell inoculation and medium changing.

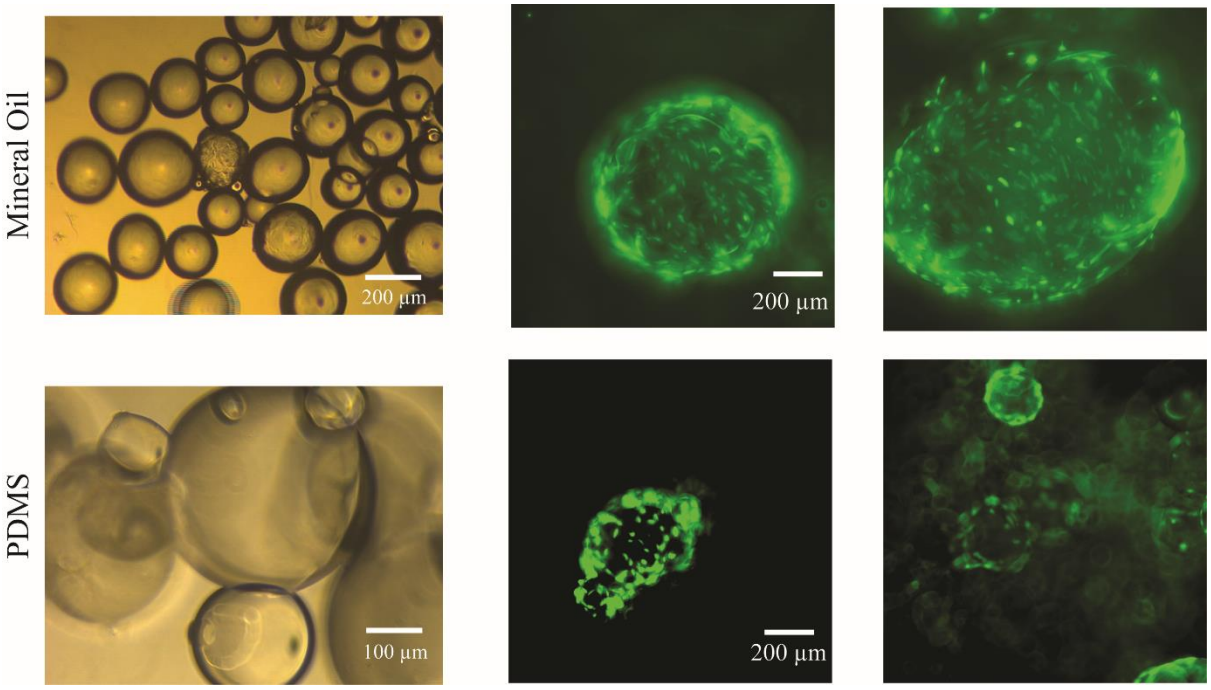

Figure 4.8. MSC cultured on non-fluorinated oil-based emulsion. Bright field microscope images (left) of mineral oil emulsion (top) and PDMS emulsion (bottom) left for 3 days. Epifluorescence microscopy images (right) of MSC (green, calcein staining) cultured on the corresponding oil emulsions for 7 days. Emulsion was prepared by 0.1 mg/mL 1:1 ratio mixture of SBC and HDC, functionalised with PLL/FN nanosheets.

4.3.3 Long-term Retention of MSC Phenotypes on Nanosheet-Stabilised Emulsions

As previous works have pointed out, the enzymatic digestion used for cell harvesting breaks cell-cell junctions and cell-ECM adhesion can severely modify cell phenotype in long-term cultures. Our emulsion-based culture system allows harvesting cells via centrifugation. Due to the disadvantages of non-fluorinated oil in emulsion stability and cell inoculation, the fluorinated oil emulsion is therefore more controllable over non-fluorinated oil and was used to perform long-term cultures.

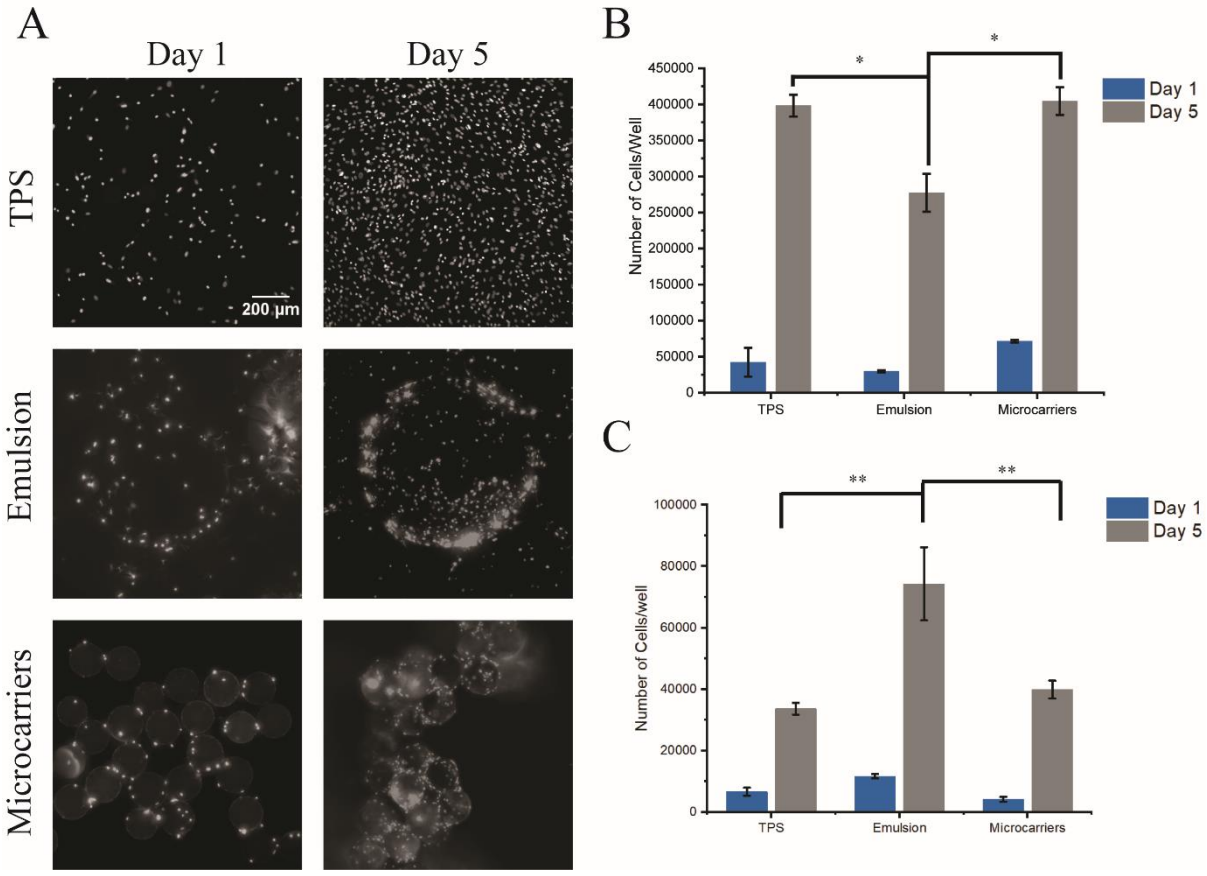

Figure 4.9. MSC proliferation on TPS, emulsion and microcarriers. (A) Epifluorescence microscopy images of Hoechst stained MSCs cultured on TPS, emulsion and microcarriers on day 1 and day 5. The corresponding MSC densities were quantified by (B) Cyquant and (C) CCK-8. Error bars are s.e.m; n represents number of experiments, n ≥ 3.

A commercially available microcarrier (Synthemax II) recommended for MSC culture was also included in the long-term study to compare with TPS control and our emulsion system. Emulsions and microcarriers were transferred to 24-well plates, increasing the surface area roughly 2.53- and 3.79-

fold respectively, with total culture areas to 4.8 and 7.2 cm^2, respectively. To avoid any potential differentiation induced by over-confluent cells, 6-well plates, which provide surface area of 9.6 cm^2 per well, were used for cell culture on TPS. A Cyquant assay was used to quantify the DNA amount which was subsequently converted into the density of cells on different substrates via a standard curve (Appendix Figure 1), reflecting that MSC density on emulsions after a 5-day culture was significantly lower than that of TPS and microcarriers (Figure 4.9B). Apparently, the surface area was lower for emulsions than for the other culture substrates, what could lead to a lower cell output. However, in terms of unit area output, the cell densities were similar on emulsion and microcarriers. Both were significantly higher than that of TPS on day 5 (Figure 4.10). In the metabolic activity measurement, it was observed that MSCs on emulsion proliferated significantly more than on TPS and microcarriers on day 5 (Figure 4.9C), exactly the opposite to what the Cyquant assay suggested, although the metabolic assay is not very sensitive at higher cell densities as we mentioned above.

The primary human bone marrow derived MSCs were received, expanded and further cryopreserved at passage 2. After further expansion on tissue culture flask, some of the MSCs harvested were used to perform flow cytometry immuno-phenotyping and RT-PCR experiments to determine their phenotype at an early passage. The rest of the MSCs were cultured on the corresponding substrates for long-term study from passage 3 onwards. Culturing MSCs for 5 days allows cells to be sufficiently confluent (70-80 coverage) on the substrates. The majority of the cells were harvested for flow cytometry, RT-PCR, adhesion or differentiation studies whereas the rest of them were passaged via enzymatic digestion (TPS) or carrier-to-carrier transfer (emulsions and microcarriers) to fresh substrates for continuous culture. Such process was repeated (Passage 6 and 8 proliferation results shown in Appendix Figure 3) until cell proliferation rates were significantly reduced (at passage 10 where no significant proliferation was observed between day 1 and day 7, Figure 4.10). All the characterisation of cell behaviour and phenotypes were carried out every two passages (at Passage 4, 6, 8, 10).

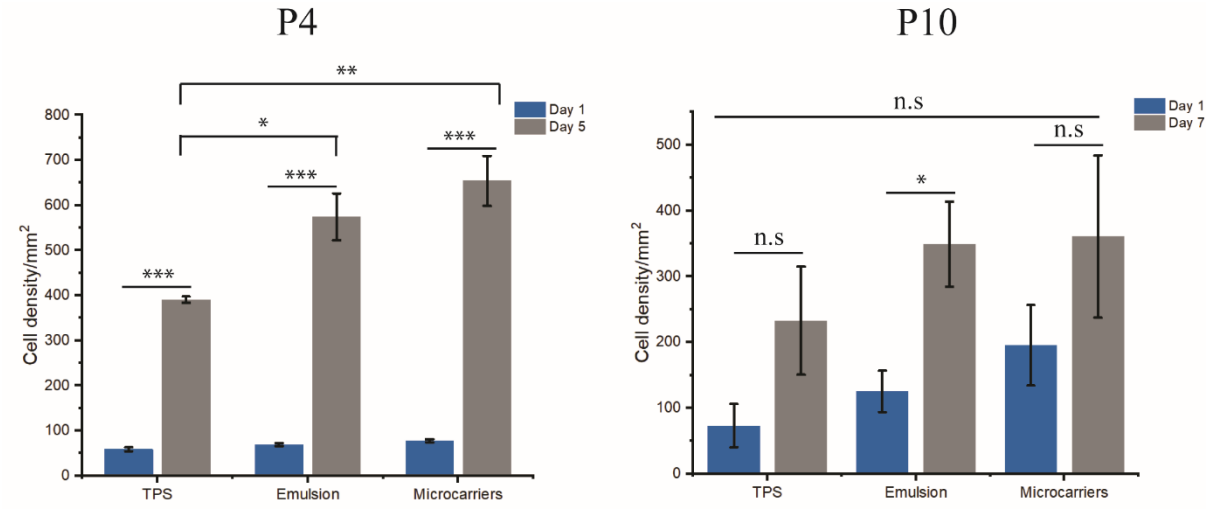

Figure 4.10. MSC proliferation on TPS, emulsion and microcarries is reduced at later passage. MSC densities were measured via cyquant assay and converted into number of cells per mm^2 at passage 4 (left) and 10 (right). Error bars are s.e.m; n represents number of experiments, n ≥ 3.

4.3.3.1 Long-term Adhesion Behaviour

To examine cell morphology and spreading, we examined important markers associated with changes in cell phenotype. MSCs were harvested from different substrates and re-seeded on FN-coated glass slides for 24 hours before characterisation by immunostaining. Cell spreading gradually increased during the long-term culture and was significantly higher at later passages (in particular passage 10), presumably as a result of cell senescence.[282,283] At passage 10, cell spreading areas were almost twice the size of that of cells at passage 3 on all substrates (Figure 4.11B). No significant difference was found between different substrates throughout the culture period when comparing them at one specific time point since MSCs morphologies were very similar regardless of the culture substrate selected. At passage 10, folds in the actin structure indicative of membrane ruffles[304,305] were found at the cell periphery on TPS and microcarrier-cultured cells. Actin stress fibers were also poorly organised (Figure 4.11A). Since membrane ruffling was believed to be an indicator of inefficient lamellipodia adhesion and enhanced motility,[304–306] these findings could suggest poor cell adhesion and poor cytoskeleton assembly, which are also regarded as characteristics of senescent cells.[282] In the case of cell circularity, no dramatic changes were observed and MSCs on all substrates at all the time points maintained an elongated shape with circularity around 0.23 (Figure 4.11C).

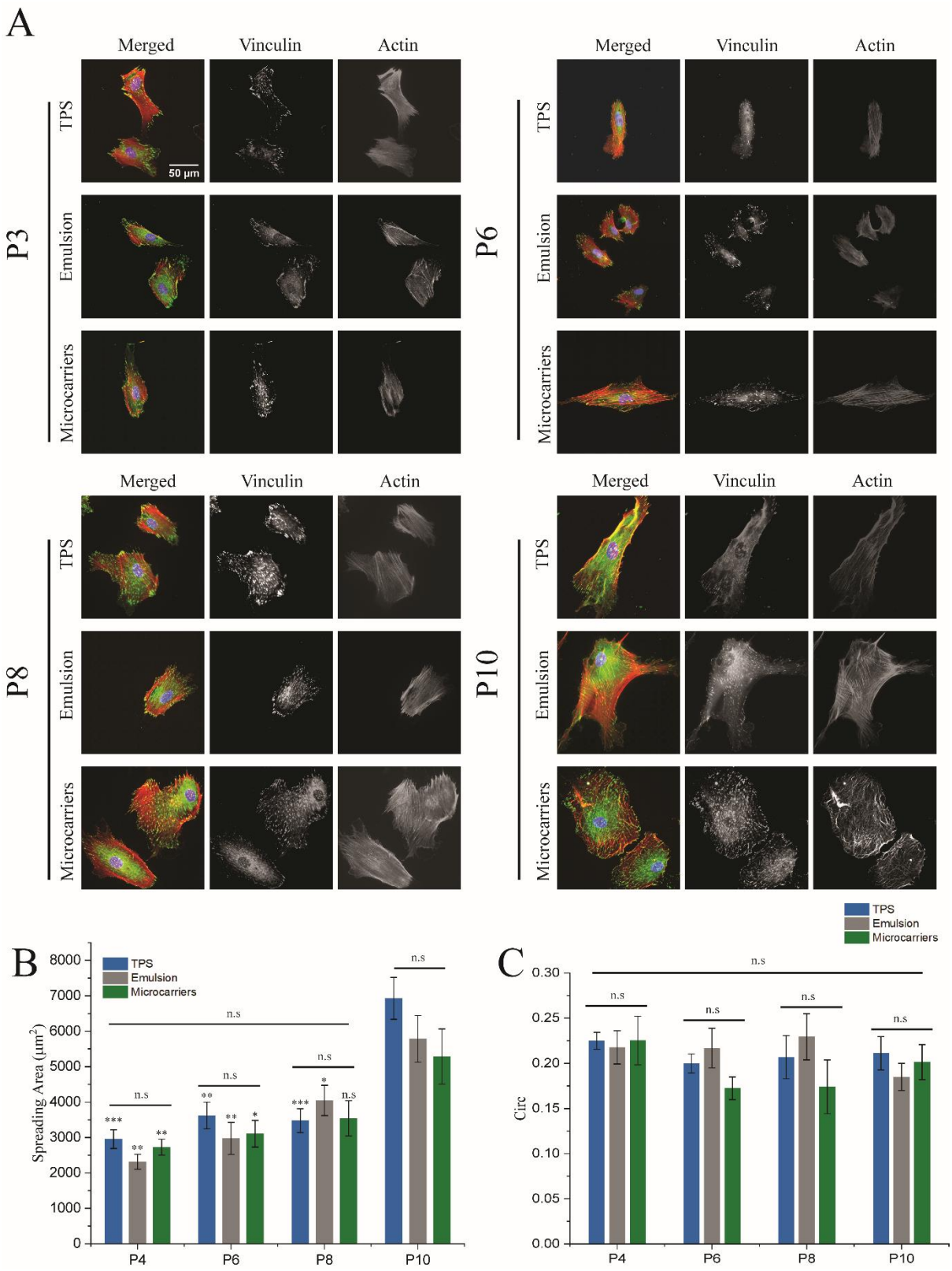

Figure 4.11. MSC spread similarly on TPS, emulsion and microcarriers over a long-term culture. (A) Confocal microscope images of MSCs harvested and transferred to FN-coated glass slides for 24 hours, green, vinculin; red, actin. Summarised spreading area (B) and circ (C) of the corresponding cells calculated from actin images. Error bars are s.e.m; n represents number of experiments, n ≥ 3, more than 40 cells for each condition were measured in each experiment.

MSC adhesion on these substrates was also showing a similar trend during the long-term culture. FAs of MSCs cultured on different substrates did not show any difference in terms of area, circularity and aspect ratio during the whole period of the long-term culture. However, the amount of FA per cell was found significantly increased on TPS and emulsion at passage 10 relative to that of P3 (Figure 4.12A). This increased FA density at later passage was possibly in response to or resulting in the increased spreading area. The histogram of FA size distribution (Figure 4.12E) revealed that the majority of FAs were smaller than 2 μm^2 and there was an increased percentage of FAs below 1 μm^2 from P4 (around 33%) to P10 (more than 35%). Adhesion areas below 1 μm^2 are identified as focal complexes instead of FAs, which serve as precursors of FAs.[3,31] The increased amount of focal complexes suggested the increased mobility of P10 MSCs.

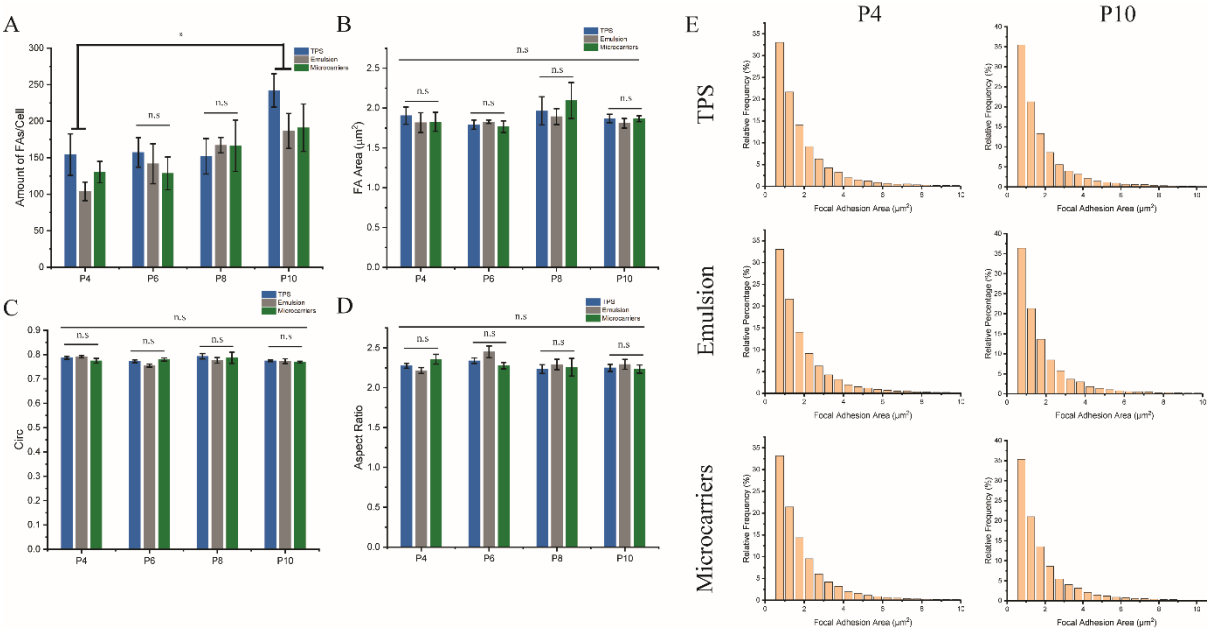

Figure 4.12. MSC adhere similarly on TPS, emulsion and microcarriers over a long-term culture. Summarised (A) amount of focal adhesion per cell, (B) focal adhesion area, (C) circ of focal adhesion and (D) aspect ratio of focal adhesion. Error bars are s.e.m; n represents number of experiments, n ≥ 3, more than 40 cells for each condition were measured in each experiment. (E) Histogramme of focal adhesion area distributions.

4.3.3.2 Long-term Phenotypic Characterisation

According to the ISCT, MSCs must express CD105, CD90 and CD73, at the same time, lack the expression of CD45, CD34, CD14 or CD11b, CD79a or CD19 and HLA-DR.[277] Hence immuno-phenotyping flow cytometry was conducted to monitor MSC expression of these surface molecules. Flow cytometry was performed as described in 4.2 Materials and Methods. For data analysis, gating was performed to discard dead cells, debris and cell doublets before CD73 positive cells were selected on histograms first (CD73 is highly expressed thus can be easily discriminated from negative signals in histograms) based on the FMO control. Cells co-expressing CD105 and CD90 were then sub-gated from the dot plot as shown in Figure 4.13B, based on the corresponding FMO control. As shown in Figure 4.13A, MSCs gradually lost their co-expression of these three markers over time, the expression was significantly reduced in P10 cells on TPS and emulsion compared to P4 but no difference was found between different substrates throughout the passages. Figure 4.14A showed the trend of each individual marker, CD73 was maintained at a very high expression level on all the substrates throughout the culture, whereas the expressions of both CD90 and CD105 was reduced at later passages. CD90, also known as Thy-1, is a small glycoprotein present at the surface of cells, attached through a glycosylphosphatidylinositol anchor,[307,308] and functioning as a signalling modulator in regulating cell proliferation, adhesion and migration.[308] More recent studies suggested that CD90 may also be involved in MSC differentiation, as reviewed by Anja Saalbach and Ulf Anderegg,[307] indicating that CD90 may play an important role in balancing the osteogeneic and adipogenic differentiation of MSCs. CD105, also known as endoglin, is a cell membrane glycoprotein receptor for the transforming growth factor β (TGF-β) superfamily, and has been widely recognised for its role in angiogenesis.[309] Studies on MSCs also addressed its role in osteogenesis and adipogenesis,[310,311] but other studies suggest its role in chondrogenesis, although this remains unclear.[312,313] The downregulation of these surface markers is not unexpected, as it indicates the change of MSC phenotypes during long-term culture. It is also worth noting that MSCs are notoriously autofluorescent,[314] larger cell sizes at later passage would increase the autofluorescence signal, which could mask the signal of weakly expressed

surface markers. Autofluorescence, generally arising from endogenous fluorophores such as nicotinamide adenine dinucleotide (NADH), flavin adenine dinucleotide (FAD) or structural proteins including COL and elastin.[284] MSCs passaged on emulsions and microcarriers via bead-to-bead transfer may prove to be more difficult to characterise by flow cytometry due to this autofluorescence, as the enzymatic digestion was only conducted prior to the measurements while the lack of enzymatic digestion during passages could leave cells with more residual ECM proteins when performing the experiment that further enhance the autofluorescence, resulting in higher threshold for positive populations. As shown in Figure 4.13B, the gating for MSCs that co-expressed CD90 and CD105 on emulsion and microcarriers were generally higher than that of TPS. However, in the histogram of each individual marker is showing that the intensity was mostly the same (Figure 4.14B), MSCs on TPS even showed slightly lower expression of CD90 and CD105 at passage 10. Some evidences also suggests that the autofluorescence is an indicator of MSC proliferation[315] and senescence.[284]

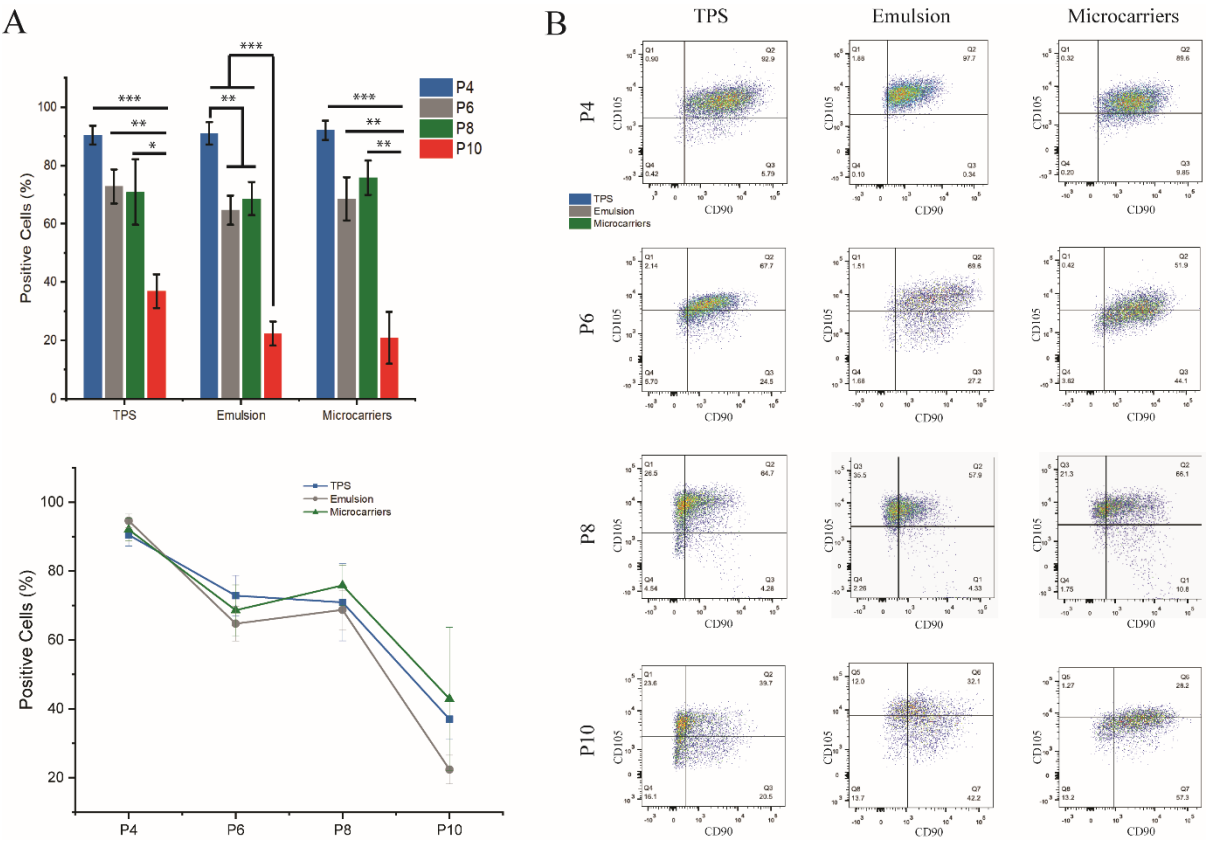

Figure 4.13. MSCs retain surface markers similarly on TPS, emulsion and microcarriers over a long-term culture. (A) Bar chart of percentage of MSCs co-expressing CD73, CD90 and CD105, and (B) the

corresponding line chart showing the trend. Error bars are s.e.m; n represents number of experiments, n ≥ 3. (C) Examples of the dot plots of CD105 against CD90 in CD73 positive gating.

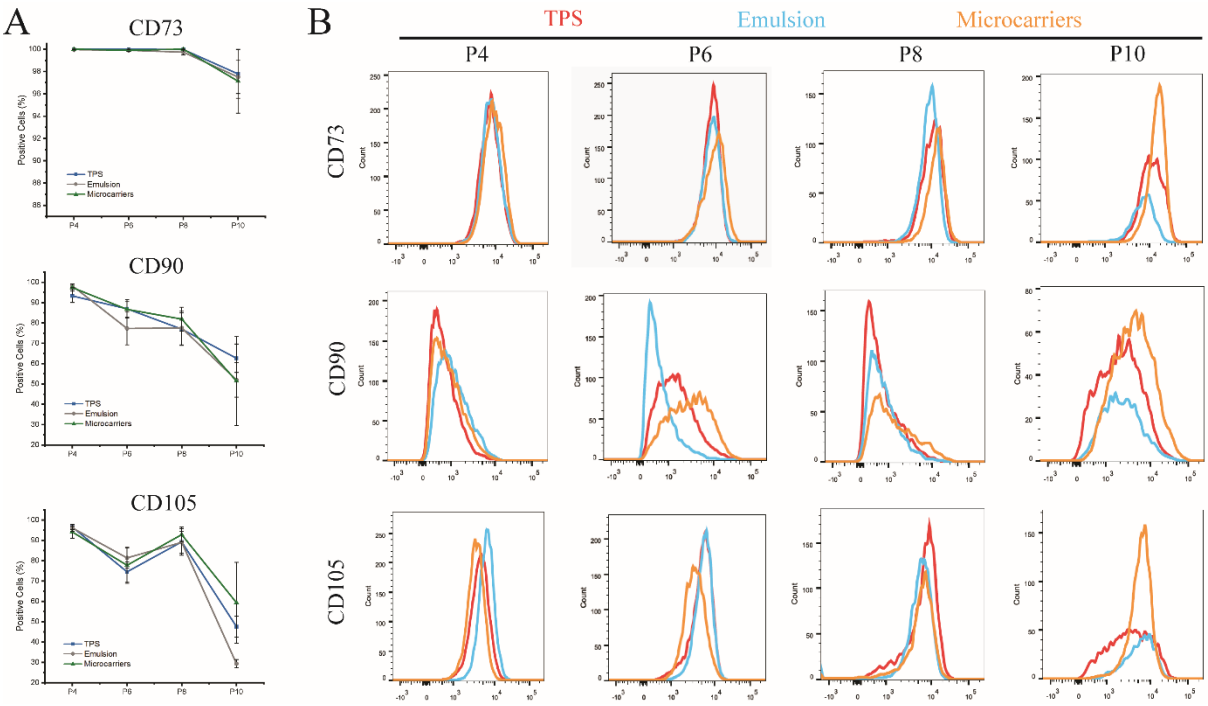

Figure 4.14. MSCs retain each individual surface marker differently over a long-term culture. (A) Line chart of the percentage of MSCs positive individually to CD73 (top), CD90 (middle) and CD105 (bottom). Error bars are s.e.m; n represents number of experiments, n ≥ 3. (B) Examples of the fluorescence intensity histogramme of each individual surface markers. Red, TPS; blue, emulsion; light brown, microcarriers.

The expression of stemness markers namely THY, NES and VCAM-1 were also monitored at gene level and no significant difference was found (Figure 4.15). THY is also known as CD90, the expression of which was downregulated at later passage in flow cytometry measurements, as mentioned above. In contrast, its gene expression was found upregulated, which suggests that the high expression of THY does not necessary translate into surface marker presentation. Nestin is normally considered as a neural marker, but its role in cell-cell junction and signalling in the niche, especially its role in hematopoietic stem cell (HSC) homing is of particular interest in mimicking the microenvironment of bone marrow.[316,317] It is also believed that nestin is upregulated upon culture on soft substrates.[7]

However, this is not the case on the nanosheets assembled emulsions where nestin expression remained low throughout the culture. This suggests that either the curvature of emulsions altered such process or culture on emulsions allowed to retain MSC stemness and prevented differentiation towards neural lineages. VCAM-1, also known as CD106, is an adhesion molecule that has been reported to mediate homing, migration and adhesion of MSCs.[318,319] The unchanged gene expression level is in agreement with the adhesion study. Some studies also suggested that VCAM-1 may be indicative of adipogenic and osteogenic potential of MSCs[319] as VCAM-1 positive MSCs were found to be less osteogenic but more adipogenic than VCAM-1 negative MSCs'.[320]

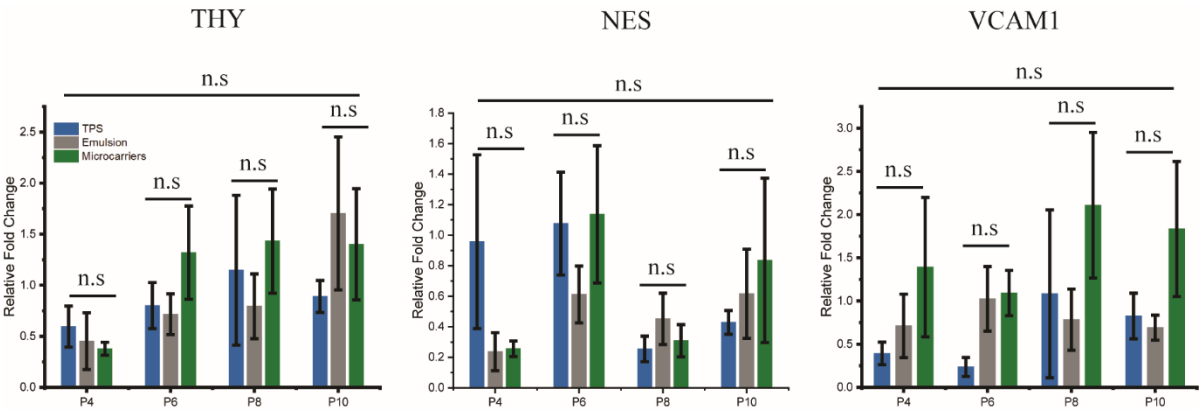

Figure 4.15. MSCs retain stemness similarly on TPS, emulsion and microcarriers over a long-term culture. RNA was directly extracted from MSC cultured on TPS, emulsion and microcarriers for the given times and reverse transcribed into cDNA for PCR experiments. Results were shown as relative fold change of gene expressed by MSCs on different substrates relative to that of newly thawed MSC on TPS. Error bars are s.e.m; n represents number of experiments, n ≥ 3.

The multi-potency of MSCs was studied by inducing MSCs differentiation towards three lineages (adipogenic, osteogenic and chondrogenic) in their corresponding differentiation media after transferring to TPS (as the ECM biochemistry and mechanics is also able to regulate differentiation). Adipogenesis was studied by Oil Red staining of lipid droplets (Figure 4.16B) showing very clear adipogenesis in differentiation medium compared to the control group cultured in growth medium. The Oil Red staining also suggested that MSCs from different substrates differentiated similarly, which was confirmed by RT-PCR with two commonly used adipogenesis marker genes (FABP4 and LPL). No

statistically significant difference was found between expression of these genes in cells cultured on the different substrates studied at the same passage (Figure 4.16A). However, it was clear that MSCs gradually lost their adipogenesis potential on prolonged culture. Since MSCs do not express differentiation markers when culture in growth medium, the relative fold change of gene expression was normalised to P3 MSCs on TPS in differentiation medium. Although it is unfair to perform statistical analysis between the gene expression of MSCs on TPS at P3 and that of later passages (as the expression of P3 is normalised to 1), the expression of both genes on TPS was clearly downregulated at later passage. The expression of FABP4 on MSCs growing on microcarriers were significantly downregulated at P6 compared to P3. Although FABP4 is an early indicator of adipogenesis, it does not necessary suggest the adipogenesis was halted as the later marker LPL at the same passage remained expressed at a comparable level, which is in consistent with the staining. MSCs cultured on emulsions retained the expression of both genes to some level, perhaps reflecting the role of substrate stiffness in priming for differentiation, as it is widely accepted that softer substrates would better support differentiation towards adipogenic lineages.[7]

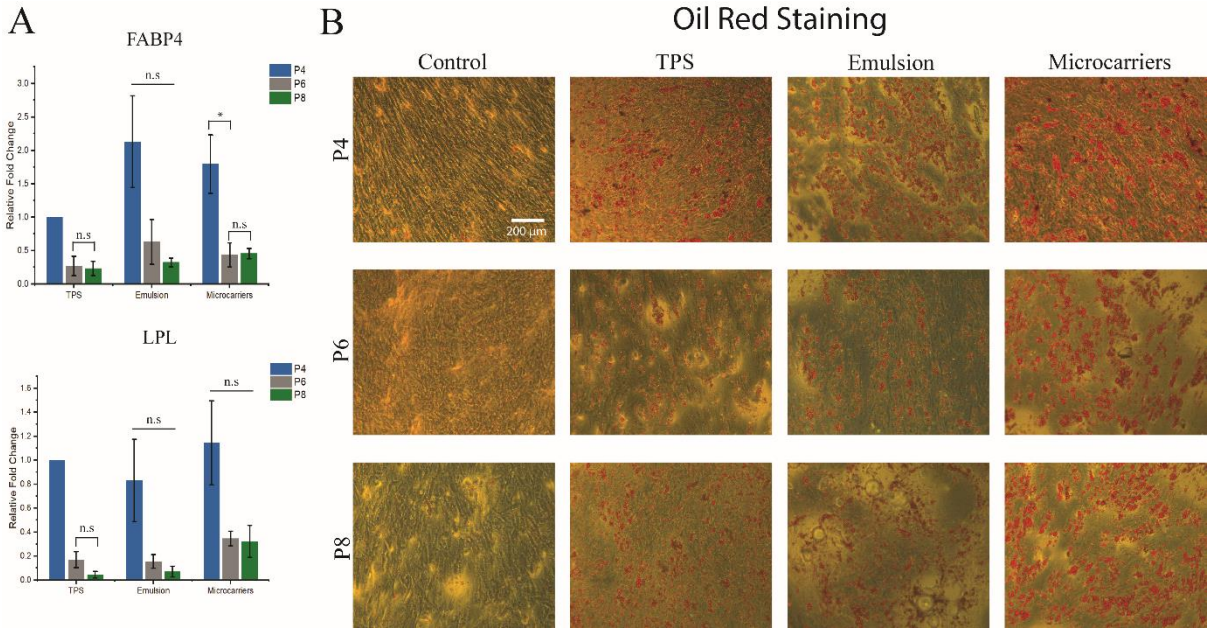

Figure 4.16. MSCs retain adipogenic differentiation potential over a long-term culture on TPS, emulsion and microcarriers. (A) Relative fold change of gene expressed by MSCs harvested from different substrates cultured on TPS in adipogenic differentiation medium for 14 days relative to that of P4 MSC on TPS in differentiation medium. Error bars are s.e.m; n represents number of

experiments, n ≥ 3. (B) Bright field images of Oil Red staining of the corresponding samples, controls were MSCs of the same passage harvested from TPS cultured in growth medium.

MSC osteogenesis has been identified as a multi-step process, as it starts with a proliferation stage to reach a high cell confluence, followed by a matrix maturation step, at which point the expression of ALP and RUNX2 becomes detectable. The expression of RUNX2 indicates MSC commitment towards osteogenic lineage, activating the expression of type I COL and triggering matrix mineralisation, involving OCN and osteopontin deposition, as well as calcium deposition.[321,322] Early osteogenesis was characterised by ALP staining. As shown in Figure 4.17B, similar ALP activity can be observed for cells cultured on all three substrates, even at late passages, confirming their ability to differentiate into osteoblasts. Interestingly, ALP activity was also observed in the control group at passage 8 in growth medium, which is consistent with previous findings[7] showing that prolonged culture of MSCs on rigid substrates (TPS) induces osteogenic differentiation. Calcium deposition was visualised by Alizarin Red staining, characterising the mineralisation of the matrix by MSCs (Figure 4.17C). Although calcium deposition was observed on all substrates, there is a clear decrease after long-term culture. However, trends in gene expression were less clear (Figure 4.17A) and the interpretation of the results is rather challenging. BMP-2 has been widely studied and recognised as an important factor stimulating RUNX2 expression,[322,323] which subsequently activates COL1A1. Therefore, the up-regulation of BMP2 expression and down-regulation of RUNX2 and COL1A1 expression at later passages may suggest that the osteogenesis process was slowing down at passage 8. However, the role of BMP-2 for matrix mineralisation has also been widely demonstrated.[322] COL1A1, ALP and RUNX2 expression was reported to decline upon initiation of matrix mineralisation.[324] Thus the RT-PCR results can also imply that the osteogenesis was favoured at later passages, a conclusion that conflicts with the functional assays quantifying ALP activity and mineralisation via Alizarin Red staining. Similar conflicting trends have also been reported in the literature, some suggesting that cell senescence may promote the osteogenic differentiation, whereas other suggested the promotion of adipogenic commitment.[282,283] In other reports, senescence impaired differentiation towards all lineages.[284] In our study, ALP activity

at P8 was similar to P4 whereas the calcium deposition was reduced, since ALP activity would also decline at mineralisation step, it was more likely that osteogenesis was slowed down at P8. However, overall the osteogenic potential of MSCs cultured on the three substrates studied was comparable.

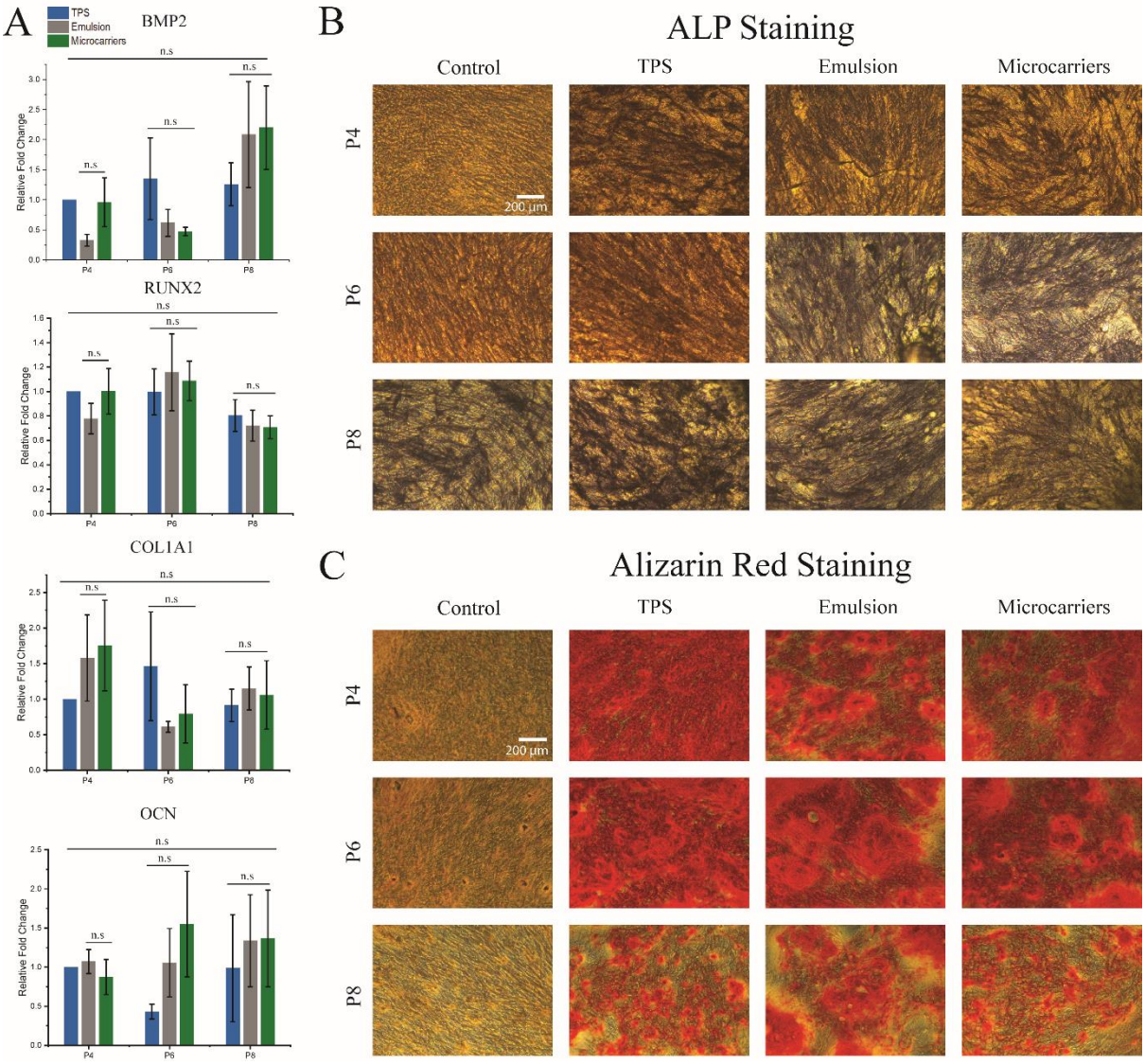

Figure 4.17. MSCs retain osteogenic differentiation potential over a long-term culture on TPS, emulsion and microcarriers. (A) Relative fold change of gene expressed by MSCs harvested from different substrates cultured on TPS in osteogenic differentiation medium for 14 days relative to that of P4 MSC on TPS in differentiation medium. Error bars are s.e.m; n represents number of experiments, n ≥ 3. Bright field images of (B) ALP staining and (C) Alizarin Red staining of the corresponding samples, controls were MSCs of the same passage harvested from TPS cultured in growth medium.

Chondrogenesis was induced on spheroid cultures, and Alcian Blue staining was performed to characterise the secretion of the cartilage matrix protein aggrecan. During the process of

chondrogenic differentiation, MSCs aggregate and condensate into pre-cartilaginous nodules and secret cartilage specific ECM matrix (such as aggrecan, decorin, biglycan, fibromodulin and type II COL) filling gaps between cells as they differentiate into chondrocytes.[325,326] As shown in Figure 4.18B, the formation of spheroids was observed in all conditions, although cells cultured in basal DMEM displayed lighter staining, whilst cells cultured in differentiation medium showed a dark blue colour, confirming the upregulation of the secretion of aggrecan. It is also noticeable that the colour was lighter at later passages, indicating again a reduction of the chondrogenesis potential. Although no statistically significant differences were found between P4 and P8 MSCs in the expression of chondrogenesis-related genes (SOX9, COL2A1 and COL10A1), there was a trend of gradual reduction in the expression of these genes at later passages. COL2A1, in particular, which is an important gene for the formation of articular cartilage.[327] SOX9 is expressed by proliferative chondrocytes in growth cartilage,[326] and is reported to induce the secretion of the major cartilage matrix components, type II and type X COL by activating the expression of COL2A1 and COL10A1 genes.[321,326,327] However, despite its role in promoting mineralisation of cartilage, COL10A1 is also associated with hypertrophic cartilage, which is undesirable for chondrogenesis at late point.[327,328] Since SOX9 is hardly expressed by hypertrophic chondrocyte,[326] the similar expression profile of SOX9 and COL10A1 in our experiment suggests that chondrocytes remained in growth stage over the whole period of the experiment. Thus, the downregulation of COL10A1 in this case was an indication of loss of chondrogenic potential rather than chondrocyte hypertrophy.

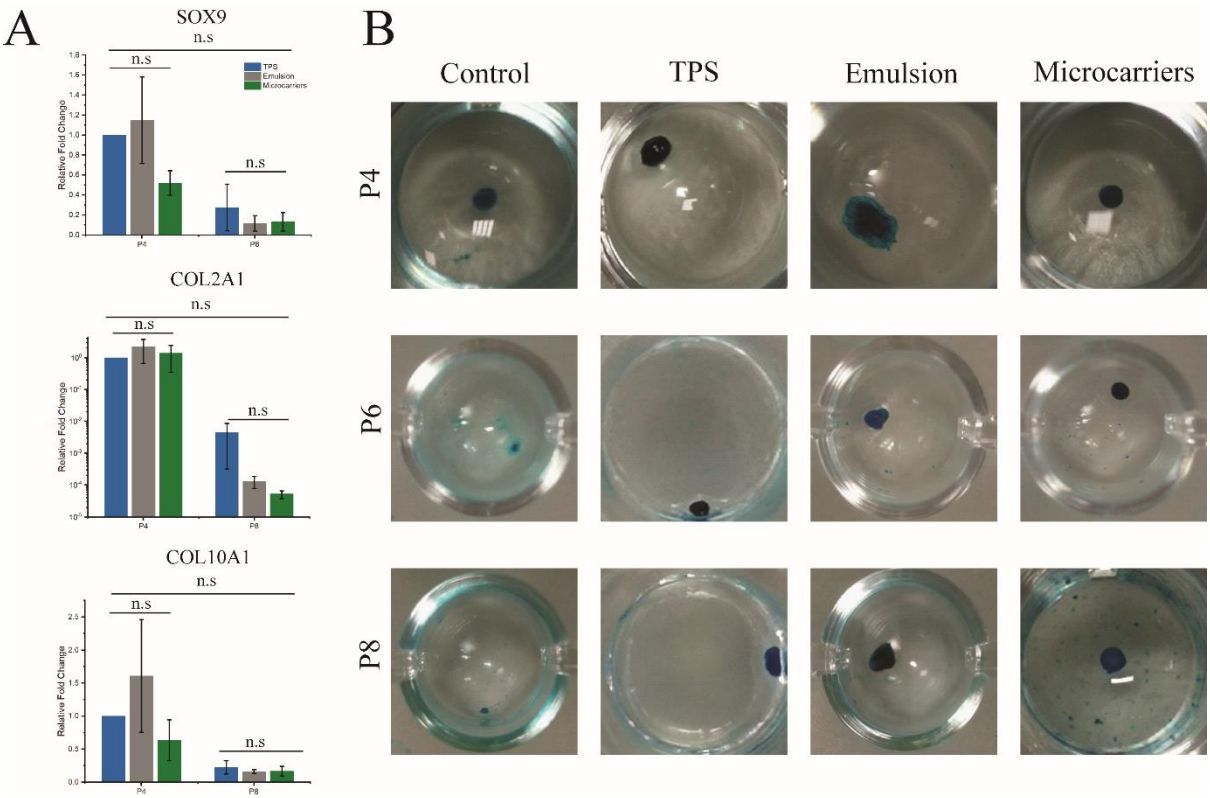

Figure 4.18. MSCs retain chondrogenic differentiation potential over a long-term culture on TPS, emulsion and microcarriers. (A) Relative fold change of genes expressed by MSCs harvested from different substrates cultured on TPS in spheroids in chondrogenic differentiation medium for 21 days relative to that of P4 MSC on TPS in differentiation medium. Error bars are s.e.m; n represents number of experiments, n ≥ 3. (B) Bright images of Alcian Blue staining of MSCs from the corresponding samples, controls were MSCs of the same passage harvested from TPS cultured in DMEM for 21 days.

4.3.4 Conclusions

In this chapter, based on the previous studies on nanosheet assembly at liquid interfaces, we developed a nanosheet assembled oil-based emulsion for the culture of MSCs. The protein nanosheets functioned as an emulsifier, providing steric and electrostatic repulsion, preventing emulsions from coalescence. Nanosheets assembled at the interface and displayed birefringent structures with the assistance of pro-surfactants, which leads to improved strength to support cell adhesion and proliferation. The culture of MSCs was found to be supported by fluorinated oil-based emulsions as well as non-fluorinated oil-based systems. We demonstrated the proof-of-concept of MSC expansion on emulsions and the simple transfer and harvest of cells from corresponding emulsions. Such emulsion systems provide higher surface-to-volume ratio than conventional 2D plastic culture plates

and allow simple transfer for passaging, instead of labour intensive digestion and re-seeding process. Therefore, we find that emulsions offer advantages in terms of processability and cost-effectiveness for industrial scale-up of cell expansion. Since emulsions are based on liquid substrates, they offer the advantage of by-passing enzymatic digestion for cell harvesting over solid microcarriers. Emulsion systems could be a potential replacement for currently applied solid microcarrier-based culture systems and for fabricating cell sheets.[202] Given that enzymatic digestion was widely considered as harmful and a potential modifying agent of cell phenotypes,[272,273,329] we compared the impact of prolonged culture on MSC phenotype to investigate the retention of cell phenotype upon culture on different substrates. Although MSC adhesion, proliferation and the expression of surface markers declined at passage 10, no major significant differences were found between TPS, emulsions and microcarriers. Since the accutase-solution we used for digestion is a less invasive enzyme compared to trypsin, the results may suggest that senescence dominate MSC phenotype at late passages, independent of enzymatic treatment. In the case of MSC multi-potency, MSCs retained its potential of differentiating towards three lineages (osteogenic, adipogenic and chondrogenic) at relatively late passage (passage 8). Despite the fact that the staining studies (Oil Red, Alizarin Red and Alcian Blue stainings) suggested osteogenic, adipogenic and chondrogenic potentials, these potentials decrease over time in culture. RT-PCR studies of differentiation markers showed small differences in gene expression among the three culture methods. Although long-term culture experiments suggests that no significant phenotype retention by reducing or avoiding the use of enzymatic digestion, the similar phenotype (especially for osteogenic and chondrogenic differentiation) confirmed that MSC phenotypes were not affected by prolonged culture on a relatively soft substrate (emulsion). This is showing that emulsions can be used as an alternative to solid microcarrier-based systems for long-term MSC expansion.

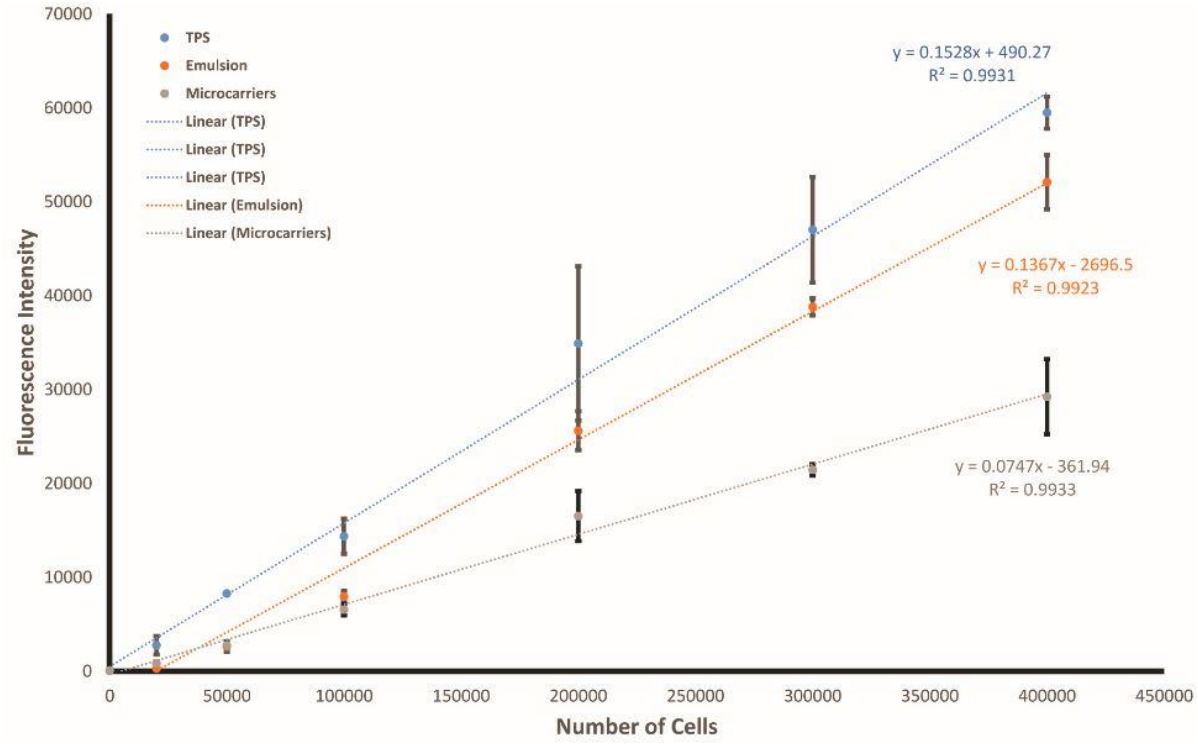

Appendix Figure 1. Calibration curve for cell counting via a Cyquant assay. Standard curve and the corresponding fitting of cyquant assay measurements on MSCs cultured on TPS (blue), emulsion (orange) and microcarriers (grey). Error bars are s.e.m; n represents number of experiments, n = 3.

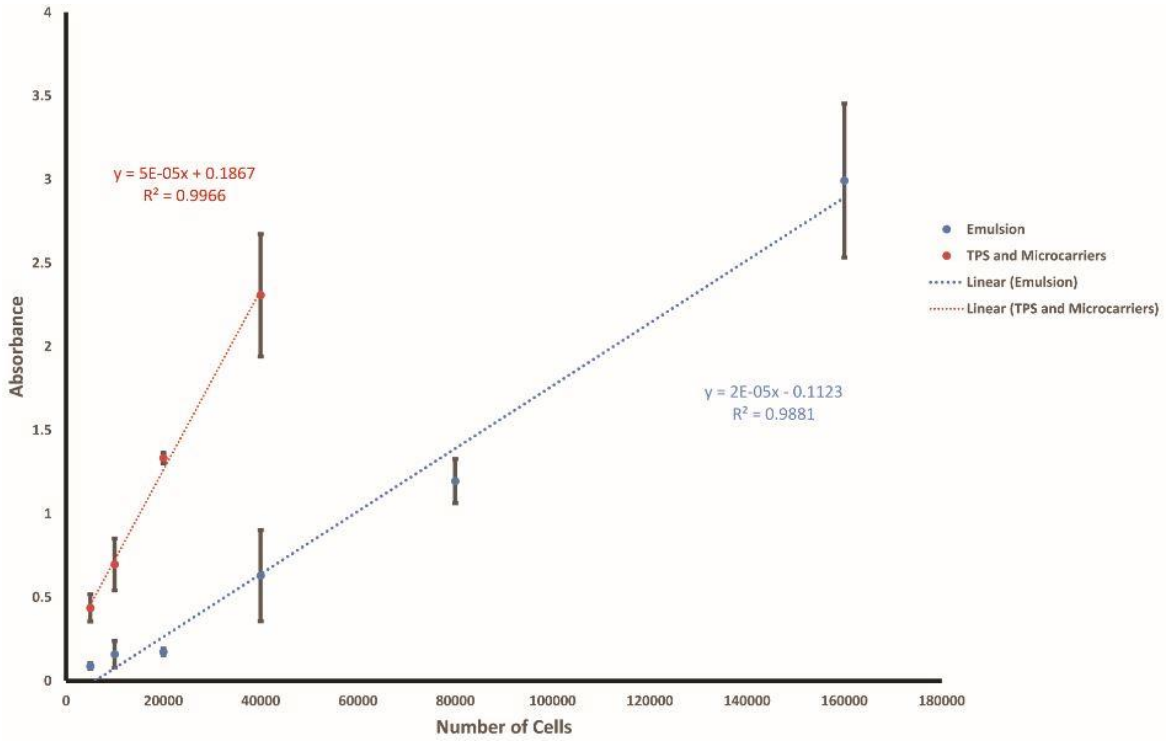

Appendix Figure 2. Calibration curve for cell counting via a metabolic assay. Standard curve and the corresponding fitting of metabolic assay (CCK-8) measurements on MSCs cultured on TPS and microcarriers (blue), emulsion (red). MSCs on emulsion were used a separate fitting as the emulsion stays at the well bottom, could shield some metabolic products of the cells from reacting with the kit. Error bars are s.e.m; n represents number of experiments, n = 3.

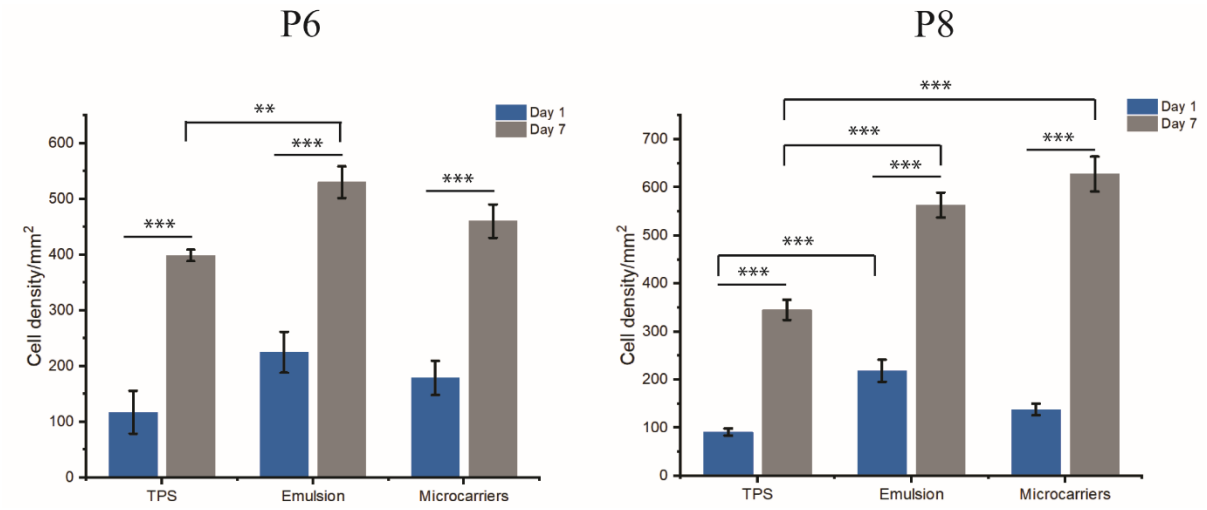

Appendix Figure 3. MSC proliferation on TPS, emulsion and microcarries at passage 6 and passage 8. MSC densities were measured via cyquant assay and converted into number of cells per mm^2 at passage 6 (left) and 8 (right). Error bars are s.e.m; n represents number of experiments, n ≥ 3.

Chapter 5

Conclusions and Future Directions

5.1 Conclusions

In this project, we focused on the design of protein nanosheets assembled at liquid interfaces for the culture of MSCs. This work was inspired by the pioneering works of Keese and Giaever who had reported the culture of fibroblast at the surface of fluorinated oils. Their study highlighted the importance of surfactant molecules in cell expansion, but without identifying molecular mechanisms enabling cell adhesion and proliferation. The reconfigurable and dynamic properties of protein nanosheets assembled at liquid-liquid interfaces make these an adaptive system that is particularly interesting for the regulation of stem cell fate. Our works adapted such system for the culture of MSCs, for applications in tissue engineering and regenerative medicine.

We contribute to the existing knowledge of the field by highlighting the importance of the interfacial mechanical properties modulated by these nanosheets. These properties, including interfacial moduli and viscoelasticity, depend on the assembly of protein nanosheets at corresponding interfaces. By characterising the interface with interfacial rheology, magnetic tweezer, XPS, ellipsometry and polarised optical microscopy, we explored the impact of the oil, protein, pH and pro-surfactant on the assembly of these nanosheets. Upon the adjustment of these factors, the inter- and intra-molecular interactions regulating such nanosheet assembly could vary significantly, resulting in interfaces with interfacial storage moduli ranging from 3.67 ± 1.4 mN/m (PLL nanosheet formed at pH 8.5 on Novec 7500 with 1.25 µg/mL PFBC) to 2.30 ± 0.61 N/m (PLL nanosheet formed at pH 10.5 on PDMS containing 0.1 mg/mL HDC). Specifically, we highlighted the role that the pro-surfactant plays in assisting the adsorption of PLL at the interface. We propose that the assembly of PLL is mediated by reaction with the acyl chloride pro-surfactants, forming corresponding amides that pin PLL molecules at the liquid interface.

The designed PLL-based nanosheets have been successfully applied for the culture of MSCs after further coating with cell adhesive components (FN, VN and COL), presenting sufficient cell adhesion and proliferation. This suggests that the mechanical properties conferred by the nanosheets are

sufficient to counterbalance the shear forces exerted by cells. MSCs on oil surfaces with stiffer PLL nanosheets established more structured actin cytoskeleton than those on the surface with softer nanosheets. MSC adhesion at liquid-liquid interfaces is regulated by the interfacial mechanics, similarly to the regulation of cell adhesion by the bulk mechanics of solid substrates and hydrogels, mediated by classical integrin adhesion and acto-myosin contractility. However, the fracture of nanosheets constitutes a major hurdle affecting cell yield at liquid interfaces. Most interestingly, we highlight a clear correlation between the elasticity (and lack of fracture) of the nanosheets and MSC proliferation. Therefore, nanosheet viscoelasticity appears to play an essential role in regulating MSC proliferation at liquid interfaces. This correlation could provide a helpful guideline for the design of protein nanosheets at oil interfaces, for cell expansion in bioreactors. This system could also be a useful platform for the investigation of cell behaviour on substrates displaying defined viscoelastic properties. Most importantly, by broadening such protein nanosheet-assembled liquid interface system to other oil and pro-surfactant combinations, we demonstrated the universality of this system and its broad applicability for adherent cell expansion.

Furthermore, inspired by the application of solid microcarriers for *in vitro* cell expansion, we have generated stable O/W emulsions by using the designed protein nanosheets as emulsifiers and have also demonstrated the proof-of-concept of MSC expansion on emulsions. Similar to the microcarriers, the emulsion system also has large surface-to-volume ratio, providing sufficiently large surface areas than conventional planar culture platform. However, unlike the microcarriers, cells on the emulsion can be harvested via centrifugation thus avoids the harsh enzymatic treatment required for cell harvesting for solid substrates. We conducted a side-by-side comparison of the emulsions, the microcarriers and TPS over the performance for a prolong MSC culture. As a result, no statistically significant difference was found in terms of cell adhesion, expression of surface markers, proliferation and differentiation between three substrates. We concluded that cell senescence, at higher passage numbers, had a far stronger impact on MSC phenotype than the culture on the different systems tested. Enzymatic digestion, when using gentle enzymatic treatment (e.g. accutase) was therefore

fond to have a moderate impact on cell phenotype. Although results did not suggest that emulsions are not superior to microcarriers in retaining MSC phenotypes upon long-term culture, it is worth noting that MSC on the emulsion showed comparable osteogenesis and chondrogenesis levels to that of cells culture on microcarriers, which was unexpected on such soft substrates. Overall, our results indicate that emulsions could be a promising alternative to microcarriers at least for MSC expansion. We also note that emulsions are considerably less expensive to produce than solid microcarriers and could more conveniently recycled to avoid plastic microparticulate waste (and potentially bypass their phasing out from products used in healthcare).

5.2 Future Directions

In this thesis, we have developed protein nanosheets that are sufficiently strong to support the adhesion and proliferation of MSCs; the emulsions developed from such nanosheets also showed potential as a replacement of microcarriers for the large scale expansion of MSCs. However, there remain few challenges that need to be tackled for further improvement and wider applications.

As we mentioned before, nanosheets are strong enough to support cell adhesion initially but they might not be able to sustain contractile forces exerted by cells when a high cell confluency is reached. Nanosheet fracture remains a concern for MSC proliferation on such systems. A nanosheet toughening is therefore required. Our preliminary results on PLL/HA/COL nanosheets also suggested that HA/COL pairs are more sustainable to the contraction of MSC, probably due to the fibrillogenesis of COL. However, toughened nanosheets may make emulsions become too stable to be disrupted by centrifugation for cell harvesting. Therefore, these aspects should be taken into consideration for cell manufacturing scale-up.

In the long-term culture of MSCs on emulsions, MSCs tend to aggregate into clusters after several passages. Such aggregation was also found on microcarriers, which may be the result of insufficient agitation and beads-to-beads collision that ultimately leads to inhomogeneous beads-to-beads cell

transfer and cell adhesion to multiple carriers (potentially involving matrix deposition bridging microcarriers). Stronger agitation in a spinner flask should reduce such issue but its impact on the stability of emulsion and MSC phenotypes (higher agitation speed could induce MSC osteogenesis and it may also affect cell viability) also need to be systematically investigated. Moreover, a narrower size distribution of emulsions might also help as different droplets could have similar cell confluency at the same time. Our groups are currently working on generating more homogeneous emulsion via microfluidic systems.

Although we have showed successful culture of MSCs on non-fluorinated oil-based emulsions, protocols for more controllable generation of these emulsions need to be developed as non-fluorinated oils are generally cheaper and more accessible than fluorinated oil. Meanwhile, the nanosheets we focused on were PLL/FN assembled, they performed well in stabilising the emulsion as well as supporting the culture of MSC, but they could be further improved from an industrial perspective, as the cost of PLL and FN is relatively high. Other cheaper options need to be explored.

Reference

1. Di Cio, S. & Gautrot, J. E. Cell sensing of physical properties at the nanoscale: Mechanisms and control of cell adhesion and phenotype. *Acta Biomater.* **30,** 26–48 (2016).

2. Humphrey, J. D., Dufresne, E. R. & Schwartz, M. A. Mechanotransduction and extracellular matrix homeostasis. *Nat. Rev. Mol. Cell Biol.* **15,** 802–812 (2014).

3. Geiger, B., Bershadsky, A., Pankov, R. & Yamada, K. M. Transmembrane extracellular matrix-cytoskeleton crosstalk. *Nat. Rev. Mol. Cell Biol.* **2,** 793–805 (2001).

4. Discher, D. E., Mooney, D. J. & Zandstra, P. W. Growth factors, matrices, and forces combine and control stem cells. *Science (80-.).* **324,** 1673–1677 (2009).

5. Sun, Z., Guo, S. S. & Fässler, R. Integrin-mediated mechanotransduction. *J. Cell Biol.* **215,** 445–456 (2016).

6. Janmey, P. A. & Weitz, D. A. Dealing with mechanics: Mechanisms of force transduction in cells. *Trends Biochem. Sci.* **29,** 364–370 (2004).

7. Engler, A. J., Sen, S., Sweeney, H. L. & Discher, D. E. Matrix Elasticity Directs Stem Cell Lineage Specification. *Cell* **126,** 677–689 (2006).

8. Ohashi, K., Fujiwara, S. & Mizuno, K. Roles of the cytoskeleton, cell adhesion and rho signalling in mechanosensing and mechanotransduction. *J. Biochem.* **161,** mvw082 (2017).

9. Popov, S. V., Svitkina, T. M., Margolis, L. B. & Tsong, T. Y. Mechanism of cell protrusion formation in electrical field: the role of actin. *BBA - Biomembr.* **1066,** 151–158 (1991).

10. Le Clainche, C. & Carlier, M. F. Regulation of actin assembly associated with protrusion and adhesion in cell migration. *Physiol. Rev.* **88,** 489–513 (2008).

11. DeMali, K. A. & Burridge, K. Coupling membrane protrusion and cell adhesion. *J. Cell Sci.* **116,** 2389–2397 (2003).

12. Mattila, P. K. & Lappalainen, P. Filopodia: Molecular architecture and cellular functions. *Nat. Rev. Mol. Cell Biol.* **9,** 446–454 (2008).

13. Footer, M. J., Kerssemakers, J. W. J., Theriot, J. A. & Dogterom, M. Direct measurement of force generation by actin filament polymerization using an optical trap. *Proc. Natl. Acad. Sci. U. S. A.* **104,** 2181–2186 (2007).

14. Parekh, S. H., Chaudhuri, O., Theriot, J. A. & Fletcher, D. A. Loading history determines the velocity of actin-network growth. *Nat. Cell Biol.* **7,** 1119–1123 (2005).

15. Tobergte, D. R. & Curtis, S. *Molecular biology of the cell*. *Journal of Chemical Information and Modeling* **53,** (2013).

16. Alberts, B. *Molecular biology of the cell*. (fifth edition. New York : Garland Pub., [2008] ©2008).

17. Mullins, R. D., Heuser, J. A. & Pollard, T. D. The interaction of Arp2/3 complex with actin: Nucleation, high affinity pointed end capping, and formation of branching networks of filaments. *Proc. Natl. Acad. Sci.* **95,** 6181–6186 (1998).

18. Mejillano, M. R. *et al.* Lamellipodial Versus Filopodial Mode of the Actin Nanomachinery. *Cell*

118, 363–373 (2004).

19. Mccullough, B. R., Blanchoin, L., Martiel, J. & La, E. M. De. NIH Public Access. *J. Mol. …* **381,** 550–558 (2009).

20. Otto, J. J. Actin-bundling proteins. *Curr. Opin. Cell Biol.* **6,** 105–109 (1994).

21. Hoffman, B. D., Grashoff, C. & Schwartz, M. A. Dynamic molecular processes mediate cellular mechanotransduction. *Nature* **475,** 316–323 (2011).

22. Khurana, S. & George, S. P. The role of actin bundling proteins in the assembly of filopodia in epithelial cells. *Cell Adh. Migr.* **5,** 409–420 (2011).

23. Svitkina, T. M. *et al.* Mechanism of filopodia initiation by reorganization of a dendritic network. *J. Cell Biol.* **160,** 409–421 (2003).

24. Hynes, R. O. Integrins: Bidirectional, allosteric signaling machines. *Cell* **110,** 673–687 (2002).

25. Roca-Cusachs, P., Gauthier, N. C., Del Rio, A. & Sheetz, M. P. Clustering of alpha(5)beta(1) integrins determines adhesion strength whereas alpha(v)beta(3) and talin enable mechanotransduction. *Proc. Natl. Acad. Sci. U. S. A.* **106,** 16245–16250 (2009).

26. Shattil, S. J., Kim, C. & Ginsberg, M. H. The final steps of integrin activation: the end game. *Nat. Rev. Mol. Cell Biol.* **11,** 288–300 (2010).

27. Butler, B., Gao, C., Mersich, A. T. & Blystone, S. D. Purified integrin adhesion complexes exhibit actin-polymerization activity. *Curr. Biol.* **16,** 242–251 (2006).

28. Yu, C. -h., Law, J. B. K., Suryana, M., Low, H. Y. & Sheetz, M. P. Early integrin binding to Arg-Gly-Asp peptide activates actin polymerization and contractile movement that stimulates outward translocation. *Proc. Natl. Acad. Sci.* **108,** 20585–20590 (2011).

29. Roca-Cusachs, P. *et al.* Integrin-dependent force transmission to the extracellular matrix by -actinin triggers adhesion maturation. *Proc. Natl. Acad. Sci.* **110,** E1361–E1370 (2013).

30. Parsons, J. T., Horwitz, A. R. & Schwartz, M. A. Cell adhesion: Integrating cytoskeletal dynamics and cellular tension. *Nat. Rev. Mol. Cell Biol.* **11,** 633–643 (2010).

31. Gardel, M. L., Schneider, I. C., Aratyn-Schaus, Y. & Waterman, C. M. Mechanical Integration of Actin and Adhesion Dynamics in Cell Migration. *Annu. Rev. Cell Dev. Biol.* **26,** 315–333 (2010).

32. Foth, B. J., Goedecke, M. C. & Soldati, D. New insights into myosin evolution and classification. *Proc. Natl. Acad. Sci.* **103,** 3681–3686 (2006).

33. Vicente-Manzanares, M., Ma, X., Adelstein, R. S. & Horwitz, a. R. Non-muscle myosin II takes centre stage in cell adhesion and migration. *Nat. Rev. Mol. Cell Biol.* **10,** 778–790 (2009).

34. Dumbauld, D. W. *et al.* How vinculin regulates force transmission. *Proc. Natl. Acad. Sci.* **110,** 9788–9793 (2013).

35. Chen, C. S. Mechanotransduction - a field pulling together? *J. Cell Sci.* **121,** 3285–3292 (2008).

36. Huang, J. *et al.* Impact of order and disorder in RGD nanopatterns on cell adhesion. *Nano Lett.* **9,** 1111–1116 (2009).

37. Malmström, J. *et al.* Large area protein patterning reveals nanoscale control of focal adhesion development. *Nano Lett.* **10,** 686–694 (2010).

38. Kegg. Focal Adhesion. 3–5 (2009). doi:10.1042/bst0320416.

39. Elosegui-Artola, A., Trepat, X. & Roca-Cusachs, P. Control of Mechanotransduction by Molecular Clutch Dynamics. *Trends Cell Biol.* **28,** 356–367 (2018).

40. Elosegui-Artola, A. *et al.* Mechanical regulation of a molecular clutch defines force transmission and transduction in response to matrix rigidity. *Nat. Cell Biol.* **18,** 540–548 (2016).

41. Bennett, M. *et al.* Molecular clutch drives cell response to surface viscosity. *Proc. Natl. Acad. Sci.* 201710653 (2018). doi:10.1073/pnas.1710653115

42. Zheng, W., Christensen, L. P. & Tomanek, R. J. Differential effects of cyclic and static stretch on coronary microvascular endothelial cell receptors and vasculogenic / angiogenic responses. *Am J Physiol Hear. Circl Physiol* **52242,** 794–800 (2008).

43. Hsu, H. J., Lee, C. F. & Kaunas, R. A dynamic stochastic model of frequency-dependent stress fiber alignment induced by cyclic stretch. *PLoS One* **4,** 1–11 (2009).

44. del Rio, A. *et al.* Stretching single talin rod molecules activates vinculin binding. *Science* **323,** 638–41 (2009).

45. Mao, Y. & Schwarzbauer, J. E. Fibronectin fibrillogenesis, a cell-mediated matrix assembly process. *Matrix Biol.* **24,** 389–399 (2005).

46. Kadler, K. E., Hill, A. & Canty-Laird, E. G. Collagen fibrillogenesis: fibronectin, integrins, and minor collagens as organizers and nucleators. *Curr. Opin. Cell Biol.* **20,** 495–501 (2008).

47. Kong, D., Nguyen, K. D. Q., Megone, W., Peng, L. & Gautrot, J. E. The culture of HaCaT cells on liquid substrates is mediated by a mechanically strong liquid-liquid interface. *Faraday Discuss.* **204,** (2017).

48. Trappmann, B. *et al.* Extracellular-matrix tethering regulates stem-cell fate. *Nat. Mater.* **11,** 742–742 (2012).

49. Attwood, S. J. *et al.* Adhesive ligand tether length affects the size and length of focal adhesions and influences cell spreading and attachment. *Sci. Rep.* **6,** 34334 (2016).

50. Baker, B. M. *et al.* Cell-mediated fibre recruitment drives extracellular matrix mechanosensing in engineered fibrillar microenvironments. *Nat. Mater.* **14,** 1262–1268 (2015).

51. Chaudhuri, O. *et al.* Hydrogels with tunable stress relaxation regulate stem cell fate and activity. *Nat. Mater.* **15,** 326–334 (2015).

52. Kong, D. *et al.* Protein Nanosheet Mechanics Controls Cell Adhesion and Expansion on Low-Viscosity Liquids. *Nano Lett.* **18,** 1946–1951 (2018).

53. Forrest, J. A. & Dalnoki-Veress, K. The glass transition in thin polymer films. *Adv. Colloid Interface Sci.* **94,** 167–196 (2001).

54. Fujie S., T. & T. Advances in Nanosheet Technology Towards Nanomedical Engineering. *Nanobiotechnology* 68–94 (2014).

55. Fujie, T. Development of free-standing polymer nanosheets for advanced medical and health-care applications. *Polym. J.* **48,** 773–780 (2016).

56. Niwa, D., Fujie, T., Lang, T., Goda, N. & Takeoka, S. Heterofunctional nanosheet controlling cell adhesion properties by collagen coating. *J. Biomater. Appl.* **27,** 131–141 (2012).

57. Endo, H., Kado, Y., Mitsuishi, M. & Miyashita, T. Fabrication of free-standing hybrid nanosheets organized with polymer Langmuir-BIodgett films and gold nanoparticles. *Macromolecules* **39,** 5559–5563 (2006).

58. Jiang, C. & Tsukruk, V. V. Freestanding nanostructures via layer-by-layer assembly. *Adv. Mater.* **18,** 829–840 (2006).

59. Fujie, T., Furutate, S., Niwa, D. & Takeoka, S. A nano-fibrous assembly of collagen–hyaluronic acid for controlling cell-adhesive properties. *Soft Matter* **6,** 4672 (2010).

60. Vendamme, R., Onoue, S.-Y., Nakao, A. & Kunitake, T. Robust free-standing nanomembranes of organic/inorganic interpenetrating networks. *Nat. Mater.* **5,** 494–501 (2006).

61. Minami, K. *et al.* Suppression of Myogenic Differentiation of Mammalian Cells Caused by Fluidity of a Liquid-Liquid Interface. *ACS Appl. Mater. Interfaces* **9,** 30553–30560 (2017).

62. Jia, X. *et al.* Adaptive Liquid Interfacially Assembled Protein Nanosheets for Guiding Mesenchymal Stem Cell Fate. *Adv. Mater.* **32,** 1–7 (2020).

63. Jia, X. *et al.* Modulation of Mesenchymal Stem Cells Mechanosensing at Fluid Interfaces by Tailored Self-Assembled Protein Monolayers. *Small* **15,** 1–6 (2019).

64. Narsimhan, G. & Xiang, N. Role of Proteins on Formation, Drainage, and Stability of Liquid Food Foams. *Annu. Rev. Food Sci. Technol.* **9,** 45–63 (2018).

65. Andrade, J. D. & Hlady, V. Protein Adsorption and Materials Biocompatibility: a Tutorial Review and Suggested Hypoteheses. *Adv. Polym. Sci.* 1–63 (1987). doi:10.1007/3-540-16422-7_6

66. Damodaran, S. Adsorbed layers formed from mixtures of proteins. *Curr. Opin. Colloid Interface Sci.* **9,** 328–339 (2004).

67. Mezzenga, R. & Fischer, P. The self-assembly, aggregation and phase transitions of food protein systems in one, two and three dimensions. *Reports Prog. Phys.* **76,** (2013).

68. Eckenrode, H. M. & Dai, H. L. Nonlinear optical probe of biopolymer adsorption on colloidal particle surface: Poly-L-lysine on polystyrene sulfate microspheres. *Langmuir* **20,** 9202–9209 (2004).

69. Lu, J. R., Su, T. J. & Penfold, J. Adsorption of serum albumins at the air/water interface. *Langmuir* **15,** 6975–6983 (1999).

70. Beverung, C. J., Radke, C. J. & Blanch, H. W. Protein adsorption at the oil/water interface: Characterization of adsorption kinetics by dynamic interfacial tension measurements. *Biophys. Chem.* **81,** 59–80 (1999).

71. Adamczyk, Z. Protein adsorption: A quest for a universal mechanism. *Curr. Opin. Colloid Interface Sci.* **41,** 50–65 (2019).

72. Rodríguez-Maldonado, L., Fernández-Nieves, A. & Fernández-Barbero, A. Dynamic light scattering from high molecular weight poly-L-lysine molecules. *Colloids Surfaces A Physicochem. Eng. Asp.* **270–271,** 335–339 (2005).

73. Morga, M., Adamczyk, Z., Gödrich, S., Oćwieja, M. & Papastavrou, G. Monolayers of poly-l-lysine on mica - Electrokinetic characteristics. *J. Colloid Interface Sci.* **456,** 116–124 (2015).

74. Choi, J. H. *et al.* Influence of pH and Surface Chemistry on Poly(l -lysine) Adsorption onto Solid Supports Investigated by Quartz Crystal Microbalance with Dissipation Monitoring. *J. Phys. Chem. B* **119,** 10554–10565 (2015).

75. Firkowska-Boden, I., Zhang, X. & Jandt, K. D. Controlling Protein Adsorption through Nanostructured Polymeric Surfaces. *Adv. Healthc. Mater.* **7,** 1–19 (2018).

76. Shiratori, S. S. & Rubner, M. F. pH-dependent thickness behavior of sequentially adsorbed

layers of weak polyelectrolytes. *Macromolecules* **33,** 4213–4219 (2000).

77. Thompson, M. T., Berg, M. C., Tobias, I. S., Rubner, M. F. & Van Vliet, K. J. Tuning compliance of nanoscale polyelectrolyte multilayers to modulate cell adhesion. *Biomaterials* **26,** 6836–6845 (2005).

78. Crouzier, T., Boudou, T. & Picart, C. Polysaccharide-based polyelectrolyte multilayers. *Current Opinion in Colloid and Interface Science* **15,** 417–426 (2010).

79. Boddohi, S., Killingsworth, C. E. & Kipper, M. J. Polyelectrolyte multilayer assembly as a function of pH and ionic strength using the polysaccharides chitosan and heparin. *Biomacromolecules* **9,** 2021–2028 (2008).

80. Richert, L. *et al.* Layer by Layer Buildup of Polysaccharide Films: Physical Chemistry and Cellular Adhesion Aspects. *Langmuir* **20,** 448–458 (2004).

81. Maroni, P., Montes Ruiz-Cabello, F. J., Cardoso, C. & Tiraferri, A. Adsorbed mass of polymers on self-assembled monolayers: Effect of surface chemistry and polymer charge. *Langmuir* **31,** 6045–6054 (2015).

82. Maroni, P., Montes Ruiz-Cabello, F. J. & Tiraferri, A. Studying the role of surface chemistry on polyelectrolyte adsorption using gold-thiol self-assembled monolayer with optical reflectivity. *Soft Matter* **10,** 9220–9225 (2014).

83. Bergfreund, J., Bertsch, P., Kuster, S. & Fischer, P. Effect of Oil Hydrophobicity on the Adsorption and Rheology of β-Lactoglobulin at Oil-Water Interfaces. *Langmuir* **34,** 4929–4936 (2018).

84. Roach, P., Farrar, D. & Perry, C. C. Surface tailoring for controlled protein adsorption: Effect of topography at the nanometer scale and chemistry. *J. Am. Chem. Soc.* **128,** 3939–3945 (2006).

85. Rechendorff, K., Hovgaard, M. B., Foss, M., Zhdanov, V. P. & Besenbacher, F. Enhancement of protein adsorption induced by surface roughness. *Langmuir* **22,** 10885–10888 (2006).

86. Piradashvili, K., Alexandrino, E. M., Wurm, F. R. & Landfester, K. Reactions and polymerizations at the liquid-liquid interface. *Chem. Rev.* **116,** 2141–2169 (2016).

87. MacRitchie, F. Mechanism of interfacial polymerization. *Trans. Faraday Soc.* **65,** 2503–2507 (1969).

88. Beaman, R. G., Morgan, P. W., Koller, C. R., Wittbecker, E. L. & Magat, E. E. Interfacial polycondensation. III. Polyamides. *J. Polym. Sci.* **40,** 329–336 (1959).

89. Kong, D., Peng, L., Di Cio, S., Novak, P. & Gautrot, J. E. Stem Cell Expansion and Fate Decision on Liquid Substrates Are Regulated by Self-Assembled Nanosheets. *ACS Nano* **12,** 9206–9213 (2018).

90. Maldonado-Valderrama, J. & Patino, J. M. R. Interfacial rheology of protein-surfactant mixtures. *Curr. Opin. Colloid Interface Sci.* **15,** 271–282 (2010).

91. Otzen, D. Protein-surfactant interactions: A tale of many states. *Biochim. Biophys. Acta - Proteins Proteomics* **1814,** 562–591 (2011).

92. Bos, M. A. & Van Vliet, T. Interfacial rheological properties of adsorbed protein layers and surfactants: A review. *Adv. Colloid Interface Sci.* **91,** 437–471 (2001).

93. Day, J. P. R., Pudney, P. D. A. & Bain, C. D. Ellipsometric study of the displacement of milk proteins from the oil-water interface by the non-ionic surfactant C10E8. *Phys. Chem. Chem.*

Phys. **12,** 4590–4599 (2010).

94. Sundararajan, P. R., Singh, S. & Moniruzzaman, M. Surfactant-induced crystallization of polycarbonate. *Macromolecules* **37,** 10208–10211 (2004).

95. Hammond, M. R. & Mezzenga, R. Supramolecular routes towards liquid crystalline side-chain polymers. *Soft Matter* **4,** 952–961 (2008).

96. Schmidt, S. *et al.* Control of cell adhesion by mechanical reinforcement of soft polyelectrolyte films with nanoparticles. *Langmuir* **28,** 7249–7257 (2012).

97. Ariga, K., Ji, Q., Hill, J. P., Bando, Y. & Aono, M. Forming nanomaterials as layered functional structures toward materials nanoarchitectonics. *NPG Asia Mater.* **4,** e17 (2012).

98. Gand, A. *et al.* Fibronectin-based multilayer thin films. *Colloids Surfaces B Biointerfaces* **156,** 313–319 (2017).

99. Miller, M. D. & Bruening, M. L. Correlation of the swelling and permeability of polyelectrolyte multilayer films. *Chem. Mater.* **17,** 5375–5381 (2005).

100. Harris, J. J. & Bruening, M. L. Electrochemical and in situ ellipsometric investigation of the permeability and stability of layered polyelectrolyte films. *Langmuir* **16,** 2006–2013 (2000).

101. and, S. E. B. & Barrett*, C. J. pH-Responsive Properties of Multilayered Poly(l-lysine)/Hyaluronic Acid Surfaces. 1773–1783 (2003). doi:10.1021/BM034184W

102. Ghosh, S., Kobal, I., Zanette, D. & Reed, W. F. Conformational Contraction and Hydrolysis of Hyaluronate in Sodium Hydroxide Solutions. *Macromolecules* **26,** 4685–4693 (1993).

103. Picart, C. *et al.* Buildup Mechanism for Poly(l -lysine)/Hyaluronic Acid Films onto a Solid Surface. *Langmuir* **17,** 7414–7424 (2001).

104. Ai, H., Jones, S. A. & Lvov, Y. M. Biomedical Applications of Electrostatic Layer-by-Layer Nano-Assembly of Polymers, Enzymes, and Nanoparticles. *Cell Biochem. Biophys.* **39,** 23–44 (2003).

105. Lee, J. Y. & Spicer, A. P. Hyaluronan: A multifunctional, megaDalton, stealth molecule. *Curr. Opin. Cell Biol.* **12,** 581–586 (2000).

106. Kidambi, S., Lee, I. & Chan, C. Controlling primary hepatocyte adhesion and spreading on protein-free polyelectrolyte multilayer films. *J. Am. Chem. Soc.* **126,** 16286–16287 (2004).

107. Han, L., Mao, Z., Wu, J., Zhang, Y. & Gao, C. Influences of surface chemistry and swelling of salt-treated polyelectrolyte multilayers on migration of smooth muscle cells. *J. R. Soc. Interface* **9,** 3455–3468 (2012).

108. Ricotti, L. *et al.* Quantification of growth and differentiation of C2C12 skeletal muscle cells on PSS-PAH-based polyelectrolyte layer-by-layer nanofilms. *Biomed. Mater.* **6,** (2011).

109. Liu, Z. M., Gu, Q., Xu, Z. K. & Groth, T. Synergistic effect of polyelectrolyte multilayers and osteogenic growth medium on differentiation of human mesenchymal stem cells. *Macromol. Biosci.* **10,** 1043–1054 (2010).

110. Ren, K., Fourel, L., Rouvière, C. G., Albiges-Rizo, C. & Picart, C. Manipulation of the adhesive behaviour of skeletal muscle cells on soft and stiff polyelectrolyte multilayers. *Acta Biomater.* **6,** 4238–4248 (2010).

111. Richert, L. *et al.* Improvement of Stability and Cell Adhesion Properties of Polyelectrolyte Multilayer Films by Chemical Cross-Linking. *Biomacromolecules* **5,** 284–294 (2004).

112. Semenov, O. V., Malek, A., Bittermann, A. G., Vörös, J. & Zisch, A. H. Engineered Polyelectrolyte Multilayer Substrates for Adhesion, Proliferation, and Differentiation of Human Mesenchymal Stem Cells. *Tissue Eng. Part A* **15,** 2977–2990 (2009).

113. Schneider, A. *et al.* Polyelectrolyte Multilayers with a Tunable Young ' s Modulus : Influence of Film Stiffness on Cell Adhesion. *Langmuir* **22,** 1193–1200 (2006).

114. Liu, M. *et al.* Stabilized hemocompatible coating of nitinol devices based on photo-cross-linked alginate/heparin multilayer. *Langmuir* **23,** 9378–9385 (2007).

115. Vázquez, C. P. *et al.* Variation of polyelectrolyte film stiffness by photo-cross-linking: A new way to control cell adhesion. *Langmuir* **25,** 3556–3563 (2009).

116. Gribova, V., Auzely-Velty, R. & Picart, C. Polyelectrolyte multilayer assemblies on materials surfaces: From cell adhesion to tissue engineering. *Chem. Mater.* **24,** 854–869 (2012).

117. Francius, G. *et al.* Stiffening of soft polyelectrolyte architectures by multilayer capping evidenced by viscoelastic analysis of AFM indentation measurements. *J. Phys. Chem. C* **111,** 8299–8306 (2007).

118. Kocgozlu, L. *et al.* Selective and uncoupled role of substrate elasticity in the regulation of replication and transcription in epithelial cells. *J. Cell Sci.* **123,** 29–39 (2010).

119. Salomaki, M. & Kankare, J. Influence of synthetic polyelectrolytes on the growth and properties of hyaluronan-chitosan multilayers. *Biomacromolecules* **10,** 294–301 (2009).

120. Srivastava, S. & Kotov, N. A. Composite Layer-by-Layer (LBL) assembly with inorganic nanoparticles and nanowires. *Acc. Chem. Res.* **41,** 1831–1841 (2008).

121. Lee, W. C. *et al.* Origin of enhanced stem cell growth and differentiation on graphene and graphene oxide. *ACS Nano* **5,** 7334–7341 (2011).

122. Jin, L. *et al.* Synergistic effects of a novel free-standing reduced graphene oxide film and surface coating fibronectin on morphology, adhesion and proliferation of mesenchymal stem cells. *J. Mater. Chem. B* **3,** 4338–4344 (2015).

123. Qi, W., Xue, Z., Yuan, W. & Wang, H. Layer-by-layer assembled graphene oxide composite films for enhanced mechanical properties and fibroblast cell affinity. *J. Mater. Chem. B* **2,** 325–331 (2014).

124. Di Lullo, G. A., Sweeney, S. M., K??rkk??, J., Ala-Kokko, L. & San Antonio, J. D. Mapping the ligand-binding sites and disease-associated mutations on the most abundant protein in the human, type I collagen. *J. Biol. Chem.* **277,** 4223–4231 (2002).

125. Gaudet, C. *et al.* Influence of Type I Collagen Surface Density on Fibroblast Spreading, Motility, and Contractility. *Biophys. J.* **85,** 3329–3335 (2003).

126. CR Keese, I. G. Cell Growth on Liquid Microcarriers. *Science (80-.).* **219,** 1448–1449 (1983).

127. Keese, C. R. & Giaever, I. Cell growth on liquid interfaces: Role of surface active compounds. *Proc. Natl. Acad. Sci. U. S. A.* **80,** 5622–5626 (1983).

128. Keese, C. R. & Giaever, I. Substrate mechanics and cell spreading. *Exp. Cell Res.* **195,** 528–532 (1991).

129. Giaever, I. & Keese, C. R. Behavior of cells at fluid interfaces. *Proc. Natl. Acad. Sci. U. S. A.* **80,** 219–222 (1983).

130. McCLmenets, D. J. *Food Emulsions Principles, Practices, and Techniques*. (2015).

doi:10.1201/9781420029581.ch9

131. Rayner, M. Scales and Forces in Emulsification. 3–32 (2015). doi:10.1201/b18436-3

132. Adams, F. *et al. Modern Aspects of Emulsion Science*. (The Royal Society of Chemistry, 1998). doi:10.1039/9781847551474

133. Tadros, T. F. Emulsion Formation and Stability. *Emuls. Form. Stab.* (2013). doi:10.1002/9783527647941

134. Karbstein, H. & Schubert, H. Developments in the continuous mechanical production of oil-in-water macro-emulsions. *Chem. Eng. Process. Process Intensif.* **34,** 205–211 (1995).

135. Dickinson, E. Hydrocolloids as emulsifiers and emulsion stabilizers. *Food Hydrocoll.* **23,** 1473–1482 (2009).

136. Tokle, T. & McClements, D. J. Physicochemical properties of lactoferrin stabilized oil-in-water emulsions: Effects of pH, salt and heating. *Food Hydrocoll.* **25,** 976–982 (2011).

137. Wilde, P., Mackie, A., Husband, F., Gunning, P. & Morris, V. Proteins and emulsifiers at liquid interfaces. *Adv. Colloid Interface Sci.* **108–109,** 63–71 (2004).

138. Bouyer, E. *et al.* Stabilization mechanism of oil-in-water emulsions by β-lactoglobulin and gum arabic. *J. Colloid Interface Sci.* **354,** 467–477 (2011).

139. Evans, M., Ratcliffe, I. & Williams, P. A. Emulsion stabilisation using polysaccharide-protein complexes. *Curr. Opin. Colloid Interface Sci.* **18,** 272–282 (2013).

140. Erni, P. *et al.* Interfacial rheology of surface-active biopolymers: Acacia senegal gum versus hydrophobically modified starch. *Biomacromolecules* **8,** 3458–3466 (2007).

141. Islam, A. M., Phillips, G. O., Sljivo, A., Snowden, M. J. & Williams, P. A. A review of recent developments on the regulatory, structural and functional aspects of gum arabic. *Food Hydrocoll.* **11,** 493–505 (1997).

142. Leroux, J., Langendorff, V., Schick, G., Vaishnav, V. & Mazoyer, J. Emulsion stabilizing properties of pectin. *Food Hydrocoll.* **17,** 455–462 (2003).

143. Hou, C., Wu, S., Xia, Y., Phillips, G. O. & Cui, S. W. A novel emulsifier prepared from Acacia seyal polysaccharide through Maillard reaction with casein peptides. *Food Hydrocoll.* **69,** 236–241 (2017).

144. Zhang, J. B., Wu, N. N., Yang, X. Q., He, X. T. & Wang, L. J. Improvement of emulsifying properties of Maillard reaction products from β-conglycinin and dextran using controlled enzymatic hydrolysis. *Food Hydrocoll.* **28,** 301–312 (2012).

145. Kato, A., Minaki, K. & Kobayashi, K. Improvement of Emulsifying Properties of Egg White Proteins by the Attachment of Polysaccharide through Maillard Reaction in a Dry State. *J. Agric. Food Chem.* **41,** 540–543 (1993).

146. Shu, Y. W., Sahara, S., Nakamura, S. & Kato, A. Effects of the Length of Polysaccharide Chains on the Functional Properties of the Maillard-Type Lysozyme-Polysaccharide Conjugate. *J. Agric. Food Chem.* **44,** 2544–2548 (1996).

147. Kato, A., Sasaki, Y., Furuta, R. & Kobayashi, K. Functional Protein-Polysaccharide Conjugate Prepared by Controlled Dry-heating of Ovalbumin-Dextran Mixtures. *Agric. Biol. Chem.* **54,** 107–112 (1990).

148. Dickinson, E. & Galazka, V. B. Emulsion stabilization by ionic and covalent complexes of β-

lactoglobulin with polysaccharides. *Top. Catal.* **5,** 281–296 (1991).

149. Dickinson, E. Milk protein interfacial layers and the relationship to emulsion stability and rheology. *Colloids Surfaces B Biointerfaces* **20,** 197–210 (2001).

150. Pichot, R., Spyropoulos, F. & Norton, I. T. O/W emulsions stabilised by both low molecular weight surfactants and colloidal particles: The effect of surfactant type and concentration. *J. Colloid Interface Sci.* **352,** 128–35 (2010).

151. Pichot, R., Spyropoulos, F. & Norton, I. T. Mixed-emulsifier stabilised emulsions: Investigation of the effect of monoolein and hydrophilic silica particle mixtures on the stability against coalescence. *J. Colloid Interface Sci.* **329,** 284–291 (2009).

152. Gullapalli, R. P. & Sheth, B. B. Influence of an optimized non-ionic emulsifier blend on properties of oil-in-water emulsions. *Eur. J. Pharm. Biopharm.* **48,** 233–238 (1999).

153. Tcholakova, S., Denkov, N. ~D. & Lips, A. Comparison of solid particles, globular proteins and surfactants as emulsifiers. *Phys. Chem. Chem. Phys. (Incorporating Faraday Trans.* **10,** 1608 (2008).

154. Binks, B. P. & Lumsdon, S. O. Influence of particle wettability on the type and stability of surfactant-free emulsions. *Langmuir* **16,** 8622–8631 (2000).

155. Hunter, T. N., Pugh, R. J., Franks, G. V. & Jameson, G. J. The role of particles in stabilising foams and emulsions. *Adv. Colloid Interface Sci.* **137,** 57–81 (2008).

156. Drelich, A., Gomez, F., Clausse, D. & Pezron, I. Evolution of water-in-oil emulsions stabilized with solid particles. Influence of added emulsifier. *Colloids Surfaces A Physicochem. Eng. Asp.* **365,** 171–177 (2010).

157. Binks, B. P. & Whitby, C. P. Nanoparticle silica-stabilised oil-in-water emulsions: Improving emulsion stability. *Colloids Surfaces A Physicochem. Eng. Asp.* **253,** 105–115 (2005).

158. Lagaly, G., Reese, M. & Abend, S. Smectites as colloidal stabilizers of emulsions I. Preparation and properties of emulsions with smectites and nonionic surfactants. *Appl. Clay Sci.* **14,** 83–103 (1999).

159. Shields, M., Ellis, R. & Saunders, B. R. A creaming study of weakly flocculated and depletion flocculated oil-in-water emulsions. *Colloids Surfaces A Physicochem. Eng. Asp.* **178,** 265–276 (2001).

160. Goodarzi, F. & Zendehboudi, S. A Comprehensive Review on Emulsions and Emulsion Stability in Chemical and Energy Industries. *Can. J. Chem. Eng.* **97,** 281–309 (2019).

161. Chanamai, R. & McClements, D. J. Dependence of creaming and rheology of monodisperse oil-in-water emulsions on droplet size and concentration. *Colloids Surfaces A Physicochem. Eng. Asp.* **172,** 79–86 (2000).

162. Kingdom, U. Creaming and Flocculation of Oil-in-Water Emulsions Containing Sodium Caseinate. **529,** 515–529 (1997).

163. Pinfield, V. J., Dickinson, E. & Povey, M. J. W. Modeling of combined creaming and flocculation in emulsions. *J. Colloid Interface Sci.* **186,** 80–89 (1997).

164. Ivanov, I. B., Danov, K. D. & Kralchevsky, P. A. Flocculation and coalescence of micron-size emulsion droplets. *Colloids Surfaces A Physicochem. Eng. Asp.* **152,** 161–182 (1999).

165. Kabalnov, A. Thermodynamic and theoretical aspects of emulsions and their stability. *Curr.*

Opin. Colloid Interface Sci. **3,** 270–275 (1998).

166. Kabalnov, A. S. & Shchukin, E. D. Ostwald ripening theory: applications to fluorocarbon emulsion stability. *Adv. Colloid Interface Sci.* **38,** 69–97 (1992).

167. Zeeb, B., Gibis, M., Fischer, L. & Weiss, J. Influence of interfacial properties on Ostwald ripening in crosslinked multilayered oil-in-water emulsions. *J. Colloid Interface Sci.* **387,** 65–73 (2012).

168. Dickinson, E., Ritzoulis, C., Yamamoto, Y. & Logan, H. Ostwald ripening of protein-stabilized emulsions: Effect of transglutaminase crosslinking. *Colloids Surfaces B Biointerfaces* **12,** 139–146 (1999).

169. Mun, S. & McClements, D. J. Influence of interfacial characteristics on ostwald ripening in hydrocarbon oil-in-water emulsions. *Langmuir* **22,** 1551–1554 (2006).

170. Santos, F. dos *et al.* Toward a Clinical-Grade Expansion of Mesenchymal Stem Cells from Human Sources: A Microcarrier-Based Culture System Under Xeno-Free Conditions. *Tissue Eng. Part C Methods* **17,** 1201–1210 (2011).

171. Jones, M. K., Lu, B., Girman, S. & Wang, S. Cell-based therapeutic strategies for replacement and preservation in retinal degenerative diseases. *Prog. Retin. Eye Res.* **58,** 1–27 (2017).

172. Assinck, P., Duncan, G. J., Hilton, B. J., Plemel, J. R. & Tetzlaff, W. Cell transplantation therapy for spinal cord injury. *Nat. Neurosci.* **20,** 637–647 (2017).

173. Walia, B., Satija, N., Tripathi, R. P. & Gangenahalli, G. U. Induced Pluripotent Stem Cells: Fundamentals and Applications of the Reprogramming Process and its Ramifications on Regenerative Medicine. *Stem Cell Rev. Reports* **8,** 100–115 (2012).

174. Wang, S., Qu, X. & Zhao, R. C. Clinical applications of mesenchymal stem cells. *Journal of Hematology and Oncology* **5,** 1 (2012).

175. McGuirk, J. P., Robert Smith, J., Divine, C. L., Zuniga, M. & Weiss, M. L. Wharton's jelly-derived mesenchymal stromal cells as a promising cellular therapeutic strategy for the management of graft-versus-host disease. *Pharmaceuticals* **8,** 196–220 (2015).

176. Le Blanc, K. *et al.* Mesenchymal stem cells for treatment of steroid-resistant, severe, acute graft-versus-host disease: a phase II study. *Lancet* **371,** 1579–1586 (2008).

177. Rafiq, Q. A., Coopman, K. & Hewitt, C. J. Scale-up of human mesenchymal stem cell culture: Current technologies and future challenges. *Curr. Opin. Chem. Eng.* **2,** 8–16 (2013).

178. Tavassoli, H. *et al.* Large-scale production of stem cells utilizing microcarriers: A biomaterials engineering perspective from academic research to commercialized products. *Biomaterials* **181,** 333–346 (2018).

179. Badenes, S. M., Fernandes, T. G., Rodrigues, C. A. V., Diogo, M. M. & Cabral, J. M. S. Microcarrier-based platforms for in vitro expansion and differentiation of human pluripotent stem cells in bioreactor culture systems. *J. Biotechnol.* **234,** 71–82 (2016).

180. Chen, A. K.-L., Reuveny, S. & Oh, S. K. W. Application of human mesenchymal and pluripotent stem cell microcarrier cultures in cellular therapy: Achievements and future direction. *Biotechnol. Adv.* **31,** 1032–1046 (2013).

181. Oh, S. K. W. *et al.* Long-term microcarrier suspension cultures of human embryonic stem cells. *Stem Cell Res.* **2,** 219–230 (2009).

182. Rafiq, Q. A. *et al.* Qualitative and quantitative demonstration of bead-to-bead transfer with

bone marrow-derived human mesenchymal stem cells on microcarriers: Utilising the phenomenon to improve culture performance. *Biochem. Eng. J.* **135,** 11–21 (2018).

183. Leber, J. *et al.* Microcarrier choice and bead-to-bead transfer for human mesenchymal stem cells in serum-containing and chemically defined media. *Process Biochem.* **59,** 255–265 (2017).

184. Simaria, A. S. *et al.* Allogeneic cell therapy bioprocess economics and optimization: Single-use cell expansion technologies. *Biotechnol. Bioeng.* **111,** 69–83 (2014).

185. Cherian, D. S., Bhuvan, T., Meagher, L. & Heng, T. S. P. Biological Considerations in Scaling Up Therapeutic Cell Manufacturing. *Front. Pharmacol.* **11,** 1–25 (2020).

186. Van Wezel, A. L. Growth of cell-strains and primary cells on micro-carriers in homogeneous culture. *Nature* **216,** 64–65 (1967).

187. Rafiq, Q. A., Coopman, K., Nienow, A. W. & Hewitt, C. J. Systematic microcarrier screening and agitated culture conditions improves human mesenchymal stem cell yield in bioreactors. *Biotechnol. J.* **11,** 473–486 (2016).

188. Fischer, E. M., Layrolle, P., van Blitterswijk, C. A. & de Bruijn, J. D. Bone Formation by Mesenchymal Progenitor Cells Cultured on Dense and Microporous Hydroxyapatite Particles. *Tissue Eng.* **9,** 1179–1188 (2003).

189. Li, B. *et al.* Past, present, and future of microcarrier-based tissue engineering. *J. Orthop. Transl.* **3,** 51–57 (2015).

190. de Soure, A. M., Fernandes-Platzgummer, A., da Silva, C. L. & Cabral, J. M. S. Scalable microcarrier-based manufacturing of mesenchymal stem/stromal cells. *J. Biotechnol.* **236,** 88–109 (2016).

191. Choi, S. W., Zhang, Y., Yeh, Y. C., Lake Wooten, A. & Xia, Y. Biodegradable porous beads and their potential applications in regenerative medicine. *J. Mater. Chem.* **22,** 11442–11451 (2012).

192. Kumar, A. & Starly, B. Large scale industrialized cell expansion: Producing the critical raw material for biofabrication processes. *Biofabrication* **7,** 44103 (2015).

193. Schmidt, J. J., Jeong, J. & Kong, H. The interplay between cell adhesion cues and curvature of cell adherent alginate microgels in multipotent stem cell culture. *Tissue Eng. - Part A* **17,** 2687–2694 (2011).

194. Pieuchot, L. *et al.* Curvotaxis directs cell migration through cell-scale curvature landscapes. *Nat. Commun.* **9,** (2018).

195. Werner, M. *et al.* Surface Curvature Differentially Regulates Stem Cell Migration and Differentiation via Altered Attachment Morphology and Nuclear Deformation. *Adv. Sci.* **4,** 1–11 (2017).

196. Alfred, R. *et al.* Large-scale production of murine embryonic stem cell-derived osteoblasts and chondrocytes on microcarriers in serum-free media. *Biomaterials* **32,** 6006–6016 (2011).

197. Frauenschuh, S. *et al.* A Microcarrier-Based Cultivation System for Expansion of Primary Mesenchymal Stem Cells. *Biotechnol. Prog.* **23,** 187–193 (2007).

198. Chen, A. K. L., Chen, X., Choo, A. B. H., Reuveny, S. & Oh, S. K. W. Critical microcarrier properties affecting the expansion of undifferentiated human embryonic stem cells. *Stem Cell Res.* **7,** 97–111 (2011).

199. Jin, S., Yao, H., Weber, J. L., Melkoumian, Z. K. & Ye, K. A Synthetic, Xeno-Free Peptide Surface

for Expansion and Directed Differentiation of Human Induced Pluripotent Stem Cells. *PLoS One* **7,** (2012).

200. Hervy, M. *et al.* Long term expansion of bone marrow-derived hMSCs on novel synthetic microcarriers in xeno-free, defined conditions. *PLoS One* **9,** 1–7 (2014).

201. Curran, J. M., Chen, R. & Hunt, J. A. Controlling the phenotype and function of mesenchymal stem cells in vitro by adhesion to silane-modified clean glass surfaces. *Biomaterials* **26,** 7057–7067 (2005).

202. Matsuda, N., Shimizu, T., Yamato, M. & Okano, T. Tissue Engineering Based on Cell Sheet Technology. *Adv. Mater.* **19,** 3089–3099 (2007).

203. LI, M., MA, J. U. N., GAO, Y. & YANG, L. E. I. Cell sheet technology: a promising strategy in regenerative medicine. *Cytotherapy* **21,** 3–16 (2019).

204. Nagase, K., Kobayashi, J. & Okano, T. Temperature-responsive intelligent interfaces for biomolecular separation and cell sheet engineering. *J. R. Soc. Interface* **6,** (2009).

205. Yang, H. S., Jeon, O., Bhang, S. H., Lee, S. H. & Kim, B. S. Suspension culture of mammalian cells using thermosensitive microcarrier that allows cell detachment without proteolytic enzyme treatment. *Cell Transplant.* **19,** 1123–1132 (2010).

206. Tamura, A. *et al.* Simultaneous enhancement of cell proliferation and thermally induced harvest efficiency based on temperature-responsive cationic copolymer-grafted microcarriers. *Biomacromolecules* **13,** 1765–1773 (2012).

207. Tamura, A., Kobayashi, J., Yamato, M. & Okano, T. Temperature-responsive poly(N-isopropylacrylamide)-grafted microcarriers for large-scale non-invasive harvest of anchorage-dependent cells. *Biomaterials* **33,** 3803–3812 (2012).

208. Yuan, Yifan; Kallos, M. S. C. H. and A. S. Improved expansion of human bone marrow-derived mesenchymal stem cells in microcarrier-based suspension culture. *J. Tissue Eng. Regen. Med.* **17,** 1201–1210 (2012).

209. Chen, X., Xu, H., Wan, C., McCaigue, M. & Li, G. Bioreactor Expansion of Human Adult Bone Marrow-Derived Mesenchymal Stem Cells. *Stem Cells* **24,** 2052–2059 (2006).

210. Moore, S. W., Roca-Cusachs, P. & Sheetz, M. P. Stretchy proteins on stretchy substrates: The important elements of integrin-mediated rigidity sensing. *Dev. Cell* **19,** 194–206 (2010).

211. Mezei, A. *et al.* Self assembly of pH-sensitive cationic lysine based surfactants. *Langmuir* **28,** 16761–16771 (2012).

212. Takehara, M. Properties and applications of amino acid based surfactants. *Colloids and Surfaces* **38,** 149–167 (1989).

213. Sharma, V., Jaishankar, A., Wang, Y. C. & McKinley, G. H. Rheology of globular proteins: Apparent yield stress, high shear rate viscosity and interfacial viscoelasticity of bovine serum albumin solutions. *Soft Matter* **7,** 5150–5160 (2011).

214. Szyk-Warszyńska, L., Piekoszewska, J. & Warszyński, P. Formation and stability of poly-L-lysine/casein multilayers. *Adsorption* **16,** 241–248 (2010).

215. Ogieglo, W., Wormeester, H., Eichhorn, K. J., Wessling, M. & Benes, N. E. In situ ellipsometry studies on swelling of thin polymer films: A review. *Prog. Polym. Sci.* **42,** 42–78 (2015).

216. Halthur, T. J. & Elofsson, U. M. Multilayers of charged polypeptides as studied by in situ

ellipsometry and quartz crystal microbalance with dissipation. *Langmuir* **20,** 1739–1745 (2004).

217. Bouyer, E., Mekhloufi, G., Rosilio, V., Grossiord, J. L. & Agnely, F. Proteins, polysaccharides, and their complexes used as stabilizers for emulsions: Alternatives to synthetic surfactants in the pharmaceutical field? *Int. J. Pharm.* **436,** 359–378 (2012).

218. Lee, H. *et al.* Substrate-independent layer-by-layer assembly by using mussel-adhesive-inspired polymers. *Adv. Mater.* **20,** 1619–1623 (2008).

219. Engelhardt, K. *et al.* Protein adsorption at the electrified air-water interface: Implications on foam stability. *Langmuir* **28,** 7780–7787 (2012).

220. Alahverdjieva, V. S. *et al.* Competitive adsorption from mixed hen egg-white lysozyme/surfactant solutions at the air-water interface studied by tensiometry, ellipsometry, and surface dilational rheology. *J. Phys. Chem. B* **112,** 2136–2143 (2008).

221. Dickinson, E., Horne, D. S., Phipps, J. S. & Richardson, R. M. A Neutron Reflectivity Study of the Adsorption of β-Casein at Fluid Interfaces. *Langmuir* **9,** 242–248 (1993).

222. Hirsa, A., Korenowski, G. M., Logory, L. M. & Judd, C. D. Determination of surface viscosities by surfactant concentration and velocity field measurements for an insoluble monolayer. *Langmuir* **13,** 3813–3822 (1997).

223. Kim, G., Gurau, M., Kim, J. & Cremer, P. S. Investigations of lysozyme adsorption at the air/water and quartz/water interfaces by vibrational sum frequency spectroscopy. *Langmuir* **18,** 2807–2811 (2002).

224. Lam, A. T. L. *et al.* Conjoint propagation and differentiation of human embryonic stem cells to cardiomyocytes in a defined microcarrier spinner culture. *Stem Cell Res. Ther.* **5,** 1–15 (2014).

225. De Castro, M., Orive, G., Hernández, R. M., Gascón, A. R. & Pedraz, J. L. Comparative study of microcapsules eleborated with three polycations (PLL, PDL, PLO) for cell immobilization. *J. Microencapsul.* **22,** 303–315 (2005).

226. Wilson, J. L. & Mcdevitt, T. C. Stem cell microencapsulation for phenotypic control, bioprocessing, and transplantation. *Biotechnol. Bioeng.* **110,** 667–682 (2013).

227. Haque, T. *et al.* Superior cell delivery features of poly(ethylene glycol) incorporated alginate, chitosan, and poly-L-lysine microcapsules. *Mol. Pharm.* **2,** 29–36 (2005).

228. Murua, A. *et al.* Cell microencapsulation technology: Towards clinical application. *J. Control. Release* **132,** 76–83 (2008).

229. Chittchang, M. *et al.* Poly(L-lysine) as a model drug macromolecule with which to investigate secondary structure and microporous membrane transport, part 2: diffusion studies. *J. Pharm. Pharmacol.* **54,** 1497–1505 (2002).

230. Shan, C. *et al.* Water-soluble graphene covalently functionalized by biocompatible poly-L-lysine. *Langmuir* **25,** 12030–12033 (2009).

231. Satake, I. & Yang, J. T. Effect of temperature and pH on the β–helix transition of poly(L-lysine) in sodium dodecyl sulfate solution. *Biopolymers* **14,** 1841–1846 (1975).

232. Brown, E. M. & Groves, M. L. Effect of temperature on the circular dichroism spectra of β2-microglobulins. *FEBS Lett.* **184,** 36–39 (1985).

233. Lee, A. T. & McHugh, A. J. The effect of simple shear flow on the helix-coil transition of poly-L-lysine. *Biopolymers* **50,** 589–594 (1999).

234. Kong, D., Peng, L., Di Cio, S., Novak, P. & Gautrot, J. E. Stem Cell Expansion and Fate Decision on Liquid Substrates Are Regulated by Self-Assembled Nanosheets. *ACS Nano* **12,** (2018).

235. Sarkar, R. & Rybenkov, V. V. A Guide to Magnetic Tweezers and Their Applications. *Front. Phys.* **4,** (2016).

236. Yao, M. *et al.* Mechanical activation of vinculin binding to talin locks talin in an unfolded conformation. *Sci. Rep.* **4,** (2014).

237. Chronopoulos, A. *et al.* ATRA mechanically reprograms pancreatic stellate cells to suppress matrix remodelling and inhibit cancer cell invasion. *Nat. Commun.* **7,** (2016).

238. Goudoulas, T. B. & Germann, N. Viscoelastic properties of polyacrylamide solutions from creep ringing data. *J. Rheol. (N. Y. N. Y).* **60,** 491–502 (2016).

239. Pavlovsky, L., Younger, J. G. & Solomon, M. J. In situ rheology of Staphylococcus epidermidis bacterial biofilms. *Soft Matter* **9,** 122–131 (2013).

240. Jaishankar, A., Sharma, V. & McKinley, G. H. Interfacial viscoelasticity, yielding and creep ringing of globular protein-surfactant mixtures. *Soft Matter* **7,** 7623–7634 (2011).

241. Program, T., Lake, S., Data, O., Ewoldt, R. H. & Mckinley, G. H. Help with Ringing , Dumbbells , Relaxation Times Also : Notable Passing : Hershel Markovitz in Step Stress Tests ! *Rheology* **76,** (2007).

242. Bui, B. T. & Tutuncu, A. N. Creep-recovery test: A critical tool for rheological characterization of drilling fluids. *Unconv. Resour. Technol. Conf. 2013, URTC 2013* 1045–1059 (2013). doi:10.1190/urtec2013-107

243. Noskovy, B. A., Latnikova, A. V., Lin, S. Y., Loglio, G. & Miller, R. Dynamic surface elasticity of β-casein solutions during adsorption. *J. Phys. Chem. C* **111,** 16895–16901 (2007).

244. Hermel, H. & Miller, R. Effect of the secondary structure of poly-L-lysine on the adsorption at the water/dodecane interface. *Colloid Polym. Sci.* **273,** 387–391 (1995).

245. Morris, V. J. & Gunning, A. P. Microscopy, microstructure and displacement of proteins from interfaces: implications for food quality and digestion. *Soft Matter* **4,** 943–951 (2008).

246. Leiss, M., Beckmann, K., Girós, A., Costell, M. & Fässler, R. The role of integrin binding sites in fibronectin matrix assembly in vivo. *Curr. Opin. Cell Biol.* **20,** 502–507 (2008).

247. Van der Flier, A. & Sonnenberg, A. Function and interactions of integrins. *Cell Tissue Res.* **305,** 285–298 (2001).

248. Horton, M. A. The αvβ3 integrin 'vitronectin receptor'. *Int. J. Biochem. Cell Biol.* **29,** 721–725 (1997).

249. Emsley, J., Knight, C. G., Farndale, R. W. & Barnes, M. J. Structure of the Integrin α2β1-binding Collagen Peptide. *J. Mol. Biol.* **335,** 1019–1028 (2004).

250. Ang, Y. U. L. I. W. Cell locomotion and focal adhesions are regulated by. *Proc. Natl. Acad. Sci.* **94,** 13661–13665 (1997).

251. Di Cio, S., Iskratsch, T., Connelly, J. T. & Gautrot, J. E. Contractile myosin rings and cofilin-mediated actin disassembly orchestrate ECM nanotopography sensing. *Biomaterials* **232,** 119683 (2020).

252. Di Cio, S., Bøggild, T. M. L., Connelly, J., Sutherland, D. S. & Gautrot, J. E. Differential integrin expression regulates cell sensing of the matrix nanoscale geometry. *Acta Biomater.* **50,** 280–

292 (2017).

253. Rowlands, A. S., George, P. A. & Cooper-White, J. J. Directing osteogenic and myogenic differentiation of MSCs: Interplay of stiffness and adhesive ligand presentation. *Am. J. Physiol. - Cell Physiol.* **295,** 1037–1044 (2008).

254. Chaudhuri, O. *et al.* Substrate stress relaxation regulates cell spreading. *Nat. Commun.* **6,** 1–7 (2015).

255. Discher, D. E., Janmey, P. & Wang, Y. L. Tissue cells feel and respond to the stiffness of their substrate. *Science (80-.).* **310,** 1139–1143 (2005).

256. Verdier, C., Etienne, J., Duperray, A. & Preziosi, L. Review: Rheological properties of biological materials. *Comptes Rendus Phys.* **10,** 790–811 (2009).

257. Cameron, A. R., Frith, J. E. & Cooper-White, J. J. The influence of substrate creep on mesenchymal stem cell behaviour and phenotype. *Biomaterials* **32,** 5979–5993 (2011).

258. Gong, Z. *et al.* Matching material and cellular timescales maximizes cell spreading on viscoelastic substrates. (2018). doi:10.1073/pnas.1716620115

259. Pilarek, M., Grabowska, I., Ciemerych, M. A., Dabkowska, K. & Szewczyk, K. W. Morphology and growth of mammalian cells in a liquid/liquid culture system supported with oxygenated perfluorodecalin. *Biotechnol. Lett.* **35,** 1387–1394 (2013).

260. Hanga, M. P. *et al.* Expansion of bone marrow-derived human mesenchymal stem/stromal cells (hMSCs) using a two-phase liquid/liquid system. *J. Chem. Technol. Biotechnol.* **92,** 1577–1589 (2017).

261. Bauer, A. *et al.* Hydrogel substrate stress-relaxation regulates the spreading and proliferation of mouse myoblasts. *Acta Biomater.* **62,** 82–90 (2017).

262. Helfand, B. T., Mendez, M. G., Pugh, J., Delsert, C. & Goldman, R. D. Maintaining the Shape of Nerve Cells □. *Mol. Biol. Cell* **14,** 5069–5081 (2003).

263. Anthis, N. J. *et al.* β integrin tyrosine phosphorylation is a conserved mechanism for regulating talin-induced integrin activation. *J. Biol. Chem.* **284,** 36700–36710 (2009).

264. Pasapera, A. M., Schneider, I. C., Rericha, E., Schlaepfer, D. D. & Waterman, C. M. Myosin II activity regulates vinculin recruitment to focal adhesions through FAK-mediated paxillin phosphorylation. *J. Cell Biol.* **188,** 877–890 (2010).

265. Chen, B., Ji, B. & Gao, H. Modeling Active Mechanosensing in Cell–Matrix Interactions. *Annu. Rev. Biophys.* **44,** 1–32 (2015).

266. Schaller, M. D. Paxillin: A focal adhesion-associated adaptor protein. *Oncogene* **20,** 6459–6472 (2001).

267. Turner, C. E. Paxillin and focal adhesion signalling. *Nature Cell Biology* **2,** 231–236 (2000).

268. Werner, M., Petersen, A., Kurniawan, N. A. & Bouten, C. V. C. Cell-Perceived Substrate Curvature Dynamically Coordinates the Direction, Speed, and Persistence of Stromal Cell Migration. *Adv. Biosyst.* **3,** (2019).

269. Lee, S. J. & Yang, S. Substrate Curvature Restricts Spreading and Induces Differentiation of Human Mesenchymal Stem Cells. *Biotechnol. J.* **12,** 1–10 (2017).

270. Uto, K., Mano, S. S., Aoyagi, T. & Ebara, M. Substrate Fluidity Regulates Cell Adhesion and Morphology on Poly(ε-caprolactone)-Based Materials. *ACS Biomater. Sci. Eng.* **2,** 446–453

(2016).

271. Terada, S., Sato, M., Katayama, R. & Shinozawa, T. Recovery of intact membrane proteins from adherent animal cells grown in a liquid-liquid interface. *J. Ferment. Bioeng.* **74,** 330–332 (1992).

272. Baumann, H. & Doyle, D. Effect of Trypsin Culture Cells on the Cell Surface Proteins of Hepatoma Tissue Culture Cells. *J. Biol. Chem.* **254,** 3935–3946 (1979).

273. Jones, P. H. & Watt, F. M. Separation of human epidermal stem cells from transit amplifying cells on the basis of differences in integrin function and expression. *Cell* **73,** 713–724 (1993).

274. Friedenstein, A. J., Latzinik, N. V., Gorskaya, U. F. & Sidorovich, S. Y. Radiosensitivity and postirradiation changes of bone marrow clonogenic stromal mechanocytes. *Int. J. Radiat. Biol.* **39,** 537–546 (1981).

275. Ullah, I., Subbarao, R. B. & Rho, G. J. Human mesenchymal stem cells - Current trends and future prospective. *Biosci. Rep.* **35,** (2015).

276. Wei, X. *et al.* Mesenchymal stem cells: a new trend for cell therapy. *Acta Pharmacol. Sin.* **34,** 747–754 (2013).

277. Dominici, M. *et al.* Minimal criteria for defining multipotent mesenchymal stromal cells. The International Society for Cellular Therapy position statement. *Cytotherapy* **8,** 315–317 (2006).

278. Okolicsanyi, R. K. *et al.* Human mesenchymal stem cells retain multilineage differentiation capacity including neural marker expression after extended in vitro expansion. *PLoS One* **10,** 1–29 (2015).

279. Lazarus, H. M., Haynesworth, S. E., Gerson, S. L., Rosenthal, N. S. & Caplan, A. I. Ex vivo expansion and subsequent infusion of human bone marrow-derived stromal progenitor cells (mesenchymal progenitor cells): implications for therapeutic use. *Bone Marrow Transplant.* **16,** 557—564 (1995).

280. Leng, Z. *et al.* Transplantation of ACE2- Mesenchymal stem cells improves the outcome of patients with covid-19 pneumonia. *Aging Dis.* **11,** 216–228 (2020).

281. Metcalfe, S. M. Mesenchymal stem cells and management of COVID-19 pneumonia. *Med. Drug Discov.* **5,** 100019 (2020).

282. Książek, K. A comprehensive review on mesenchymal stem cell growth and senescence. *Rejuvenation Res.* **12,** 105–116 (2009).

283. Turinetto, V., Vitale, E. & Giachino, C. Senescence in human mesenchymal stem cells: Functional changes and implications in stem cell-based therapy. *Int. J. Mol. Sci.* **17,** 1–18 (2016).

284. Bertolo, A., Baur, M., Guerrero, J., Pötzel, T. & Stoyanov, J. Autofluorescence is a Reliable in vitro Marker of Cellular Senescence in Human Mesenchymal Stromal Cells. *Sci. Rep.* **9,** 1–15 (2019).

285. Park, I. H. *et al.* Reprogramming of human somatic cells to pluripotency with defined factors. *Nature* **451,** 141–146 (2008).

286. Tang, H. *et al.* Dual expression of hTERT and VEGF prolongs life span and enhances angiogenic ability of aged BMSCs. *Biochem. Biophys. Res. Commun.* **440,** 502–508 (2013).

287. Kawasaki, H., Guan, J. & Tamama, K. Hydrogen gas treatment prolongs replicative lifespan of bone marrow multipotential stromal cells in vitro while preserving differentiation and paracrine potentials. *Biochem. Biophys. Res. Commun.* **397,** 608–613 (2010).

288. Zanichelli, F. *et al.* Low concentrations of isothiocyanates protect mesenchymal stem cells from oxidative injuries, while high concentrations exacerbate DNA damage. *Apoptosis* **17,** 964–974 (2012).

289. Hendriks, J., Riesle, J. & Blitterswijk, A. van, C. Expansion of mesenchymal stem cells using a microcarrier-based cultivation system: growth and metabolism. *J. Tissue Eng. Regen. Med.* **2,** 126–135 (2008).

290. Gupta, P. *et al.* Optimization of agitation speed in spinner flask for microcarrier structural integrity and expansion of induced pluripotent stem cells. *Cytotechnology* **68,** 45–59 (2016).

291. Eibes, G. *et al.* Maximizing the ex vivo expansion of human mesenchymal stem cells using a microcarrier-based stirred culture system. *J. Biotechnol.* **146,** 194–197 (2010).

292. Panchalingam, K. M., Jung, S., Rosenberg, L. & Behie, L. A. Bioprocessing strategies for the large-scale production of human mesenchymal stem cells: a review. *Stem Cell Res. Ther.* **6,** 225 (2015).

293. Petry, F. *et al.* Manufacturing of Human Umbilical Cord Mesenchymal Stromal Cells on Microcarriers in a Dynamic System for Clinical Use. *Stem Cells Int.* **2016,** (2016).

294. McKee, C. & Chaudhry, G. R. Advances and challenges in stem cell culture. *Colloids Surfaces B Biointerfaces* **159,** 62–77 (2017).

295. Dolley-Sonneville, P. J., Romeo, L. E. & Melkoumian, Z. K. Synthetic Surface for Expansion of Human Mesenchymal Stem Cells in Xeno-Free, Chemically Defined Culture Conditions. *PLoS One* **8,** 1–12 (2013).

296. Finkle, P., Draper, H. D. & Hildebrand, J. H. The theory of emulsification. *J. Am. Chem. Soc.* **45,** 2780–2788 (1923).

297. Rousseau, Â. Fat crystals and emulsion stability. *Food Res. Int.* **33,** (2000).

298. McClements, D. J. & Demetriades, K. An integrated approach to the development of reduced-fat food emulsions. *Crit. Rev. Food Sci. Nutr.* **38,** 511–536 (1998).

299. Douaire, M. *et al.* Fat crystallisation at oil-water interfaces. *Adv. Colloid Interface Sci.* **203,** 1–10 (2014).

300. Fredrick, E., Walstra, P. & Dewettinck, K. Factors governing partial coalescence in oil-in-water emulsions. *Adv. Colloid Interface Sci.* **153,** 30–42 (2010).

301. Picart, C. *et al.* Molecular basis for the explanation of the exponential growth of polyelectrolyte multilayers. *Proc. Natl. Acad. Sci. U. S. A.* **99,** 12531–12535 (2002).

302. Pawar, A. B., Caggioni, M., Ergun, R., Hartel, R. W. & Spicer, P. T. Arrested coalescence in Pickering emulsions. *Soft Matter* **7,** 7710–7716 (2011).

303. Burke, S. E. & Barrett, C. J. pH-responsive properties of multilayered poly(L-lysine)/hyaluronic acid surfaces. *Biomacromolecules* **4,** 1773–1783 (2003).

304. Borm, B., Requardt, R. P., Herzog, V. & Kirfel, G. Membrane ruffles in cell migration: Indicators of inefficient lamellipodia adhesion and compartments of actin filament reorganization. *Exp. Cell Res.* **302,** 83–95 (2005).

305. Hoon, J.-L., Wong, W.-K. & Koh, C.-G. Functions and Regulation of Circular Dorsal Ruffles. *Mol. Cell. Biol.* **32,** 4246–4257 (2012).

306. Innocenti, M. New insights into the formation and the function of lamellipodia and ruffles in

mesenchymal cell migration. *Cell Adhes. Migr.* **12,** 401–416 (2018).

307. Saalbach, A. & Anderegg, U. Thy-1: more than a marker for mesenchymal stromal cells. *FASEB J.* **33,** 6689–6696 (2019).

308. Rege, T. A. & Hagood, J. S. Thy-1, a versatile modulator of signaling affecting cellular adhesion, proliferation, survival, and cytokine/growth factor responses. *Biochim. Biophys. Acta - Mol. Cell Res.* **1763,** 991–999 (2006).

309. Fonsatti, E. *et al.* Endoglin: An accessory component of the TGF-β-binding receptor-complex with diagnostic, prognostic, and bioimmunotherapeutic potential in human malignancies. *J. Cell. Physiol.* **188,** 1–7 (2001).

310. Kim, Y.-K. *et al.* Osteogenic Potential of Mouse Periosteum-Derived Cells Sorted for CD90 In Vitro and In Vivo. *Stem Cells Transl. Med.* **5,** 227–234 (2016).

311. Jin, H. J. *et al.* Down-regulation of CD105 is associated with multi-lineage differentiation in human umbilical cord blood-derived mesenchymal stem cells. *Biochem. Biophys. Res. Commun.* **381,** 676–681 (2009).

312. Cleary, M. A. *et al.* Expression of CD105 on expanded mesenchymal stem cells does not predict their chondrogenic potential. *Osteoarthr. Cartil.* **24,** 868–872 (2016).

313. Izgi, K., Sonmez, M. F., Canatan, H. & Iskender, B. Long Term Exposure to Myrtucommulone-A Changes CD105 Expression and Differentiation Potential of Mesenchymal Stem Cells. *Tissue Eng. Regen. Med.* **14,** 113–121 (2017).

314. Bohn, A. B., Moller, B. K. & Petersen, M. S. Flow cytometry and compensation of highly autofluorescent cells: the example of mesenchymal stem cells. *Stem Cell Biol. Res.* **2,** 4 (2015).

315. Anwer, A. G., Gosnell, M. E., Perinchery, S. M., Inglis, D. W. & Goldys, E. M. Visible 532 nm laser irradiation of human adipose tissue-derived stem cells: Effect on proliferation rates, mitochondria membrane potential and autofluorescence. *Lasers Surg. Med.* **44,** 769–778 (2012).

316. Lewis, E. E. L. *et al.* A Quiescent, Regeneration-Responsive Tissue Engineered Mesenchymal Stem Cell Bone Marrow Niche Model via Magnetic Levitation. *ACS Nano* **10,** 8346–8354 (2016).

317. Méndez-Ferrer, S. *et al.* Mesenchymal and haematopoietic stem cells form a unique bone marrow niche. *Nature* **466,** 829–834 (2010).

318. Jung, E. M. *et al.* Evidences for correlation between the reduced VCAM-1 expression and hyaluronan synthesis during cellular senescence of human mesenchymal stem cells. *Biochem. Biophys. Res. Commun.* **404,** 463–469 (2011).

319. Boxall, S. A. & Jones, E. Markers for Characterization of Bone Marrow Multipotential Stromal Cells. *Stem Cells Int.* **2012,** 1–12 (2012).

320. Fukiage, K. *et al.* Expression of vascular cell adhesion molecule-1 indicates the differentiation potential of human bone marrow stromal cells. *Biochem. Biophys. Res. Commun.* **365,** 406–412 (2008).

321. Tsang, K. Y., Chan, D. & Cheah, K. S. E. Fate of growth plate hypertrophic chondrocytes: Death or lineage extension? *Dev. Growth Differ.* **57,** 179–192 (2015).

322. Huang, Z., Nelson, E. R., Smith, R. L. & Goodman, S. B. The sequential expression profiles of growth factors from osteroprogenitors to osteoblasts in vitro. *Tissue Eng.* **13,** 2311–2320 (2007).

323. Jeon, E. J. *et al.* Bone morphogenetic protein-2 stimulates Runx2 acetylation. *J. Biol. Chem.* **281,** 16502–16511 (2006).

324. Labbaf, S. *et al.* Spherical bioactive glass particles and their interaction with human mesenchymal stem cells in vitro. *Biomaterials* **32,** 1010–1018 (2011).

325. Richardson, S. M. *et al.* Mesenchymal stem cells in regenerative medicine: Focus on articular cartilage and intervertebral disc regeneration. *Methods* **99,** 69–80 (2016).

326. Mackie, E. J., Ahmed, Y. A., Tatarczuch, L., Chen, K. S. & Mirams, M. Endochondral ossification: How cartilage is converted into bone in the developing skeleton. *Int. J. Biochem. Cell Biol.* **40,** 46–62 (2008).

327. Barry, F., Boynton, R. E., Liu, B. & Murphy, J. M. Chondrogenic differentiation of mesenchymal stem cells from bone marrow: Differentiation-dependent gene expression of matrix components. *Exp. Cell Res.* **268,** 189–200 (2001).

328. Shen, G. The role of type X collagen in facilitating and regulating endochondral ossification of articular cartilage. *Orthod. Craniofacial Res.* **8,** 11–17 (2005).

329. Paebst, F. *et al.* Comparative immunophenotyping of equine multipotent mesenchymal stromal cells: An approach toward a standardized definition. *Cytom. Part A* **85,** 678–687 (2014).

330. Choi, C. K. *et al.* Actin and alpha-actinin orchestrate the assembly and maturation of nascent adhesions in a myosin II motor-independent manner. *Nat. Cell Biol.* **10,** 1039–50 (2008).

331. Kanchanawong, P. *et al.* Nanoscale architecture of integrin-based cell adhesions. *Nature* **468,** 580–4 (2010).